Numerical Investigation of Turbulent Hydrogen/ Air Diffusion Flames and Turbulence Radiation Interactions

Onokpe Oghenekevwe Owin (B.Eng, M.Sc)

A dissertation submitted for the degree of Doctor of Philosophy (PhD)

Heriot-Watt University

School of Engineering and Physical Sciences

April, 2011.

Abstract

An investigation of the flame structure and radiation properties of turbulent hydrogen/air diffusion flames is reported. The laminar flamelet-conserved scalar probability density function approach is used to predict the scalar distributions throughout a laboratory-scale axisymmetric buoyant hydrogen diffusion flame. Predictions are compared with published measurements of mean and root mean square (RMS) temperatures and species concentrations based on the laminar flamelet concept. Predictions of spectral intensity and received heat flux are made with a narrow-band radiation model using mean properties, stochastic and mean emission methods to evaluate the effects of turbulence radiation interactions (TRI) and modelling TRI to predict the received radiant heat flux was very important. The predictions were, on the whole in good agreement with published measured data available in the open literature.

Present study centres on the development of novel numerical models to predict TRI in turbulent hydrogen flames, implemented in a sophisticated way using enthalpy perturbation equation to account for radiative heat loss. This thesis highlights novel accomplishments in areas such as modelling lifted hydrogen jet flames, flame structures and external radiation fields where significant findings are reported. Firstly, successful extension of the lift-off model to hydrogen jet flames using strain rate as stretch parameter to accurately predict the lift-off height and affirming the small-scale strain rate model is better than the large-scale strain rate model which is different to methane lifted jet flames. Secondly, different jet flames were investigated using two different probability density functions (PDFs) and two transport equations taking into account fluctuations of temperature $\sqrt{\widetilde{T''^2}}$ and water vapours $\sqrt{\widetilde{X''^2_{H_2O}}}$. The new Truncated Gaussian PDF was confirmed to give better predictions than other methods. Lastly, of the three approaches considered in modelling TRI the stochastic method proved the most accurate to predict the spectral intensity distribution and radiative heat flux distribution.

Dedication

To my late mother Elizabeth Onokpe always remembered.

Acknowledgements

I am most grateful and indebted to my supervisor Dr. Peter Cumber, for his invaluable support, guidance and profound knowledge in turbulent combustion modelling and numerical methods. I thank my family for their emotional support and encouragement. I am deeply indebted to my brother God'stime who positioned himself into my deep heart by his exceptional support. Very special thanks to my lovely wife Ebuwa and two sons namely Onanefe and Ogheneruno who have supported me during my study and have been patient and understanding.

I would like to thank Heriot-Watt University that provided my tuition fee scholarship and also the entire staff of Mechanical and Chemical Engineering department for their tremendous assistance. Finally, special thanks to all my friends in the department who made my stay enjoyable and full of laughs.

ACADEMIC REGISTRY
Research Thesis Submission

Name*:*	ONOKPE OGHENEKEVWE OWIN		
School/PGI:	Engineering and Physical Sciences		
Version: *(i.e. First, Resubmission, Final)*	Final	Degree Sought (Award **and** Subject area)	PhD – Mechanical Engineering

Declaration

In accordance with the appropriate regulations I hereby submit my thesis and I declare that:

1) the thesis embodies the results of my own work and has been composed by myself
2) where appropriate, I have made acknowledgement of the work of others and have made reference to work carried out in collaboration with other persons
3) the thesis is the correct version of the thesis for submission and is the same version as any electronic versions submitted*.
4) my thesis for the award referred to, deposited in the Heriot-Watt University Library, should be made available for loan or photocopying and be available via the Institutional Repository, subject to such conditions as the Librarian may require
5) I understand that as a student of the University I am required to abide by the Regulations of the University and to conform to its discipline.

* *Please note that it is the responsibility of the candidate to ensure that the correct version of the thesis is submitted.*

Signature of Candidate*:*		Date:	21st April, 2011.

Submission

Submitted By *(name in capitals):*	ONOKPE OGHENEKEVWE OWIN
Signature of Individual Submitting:	
Date Submitted:	21st April, 2011.

For Completion in Academic Registry

Received in the Academic Registry by *(name in capitals):*			
Method of Submission *(Handed in to Academic Registry; posted through internal/external mail):*			
E-thesis Submitted (***mandatory* for final theses from January 2009)**			
Signature:		Date:	

Table of Contents

Lists of Tables and Figures

Nomenclature

p	Pressure
C_1, C_2, C_μ	Parameters in the k-ε turbulence model
$C_{p,j}$	Specific heat capacity of species j
$C_{s,1}$, $C_{s,2}$	Calibration constants in strain rate models
D	Mass diffusion coefficient
d	Nozzle diameter
E	Activation energy
f	Mixture fraction
f''^2	Variance of mixture fraction
k	Turbulence kinetic energy
κ_λ	Spectral absorption coefficient
l_t	Turbulence length scale
L_e	Integral length scale
M	Molecular mass of the mixture
P	Turbulence production source term, Probability density function
P_b	Probability of burning
P_{burn}	Composite probability of burning
P_c	Percolation threshold
P_d	Probability of burning relating to the location of the fluctuating flame base
q_{Rad}	Radiation heat flux
r	Radial co-ordinate
r_{st}	Radial location of the stoichiometric concentration
s	Strain rate
S_i	Source term

S_D	Scalar dissipation rate
T	Temperature
U	Stream-wise velocity
U_0	Source velocity
V	Radial velocity
w_i	Chemical production rate for species i
X_i	Mole fraction of species i
Y_i	Mass fraction of species i
z	Axial co-ordinate
z_L	Lift-off height

Greek Symbols

Δh	Enthalpy perturbation
ε	Dissipation rate of turbulence kinetic energy
φ	Generic flow variable
φ_b	Burning flamelet
φ_m	Isothermal mixing flamelet
κ	Von Karman Constant
μ_{eff}	Effective viscosity
μ_l	Laminar viscosity
μ_t	Turbulent viscosity
ν_l	Kinematic viscosity
ρ	Density
σ	Stefan Boltzmann constant

$\sigma_{\Delta h}$	Turbulent Prandtl number for specific enthalpy perturbation
σ_{ε}	Turbulent Prandtl number for the dissipation rate of turbulence kinetic energy
σ_{k}	Turbulent Prandtl number for the turbulence kinetic energy
λ	Wavelength
I_{λ}	Spectral radiation intensity
$e_{b\lambda}$	Spectral blackbody emissive power
τ_{λ}	Spectral transmissivity
$d\Omega$	Solid angle
Γ_{i}	Diffusion coefficient of species i

Subscripts:

adia	Adiabatic property
amb	Ambient value
rms	Root mean square
q	Quench value
st	Property at stoichiometric conditions
0	Initial condition or source condition

Over bars

-	Reynolds averaged quantity
~	Favre averaged quantity

Glossary

CFD	Computational fluid dynamics
CV	Control volume
CPDF	Cumulative probability density function
DNS	Direct numerical simulation
DTM	Discrete transfer method
FCV	Fuel cell vehicle
ICE	Internal combustion engine
LES	Large eddy simulation
MIE	Minimum ignition energy
PDF	Probability density function
PDFT	Probability density function transport
RANS	Reynolds average Navier Stoke
RE	Reynolds number
RMS	Root mean square
RTE	Radiative transfer equation
SNB	Statistical narrow band
TRI	Turbulent radiation interactions

List of Publications

O. Onokpe, P.S. Cumber: Modelling lifted hydrogen jet fires using the boundary layer equations. Applied thermal engineering volume 29 (2009) pages 1383-1390

O. Onokpe, P.S. Cumber: Modelling lifted hydrogen jet fires using the boundary layer equations. Conference paper at the 10^{th} UK heat transfer conference international symposium on phase change (September 10-11, 2007) Edinburgh, Scotland, United Kingdom.

Chapter 1

Introduction

Hydrogen is likely to be one of the most important future energy carrier, for many stationary and mobile applications, with the potential to make significant reductions in greenhouse gas emissions and significant improvements in energy efficiency at a global scale, especially if renewable primary energy sources are used to produce the hydrogen, coupled with fuel cells which use this hydrogen to produce electricity.

With interest in its practical applications dating back almost 200 years, hydrogen energy use is hardly a novel idea [1]. What is new is the confluence of factors since the mid-1990s that increase the attractiveness of a hydrogen energy economy. These factors include: persistent urban air pollution, demand for low or zero-emission vehicles, the need to reduce foreign oil imports, carbon dioxide (CO_2) emissions and global climate change, and the need to store renewable electricity supplies. These considerations are not confined to a single nation or region, and render hydrogen a virtually ideal energy carrier that is abundantly and equitably available to humanity [2].

The study of turbulence radiation interaction (TRI) remains a fully open research subject. Several years ago, interesting studies emerged, estimating the global effect of turbulence on radiation-heat transfer and demonstrating that this phenomenon is important. It was made known that in flames, the radiant intensity can be easily increased by 24% because of turbulent fluctuations [3]. In [4], the influence of various fluctuating radiation quantities on fluctuating reacting mixtures was studied with a wide-band model. Simulations that took account of TRI are found to be in better agreement with experimental data [5, 6]. The most important effect of accurate radiation modelling is on temperature prediction that could reduce the computed highest temperature as a result affects other important quantities that are sensitive to the temperature field. In this present investigation we use the stochastic and mean emission method to modelled TRI but with a narrow-band model.

The simulation of hydrogen jet fires is an interesting and current area of research due to the sensitivity to global warming and the potential to address this problem with ‘‘The

Hydrogen Economy" concept. To utilise hydrogen successfully requires the development of robust and accurate models to investigate new techniques for assessing the safety of operations involving hydrogen to ensure the inherent hazards of using hydrogen do not negate the benefit of reduced CO_2 emissions. It is broadly acknowledged that thermal radiative emission is often the controlling mechanism in the growth and spread of unwanted fire. Present models of fire radiation, however, are limited by our understanding of the interactions between the turbulence flame dynamics and the complex integral nature of radiative transfer. It is the goal of this thesis to study the radiative emission from hydrogen diffusion flames, characteristic of fire, and assess the significance of these interactions in order to develop more accurate models of turbulence flame radiation.

1.1 Hydrogen Safety

Hydrogen safety is known to be of vital importance to the onset and further development of the hydrogen economy. The development and introduction of hydrogen technologies, as well as the level of public acceptance of hydrogen applications, are presently being constrained by safety barriers.

The perception of "hydrogen" has been incorrectly shaped by vividly haunting images of three well-publicized events, namely the 1937 Hindenburg Airship disaster (see Figure 1.1), the development and proliferation of nuclear weapons, specifically the hydrogen bomb, and the 1986 Space Shuttle Challenger accident.

In the case of the Hindenburg, hydrogen was the buoyancy gas used to provide lift to the airship. It is true that the gas did ignite and burn; it did so quickly, upwardly, and away from the people below. Hydrogen did not cause the Hindenburg to explode, even though the average person believes that it did. If the Hindenburg had exploded, then the loss of life would have been much greater than actually occurred. Certainly, the crew and passengers would have perished in the air. The explosion was later attributed to a weather-related static electric discharge, which ignited the airship's silver-coloured, canvas exterior covering. Forensic research has revealed that the exterior covering was treated with two materials that years after the Hindenburg accident became key ingredients of solid rocket fuel. All the passengers that rode the airship down to the ground survived. Thirty-five of the thirty-seven casualties resulted from people jumping

to the ground. While the Hindenburg was not the largest loss-of-life accident with an airship, it is the most memorable. Some reasons for this are the motion picture camera footage (see fig 1.1) and the live radio broadcast.

The hydrogen bomb uses hydrogen in the form of Tritium, a hydrogen atom with three neutrons in the nucleus, and the heat and nuclear reactions from the detonation of a nuclear fission bomb, to induce a nuclear fusion reaction. Nuclear fusion is the same process by which the sun generates its energy. These nuclear reactions require enormously high temperatures and pressures, and are in no way similar to the simple chemical reactions associated with hydrogen (H_2) production, storage, distribution, and use.

The Government Commission that investigated the 1986 Challenger accident concluded that the accident was not caused by hydrogen. While the Shuttle did have hydrogen onboard as a fuel for its main rocket engines, the primary cause of the explosion was leaking hot plasma from one of its two solid-fuel booster rockets.

Hydrogen is perceived to be dangerous because it has some properties that make its behaviour during accidents different from that of most other combustible gases. It may cause material embrittlement and diffuses more easily through many conventional materials used for pipelines and vessels. Gaps that are normally small enough to seal other gases safely are found to leak hydrogen profusely. Unlike other combustible gases, it has a Joule-Thompson inversion temperature (i.e. the temperature above which the Joule-Thompson coefficient becomes negative and expansion leads to warming instead of cooling) which is well below that of many applications involving gaseous hydrogen. This makes hydrogen more susceptible to ignition after sudden releases from high pressure containment. However, the reverse Joule-Thomson effect as a source of ignition has been ruled out while diffusion ignition has been examined in some experiments [12-14]. Diffusion ignition was first proposed by Wolanski and Wojcicki [7] following their experimental study in which pressurized hydrogen was released into ambient oxidizer. The release produced a strong shock wave which gave rise to ignition regardless of total temperature of hydrogen was below its auto-ignition temperature. It was prescribed that ignition was caused by a temperature rise of the combustible mixture due to mass and heat transfer between the hydrogen and shock-heated oxygen. These properties and behaviours of hydrogen (see Figure 1.2) require special studies be

done in order to comprehend and control the safety hazards that a hydrogen economy could pose.

Hydrogen is renowned for its predisposition to auto-ignite. In some accidental scenarios, pressurized hydrogen release was found to have ignited where there was no obviously identifiable ignition source [8]. Data from accidents and anecdotal evidence from operators showed that there is a high possibility that a release of hydrogen from a high pressure source would ignite without the presence of an ignition source. An analysis of hydrogen accidental database compiled by Wen et al of Kingston University in the United Kingdom [9] contained 676 incidents involving hydrogen where in 60% of the cases, the ignition sources were unidentified. Their findings are consistent with that of Astbury and Hawksworth [8]. Notwithstanding numerous mechanisms have been hypothesized and tried in the literature of spontaneous ignition of pressurized hydrogen release [8], unambiguous understanding about ignition mechanism is yet to be achieved.

A parametric study of previous studies [10-12] were investigated by Wen et al [9] to clarify the influence of pressure boundary rupture rate on the likelihood of spontaneous ignition. Wen et al [9] demonstrated that the rupturing process of the initial pressure boundary has important influence on the spontaneous ignition of pressurized hydrogen release. Nevertheless, they did not consider the actual rupture process and the influence of the ruptured disk thickness. Perhaps, it could be the sharp edges formed by the ruptured disk as it is flattened onto the wall of the pipe could potentially promote the generation of shock waves and lead to stronger shocks which could in turn facilitate spontaneous ignition. Our investigation mainly focuses on accidental release of hydrogen fuel that finds a source of ignition it will then form a lifted jet fire based on a characteristic valve diameter and source velocities encountered.

Hydrogen can leak through tiny orifices 2.8 times faster than methane and 3.3 times faster than air because of its small molecular size [13]. It is flammable over a wider range of compositions in air than methane, propane or gasoline and its detonation range is similarly broad [13, 14]. Hydrogen's unusually high diffusion and buoyancy force in air, however, somewhat compensate for the danger posed by its fast leak rate and wide range of combustible compositions. In the open environment, hydrogen quickly disperses up and away from the source of a leak, rather than concentrating in low-lying areas, as do propane and gasoline vapours. If hydrogen does catch fire, it burns with a

nearly invisible flame that is hard to detect. Its ignition energy is lower than methane or propane at most compositions, enabling self-ignition of high-pressure leaks.

Since it is expensive and potentially hazardous to undertake experimental hydrogen release and combustion in real-scale configurations, the use of computational fluid dynamics (CFD) modelling for safety purposes is increasing in this field. Moreover CFD modelling also permits the investigation of releases in real world environments. Earlier hydrogen safety work in urban environment based on CFD methods of investigation includes the analysis of the 1983 Stockholm accident by Venetsanos, Huld, Adams, and Bartzis [15]. In the Stockholm accident, a hydrogen leak occurred from a rack of hydrogen cylinders located on a truck delivering industrial gases. In the subsequent explosion in an inner city area, several people were injured, the facade of the nearest building was heavily damaged and windows were broken within a radius of 90m.

Because the combustion behaviour of hydrogen differs from that of other fuels, it presents another set of hazards and requires diverse safety precautions. In the open air, for example, the high buoyancy and diffusivity of pure hydrogen make it very unlikely to accumulate to its threshold of flammability, which gives hydrogen an intrinsic safety feature. In enclosed spaces, however, combustible compositions can build up, and precautions such as ventilation and careful monitoring are needed. The basic kinetics and explosion limits of hydrogen/air are well known [16] for the reason that very few chemical species are involved. The ignition step in pure hydrogen/air mixtures (that is, $H_2 + \frac{1}{2}(O_2 + \frac{79}{21}N_2) \rightarrow H_2O + \frac{79}{42}N_2$), however, is essentially never involved in accidental explosions. Rather, an external heat source (for example, a spark from static electricity) or an impurity assisted lower energy dissociation reaction (for example, thermal dissociation of a lubricant or organic film) in the presence of hydrogen initiates the production of radicals and triggers a subsequent runaway chain reaction. Beyond kinetics, the hydrodynamics of hydrogen mixtures in oxygen and nitrogen are complex because of the very different masses and the broad range of transport properties such as diffusivities, viscosities and densities of the constituent gases. When chemical combustion is added to the picture, modelling and predicting flame and explosion behaviour become more complex, as the relatively unknown transport properties of the

airborne neutral radicals such as H and OH are important in modelling the turbulence characteristics of the explosion.

Example areas of application where mathematical models are used in safety analysis are high pressure plant and pipe work. The safe design and operation of high pressure plant and pipe work requires that provision be made for the relief of pressure under certain operational and emergency conditions. The consequences of a release must also be evaluated so that appropriate safety measures can be adopted during the relief process. Furthermore, assessments of the consequences associated with accidental releases of flammable material are required as the basis of safety reports and risk assessments on existing and proposed installations. For flammable gases and vapours it is necessary to be able to predict the thermal radiation fluxes that any fire might impose on its surroundings either by direct flame impingement of the fire on an item of plant or at a distance from the fire by radiation transmitted through the atmosphere. This information is in turn used to provide estimates, for example, of vessel survival times, building burning distances and escape times for personnel.

1.1.1 Hazards of Compressed Hydrogen (CompH_2)

Compressed hydrogen presents exactly the same hazards as any compressed gas, so will have all the same potential hazards as compressed natural gas (CNG). However, there are two other hazards with hydrogen—its small molecular size, and its minimum ignition energy (MIE). The small molecular size means that hydrogen will easily diffuse out of a system which is completely leak tight to other gases. It can also induce blistering and cracking of steels at elevated temperatures or where the hydrogen is generated in its atomic form, such as corrosion of steel with wet hydrogen sulphide. Here the aqueous sulphide attacks the steel and forms nascent hydrogen which permeates through the steel until it encounters a void, where it combines to form the gaseous diatomic form. This form is unable to diffuse through the steel, and so accumulates. The pressures which can be generated are significant, sufficient to rupture the steel.

Hydrogen also has a much lower MIE than any traditional hydrocarbon fuel, at 0.017mJ, as opposed to a value nearer to 0.2mJ for a hydrocarbon. This makes the hydrogen far more sensitive to ignition than any other gaseous fuel. There are some

references to hydrogen having a positive Joule-Thompson coefficient [17], and so a large reduction in pressure which occurs during a leak from a high-pressure system results in a rise in temperature, rather than a fall, due to the expansion. Whilst this would appear to offer a mechanism for leaks to always ignite, in practice leaks even from high pressure do not always ignite, and the temperature rise when expanding from 50MPa to atmospheric pressure raises the temperature by less than 18K. However, there have been many ignitions of hydrogen leaks which have not had an obvious ignition source. A review of these were undertaken by Astbury and Hawksworth [8].

1.2 Objectives and Scope of the Research

It is widely accepted that thermal radiative emission is often the controlling mechanism in the growth and spread of unwanted fire. Existing models of fire radiation, however, are limited by our understanding of the interactions between the turbulence flame dynamics and the complex integral nature of radiative transfer. It is the aim of this thesis to study the radiative emission from buoyant diffusion flames and the important flame structure fields in TRI, characteristic of fire, and assess the importance of these interactions in order to develop more accurate models of turbulence flame radiation.

This investigation will produce a complete computational model for a hydrogen jet fire which will be used to predict

- The lift-off region
- The flame structure fields important to thermal radiation
- The external radiation fields

When considering the safety of a high pressure system, storing flammable pressurized hydrogen, a typical scenario that must be considered is the possibility of an accidental leak that finds a source of ignition. This produces a jet fire characterised by a high momentum source with a flame trajectory in the near field determined by the orientation of the gas leak, further downstream the flame trajectory is modified by the atmospheric boundary layer or the jet fire might impinge on another part of the plant such as a storage vessel [18]. Jet fires are of particular concern as they represent the worst case for a storage vessel tending to induce vessel failure in a small time interval [19].

Since the nature of turbulence reacting flowfields in practical combustors is very complex, idealised flows such as non-premixed jet flames are usually used for investigation of models. Another reason for the use of idealised flows to validate models is that comprehensive measurements are rarely obtainable from the practical combustor due to the many unresolved experimental difficulties, in particular access for instrumentation.

In order to obtain a tractable problem, based on existing knowledge of flames and their radiation properties, the present investigation is limited to the fully turbulence region of the flow as opposed to the near-source region. Analysis was developed to provide predictions of the mean and turbulence properties of this flow. These predictions were employed to estimate spectral radiation intensities and heat flux distribution surrounding the hydrogen flame.

The objective of the present investigation is to study mathematically and computationally the structure and radiation properties of buoyant turbulence hydrogen flames in still air. Specific goals of the study are as follows:

- Numerically predict velocity, temperature and species concentration fields of turbulence hydrogen-air diffusion flames. Source conditions for these tests will be well-defined and operating conditions range from rim stabilised jet flames to lifted jet flames.

- Apply a turbulence hydrogen combustion model as part of a jet fire model to compare the predicted flame structure with experimental measurements in the open literature. Use both predictive measurements as well as existing data in literature to evaluate methods for predicting the structure of axisymmetric lifted and rim stabilised flames.

- Investigate a range of modelling approaches for predicting the RMS temperature field and the RMS H_2O field. Specifically, two probability density function (PDF) will be investigated and a transport equation for the RMS fields.

- Evaluate methods of predicting radiation properties of turbulence flames, with particular emphasis on spectrally resolved non-luminous infrared radiation from gas bands and the incorporation of turbulence radiation interactions.

Turbulence combustion encapsulates a fascinating combination of physical phenomena, which continues to be unravelled by a host of international academics applying experimental and computational resources. In countless cases, including this thesis, the purpose is to produce a mathematical description of combustions process using hydrogen as the fuel of choice.

The structure of the thesis is as follows. Chapter Two highlights the literature review of this investigation covering areas such as lift-off height, turbulence combustion, flame structure and turbulence modelling and turbulence interactions. It also presents modelling issues specific to hydrogen. In Chapter Three we discuss the underlying theory and concepts used in developing the computation models to predict numerical results as against measured experimental values. Chapter Four focuses attention on the prediction of hydrogen jet lift-off height as a function of source velocity. In Chapter Five, we determine the flame structure by comparing two different approaches of probability density function (PDF) taking into account the fluctuations present in turbulence flames. Chapter Six, we use the dominant fluctuations present in diffusive turbulence hydrogen flames to illustrate the spectral intensity and received heat flux reducing the temperature to account for the heat loss using an enthalpy perturbation methodology. Furthermore, in hydrogen jet flames the major participating species is H_2O hence we focus on the mean and RMS H_2O predicted and measured fields. Lastly, Chapter Seven is the concluding remarks and summary of the major findings of our investigation and a proposal for future work to be undertaken in this field of study.

The overall goal of this investigation is to achieve a better theoretical understanding of buoyant hydrogen diffusion flames. The major effort is the development of a jet fire model and to propose a radiation model which accounts for the effect of turbulence fluctuations.

Figure 1. 1: The 1937 Hindenburg Airship Disaster [20]

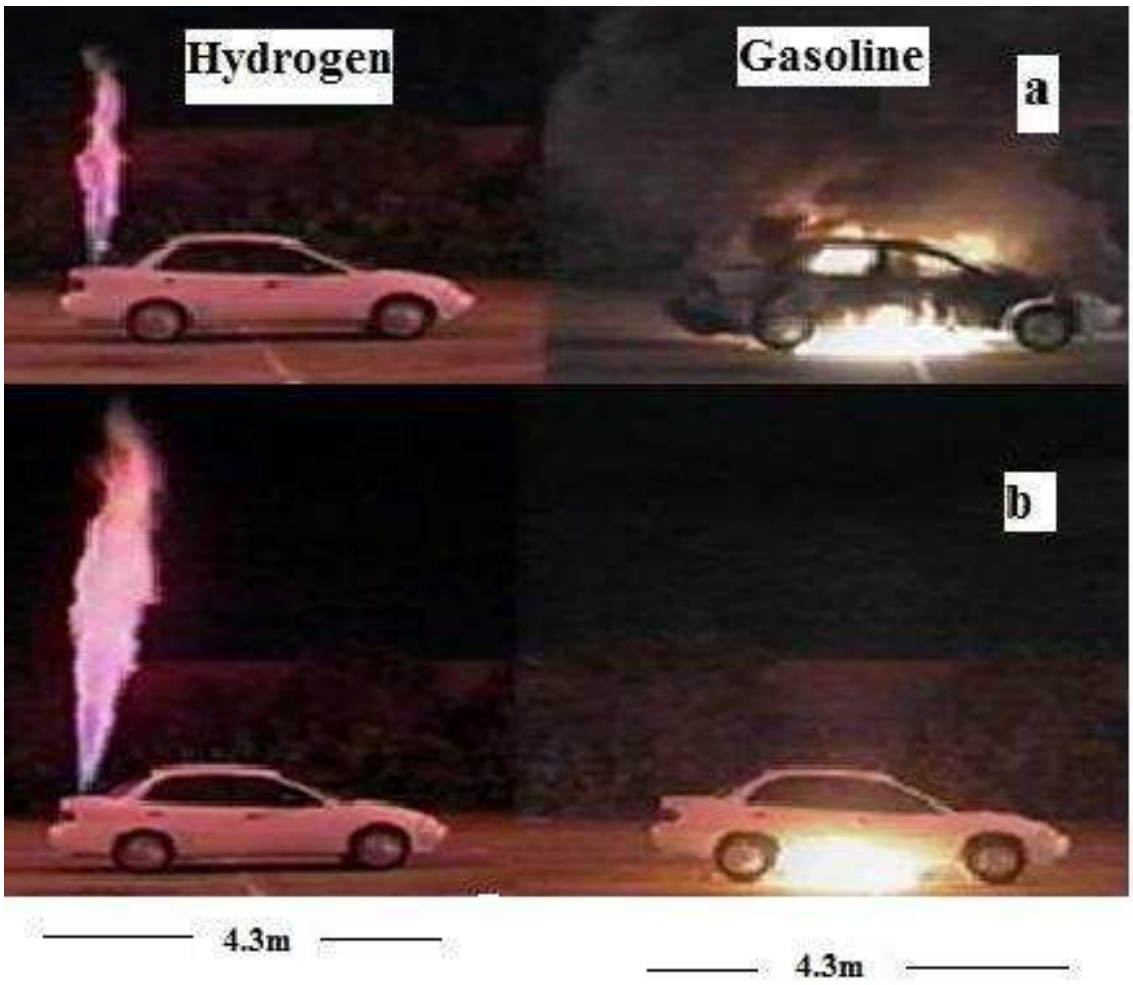

Figure 1.2: [21] a) Shows hydrogen leak and Gasoline leak after 1 minute
b) Shows hydrogen leak and Gasoline leak after 3 seconds

Chapter 2

Literature Review

The history of combustion research might start with the history of humankind [22-24] Early activities must have been far different from those in modern combustion research. The purposes would, however, be the same as those of present combustion research, that is, to find better ways to use the energy released by combustion or to mitigate the adverse effects of combustion. This dual function of combustion has been pointed out in most of the well-known textbooks on combustion [16, 22, 24-29].

The need to predict the rate of spreading of unwanted fire is readily apparent in a wide range of hazardous environments. However, the complexity of the phenomena involved and the large number of variables influencing their behaviour make modelling a formidable task. Early approaches reflect the desire to control the spread of unwanted fire and limited attempts made to examine underlying physical and chemical processes. These models, known as stochastic models, consider the probability of a specific occurrence, such as the spread of fire from one building to another, as a function of separation of the buildings and of time. The early model of Albini [30], later modified to a differential form by Thomas [31], is an example of this approach. Such stochastic models might be considered too simplistic for practical use, but in fact they do offer simple guidelines for prevention and control of fire spreading since they can embody substantial empiricism.

To understand the controlling mechanisms of fire, necessary for the improved design of buildings and fire safety devices, such as smoke detectors, a more rigorous approach is needed. Deterministic models attempt to describe in mathematical form the behaviour of fire in a given situation. Broadly, there are three types of deterministic models [32]. The physical models include experimentally determined scaling laws and correlations. The shape, size or overall characteristics of a flame, such as entrainment rate, are measured experimentally and applied to other situations using a similarity hypothesis determined from experimental results. Zone models offer a more comprehensive assessment of the overall fire system by dividing the combusting flame and its surrounding environment into zones. A set of equations are solved which describe what

happens within each zone and also the interaction between zones. The accuracy of the solution depends largely on how well the processes in each zone are described. Experimentally determined correlations are readily incorporated. In contrast, the field approach [33] attempts to solve the underlying flow field equations which describe the detail processes taking place within the system. It is, in principle, an exact approach. In practice, some terms must either be modelled or prescribed by empirical correlation. In addition, assumptions may be necessary to assist the numerical computation which would otherwise involve prohibitively expensive computer run times. Whilst in the immediate future zone models incorporating experimentally determined empirical correlations are likely to provide guidance for building codes and designers, the more precise description offered by field models may be the key to a more complete understanding of the complex phenomena associated with fire.

This study is focused on the accidental release of a hydrogen jet that encounters a source of ignition, which are (small-scale) un-impinging free jets or momentum-dominated buoyant jets. Previous work introduced a boundary layer theory approach to model the concentration layer adjacent to a ceiling wall at the impinging and far regions for small-scale hydrogen leakage [34, 35]. Houf and Schefer [36] have presented analytical and experimental investigations of small-scale unintended releases of hydrogen. They presented calculations from the model and experimental results to explain the behaviour of slow leaks over a Froude number range. Froude number can be expressed as

$$Fr = \frac{v}{(gL)^{1/2}} \tag{2.1}$$

where v is the velocity, g is the gravity and L is the characteristic linear dimension.

The turbulent round jet is the most suitable model to describe unintended hydrogen releases with circular leak geometries, such as pinholes, through which the flow of hydrogen is an axisymmetric jet. Measurements of the hydrogen distribution in a laboratory-scale hydrogen leak under flow conditions and neglecting the buoyancy effects are described by Houf et al. [37]. They reported a Froude number of 268, which is in the momentum-dominated regime where the effects of buoyancy-generated momentum are small and the Reynolds number was sufficient for fully developed turbulent flow. Their results showed that hydrogen jets behave similar to jets of helium

and conventional hydrocarbon fuels such as methane and propane in the momentum dominated regime. As with any jet flow, the hydrogen mole fraction centreline decay rate shows X^{-1} dependence where X is the axial distance from the jet exit.

The integral modelling approach was used by Agrawal and Prasad [38] to derive similarity solutions for several quantities of interest including the cross-stream velocity, Reynolds stress, the dominant turbulent kinetic energy production term, and eddy diffusivities of momentum and heat for axisymmetric and planar turbulent jets, plumes, and wakes. In this investigation, numerical predictions of results such as the centerline velocities, temperature and the species concentration at any downstream location are used with the corresponding constants for the hydrogen leakage from a momentum-dominated regime of a buoyant jet obtained by Kalghatgi [39], Faeth et al [40] and Barlow [41]. The integral modelling approach is used to derive similarity solutions for turbulence quantities such as source velocity, mean and fluctuating temperature, the mixture fraction and species concentration for the axisymmetric turbulent hydrogen jet.

2.1 Lifted Jet Flames

Combustion in non-premixed systems such as jets does not necessarily begin at the location where fuel and oxidizer mix to produce stoichiometric conditions. In numerous situations, the combustion zone is lifted above the nozzle, creating a stabilized partially premixed system several diameters above the nozzle. In many applications the flame is usually anchored at the nozzle to avoid instabilities of the pressure field, extinction and blowout for safety reasons. On the other hand, in some burner designs, lifted flames are preferred to protect the burner nozzle.

The physical mechanism that is responsible for the lifting of the flame is the competition between the flow and chemical effects, characterised by their respective time scales, the ratio of which is the Damköhler number.

$$D_a \equiv \frac{t_t\left(characteristic\ \ fluid\ time\right)}{t_c\left(characteristic\ chemical\ reaction\ rate\right)} \tag{2.2}$$

If typical chemical time scales are everywhere smaller than flow residence times, which is the inverse of the strain rate, decreases and so does the Damköhler number. At a critical exit velocity the flame can no longer be stable at the nozzle rim and lift-off

occurs. From this point increasing the fuel velocity further leads to an increase of the lift-off height proportional to the exit velocity [39].

The knowledge of the mechanisms involved in non-premixed turbulence flame stabilisation is one of the important issues of diffusion combustion, and different mechanisms have been proposed to explain lift-off [42]. In turbulence lifted flames, the flame base is distorted by large vortices responsible for incomplete mixing of the reactants, whereas micromixing mechanisms bring fuel and oxidizer to the reaction zones. In non-premixed turbulence combustion, the reaction zone is confined to the highly convoluted stoichiometric surface of the mixture. Results of analysis of diffusive-reactive layers [43] indicate that quasi-steady combustion is observed when the heat loss by diffusion and convection is balanced by the heat released within the reaction zone. The flame will undergo local quenching when the chemistry cannot produce sufficient heat compared to the heat diffusing away from the reaction zone. In turbulence flames, we anticipate large thermal gradients responsible for quenching where the velocity fluctuations generate stretching of the stoichiometric surface.

Wen and Ferrais [44] carried out a study using the large eddy simulation technique to facilitate the simulation of turbulent lifted flames. Their model was based on the linear coupling of two independent approaches for premixed and non-premixed combustion through the flame index concept which uses the fuel and oxygen gradients to detect the combustion regime. Their study covers a wide domain from the jet exit to the far-field. Good agreement with the data for the lift-off height and mean mixture fraction was obtained. However, the flame index approach adopted was unable to capture the physics in the transition zone where, even though the oxygen and fuel gradient have the same direction, the combustion is diffusion controlled [45] and their model was not tested in flows with turbulence. A wide range of small-scale, Kalghatgi [39] and Pitts [46], and large-scale experimental studies of lifted fires, Birch and Hargrave [47], exist in the open literature. There are also a number of theoretical studies, Sanders and Lamers [48], Cumber and Spearpoint [49] being examples.

The computational modelling of rim-stabilised fires is mature with good agreement between the predicted and measured mean temperature and major chemical species established, Gore et al. [40] for example. This is not the case for lifted jets where computational studies have focussed on understanding the mechanism for the location

of the combusting flame base and good agreement between predicted and measured flow properties is not universal.

The mechanism involved in flame stabilisation at the lift-off height after over three decades of research is still debated vigorously. The early accepted theory was the lift-off height was determined by the downstream location on the stoichiometric contour where the mean jet velocity equals the turbulence burning velocity. The location of the flame base is governed by the premixed nature of the fuel air mixture. Computational models using this criterion were able to predict lift-off heights for the jet fires considered by Vanquickenborne and Van Tiggelen [50]. Experimentalists were also able to correlate measured lift-off heights for a range of fuels using the premixed assumption and the turbulence burning velocity, Kalghatgi [39].

Peters and Williams [51] were the first to question this theory suggesting that insufficient premixing could occur for the premixed theory to be valid in the lifted jet fires they considered. Peters and Williams proposed another mechanism, based on laminar flamelet quenching that relies on an analysis of laminar flamelets distorted by the turbulence field. At the fluctuating flame base the lifted flame can be considered as an ensemble of laminar flamelets in the instantaneous field; the laminar flamelets varying from air–fuel mixtures at or near stoichiometric conditions to fully entrained air. Each of the flamelets can be considered to be burning or non-reacting depending on the local instantaneous composition and level of turbulence distortion or stretch the flamelet is subjected to. The location of the flame base is determined by the proportion of burning to non-reacting flamelets. A candidate property for characterising the degree of stretch of the flamelets is the scalar dissipation rate, Peters [52], although Sanders and Lamers [48] present a convincing argument against the scalar dissipation rate and suggest the strain rate as the appropriate parameter. Muller et al. [53] use a model for the strain rate of the largest eddies to predict the lift-off height, whereas Sanders and Lamers favour the small-scale strain rate. Sanders and Lamers base their conclusions on a calibration of lift-off height using isothermal simulations, the argument being the lift-off height is primarily determined by the flow upstream of the flame base.

As well as the two theories discussed above Pitts [46] analysed a number of lifted jet fires and suggested that the location of the lift-off height is determined by large-scale rather than small-scale structures in the jet, and isothermal mixing upstream of the lift-

off region is important in determining the location of the flame base. Even though Pitts presents a compelling case for his favoured mechanism he still states that models based on a premixed theory or small-scale turbulence structures cannot be discounted. Upatnicks et al. [54] using a high speed photography technique, Cinema PIV identified another mechanism for the location of the lift-off height based on an analysis of the edge of the flame. One reason for the lack of clarity as to the correct mechanism is all theories show some degree of agreement with observation, and in many experiments there is considerable overlap in prerequisite conditions for each theory to apply.

Another concept for predicting lift-off heights of turbulence diffusion flames was proposed by Bradley et al. [55] with an alternative, so called mixedness-reactedness, flamelet model. Here the combustion is considered to take place in a premixed zone in the diffusion flame. At each given mixture fraction within the flammability limits, a premixed flame is established. Because the most obvious autonomous parameter for a premixed flame is the temperature, instead of the mixture fraction, all scalar profiles are given in terms of the temperature. In this way, the heat release in temperature space is determined, and the mean heat release is calculated by integrating over independently chosen probability density functions for mixture fraction and temperature. The lift-off height is determined by the axial distance where the mean heat release begins. The obtained lift-off heights as a function of fuel exit velocity *h(U)* correspond well with the experimental data of Kalghatgi [39]. Despite the success of this method, it is not completely clear whether the assumption of premixing is justified. Furthermore apparently no threshold behaviour is contained in the model, while this is a characteristic feature of a lifting flame.

2.2 Non-premixed combustion

Fuel and oxidizer enter separately into the combustion chamber in non-premixed turbulent combustion, where they mix and burn during continuous intermixing. Non premixed combustion is a common type of flame that occurs in equipment such as diesel engines, boilers and furnaces, combustion nearly always takes place within a turbulent rather than a laminar flow field. This fact responds to two main reasons. First, turbulence increases the mixing and transport processes and in so doing enhances combustion. Second, combustion releases heat and consequently generates flow instability by buoyancy and gas expansion, which then enhances transition to

turbulence. Convection and diffusion are responsible for the turbulent mixing. The turbulence causes non uniform species and temperature fluctuations, which in turn affect the chemical reaction rates. The underlying hypothesis is that most of the fluctuations in the mole fractions and temperature that make closure for the chemical reaction rates difficult can be associated with the fluctuations of the mixture fraction. The mixture fraction describes stoichiometry of the mixture and it is a conserved scalar.

The foremost, well-substantiated concepts in non-premixed turbulent combustion are categorised in terms of their modelling of chemistry and mixing. These we discuss in more detail in the sub-sections below together with the ground-breaking experiments that have arisen from them or that they suggest for prospective research.

2.2.1 The Mixing-controlled concept

The original concept for turbulent non-premixed combustion is that combustion is fundamentally mixing controlled. The classical paper by Hawthorne et al [56] appears in the first of the post-war combustion symposia. In it the flame lengths and mean structure of turbulence jet diffusion flames are studied and are found to correlate well with mixing laws of turbulence jets. The concept is closely related to that for laminar diffusion flame as studied by Burke and Schumann [57] in the first combustion symposium held in 1928. In that early work, the mixing is by molecular diffusion in laminar flow, and the flame is situated at the surface where the fuel and the oxidant are in stoichiometric proportions – the reaction zone, itself, being very thin compared with the diameter of the flame. The main idea was that chemical reaction rates were much faster than mixing by molecular diffusion. This idea was carried across into the field of turbulence diffusion flames.

A variable, named the mixture fraction [58], can be defined that describes the stoichiometry of the mixture, and the instantaneous temperature and composition of the mixture would be distinctively related to the mixture-fraction variable. In turbulent flow, the mixture fraction at a particular point has random fluctuations, but these have statistics similar to those in non-reacting flow. Mean values of composition and temperature can be obtained by weighting their instantaneous relationship to the mixture fraction by the probability density function (PDF) of the mixture fraction. Such mean values seem to show co-existence of fuel and oxidant. This is not, however, due to the

slowness of chemical reaction, but due to the fluctuating stoichiometry: significant concentrations of both fuel and oxidant may exist at the same place, but not simultaneously.

Such a mixing-controlled concept instantly raises the question as to its range of validity. If the mixing can be made fast enough, then surely the reaction rates would be controlled by the chemistry and not by the mixing. The well-stirred reactor of Longwell and Weiss [59] used small sonic jets to produce what was thought to be a homogeneous mixture of reactants and products within the reactor. Would the length of jet diffusion be affected by limits on the reaction rate? In an esoteric study, Hottel reports [60] on experiments at MIT [61] where this was investigated by studying jet diffusion flames at a range of pressures from 0.3 to 6 atm. The novel idea was that chemical rates would go approximately as the square of the pressure whereas the Reynolds number would go linearly with pressure. The findings were that the flame lengths were still controlled by mixing but that buoyancy was more important in determining rates of mixing in such flames than was the Reynolds number. The Reynolds number (Re) can be defined as

$$\mathrm{Re} = \frac{\rho V L}{\mu} = \frac{V L}{\upsilon} \tag{2.3}$$

where V is the mean velocity, L is a characteristic linear dimension - the jet nozzle diameter, ρ is the density of the fluid, υ is the kinematic viscosity $\left(\upsilon = \mu/\rho\right)$ and μ is the dynamic viscosity of the fluid. A modified Froude number was needed to incorporate the effects of buoyancy on mixing.

In the early 1970s, interest was renewed in the effects of chemical kinetics, particularly for pollutants such as nitric oxide. This interest came as a result of sociological pressures for reduction in air pollution emissions arising from combustion processes. Nitric oxide is formed by relatively slow reactions and so could not be modelled using the mixing-controlled concept. Since the formation of nitric oxide was insignificant for the major species and overall heat release, efforts were made to correlate its production with the convective and mixing time scales in the flow. Early results on hydrogen jet diffusion flames, with Froude number held constant [62], suggested that the reactive time scale followed a power law of its reaction $t_{react} \propto \mathrm{Re}^{-1/2}$ – and so is proportional to the Kolmogoroff, or fine-scale time scale of the turbulence. Later work [63] has

indicated that radiation and differential diffusion effects are also important, particularly in hydrocarbon flames, and such attempts at simple correlation are unsustainable.

In the 1960s and 1970s, the primary emphasis of combustion research was on how the rate of mixing was affected, not only by buoyancy, but by density variation and/or fluctuations, and by the postulated phenomenon of "flame-generated turbulence" [64]. Kent and Bilger [65] studied a horizontal round jet diffusion flame of hydrogen into a co-flowing airstream, the main idea being that minimal deflection of the flame in the vertical direction and, preservation, essentially, of axisymmetry would contradict any effects of buoyancy – the chief interest was in density effects and 'flame-generated turbulence'.

The disadvantage of this approach was the introduction of new non-dimensional parameters such as the ratio of the jet to co-flow velocity and the probable increase in the influence of the boundary layer characteristics at the jet nozzle exit – something that could involve a host of new non-dimensional parameters. This development reflected the new concept for the study of non-reacting turbulence. The then classical work on self-preserving flows and equilibrium flows was superseded by attempts to describe the evolution of turbulence by partial differential equations involving several significant terms such as production, advection, turbulence diffusion and dissipation [66]. These equations were derived from Reynolds averaging of the Navier-Stokes equations. As Bray pointed out [67], many more terms would be involved in flows with strong density fluctuations. Density-Weighted or Favre averaging of the Navier-Stokes and species conservation equations [68] appeared to be a way around this problem and has enjoyed some success [69].

The modelling of chemistry was extended to include the concept of chemical equilibrium being the fast chemistry limit so that the effects of high temperature dissociations could give estimates of the concentrations of intermediate species and radicals such as H, OH, and O. This was particularly helpful for modelling nitric oxide. Previous work in hydrogen jet diffusion flames [70] assumed that the kinetics were essentially those of the Zel'dovich reduced mechanism for NO_x production [71] and that the temperature and oxygen concentrations were given by the fast chemistry concept.

As a result, the average production rate, required in the Reynolds/Favre-averaged equation for the chemical species, could be obtained by weighted instantaneous reaction rates, derived from fast-chemistry theory for the temperature and reactant species, by the probability density function of the mixture fraction [70]. An exceptional result arising from this theory was the discovery that reaction rates in flames with fast chemistry are proportional to the rate of scalar dissipation or the rate of molecular mixing (of the mixture fraction) [72] . Scalar dissipation rates in turbulent jets into still air scale with the power law $S_D \propto z^{-4}$ - so finite-rate chemistry effects would be most apparent near the nozzle exit. The bulk of the carbon monoxide burnout occurs much further downstream where the scalar dissipation rates are very low. However, Hottel [60] and Homsy [61] could find no effects of kinetic rates on flame lengths defined in terms of carbon monoxide (CO) burnout!

An immediate upshot of this discovery was the new viewpoint that the reactive species and temperature should depend not just on mixture fraction, as under the 'fast chemistry' theory, but also on local values of scalar dissipation would require high values of chemical reaction rates to balance the high rates of reactant arrival in the reaction zone from turbulence mixing. Tsuji and Yamaoka [73] has shown, in a series of investigations on laminar counter-flow diffusion flames, that the composition and temperature were dependent on the strain-rate in the flow – a quantity linearly related to the scalar dissipation of the mixture fraction. At high strain rates (scalar dissipation rates), temperatures are lowered, and there is increased overlap in the profiles of fuel and oxidant concentrations. At very high strain rates, extinction occurs. The general idea of the chemistry being dependent on the effects of scalar dissipation rates in regions where the mixture fraction is close to its stoichiometric value led, to the Sandia experiments [74, 75] on piloted jet diffusion flames.

Crucial to this experimental concept was the notion that high scalar dissipation rates should not be at the nozzle exit where the flow was subjected to the detailed minutiae of the 'initial' conditions arising from the upstream boundary layers in and outside of the jet tube or subjected to transitional 'coherent' structures. An open jet flow was also amenable to the latest advances in laser-diagnostic measurement. This experimental configuration was initially realised at the University of Sydney by Starner and Bilger [76]. Laser-diagnostic measurements by Rayleigh/Raman scattering made at Sandia

with Professor Dibble, and eventually published in Combustion and Flame [77, 78] were, the first of a long series of collaborations between Sydney University and Sandia [74, 79-81], initially with Robert Dibble and then with Robert Barlow, that has led to the superb experimental databases that provide benchmark measurements for the validation of turbulent non-premixed combustion models [74]. The high quality data made available by Sandia National Laboratories to assess the model developed in this investigation with regards to the hydrogen jet flame structure.

2.2.2 The Laminar Flamelet concept

A concept appeared in the early 1980s when Peters demonstrated [82] that the species conservation can, locally and instantaneously, be transformed into the so-called stationary laminar flamelet model (SLFM) equation by assuming terms involving transients and those involving gradients parallel to the instantaneous surface of the mixture fraction are small. The underlying theory is that flame reaction zones are thin, and their structure is essentially the same as in laminar flames subjected to the same scalar dissipation. Pre-calculated libraries of quantities such as composition, temperature, and reaction rates, as function of mixture fraction and scalar dissipation, are used to obtain closure for the chemistry-turbulence interactions. Detailed chemical reaction mechanisms and molecular diffusion processes can be included in these laminar flame calculations. A presumed joint probability density function of mixture fraction and scalar dissipation allows mean values to be predicted [83], in a manner analogous to that introduced for mixing-controlled combustion. Nevertheless, the flamelets are relatively insensitive to variations in scalar dissipation, and adequate predictions are obtained in many flows by assuming a constant mean value. This innovation has been taken on widely by combustion modelling researchers because it provides a simple and easy to implement physical picture of the turbulence flame structure. Within its range of validity, it is an attractively simple way to include effects of complex chemistry in turbulent flame calculations.

An early success [83] was the improvement in matching experimental CO concentrations, in comparison with calculations assuming chemical equilibrium. However, strong arguments have been suggested [84] against flamelet models. These include the effects of variations in scalar dissipation through flamelets, and the influence of neglected advection terms in the transport equations. It is clear that the

SLFM concept cannot remain valid in the presence of local extinction and re-ignition when unsteady and flame edge effects [85] must become relevant. However, the whole question of the range of validity of flamelet models remains contentious. It cannot be denied that the laminar flamelet concept can present an accurate description for sufficiently large turbulence scales and low turbulence intensities for combustion chemistry that is close to irreversible. It is equally evident that there is also a regime of intense turbulence, whose length and time scales are small relative to those of a laminar flame, for which laminar flamelet models will not be suitable. On the other hand, the range of validity of these models is not yet agreed.

Since the original proposal of the SLFM a number of extensions and improvements have been made to include the effects of transients [52] and to incorporate a Lagrangian viewpoint [86, 87], with associate treatment of the strong fluctuations that can occur in scalar dissipation, and to accommodate the effects of the advection terms parallel to the surfaces of constant mixture fraction. These extensions to the theory can be helpful, particularly for the modelling of extinction and re-ignition processes, and for kinetically slow species such as nitric oxide and carbon monoxide.

The laminar flamelet concept has been successfully combined with the turbulence modelling approach Large Eddy Simulation [88]. Another factor that affects the flamelet concept is the competition between the broadening of flamelets and their extinction, both of which are governed by the local Damköhler number and the level of mixture fraction fluctuations [89]. For the particular conditions of very high turbulence reported by Ratner et al. [90], the CH PLIF images indicate that the flamelets “extinguish before they broaden”. When the velocity fluctuations exceeded 10m/s, “shredded” flamelets were observed, but each CH reaction layer remained about as thin as a layer in a laminar flame (0.5-1mm). This finding implies that, for these specific conditions, the Damköhler number needed to extinguish the flamelet exceeds that needed to enter a distributed reaction regime. Nevertheless, most experiments to date have been conducted using room temperature reactants and relatively low gas velocities, which favour flamelet formation. Further work is required at elevated inlet temperatures and large mixing rates to measure the boundaries between flamelet and non-flamelet behaviour.

2.2.3 The Probability Density Function Transport (PDFT)

The mixing-controlled and stationary laminar flamelet model led to the prediction that the instantaneous composition at a point in a turbulent flame is solely determined by just one or two variables, mixture fraction (for fast-chemistry) and scalar dissipation (for the steady flamelet model). In the 1980s, single-shot Rayleigh/Raman data capable of testing these predictions became available and were presented in the form of scatter plots [77]. For hydrogen flames, the degree of scatter observed, and especially the occurrence of compositions outside those realised in steady laminar flames, indicated the need for a more general modelling approach [91]. This was provided by probability density function transport (PDFT) methods, whose development for turbulent reactive flows started in the mid-1970s [92-94]. The main advantages of the PDF approach are that independent turbulence fluctuations of all species can be represented, and that the direct effects of reaction appear in closed form in the PDFT equations [95-99]. While no modelling is required of the reaction term in the PDFT equations, a mixing model is needed to account for mixing by molecular diffusion.

The improvements in laser diagnostics led to more accurate measurements of the Sandia flames D,E, and F [75]; and the in situ adaptive tabulation (ISAT) algorithms [100, 101] facilitated the use of more detailed chemistry[102]. At the 28th combustion Symposium, quantitatively accurate calculations of these flames were reported [103, 104] based on PDFT calculations of Xu and Pope [105] accurately representing the level of local extinction in these flames as a function of jet velocity and axial distance – a feat as yet unparalleled by other approaches. Predictions in methanol flames [106] were also encouraging, even though the reaction zone is thinner. In spite of the success of these PDF calculations, there remain significant questions about the realism of the mixing models. The main models used are: Interaction-by-exchange-with-the-mean (IEM) [107] the modified curl model (MC) [108, 109]; and the Euclidean minimum spanning tree (EMST) model [110]. These are found to yield substantially different distribution (as revealed by scatter plots) [111], and also to predict extinction at substantially different Damköhler numbers [111, 112].

The three primary issues with mixing models in PDFT methods are as follows. Firstly, there is no explicit coupling between reactions and mixing although (especially in the EMST model) such coupling is implicit through the shape of the PDF. Secondly, the IEM and the MC models is non local in composition space: even at high Damköhler

number, according to the models, rich and lean mixtures can mix to form unreacted stoichiometric mixtures [113]. The EMST model was developed to overcome this shortcoming. Thirdly, none of the models include a physically realistic representation of the fluctuations in scalar dissipation. Since our notion of local extinction are based on extreme values of the scalar dissipation-many times the mean value-it remains a puzzle that PDFT models (which do not explicitly represent the distribution of scalar dissipation) are capable of calculating local extinction and re-ignition in piloted jet flames.

Considering the modelling of turbulence flows, the instantaneous flow properties fluctuate in a non-deterministic manner due to the fluctuations in the initial and boundary conditions. If we measure one physical variable in a turbulence flow with the variation of time, we may get a result similar to the one displayed in Figure 2.1a. For such cases, deterministic models are too intricate to develop due to the range of length scales present. This is the motivation for modelling the turbulence flow as a pseudo random medium and describing it with a probabilistic mathematical model.

The probability theory and statistical theory are the basis of judgement when certainty is not available or not possible. The main object of the probability method is to generalise from a given set of data to a more broadly applicable statement. The main objective of the statistical theory is to estimate the properties of a population from tests on the samples drawn from that population. In statistical analysis, the physical variables can take on many possible values, like the one shown in Figure 2.1a. With the knowledge of the statistical theory, the original time-dependent coordinate is transformed into a PDF coordinate Figure 2.1b by dividing the whole range of this fluid variable into several class intervals. The class frequency in each interval is counted. The PDF at the *i*th class interval is evaluated as:

$$f = \frac{N_i}{N_{total}} \cdot \frac{1}{\Delta x_i} \tag{2.4}$$

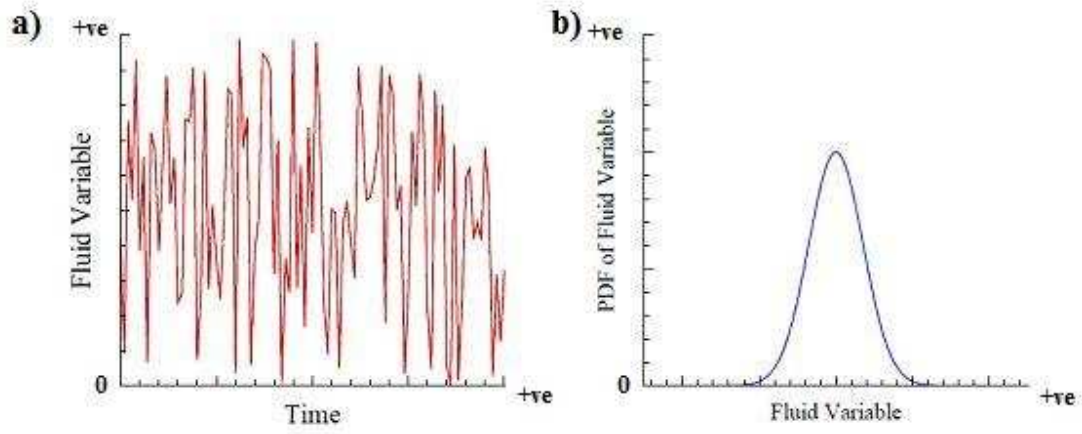

Figure 2. 1 Transformation of a time-dependent coordinate (a) to PDF Coordinate (b).

Where N_i is the frequency of class *i*; N_{total} is the total number of the available data; Δx_i is the width of the *i*th class interval. Therefore, the PDF is theoretically independent of the choice of the width of class interval while the frequency distribution function is not. Giving a joint PDF of N independent variables $\Phi_1, \Phi_2, ...\Phi_N$, the integral of the PDF in space is normalized to unity:

$$\int_{\Phi_1,\Phi_2,...\Phi_N} f\left(\Phi_1,\Phi_2,...\Phi_N\right) d\Phi_1, d\Phi_2, ...d\Phi_N = 1. \qquad (2.5)$$

The mean of an arbitrary function Z defined in Φ-space can be calculated from the PDF:

$$\langle \mathrm{Z} \rangle = \int_{\Phi_1,\Phi_2,...\Phi_N} \mathrm{Z}\left(\Phi_1,\Phi_2,...\Phi_N\right) f\left(\Phi_1,\Phi_2,...\Phi_N\right) d\Phi_1 d\Phi_2 ... d\Phi_N. \qquad (2.6)$$

The joint PDF contains all the required information to describe the flow fields. These PDFs can be extracted from experimental data or the numerical results of direct numerical simulations, Reynolds average Navier Stokes (RANS) or the PDFT method. Now the next step is to describe the shape of the PDF with mathematical tools. There are two different ways to do this. One way is to use probability theory. We presume an empirical expression which fits the real PDF. This is called “presumed PDF method”. Since the shape of the PDF usually depends on the local physical conditions, a few parameters of the PDF are computed at each location based on the balance equations of

the first several moments [114], usually the mean and variance. The presumed PDF method is often used to model one variable. It is complex to model more than one variable with a presumed joint PDF. For such problems, it is usually assumed that they are statistically independent and model the single variable with a presumed PDF:

$$f\left(\Phi_1, \Phi_2, ...\Phi_N,\right) \approx f_1(\Phi_1) f_2(\Phi_2) ... f_N(\Phi_N). \tag{2.7}$$

Another way is to use statistical theory. We derive a transport equation of the PDF, and solve it numerically as described above, the PDFT method.

With the PDFT method, the local instantaneous variables are simulated explicitly and writing closure laws directly at the macroscopic level is avoided. PDFT methods take full account of the stochastic nature of turbulence by describing the flow at each point in terms of the joint PDF of fluid variables, such as velocity, temperature, compositions. Because of this complete description, the most significant processes can be modelled without any assumptions, including the terms for convection, body force, mean pressure gradient, chemical reaction source and turbulence kinetic flow. Particularly, the PDF methods treat the turbulence chemistry interaction exactly, which makes the PDF methods very attractive in the investigation of reactive flows.

The joint PDF provides much more information than the conventional method. The independent turbulence fluctuation of all considered fluid variables can be completely represented. All the moments of fluid variables can be determined from the joint PDF, if the moments exist. However, in general, the joint PDF cannot be determined from a finite number of moments. The models developed with PDF methods are more universal than the presumed PDF approach as they depend little on external conditions, such as combustor configurations and inflow conditions. The PDF methods can handle many different inflow streams of unrelated velocities, temperature and compositions. Disadvantages of using the PDFT methods are complexity of implementation, computational cost and use of stochastic solution procedure.

2.3 Turbulence characterisation – The random nature of turbulence

The governing equations described in Chapter Three in this thesis are equally applied to laminar and turbulence flows, but in turbulence regimes, the primitive variables that

describe the flow such as instantaneous velocity, instantaneous temperature and instantaneous mass fractions behave like pseudo random variables. This means that a generic variable ϕ does not have a singular value, the same every time the experiment is repeated under a similar set of conditions. Every time the experiment is repeated, ϕ takes a different value. It does not mean that turbulence is a random phenomenon. Turbulence is governed by deterministic equations but the solutions are random like. The consistency of this statement lies in the combination of two factors: 1) in turbulence flows there are unavoidable perturbations in initial conditions, boundary conditions and material properties; 2) turbulence flows exhibit a high sensitivity to such perturbations. The perturbations are also in attendance in laminar flows but in turbulence flows, the evolution of the flow is highly sensitive to small alterations of the precise conditions.

Therefore, since turbulence is described by pseudo random variables, the instantaneous flow fields are inherently unpredictable. However, mathematical tools that characterise random variables can be used. The PDF completely characterise a pseudo random variable and it serves to represent a probability distribution in terms of integrals. Two important quantities to highlight are the mean (probability-weighted average) and the variance (mean-square fluctuation) of a random variable.

The square-root of the variance is the standard deviation. Given a random variable ϕ and its probability density function $P(\phi)$, the mean $\overline{\phi}$ and the variance $\overline{\phi'^2}$ are calculated as follows:

$$\overline{\phi} = \int_{-\infty}^{+\infty} \phi P(\phi) d\phi \tag{2.8}$$

$$\overline{\phi'^2} = \int_{-\infty}^{+\infty} \left(\phi - \overline{\phi}\right)^2 P(\phi) d\phi \tag{2.9}$$

2.3.1 Statistical techniques used in modelling turbulence

Direct Numerical Simulation of turbulent reactive flows where all the spatial and temporal scales must be resolved without the introduction of empirical information is limited to few cases due to the huge computational costs involved. In addition, and as a result of the innate time-dependent nature of a turbulence flow, the chemistry also must be resolved properly considering all the reactions, from the slowest to the fastest.

From these limitations arises the need of using statistical techniques to model turbulent flows. An ideal model should introduce the minimum amount of complexity while capturing the essence of the relevant physics [115]. The principal criteria that can assess different models are: 1) level of description; 2) completeness; 3) cost and ease of use; 4) range of applicability, and accuracy. Primarily, there are three different statistical techniques relevant to turbulence modelling:

Large Eddy Simulation (LES): Based on the average of the governing equations. The governing equations are filtered such that only the small scale turbulence must be modelled. This means the three-dimensional and transient structures of the larger turbulence scales are simulated in detail. As small scales are characterised by an isotropic structure (at least for high Reynolds numbers) and are more universal, they are easily modelled. These small turbulence eddies are modelled using a sub-grid model [44]. LES models reduce the space and time grids needed for direct numerical simulation (DNS) resolutions, but still require large computational resources for routine simulations [116].

Reynolds Averaged Navier-Stokes Simulations (RANS). This technique solves the governing equations by modelling both the large and the small scale eddies, taking a time-average of the flow variables of interest. The information supplied by these models is the time average of the variables and the fluctuating parts are not represented directly by the numerical simulation, and are included only by means of a turbulence model. These models have been extensively used for scientific and engineering calculations during the last decades. They are specially designed for high Reynolds number flows and distinguishable separation of the time scales related to the fluctuating behaviour of the variables and the time scales related to the main flow unsteady behaviour. The key advantage is the relatively low computational cost involved compared to DNS or LES calculations.

The PDFT method: This stochastic method basis is a probability distribution of the relevant stochastic quantities directly by means of a probability density function (PDF). In turbulence flows, the PDF P is a function of both, the position x and the time t. Then, $P(U;x,t)$ denotes the probability of finding a value u within the range $U \le u \le U + dU$ at the location x and time t. One of the most common PDF models

used is a joint PDF transport equation for the velocity and the scalars [117]. For reactive flows, the reactive scalars are considered; say temperature and species mass fractions. These models represent a very general statistical description of turbulence reactive flows, applicable to premixed, non-premixed and partially premixed combustion. The chemical reactions rates are exact in the PDF transport equation and account for turbulence fluctuations of the temperature and chemical species implicitly. The closure problem is shifted to the mixing of scalar gradients. From a numerical point of view, the most apparent property of the PDF transport equation is its high dimensionality. Finite volume techniques are not very attractive for this type of problem as the memory requirements increase exponentially with dimensionality. Therefore, numerical implementations of PDFT methods for turbulence reactive flows use Monte-Carlo simulation techniques which use a large number of particles (N). The particles should be considered as different realisations of the turbulence reactive flow problem and should not be confused with real fluid elements. The state of a particle is described by its position and velocity, and the values of the reactive scalars.

2.3.2 The problem of the chemical source term

The difficulties arising from the mean chemical source term have been clarified by Libby and Williams [118]. These difficulties are described and considered in this section. This analysis follows largely that accepted by Libby and Williams.

The instantaneous reaction term for a one-step irreversible reaction can be written as:

$$\dot{w}_f = -\rho^2 r Y_f Y_o \tag{2.10}$$

where r is the reaction rate constant; Y_f and Y_o are mass fraction for fuel and oxidant respectively. With Favre averaging flow, variables are mass averaged and correlations involving density fluctuations are not present. The averaged form of the chemical source term according to Libby and Williams [118] is

$$-\bar{\dot{w}}_f = \widetilde{\rho r}\left(\bar{\rho}\tilde{Y}_f\tilde{Y}_o + \overline{\rho Y_f'' Y_o''}\right) + \overline{\rho(\rho r)'' Y_o''}\tilde{Y}_f + \overline{\rho(\rho r)'' Y_f''}\tilde{Y}_o + \overline{\rho(pr)'' Y_f'' Y_o''} \tag{2.11}$$

The physical significance of various terms is described by Libby and Williams. $\tilde{r}$ is the mean rate constant and has an Arrhenius form. The instantaneous r is typically:

$$r = b \exp\left(-T_a / T\right) \tag{2.12}$$

where T_a is the activation temperature and b is the frequency factor. The relation between r'' and temperature fluctuation is only simple if the fluctuations are small and the activation energy is not large compare with the mean temperature. These are very severe limitations and no generally applicable simplification is possible.

The complication occurs in averaging the source term even for the simplest chemical reaction is clear. The range of terms describing the effective chemical behaviour in turbulence flow contributes to many closure problems. It is common practice to attempt to identify limiting cases in which some scale of simplification is attainable. This entails adoption of combustion models.

Some studies have preferred to ignore the effects of fluctuations and equation (2.11) then reduces to:

$$\overline{\dot{w}} = -\tilde{r}\,\overline{\rho}^2\,\tilde{Y}_f\,\tilde{Y}_o \tag{2.13}$$

It is insufficient to neglect the significant role of mixing in determining the reaction rates. The limiting case may be appropriate only if the chemical time scale, t_c, is large relative to the time scales of the fluctuating scalars. Under some circumstances another limit leads to the case termed “fast chemistry” which can be expressed quantitatively by the approximation, if either is zero

$$Y_f\,Y_o = 0.0, \tag{2.14}$$

that is the chemical time is small relative to the scalar time scales and the two reactants do not coexist. However, in practical application, the intermediate situation prevails, in which the chemistry is not adequately fast or slow relative to the fluctuations in scalars for either limit to be valid. Perturbation from either limit provides a potential closure of the mean source term. For non-premixed systems, $\overline{\dot{w}}$ may be attained more expressly by an integral involving the probability density function. Derivation of this will be presented more fully in Chapter Five.

The situation is further complicated for chemical reaction scheme of greater complexity. The non-linearity of the temperature dependence of the rate constant, r, initiates a difficult undertaking. One fundamental approach is to invoke a second order closure of the mean chemical source term. Equation (2.13) is altered by applying a correction factor $(1+F)$ where

$$F = F\left(\tilde{T}, \tilde{T}''^2, \tilde{Y}_f, \tilde{Y}_o, \widetilde{Y_o T''^2}, \widetilde{Y_f'' Y_o''}\right) \tag{2.15}$$

and is obtained by truncation at second order of an expansion containing covariances in increasing order. Bilger [119] gave a detailed description of this procedure. The covariances involved are obtained by second order closure and numerical solution of their balance equations. However, the series is only convergent if the fluctuations are small and the activation temperature is not large compare with the mean temperature. This procedure is as a result usually inadequate and can lead to erroneous results for high intensity combustion where temperature fluctuations are large.

A substitute approach is to model the higher moments in terms of second order and lower moments. The majority of the present methods of doing this utilize some notion of the multivariate probability density function. PDF formalism can provide a convenient means for addressing the problem of evaluating the mean chemical source term. An exact expression for $\bar{\dot{w}}_i$ is:

$$\bar{\dot{w}}_i(\underline{x}) = \iint \ldots \int \dot{w}_i\left(\rho, T, Y_j\,(j=1,2\ldots)\right) P\left(\rho, T, Y_j\,(j=1,2\ldots); \underline{x}\right) d\rho dT dY_j \quad (j=1,2\ldots) \tag{2.16}$$

Where $P(\ )$ is the joint probability density function for the variables $\rho, T, Y_j\,(j=1,2\ldots)$ at location $\underline{x}$.

In principle, this approach exposes important physical features and leads to simplified computational schemes in calculating $\bar{\dot{w}}_i$. However, this requires knowledge of the joint PDF. There is no experimental evidence available to define the structure of the multivariate PDF subject to the moment constraints. Under certain conditions the multi-dimensional PDF can be reduced to a bivariate or a univariate PDF. There are two

alternative routes which may be followed to determine the PDF. The first is to specify its general form a priori; either empirically or from some insight into flame structure. The second route is to compute the function from a modelled version of an exact balance equation describing the transport of the scalar PDF in both physical space and flow variable.

The main problems with the chemical source term have been identified. The more direct methods are shown to be difficult and impractical for further developments. More suitable routes to undertake the problems are described. The subsequent sections discuss the models that have been tried and identify their limitations for predictions of turbulence flames.

2.4 Flame structure model

In this sub-section a combustion model based on "fast" chemistry is discussed, that is, the chemical time scales are very short compared with those characteristic of the transport processes. In the fast chemistry limit the chemical source term problem in non-premixed flames is largely eliminated by introduction of a conserved scalar, (mixture fraction, f) [120]. We limit the discussion in this section to models which use an assumed form of a single scalar variable PDF.

Models of this type involve specification of relationships between instantaneous mixture fraction and instantaneous values of all scalar variables, either from a flame sheet approximation, or from an assumed chemical equilibrium. It is appropriate to define the conserved scalar quantitatively here. With the assumption of equal diffusivities the balance equation for a chemical element, β (or Schvab-Zeldovich coupling function - Williams, [121]) has no source term and is exactly similar for all elements. The element mass function may be normalised in the form:

$$f = \frac{\beta - \beta_{-\infty}}{\beta_{\infty} - \beta_{-\infty}} \tag{2.17}$$

Where ∞ and $-\infty$ denote the fuel and air stream and f is bounded between 0 and 1.

For fast chemistry and the one-step irreversible reaction there will be no oxidant present in the fuel-rich domain ($f > f_{st}$, where st denotes stoichiometric value) and no fuel present in the fuel-lean domain ($f < f_{st}$). Both will be zero in the flame sheet ($f = f_{st}$). These assumptions yield

$$\phi_F = 0, \phi_o = \phi_{o,\infty}\left[\frac{f_{st} - f}{f_{st}}\right] \quad for\ 0 \le f \le f_{st} \tag{2.18}$$

$$\phi_o = 0, \phi_o = \phi_{f,\infty}\left[\frac{f - f_{st}}{1 - f_{st}}\right] \quad for\ f_{st} \le f \le 1 \tag{2.19}$$

and

$$\phi_I = \phi_{I,\infty} + \left(\phi_{I,-\infty} - \phi_{I,\infty}\right) f \tag{2.20}$$

Where F, O and I correspond to fuel, oxidant and inert mass fractions (ϕ) respectively; and $\infty, -\infty$ denote boundary conditions corresponding to fuel and oxidant streams respectively. The mass fraction of products described is based on mass conservation

If the reaction is reversible and fast there will be both fuel and oxidant present near stoichiometric conditions. The equilibrium constants are small but finite and enable the molecular species to be calculated from elemental composition and enthalpy. The computer code developed by Gordon and McBride [122] is that most frequently used to determine the equilibrium at constant pressure. The results can be expressed as function of mixture fraction, $\phi_i = \phi_i (f)$.

The instantaneous structures of the flame sheet and chemical equilibrium give rise to different microscopic thermochemical models. These structures can form a suitable basis for turbulence non-premixed flame computation. Due to the non-linearity of these relationships, it is necessary to include the fluctuations in f. This is usually achieved via the introduction of the PDF for f.

The flame sheet model significantly simplifies the chemical source term. Bilger [119] demonstrated that with $\phi_i = \phi_i(f)$, an explicit expression for the instantaneous reaction rate $\bar{\dot{w}}_i$ results. After time averaging this may be written:

$$\bar{\dot{w}}_i = -\frac{1}{2}\bar{\rho}\int_0^1\int_0^\infty \chi \frac{d^2\phi_i}{df^2}\tilde{p}(\chi, f)\, d\chi\, df \tag{2.21}$$

where

$$\chi \simeq 2D \frac{\partial f}{\partial x_k}\frac{\partial f}{\partial x_k} \tag{2.22}$$

is the instantaneous scalar dissipation rate, and $\tilde{p}(\chi, f)$ is the joint PDF in moderate to high Reynolds number turbulence. The suffix *k* denotes repetitive summation. Bilger pointed out that for the one-step irreversible reaction

$$F + r\,O \rightarrow (r+1)\,p \tag{2.23}$$

with infinitely fast chemistry, $\frac{d^2\phi_i}{df^2}$ has the properties of a delta function at $f = f_{st}$ and

$$\bar{\dot{w}}_F = -0.5\bar{\rho}\tilde{\chi}(f_{st})\tilde{P}(f_{st})\phi_B \tag{2.24}$$

Where

$$\phi_B = \frac{\phi_{f,\infty}}{(1 - f_{st})} \tag{2.25}$$

and $\tilde{\chi}(f_{st})$ is the Favre average of χ evaluated at $f = f_{st}$. Equations (2.24) appear to describe significant features of the physical process. It is interesting to note that due to the consequence of fast chemistry the mean reaction rate is proportional to the rate of mixing out of the concentration fluctuations while the reaction is associated with the non-linearities of the instantaneous structure. The mean chemical source term of the non-premixed flame is also proportional to a particular value of the PDF for $f = f_{st}$. This suggests that predictions may be relatively sensitive to the empirical shape for the PDF of the conserved scalar.

With the instantaneous structure defined, mean and higher moments of thermodynamic variables may be obtained from the PDF of f. The individual species concentration equation and the energy balance transport equation are abandoned in favour of a probabilistic model which allows the incorporation of chemical reactions into an integral formulation for the turbulence flow fields. The time-mean scalar quantity is defined by

$$\overline{\phi_i} = \int_0^1 \phi_i \overline{P}(f)\, df \tag{2.26}$$

One of the effects of turbulence is then to increase the mean concentration of reactants above the "instantaneous thermochemical models" values at the mean mixture fraction. The mean product concentration is correspondingly reduced by the unmixedness.

2.5 Turbulence flame radiation

Tien and Lee [123] provide a comprehensive summary of radiative properties of non-homogeneous particles containing media typical of flame environments. deRis [124] surveys aspects of radiation from turbulence fires, where buoyancy influences the processes. Faeth et al [40] gave a review of methods closely followed during the present investigation. General background material on radiation in pure and particle-laden gases is provided by Siegel and Howell [125]; Ludwig et al [126], Goody [127], and Hottel and Sarofim [128].

While radiation from turbulent flames is of greatest interest, studies of laminar flames are useful since the complexities of turbulence hydrodynamics are avoided. Lloyd and co-workers [129] reported pioneering work in this area. Laminar hydrogen flames, containing no soot, were analysed using boundary layer approximations. Given the flame structure, radiation properties were found using a Statistical Narrow-band model and an Exponential Wide-band model [130]. Results were promising, with the greatest uncertainties associated with the flame structure predictions.

Several studies have used measured scalar properties in flames to test predictions of flame radiation, in order to avoid the uncertainties of flame structure predictions. Grosshandler and Sawyer [131] examined the non-luminous spectral radiation properties of methanol/air combustion products. Radiation properties were predicted

with the Goody [127] Statistical Narrow-band model, using the Curtis-Godson approximation for inhomogeneous gas paths, following Ludwig et al [126]. Measurements and predictions were in good agreement in the post-flame region. Grosshandler and co-workers [132, 133] developed a method to reduce the computations required for radiation predictions.

Karman and Steward [134] reported similar work for mixtures of propane, propylene and carbon particles (1-10μm spectral range). Mie scattering from large particles was treated following Steward and Guruz [135]. Use of measured mean scalar properties provided good predictions of spectral radiation characteristics in the post-flame region.

Souil et al [136, 137] studied radiation from turbulence flame environments. Use of measured mean temperatures, in conjunction with prescribed values of the absorption coefficient, yielded good fits to measured radiative heat flux distributions. However, a stochastic method was used by Faeth et al. [115] for modelling the interaction between the radiation and the turbulence. The assumption underlying this approach is that the flowfield consist of many statistically independent turbulent eddies. The properties within each of these eddies are considered to be uniform. The size of each eddy is equated to the dissipation length scale (L_e), determined from

$$L_e = C_\mu^{3/4} K^{3/2} / \varepsilon \tag{2.27}$$

The properties of each eddy are obtained stochastically, under the additional assumption that all the scalar properties are functions of a conserved scalar and that the statistics of this conserved scalar are known. The cumulative distribution function of this conserved scalar is constructed for each eddy. The distribution function is then sampled by selecting a random number z such that

$$z = \frac{\int_0^f pdf\left(f, \widetilde{f''^2}\right) df}{\int_0^1 pdf\left(f, \widetilde{f''^2}\right) df} \tag{2.28}$$

The process is repeated for each eddy along the path, until a single instantaneous realisation of the path is constructed. The spectral radiance for this realisation is computed and the whole process repeated until a stationary mean is achieved. Faeth et

al. [115] used the stochastic technique for predicting the spectral intensity distribution but ignored TRI in their calculation of the external radiative heat flux distribution.

Syed [138] also compared the stochastic approach with that of using mean properties for calculating the spectrally resolved emission from a buoyant methane fire - Crauford [139]. Syed [138] also found that the stochastic method tends to over estimate the radiative flame emission. This is attributed to the over estimation of the path lengths through the high temperature reaction zones, with the resultant over estimation of their emission. However, in contrast to the Faeth et al. [115] study, Syed [138] found that the use of mean properties alone tended to under-estimate the flame emission. Gore and Faeth et al. [40] extended the use of the stochastic method for calculating flame emission, by modelling hydrogen/air diffusion flames. Again the stochastic method was compared with that of using mean properties alone. The mean properties prediction tended to under-estimate the radiative emission, particularly at 2.7μm H_2O band by roughly 25%. However, the stochastic method tended to over-predict the flame emission at all points in the spectrum. Faeth et al. [40] attributed the success of the mean properties method to internal redistribution of energy by radiative emission and re-absorption within the flame.

The combined problem of predicting both turbulence diffusion flames structure and radiation properties has also been tackled. Wilcox [140] reported an early investigation, where an integral model was used to predict the structure and an exponential wide-band model (based on mean properties) was used to predict the spectral radiation intensities. Predictions were compared with measurements for a liquefied natural gas pool fire having little continuum radiation from soot [141]. The structure model concurred with measurements of bulk quantities such as flame height. The spectral radiation model gave good predictions of radiation intensities in the 4.3μm band of CO_2. The model contains substantial empiricism and its generality has not been verified.

Fishburne and Pergament [142] considered large-scale hydrogen flames burning in still air. Predictions of flame structure were based on a mixing-length model of turbulence, while Arrhenius expressions were used to prescribe turbulence reaction rates. The radiation analysis was related to Ludwig et al.[126]. Encouraging agreement was obtained between predictions and measurements, however, flame widths were not

predicted very well and use of Arrhenius expressions for turbulence diffusion flames is questionable [119].

Mean properties are often used to compute flame radiation. It is recognised however, that turbulence fluctuations make this a doubtful practice since radiation properties have non-linear temperature dependence

$$\sigma \bar{T}^4 \ll \sigma \overline{T^4} \tag{2.29}$$

Williams and Fuhs [143] treated turbulence fluctuations by assuming that a turbulence flame is a wrinkled laminar flame, but it is difficult to apply their methods to practical turbulence flames. Assuming a gray gas, Cox[3], found that fluctuating temperature intensities higher than 40 percent, which are not unusual for turbulence flames, yield radiance values which are more than twice those predicted using mean temperatures. While this result suggests a strong effect of turbulence on radiation properties, the grey gas approximation is not very appropriate for turbulence flames, where gas bands and continuum radiation from soot cause a complex variation of radiation properties with wavelength.

Kabashnikov and Kmit [144] treat combined effects of fluctuating absorption coefficient and temperature. They consider a linear variation of absorption coefficient in the Wien spectral region, where effects of fluctuations are largely due to the strong temperature dependence of the Planck function. When the radiation path is more than several times the characteristic turbulence length scale, and the optical depth of a single fluctuation is small, they show that the correct intensity can be found by using the average values of the product of the Planck function and the absorption coefficient. They state that using the conventional approach (multiplying the averages of both) could result in lower estimates of intensities by factors of 2-3. However, while the radiation model they examine yields a convenient closed form solution of the problem, it is not very representative of flame radiation properties.

Grosshandler and Joulain [145] treat effects of turbulence on flame radiation by assigning properties along a line of sight path using prescribed probability density functions for scalar properties. Both non-luminous and luminous conditions were considered. It was found that intensities could exceed predictions based on time-mean

properties by as much as a factor of two. Nonetheless, the actual intensity was lower than results based on time mean-properties for some strong sooting situations. While radiation analysis used by Grosshandler and Joulain is state-of-the-art, their prescription for scalar fluctuations along the path is relatively ad hoc; as a result, whether turbulence/radiation interactions can yield effects of this type and magnitude must still be established.

There are few available measurements of radiance fluctuations for flames. An exception is Portscht [146] who reported direct measurements of the frequency spectrum of flame radiation, considering both non-luminous and luminous flames. Power spectral densities for various detectors and flames were measured. The results showed interesting spikes characteristic of pulsations of the entire flame structure; however, no effort was made to analyse the phenomena in terms of fundamental radiation or turbulence.

It is evident that capabilities for predicting radiation from turbulence diffusion flames rest on accurate scalar structure predictions. Many radiation models have been developed to calculate radiative heat transfer, many of which are based on the solution of the radiative transfer equation (RTE). This is an integro-differential equation with seven independent variables: three spatial coordinates, two angular coordinates, which define the direction of propagation, one spectral variable, and time. The dependence on time is negligible for most practical applications, including turbulence reactive flows, because radiation travels at the speed of light, which exceeds typical velocities in such flows by several orders of magnitude. Despite this, six independent variables remain, which makes the numerical solution of the RTE a difficult task. This difficulty is greatly enhanced by the need to calculate the radiative properties of the medium. In the case of reactive flows, CO_2 and H_2O are the most important radiant gaseous species. The absorption coefficient of these species is constituted of hundreds of thousands of spectral lines, and it is not feasible to account for each individual line in practical problems. Accordingly, a model for the radiative properties of the medium is needed. The possible presence of particles, such as soot, char, or fly ash, generally makes the problem even more difficult. Consequently, scalar property predictions must include particulate properties which are relevant to radiation. The findings of Grosshandler and Sawyer [147] and Karman and Steward [134] suggest the use of mean scalar properties, along with the state-of-the-art narrow-band radiation models, provides good prediction of spectral radiation intensities in the post-flame region. Similarly, Jeng and Faeth

[148] and Jeng et al [115] find relatively small effects of turbulence/radiation interactions for propane and methane jet flames respectively. On the other hand, some studies [3, 143-145] found that turbulence/radiation interactions cause radiance levels in flames to be significantly higher (by factors of two to three) than estimates based on mean properties.

2.5.1 Turbulence-radiation interactions

Although turbulence and radiative heat transfer are formidable problems by themselves, in our investigation we are not concerned with such problems individually, but rather with their interaction. These two phenomena have traditionally been treated as independent using mean properties to calculate radiative transfer. This approach is satisfactory in the case of nonreactive hot flows of radiant species, such as CO_2 and H_2O that take place in the exhaust of most combustors, since the scalar fluctuations in such flows are substantially smaller than in flames [149]. However, neglecting turbulence fluctuations in reactive flows may yield very large errors, that is, the time-averaged radiation intensity and heat fluxes may differ significantly from the radiation intensity and heat fluxes calculated from mean temperature and mean species concentration. This phenomenon, which is mainly due to the highly nonlinear coupling between fluctuations of the radiation intensity and fluctuations of temperature and species concentrations, arising from turbulence, is referred to as turbulence-radiation interaction (TRI). The interaction between turbulence and radiation is presently well established, both theoretically and experimentally [150]. In fact, many works have reported that turbulence fluctuations influence radiative transfer, as described in chapter three.

2.5.2 Influence of radiation on turbulence

Little work has been done on the influence of radiation on the turbulence. Radiative transfer in reactive flows, and also on the atmosphere, acts as a dissipative process, especially for large-scale structures for which the optical thickness becomes important. This was first pointed out by Spiegel [151] and Townsend [152], who combined the analysis of the equations of the mean-square fluctuations of the velocity and temperature with the radiation field. Radiative transfer enhances the dissipation of large thermal eddies and tends to smooth temperature fluctuations. This effect is especially relevant if turbulence dissipation due to molecular diffusion is small compared to the

radiative dissipation. Gas and particle radiation may significantly influence the structure of the spectrum of temperature fluctuations in the planetary boundary layer.

Similar to turbulence-chemistry interactions, turbulence-radiation interactions (TRI's) arise from the highly nonlinear dependence of radiative transfer on temperature and species concentrations. Turbulence influences radiative transfer through fluctuations in temperature and species concentrations, and those in turn influence the blackbody intensity and the absorption and scattering coefficients of the radiatively participating medium. At the same time, radiation influences turbulence through its intimate coupling with flame structure, such as temperature and density distributions. As radiative transfer takes place at the speed of the light, turbulence fluctuations are reflected instantaneously in the radiative heat flux and its divergence.

PDF-based approaches to TRI's can be divided into two groups namely: presumed PDF methods and transported PDF methods. The presumed PDF methods provide a general framework in which a number of turbulence reaction and mixing models may be implemented, such as the popular laminar flamelet models. Typical choices of PDF shapes include the beta function and the clipped Gaussian distribution. The presumed PDF method is the most common approach to TRI's; examples include Gore et al. [40] and Coelho et al. [153]. Transported PDF methods have the advantage of treating TRIs rigorously and exactly (only the emission part, the correlation between absorption coefficient and Planck function). Investigations of TRI using this approach have been conducted by the research group of Modest [149]. Modest employed a velocity-composition joint PDF method, and used a composition PDF method in their simulations of methane-air turbulence diffusion flames. He also investigated the importance of the various TRI correlations to the total TRI effect by freezing species concentration and temperature fields. They concluded that consideration of the temperature self correlation alone is not sufficient to capture TRI and the absorption coefficient-Planck function correlation also must be included.

The influence of radiation on turbulence in high temperature flows was investigated by Soufiani [154]. He reported a theoretical study of this influence in the case of homogeneous and isotropic turbulence. This study was based on the solution of the equation for the temperature spectrum, which was closed using an Onsager-type model. The radiative properties of the gases were evaluated using a statistical narrow band

(SNB) model. It was assumed that the temperature fluctuations were small compared to the mean temperature, and that the thermo-physical and radiative properties of the medium were independent of the temperature fluctuations, depending only on the mean temperature. The analysis has shown that radiation may greatly modify the structure of the energy density spectra of the temperature fluctuations of radiating gases by smoothing the intensity of temperature fluctuations. The effects of radiation increase with temperature, but decrease with the dissipation rate of turbulence kinetic energy.

2.6 Experimental studies of jet flames

In the last two decades, there has been significant improvement in both experimental and computational research on turbulent non-premixed combustion. In our investigation we will strengthen some aspects of this improvement by identifying sets of well documented and relatively simple flames available in the open literature that can serve as benchmark cases for comparison with model predictions.

Kalghatgi [39] carried out experimental studies of the lift-off heights and visible flame lengths of jet diffusion flames in still air for hydrogen. Kalghagti's work describes a systematic study of the factors affecting lift-off height, the distance between the burner exit plane and the base of the lifted flame. Nearly all the previously published results for lift-off height have been for methane flames. Consequently, in our investigation we use the developed lift-off model to predict lift-off height in turbulent hydrogen air flames and compare against experimental data presented by Kalghatgi [39].

Janicka et al [155-157] carried out experimental studies to have full description of some well defined simple turbulent non-premixed jet flames, including boundary conditions. The burner was a straight tube with an inner diameter of 8mm which ended in a 0.2mm thick rim. This was centered in a coflow emanating from a contoured nozzle with an outflow diameter of 300 mm. The coflow air velocity was $0.2ms^{-1}$, and the flame was attached and unconfined. The coflow air temperature was 298K, and the humidity ratio in the coflow varied during the course of the experiments. The fuel exit temperature was also 298K. Fully developed turbulent pipe flow may have been assumed at the nozzle exit with maximum exit velocity of $34.5ms^{-1}$. Mixtures of H_2 and N_2 (50%:50%) are used as fuel. The Reynolds number used is 10,000. The diffusion flames were measured on the axis from x/d=0 to 100 with a spacing of $\Delta x/d=5$. The radial profiles

were measured at levels x/d=5, 20, 40, 60, 80 with variable spacings from 0.5mm to 3mm. Many of their results were compared to Reynolds-stress model predictions and to calculations with reduced chemistry mechanisms. In our investigation we chose not to use Janicka et al [155-157] data because the jet flame speed is low, large nozzle inner diameter and the fuel composition is highly diluted with nitrogen.

Barlow [41] combined the use of spontaneous Raman scattering, Rayleigh scattering and laser-induced fluorescene to obtain measurements of the major species and temperature in jet flames of hydrogen and helium diluted hydrogen. The burner was a straight tube with a square-off end (inner diameter, d=3.75mm; outer diameter 4.84mm). This was centered at the exit (30cm by 30cm) of a vertical wind tunnel contraction. The coflow air velocity was 1.0ms^{-1} and the flames were attached and unconfined. The coflow air temperature was 294K (±2K), and the humidity ratio was between 0.006 and 0.008kg/kg-air during the course of the experiments. The fuel exit temperature was 295K (±2K). Fully developed turbulent pipe flow was assumed at the nozzle exit with maximum exit velocity of 296 ms^{-1}. Barlow [41] presented experimental data set that includes radial profiles at several streamwise locations along the visible flame length for each of the flames studied: undiluted H_2 with Reynolds number 10,000; 20% He dilution with Reynolds number 9,800; and 40% He dilution with Reynolds number 8,300. We used these data from Barlow to validate our model in predicting the flame structure in Chapter Five because of the composition of the fuel diluted with inert gas (helium), speed of the jet and the diameter of the burner.

The emphasis of this investigation is on fundamental issues of turbulence radiation interactions (TRI) in non-sooting flames like hydrogen flames. Previous research work for examples Fishburne and Pergament [142] and Ludwig et al [126] ignored TRI and based predictions on mean scalar properties. Prompted by this omission Faeth et al [40] carried out experimental and numerical study of spectral and total radiation properties of turbulent hydrogen/air flames. Faeth et al [40] in their experimental study injected hydrogen vertically upward from a water-cooled burner, into still air. The burner had a screen plenum, followed by a 25:1 contraction which terminated in a 5mm diameter exit passage. Spectral radiation intensities were measured for radial paths through the flame using a 250mm grating monochromator with a pyroelectric detector. Uncertainties in these measurements were less than 20% [158]. Total radiative heat flux distributions were measured along the base and the axis of the turbulent flames using a gas-purged,

water-cooled sensor with a 150^0 viewing angle. The sensor was positioned so that the flame boundaries were entirely within the viewing angle, except for points far from the burner exit, which contributes very little to the radiative flux in any event [40]. Uncertainties in these measurements were less than 10% [158]. We have modelled TRI using Faeth et al [40] experimental data but we accounted for radiative heat loss ignored by Faeth et al [40] using enthalpy perturbation equations.

2.7 Modelling issues specific to hydrogen

In turbulent combustion at high Reynolds and Damköhler numbers the essential rate-controlling processes of molecular mixing and chemical reaction occur at the smallest scales which are much thinner than the resolved large scales [87]. Consequently, these transport processes have to be modelled. Large Eddy Simulation (LES) may provide a more reliable turbulence model than Reynolds Averaged Navier-Stokes (RANS) especially if there are large-scale unsteady motions. Nevertheless, the rate-controlling combustion processes require the same modelling as in RANS [159].

The vitality of RANS is caused mainly by an affordable computational cost applied to practical flows compared to conventional LES [160]. A huge amount of work has been and is currently being performed to develop, calibrate and validate semi-empirical turbulence models needed for RANS closure. As a result, hundreds of models have been developed from the simple algebraic ones, originating from the classical Prandtl's mixing length hypothesis to advanced differential Reynolds stress transport model which is no better than the $k-\varepsilon$ model used in our investigation.

Unlike other fuels, hydrogen has a high diffusion coefficient and a relatively low density compared to air, which allows hydrogen to travel upwards without the need for any wind or ventilation. Hence, due to its natural buoyancy, hydrogen jet produces some interesting modelling issues such as

- Fast chemical reaction is relevant due to the reactivity of hydrogen in air. We are only interested in the major species so can use a flamelet model based on fast chemistry.

- Reverse Joule Thomson Effect - Interesting but for subsonic turbulent flow less important.

- Turbulence-Radiation Interaction importance is believed to be due to large temperature gradient near the stoichiometric point.

- An additional gap in knowledge of hydrogen jet flame structure. The mean properties predicted well but the capability to predict Root Mean Square (RMS) properties is unknown.

In conclusion, improvements are required in models to account for the complex influences of buoyancy on a flow with large density variations and high initial momentum. Experimental data in relation to turbulence fluxes are taken from open literature to assist effective modelling of these influences. Current turbulence models do not account for the initial part of the flow before the turbulence is fully developed. Studies of the flow parameters in this region may help the development of more realistic descriptions. Finally, the treatment of flame radiation relies heavily on empirical assumptions regarding the flame structure. Numerical studies to clarify our understanding of detailed flame properties are required such that models of turbulence, combustion and radiation may be advanced.

In this chapter we extensively looked at the various works and studies of researchers in jet fire modelling and predictions. In Chapter Three we will present the underlying principles and fundamentals involved in modelling a jet fire.

Chapter 3

Transport equations

In turbulent combustion a large number of different processes are taking place. These processes include physical transport mechanisms and chemical reactions. Many of the processes are linked to each other and this makes numerical simulation of turbulence combustion a complex task. In principle, all of these processes can be described by molecular considerations. However, to describe all occurring processes from a molecular viewpoint would lead to an overwhelming simulation task, even for the most powerful computers of today. Also, the underlying physics for some of the processes are not fully understood and empirical data and models have to be used.

3.1 Properties of the gas mixtures

To solve the conservation equations, properties that describe the gas mixture are needed. For the operating conditions of the flames studied in the present work, the gas mixture can be assumed to behave as real-gas. This means that the temperature, density, and pressure of the mixture are related by the real-gas equation of state [161].

$$p = \rho \frac{R_u}{M} T \tag{3.1}$$

Where M is the molecular mass of the mixture and is calculated as a mole-fraction average of the component molecular masses:

$$M = \sum_{k=1}^{n_s} X_k M_k \tag{3.2}$$

where X_k is the mole fraction of species k.

The enthalpy for a real-gas mixture is found from the enthalpy of the components.

$$h = \sum_{k=1}^{n_s} Y_k h_k \tag{3.3}$$

Where Y_k is the mass fraction of species *k*. For a real-gas the enthalpy is a unique function of temperature, and the enthalpy at a given temperature is calculated from

$$h_k(T) = h_k^o + \int_{T^o}^{T} c_{p,k}(T)dT \tag{3.4}$$

where h_k^o is the specific enthalpy of formation at a reference temperature T^o, and $c_{p,k}(T)$ is the specific heat capacity at constant pressure for the same species.

$$c_{p,k} = \left(\frac{\partial h}{\partial T}\right)_p \tag{3.5}$$

3.2 Molecular transport

In laminar flow all transport processes except for the bulk transport and radiation takes place on a molecular level. In turbulence flow, the transport is enhanced by the turbulence fluctuations. In most turbulence flows, the transport due to the turbulence fluctuations is much stronger than the molecular transport and, if the turbulence is intense, molecular transport can be neglected. Due to this difference in strength between the transport mechanisms, and the fact that the focus of the present work is turbulence combustion, simplified expressions can be used to model the molecular transport.

3.2.1 Momentum flux

In laminar flow, the molecular transport of momentum is dependent on the molecular viscosity, μ, of the fluid. The viscous stress tensor represents the molecular flux of momentum in the flow. For a Newtonian fluid, this is given by [162]

$$\tau_{kj} = \mu\left(\frac{\partial v_k}{\partial x_j} + \frac{\partial v_j}{\partial x_k}\right) + \left(\mu_B - \frac{2}{3}\mu\right)\frac{\partial v_l}{\partial x_l}\delta_{kj} \tag{3.6}$$

where μ_B is the bulk viscosity and expresses the resistance of the fluid against rapid changes in volume. In the present work $\mu_B = 0$ has been used. This is known as the Stokes-hypothesis. The correctness of this hypothesis has been questioned by several

scientists but in general the numerical value of μ_B is unknown; therefore, employment of the Stokes-hypothesis has become the usual practice.

The viscous stress tensor may also be interpreted as the viscous force on a fluid element. The viscosity of a pure species (μ_k) is a function of temperature and can be calculated from kinetic theory [163].

3.2.2 Mass flux

The molecular mass flux of species *k* in the x_j direction, j_j^k, generally has three components. These are known as mass diffusion, pressure diffusion, and thermal diffusion (Soret effect) [163]. For most combustion processes, the pressure diffusion and Soret effect may be neglected [164] and this practice has been adapted in the present work. The diffusion flux of species *k* in the *j*-direction is given by Fick's law

$$-j_j^k = \rho D \frac{\partial Y_k}{\partial x_j} \tag{3.7}$$

The diffusion coefficient *D* will be different for different species, and it will be a function of the concentrations of all other species in the mixture. As the focus of the present work is on turbulent flames, the simplification is made that all species have the same diffusion coefficient. In most turbulent flows, turbulence transport will dominate. The turbulence fluctuations also make it necessary to treat the conservation equations in a statistical manner, and the resulting equations are simplified if a single diffusion coefficient is used, however, it is worth mentioning that hydrogen has a diffusion coefficient. Also, the turbulence combustion model becomes over complex if species-dependent diffusion coefficients are used.

The description of mass flux is further simplified by introducing the non-dimensional Schmidt number

$$\sigma_y = \frac{\mu}{\rho D} \tag{3.8}$$

The mass flux may now be expressed by the viscosity and Schmidt number

$$-j_j^k = \frac{\mu}{\sigma_y}\frac{\partial Y_k}{\partial x_j} \tag{3.9}$$

3.2.3 Energy flux

The thermal energy flux can be divided into three components.

$$j_j^q = (j_c^q)_j + (j_d^q)_j + (j_D^q)_j \tag{3.10}$$

where $\left(j_c^q\right)_j$ is energy flux due to conduction, $\left(j_d^q\right)_j$ is energy flux due to species diffusion, and $\left(j_D^q\right)_j$ is energy flux due to concentration gradients, the Dufor-effect, all in the x_j direction. The latter of these components, the Dufor-effect is usually much smaller than the other two components [162], and has been ignored in this investigation.

The energy flux due to conduction is expressed by Fourier's law with λ being the thermal conductivity.

$$-\left(j_c^q\right)_j = \lambda\frac{\partial T}{\partial x_j} \tag{3.11}$$

In the following section a conservation equation for energy is presented in which the energy flux is included. Consequently, it is desirable to express the energy flux due to conduction as a function of enthalpy instead of temperature. The following expression is obtained by combining equations(3.3),(3.4) and (3.5)

$$\left(j_c^q\right)_j = \frac{\lambda}{c_p}\left(\sum_{k=1}^{n_s} h_k\frac{\partial Y_k}{\partial x_j} - \frac{\partial h}{\partial x_j}\right) \tag{3.12}$$

Energy flux due to diffusion occurs, as indicated by the name, due to diffusion of species with different enthalpy and can be expressed as

$$\left(j_d^q\right)_j = \sum_{i=k}^{n_s} h_k\, j_j^k \tag{3.13}$$

Similar to the introduction of the Schmidt number in the section on mass flux, the Prandtl number (σ) is introduced to simplify the description of the energy flux

$$\sigma = \frac{\mu c_p}{\lambda} \tag{3.14}$$

The Lewis number (Le) is the ratio of the Schmidt and Prandtl numbers

$$Le = \frac{\sigma_y}{\sigma} \tag{3.15}$$

By introducing equations(3.9), (3.14) and (3.15) into equations (3.12) and (3.13), the total energy flux may be written as

$$j_j^q = \frac{\mu}{\sigma}\left[-\frac{\partial h}{\partial x_j} + \left(1 - \frac{1}{Le}\right)\sum_{k=1}^{n_s} \frac{\partial Y_k}{\partial x_j} \right] \tag{3.16}$$

For most gases the Lewis number is close to unity [165] and we assumed Le=1 to further simplify the expression for the energy flux.

3.3 Conservation equations

To describe turbulence combusting flows mathematically, a set of partial differential equations are used as a basis. These differential equations are statements of conservation of the fundamental properties of mass, momentum and energy in the system. The equations are presented in standard Cartesian tensor notation.

3.3.1 Conservation of mass

The Conservation equation for a single species *k* expressed as a mass fraction Y_k, is [162, 166]

$$\frac{\partial}{\partial t}\left(\rho Y_k\right) + \frac{\partial}{\partial x_j}\left(\rho Y_k v_j\right) = \frac{\partial}{\partial x_j}\left(-j_j^k\right) + \rho\omega_k \tag{3.17}$$

where ρ is the density and v_j is the velocity in the x_j direction. The first term in the equation is the time rate change of the concentration of species *k* per unit volume. The

second term represents the convective transport of the same species. The last term of the equation $(\rho\omega_k)$ is the net production rate of species *k* due to chemical reaction. The term $-j_j^k$ represents the diffusion flux of species *k* in the *j*-direction given by Fick's law, equation(3.7). By introducing the Schmidt number equation(3.8), and assuming a Lewis number of unity equation(3.15), the conservation of species *k* can be written as

$$\frac{\partial}{\partial t}(\rho Y_k)+\frac{\partial}{\partial x_j}(\rho Y_k v_j)=\frac{\partial}{\partial x_j}\left(\frac{\mu}{\sigma}\frac{\partial Y_k}{\partial x_j}\right)+\rho\omega_k \tag{3.18}$$

By summing up the conservation equations for all the species the conservation equation for overall mass appears. This equation is usually called the continuity equation [162]

$$\frac{\partial \rho}{\partial t}+\frac{\partial}{\partial x_j}(\rho v_j)=0 \tag{3.19}$$

3.3.2 Conservation of momentum

The velocity field of the system is determined by the forces acting on the system. Newton's second law of motion relates the sum of all forces acting on the system and the linear momentum of the system

$$\sum F_j=\frac{D(mv_j)}{D_t} \tag{3.20}$$

where the operator D/D_t is the substantial or material derivative. By applying Newton's second law to an infinitesimal control volume fixed in space, the conservation equation for linear momentum may be derived [162, 166, 167].

$$\frac{\partial}{\partial t}(\rho v_k)+\frac{\partial}{\partial x_j}(\rho v_k v_j)=-\frac{\partial \rho}{\partial x_k}+\frac{\partial}{\partial x_j}(\tau_{kj})+\rho b_k \tag{3.21}$$

where τ_{kj} is the viscous stress and is given by equation (3.6) and ρb_k is the body force due to buoyancy. To better understanding the effects of buoyancy, our research focussed on non-premixed hydrogen flames propagating in fully developed turbulence. We imagine that the most significant role of buoyancy forces on these flames is to

influence their flow fields through a coupling with mean and fluctuating temperature fields.

3.3.3 Conservations of energy

The first law of thermodynamics states that the total energy of a system and its surroundings is conserved. For an open system this principle can be expressed by the following equation [162, 165, 166]

$$\frac{\partial}{\partial t}\left(\rho e_t\right)+\frac{\partial}{\partial x_j}\left(\rho e_t v_j\right)=-\frac{\partial j_j^q}{\partial x_j}+Q-\frac{\partial}{\partial x_j}\left(pv_j\right)+\frac{\partial}{\partial x_j}\left(\tau_{ij}u_i\right) \qquad (3.22)$$

Where e_t is the total energy of the fluid. The total energy e_t is the sum of the internal energy (u), potential energy (Φ), and kinetic energy $\left(\frac{1}{2}v_i v_i\right)$. j_j^q is the thermal energy flux in the x_j direction and Q is the internal production rate of thermal energy, for example due to radiation. The last two terms in equation (3.22) represent the work done on the fluid by pressure forces and viscous forces respectively.

In numerical simulations of turbulent combustion, it is often desirable to use an equation for temperature or enthalpy instead of the total energy. In the present case an equation for enthalpy (*h*) has been used. A conservation equation for the enthalpy may be derived from the first law of thermodynamics in several ways. The enthalpy is linked to the internal energy by its definition

$$h=u+\frac{p}{\rho} \qquad (3.23)$$

by subtracting equations for the kinetic and potential energy from equation (3.22) an equation for the internal energy is found. The conservation equation for kinetic energy may be found by multiplying the conservation equation of linear momentum (equation(3.21)) with v_i, resulting in

$$\frac{\partial}{\partial t}\left(\rho\frac{1}{2}v_i v_i\right)+\frac{\partial}{\partial x_j}\left(\rho\frac{1}{2}v_i v_i v_j\right)=-v_i\frac{\partial p}{\partial x_i}+v_i\frac{\partial \tau_{ij}}{\partial x_j}+\rho v_j b_j \qquad (3.24)$$

an equation for the potential energy is found by multiplying the equation of continuity (3.19) with the stationary potential Φ defined as

$$b_j = -\frac{\partial \Phi}{\partial x_j} \tag{3.25}$$

the following equation is obtained

$$\frac{\partial}{\partial t}(\rho \Phi) + \frac{\partial}{\partial x_j}(\rho \Phi v_j) = -\rho v_j b_j \tag{3.26}$$

by subtracting equations (3.24) and (3.26) from equation (3.22) and using the definition of enthalpy (3.23) the conservation equation for enthalpy is finally obtained.

$$\frac{\partial}{\partial t}(\rho h) + \frac{\partial}{\partial x_j}(\rho h v_j) = \frac{\partial p}{\partial t} + v_j \frac{\partial p}{\partial x_j} - \frac{\partial j_j^q}{\partial x_j} + \tau_{ij} \frac{\partial v_i}{\partial x_j} + Q \tag{3.27}$$

The molecular $\left(j_j^q\right)$ energy flux is given by equation (3.16) where Le=1 is assumed. The equation is further simplified by ignoring the terms dp/dt, $v_j \partial p/\partial x_j$ and $\tau_{ij} \partial v_i/\partial x_j$. This assumption is justified as long as there are no extreme pressure gradients occurring in the system [97]. This assumption leads to the simplified energy equation

$$\frac{\partial}{\partial t}(\rho h) + \frac{\partial}{\partial x_j}(\rho h v_j) = \frac{\partial}{\partial x_j}\left(\frac{\mu}{\sigma}\frac{\partial h}{\partial x_j}\right) + Q \tag{3.28}$$

3.3.4 The General Transport equation

By assessment of the conservation equations it is apparent that they have a similar form. Due to this similarity, the same numerical procedure can be followed to solve all the conservation equations. The equations can be represented by a general transport equation.

$$\frac{\partial}{\partial t}(\rho \phi_i) + \frac{\partial}{\partial x_j}(\rho \phi_i v_j) = \frac{\partial}{\partial x_j}\left(\Gamma_i \frac{\partial \phi_i}{\partial x_j}\right) + S_i \tag{3.29}$$

Where ϕ_i represent a scalar variable, for example v_j or h, while Γ_i and S_i are the corresponding diffusion coefficient and source term, respectively.

3.4 Chemical kinetics

The source term ω_k in equation (3.18) represents the net production rate of species *k* due to chemical reactions. In gaseous combustion this reaction rate is found by using an appropriate reaction mechanism. This reaction mechanism consists of a set of elementary reactions with corresponding rate parameters. If the reaction mechanism consists of n_s species and n_{cr} chemical reactions, an arbitrary reaction in the reaction mechanism can be expressed as [164, 165]

$$\sum_{i=1}^{n_s} \nu'_{il} A_i \rightarrow \sum_{i=1}^{n_s} \nu''_{il} A_i \qquad l = 1, \ldots, n_{cr} \tag{3.30}$$

Where ν'_{il} and ν''_{il} are the stoichiometric coefficients of reactants or products of species *i* in reaction *l* and A_i is the specification of species *i*.

The Chemical production rate for species *i* is now expressed as [164]

$$\omega_i = \frac{M_i}{\rho} \sum_{l=1}^{n_{cr}} k_l \left(\nu''_{il} - \nu'_{il}\right) \prod_{k=1}^{n_s} c_k^{\nu'_{il}} \tag{3.31}$$

with c_k being the concentration of species *k*. k_l is the rate coefficient for reaction *l* and is calculated from a modified Arrhenius expression

$$k_l = A_l T^{b_l} \exp\left(\frac{E_{a,l}}{R_u T}\right) \tag{3.32}$$

where A_l is the pre-exponential factor, b_l is the temperature exponent and $E_{a,l}$ is the activation energy. These rate parameters, together with the selection of elementary reactions and their stoichiometric coefficient, make up the reaction mechanism.

3.5 Modelling of turbulent transport terms

The nature of turbulent flow is irregular with rapid fluctuations in velocity, density, temperature, and composition. This fluctuating nature makes turbulence flow highly diffusive as instantaneous fluid property gradients are large resulting in enhanced transport of momentum, mass, and energy. The basic physics of these transport mechanisms is the same as for laminar flow, and the expressions for molecular transport

presented earlier in this chapter, are still valid for turbulence flow. If the turbulence levels are low, the transport equations (see Section 3.3) can be solved to yield the instantaneous values for velocity, temperature and composition. This is called direct numerical simulation (DNS). However, in most practical turbulence flows, the task of resolving the fluctuations would require extremely fine grids and high time resolution. Even for modern computers this would be an impracticable task.

An approach to reduce the computational task is to apply a statistical treatment of the transport equations. The instantaneous variables are decomposed into a mean and a fluctuating component. Instead of solving transport equations for instantaneous quantities, transport equations for mean quantities are solved. This approach requires turbulence models which relate the turbulence fluctuations to the mean quantities.

The introduction of mean quantities makes the numerical handling of turbulent flow simpler. However, it also causes new challenges, especially related to the handling of chemical kinetics. The source terms in the Favre-averaged transport equations for the individual species are exponential functions of temperature in equations (3.17) and (3.18). Using the mean temperature to compute a mean source term will lead to an erroneous result. Accordingly, the averaged chemical production rates need special treatment and are approximated or replaced by a combustion model.

3.5.1 Favre-averaged conservation equations

To average the equations the instantaneous variables are decomposed into a mean value and a fluctuation.

$$\varphi = \overline{\varphi} + \varphi', \tag{3.33}$$

where $\overline{\varphi}$ is the mean value and φ' the fluctuation. When modelling turbulent flows with a varying density such as occurs in turbulent combustion, it is often useful to use a density-weighted mean [20]

$$\varphi = \tilde{\varphi} + \varphi'', \tag{3.34}$$

where $\tilde{\varphi}$ is the density-weighted mean defined as

$$\tilde{\varphi} = \frac{\overline{\rho \varphi}}{\overline{\rho}}. \tag{3.35}$$

By introducing equation (3.34) into the conservation equations (3.17) and performing the averaging, the Favre-averaged conservation equations are obtained:

Mass Conservation of Species *k*

$$\frac{\partial}{\partial t}\left(\overline{\rho}\tilde{Y}_k\right) + \frac{\partial}{\partial x_j}\left(\overline{\rho}\tilde{Y}_k \tilde{v}_j\right) = \frac{\partial}{\partial x_j}\left(\frac{\mu}{\sigma}\frac{\partial \tilde{Y}_k}{\partial x_j} - \overline{\rho} Y_k'' v_j''\right) + \overline{\rho}\tilde{\omega}_k \tag{3.36}$$

Conservation of overall mass

$$\frac{\partial \overline{\rho}}{\partial t} + \frac{\partial}{\partial x_j}\left(\overline{\rho}\tilde{v}_j\right) = 0 \tag{3.37}$$

Conservation of momentum

$$\frac{\partial}{\partial t}\left(\overline{\rho}\tilde{v}_k\right) + \frac{\partial}{\partial x_j}\left(\overline{\rho}\tilde{v}_k\tilde{v}_j\right) = -\frac{\partial \overline{p}}{\partial x_k} + \frac{\partial}{\partial x_j}\left(\overline{\tau}_{kj} - \overline{\rho} v_k'' v_j''\right) + \overline{\rho}\tilde{b}_k. \tag{3.38}$$

Conservation of energy

$$\frac{\partial}{\partial t}\left(\overline{\rho}\tilde{h}\right) + \frac{\partial}{\partial x_j}\left(\overline{\rho}\tilde{h}\,\tilde{v}_j\right) = \frac{\partial\, \overline{p}}{\partial t} + \frac{\partial}{\partial x_j}\left(\frac{\mu}{\sigma}\frac{\partial \tilde{h}}{\partial x_j} - \overline{\rho}\, h'' v_j''\right) + \overline{\rho}\,\tilde{Q}\,. \tag{3.39}$$

Conservation of a general scalar variable ϕ_i

$$\frac{\partial}{\partial t}\left(\overline{\rho}\tilde{\phi}_i\right) + \frac{\partial}{\partial x_j}\left(\overline{\rho}\tilde{\phi}_i\tilde{v}_j\right) = \frac{\partial}{\partial x_j}\left(\Gamma_i \frac{\partial \tilde{\phi}_i}{\partial x_j} - \overline{\rho}\phi_i'' v_j''\right) + \overline{S}_i\,. \tag{3.40}$$

Compared to the equations for the instantaneous variables presented in section 3.3, several new terms have appeared due to the averaging. These new terms are known as turbulence stresses or Reynolds stresses $-\overline{\rho} v_k'' v_j''$, and turbulence fluxes $-\overline{\rho}\, Y_k'' v_j''$, $-\overline{\rho} h_k'' v_j''$, and $-\overline{\rho}\phi_k'' v_j''$. These terms are unknown and to make it possible to solve the averaged conservation equations, they have to be approximated in some way. Methods

for approximating these unknown terms are called turbulence models. A large number of turbulence models have been developed. However, for simulating turbulence combustion there are mainly two different types of models which are in use at present. The most commonly used model today is the $k-\varepsilon$ model and this model has been used in this investigation. Furthermore, a class of models called Reynolds-Stress-Transport-Equation (RSTE) models or second closure models are often used although due to the plane jet - round jet anomaly [168] do not yield more accurate results than the $k-\varepsilon$ turbulence model.

3.5.2 $k-\varepsilon$ Turbulence model

The $k-\varepsilon$ model was developed by Jones and Launder [169] and is based on the assumption that the transport of turbulence eddies is analogous to molecular transport can be described by using an effective viscosity

$$\mu_{eff} = \mu + \mu_t, \tag{3.41}$$

where μ_t is the eddy (or turbulence) viscosity. The turbulence stresses are expressed by the eddy viscosity using an analogy to the expression for viscous stresses Equation (3.6) [166].

$$-\bar{\rho}\widetilde{v_k'' v_j''} = \mu_t\left(\frac{\partial \tilde{v}_k}{\partial x_j} + \frac{\partial \tilde{v}_j}{\partial x_k}\right) - \frac{2}{3}\left(\bar{\rho}k + \mu_t \frac{\partial \tilde{v}_l}{\partial x_l}\right)\delta_{kj}, \tag{3.42}$$

where k is the turbulence kinetic energy and δ_{kj} is a Dirac function. The turbulence fluxes are modelled in analogy with the molecular fluxes. For a general scalar variable the turbulence flux is expressed as [166]

$$-\bar{\rho}\phi_i'' v_j'' = \frac{\mu_t}{\sigma_t}\frac{\partial \tilde{\varphi}_i}{\partial x_j} \tag{3.43}$$

Where σ_t is the turbulent Prandtl-Schmidt number.

To complete the model the variables μ_t, σ_t and k must be derived or given values. The turbulence kinetic energy is defined as

$$k = \frac{1}{2} v_l'' v_l''. \tag{3.44}$$

By the aid of the instantaneous and the Favre-averaged momentum equations, a transport equation for k can be obtained [166]. However, in this transport equation there are several terms which have to be modelled. In this investigation the modelled equation suggested by Jones and Launder [169] has been used.

$$\frac{\partial}{\partial t}(\bar{\rho} k) + \frac{\partial}{\partial x_j}(\bar{\rho} k \tilde{v}_j) = \frac{\partial}{\partial x_j}\left[\left(\mu + \frac{\mu_t}{\sigma_k}\right)\frac{\partial k}{\partial x_j}\right] + \bar{\rho} P_k - \bar{\rho}\varepsilon \tag{3.45}$$

σ_k	σ_ε	$C_{\varepsilon 1}$	$C_{\varepsilon 2}$	C_μ
1.0	*1.3*	*1.44*	*1.92*	*0.09*

Table 3. 1: Constants in the $k-\varepsilon$ model [66]

The variable ε represents the dissipation of turbulence kinetic energy into heat. The dissipation of turbulence kinetic energy is found from a modelled transport equation

$$\frac{\partial}{\partial t}(\bar{\rho}\varepsilon) + \frac{\partial}{\partial x_j}(\bar{\rho}\varepsilon\tilde{v}_j) = \frac{\partial}{\partial x_j}\left[\left(\mu + \frac{\mu_t}{\sigma_\varepsilon}\right)\frac{\partial \varepsilon}{\partial x_j}\right] + C_{\varepsilon 1}\frac{\varepsilon}{k}\bar{\rho} P_k - C_{\varepsilon 2}\frac{\varepsilon}{k}\bar{\rho}\varepsilon. \tag{3.46}$$

The term P_k present in the two transport equations, is the production of turbulence kinetic energy [166, 169]

$$\bar{\rho} P_k = \mu_t\left(\frac{\partial \tilde{v}_k}{\partial x_j} + \frac{\partial \tilde{v}_j}{\partial x_k}\right)\frac{\partial \tilde{v}_k}{\partial x_j} - \frac{2}{3}\left(\bar{\rho} k + \mu_t \frac{\partial \tilde{v}_l}{\partial x_l}\right)\frac{\partial \tilde{v}_j}{\partial x_j}. \tag{3.47}$$

The eddy viscosity is expressed as

$$\mu_t = C_\mu \bar{\rho}\frac{k^{1.5}}{\varepsilon} \tag{3.48}$$

The parameters $\sigma_k, \sigma_\varepsilon, C_{\varepsilon 1}, C_{\varepsilon 2}$ and C_μ are model constants. In the present investigations, the values suggested by Launder and Spalding [66] have been used, see

Table 3.1. The $k-\varepsilon$ model is now complete and the unknown stresses and turbulence fluxes can be found from equations (3.42) and (3.43) once the transport equations for k and ε have been solved.

3.5.3 Mean and variance mixture fraction

The simplifications that are introduced into the modelling of turbulence diffusion flames by assigning to a conserved scalar the role of describing the fluctuating composition and temperature fields are now well known. In particular, the problem of modelling the influence of turbulence on the chemical reaction is largely removed if local composition and temperature can be related unambiguously to the local value of a conserved scalar. The mean and second moments of all thermodynamic variables are obtainable from the knowledge of the statistics of the conserved scalar; the most suitable method of introducing the required statistical information is through the introduction of the probability density function for the conserved scalar. This method is typically called the conserved scalar method. In this section we present the definition of the conserved scalar with a complete description of the mean and variance scalar. Our conserved scalar in this investigation is the mixture fraction *f*.

From the general transport equation developed in equation (3.29) the conserved scalar (or mixture fraction) cannot be generated or destroyed as atoms are conserved thus satisfies the balance equation

$$\frac{\partial(\rho f)}{\partial t}+\frac{\partial}{\partial x_k}(\rho u_k f)=\frac{\partial}{\partial x_k}\left(\rho D\frac{\partial f}{\partial x_k}\right) \tag{3.49}$$

where D is the mass diffusion coefficient.

For stationary turbulent flows of moderate to high Reynolds number molecular transport can be neglected as it is much smaller than mass transfer due to turbulent fluctuations. Under these assumptions the Favre average mean mixture fraction balance equation is

$$\frac{\partial}{\partial x_k}\left(\bar{\rho}\tilde{u}_k\tilde{f}\right)=-\frac{\partial}{\partial x_k}\left(\overline{\rho u_k'' f''}\right) \tag{3.50}$$

From the simplified energy equation (3.28) developed in this chapter replacing enthalpy with mixture fraction and using the usual eddy or gradient transport model equation (3.50) becomes

$$\frac{\partial}{\partial x_k}\left(\bar{\rho}\tilde{u}_k\,\tilde{f}\right) = -\frac{\partial}{\partial x_k}\left(\frac{\mu_t}{\sigma_f}\frac{\partial \tilde{f}}{\partial x_k}\right) \tag{3.51}$$

The scalar flux $\bar{\rho}u_k''f''$ derived in this chapter is closed using the conventional eddy transport model. This is obtained by modelling the scalar flux in terms of the gradient of the mean property, namely

$$-\bar{\rho}\,u_k''\,f'' = \frac{\mu_t}{\sigma_f}\frac{\partial \tilde{f}}{\partial x_k} \tag{3.52}$$

where the effective Schmidt number σ_f is a constant typically equal to 0.7.

The balance equation for the mixture fraction variance $\tilde{f}''^2$ is obtained by multiplying the instantaneous equation for *f* equation (3.49) by f'' and averaging

$$\bar{\rho}\tilde{u}_k\frac{\partial \tilde{f}''^2}{\partial x_k} = -2\overline{\rho u_k'' f''}\frac{\partial \tilde{f}}{\partial x_k} - \frac{\partial}{\partial x_k}\left(\overline{\rho u_k'' f''^2}\right) - 2\overline{\rho D\frac{\partial f''}{\partial x_k}\frac{\partial f''}{\partial x_k}} \tag{3.53}$$

The terms on the right hand side represent, respectively, the production by the mean gradient, diffusion by the velocity fluctuations, and the dissipation by molecular diffusion. The three terms on the right hand side can be modelled in the same way as Spalding's "concentration fluctuation" equation or $\tilde{g}$ equation [170]. The first term becomes

$$-2\,\overline{\rho\,u_k''\,f''}\,\frac{\partial \tilde{f}}{\partial x_k} = Cg_1\,\mu_t\left(\frac{\partial \tilde{f}}{\partial x_k}\right)^2 \tag{3.54}$$

The second term:

$$-\overline{\rho\,u_k''\,\tilde{f}''^2} = \frac{\mu_t}{\sigma_{f''^2}}\frac{\partial \tilde{f}''^2}{\partial x_k} \tag{3.55}$$

The third term

$$-2\overline{\rho D\frac{\partial f''}{\partial x_k}\frac{\partial f''}{\partial x_k}} = Cg_2\,\bar{\rho}\,\tilde{\varepsilon}\,\tilde{f}''^2 \Big/ \tilde{k} \tag{3.56}$$

where $\sigma_{f''^2}$, Cg_1 and Cg_2 are modelled constants and have values 0.7, 2.7 and 1.79.

With the knowledge of the chemical species and temperature and under the conditions stated above the thermochemical structure can be expressed at a constant pressure as a function of f alone. In the crucial conditions identified earlier we argued against the influence of differential mass diffusivities which would prevent the use of element conservation in the specification of a conserved scalar. This is a considerable constraint only in the hydrogen-air laminar diffusion flame where the diffusion coefficient for H_2 is four times greater than the typical mixture diffusion coefficient (N_2). However, it is believed that the equal diffusivities assumption is acceptable as effective turbulence diffusivity is several orders of magnitude higher than laminar species diffusivities. This assumption is also consistent with previous studies [40]. The influence of variable mass diffusion is less apparent in hydrocarbon flames which have higher molecular-weights. In chapter five of this thesis we will look at how $\phi_i = \phi_i(f)$ is averaged and computed in a turbulence non-premixed flame in the turbulence ensemble.

3.5.4 Parabolised Reynolds averaged equations

The overall computational framework used in this study is a parabolic flow solver, utilising the boundary layer equations, similar to GENMIX, Spalding [171], extended to include elliptic features found in lifted fires. In lifted jet fires the important elliptic features are the feedback mechanisms downstream of the lift-off region that determines the lift-off height and local flame structure. In the context of the lift-off model implemented here the elliptic feedback mechanism is introduced through the probability of burning field. The details of implementation are considered further below in section 3.8.2. As jet fires have a dominant flow direction it is common for the flame structure of a rim-stabilised jet fire to be calculated in this way, Gore et al. [40].

The computational advantages of a parabolic flow model over a fully elliptic solver are clear, as no iteration cycle of a pressure correction algorithm is required in its solution

as the dominant flow direction has a time like quality allowing a marching procedure in the dominant flow direction. This makes it possible to calculate complex flame structures using readily available computational resources. For example Wang and Chen [172] have reported the computation of a laboratory scale rim-stabilised flame, the simulation is calculated using a Probability Density Function (PDF) Transport Model with detailed chemistry, including 53 species and 32 elemental reactions and a multi-time-scale $k-\varepsilon$ turbulence model. Either of these modelling approaches in isolation would make the jet fire calculation prohibitively computationally intensive when combined with an elliptic solver on a standard PC. Using a flow solver based on the boundary layer equations Wang and Chen reported a run-time of the order of 1 week on a relatively high specification PC. The use of a parabolic solver is not only an issue of convenience as it makes it relatively simple to demonstrate mesh independence in any predicted flow fields presented. In addition any model calibration is purely dependent on the quality of the experimental data used in the calibration. The issue of robust calibration is a particularly important one as without it, model development looses rigour. Cumber and Spearpoint [49] showed that Sanders and Lamers [48] adoption of the small-scale strain rate model for lifted methane jet fires was incorrect as the large-scale strain rate model gave far closer agreement with observed lift-off heights once both models were calibrated appropriately.

The basis of the flow equations is the parabolised Favre averaged Navier Stokes equations in an axisymmetric coordinate system. The system is closed using a variant of the $k-\varepsilon$ turbulence model.

$$\frac{\partial \bar{\rho}\tilde{U}k}{\partial z}+\frac{1}{r}\frac{\partial r\bar{\rho}\tilde{V}k}{\partial r}=\frac{1}{r}\frac{\partial}{\partial r}\left(r\frac{\mu_{eff}}{\sigma_k}\frac{\partial k}{\partial r}\right)+\bar{\rho}\left(P_k-\varepsilon\right)$$

$$\frac{\partial \bar{\rho}\tilde{U}\varepsilon}{\partial z}+\frac{1}{r}\frac{\partial r\bar{\rho}\tilde{V}\varepsilon}{\partial r}=\frac{1}{r}\frac{\partial}{\partial r}\left(r\frac{\mu_{eff}}{\sigma_\varepsilon}\frac{\partial \varepsilon}{\partial r}\right)+\bar{\rho}\frac{\varepsilon}{k}\left(C_1P_k-C_2\varepsilon\right)$$

$$P_k=\mu_{eff}\left(\frac{\partial \tilde{U}}{\partial r}\right)^2,\quad \mu_{eff}=\mu_1+\frac{C_\mu\bar{\rho}k^2}{\varepsilon},\quad C_1=1.4-3.4\left(\frac{k}{\varepsilon}\frac{d\tilde{U}}{dz}\right)_{cl}^3 \qquad (3.57)$$

$$C_\mu=0.09,\quad C_2=1.84,\quad \sigma_k=1,\quad and\quad \sigma_\varepsilon=1.3$$

The version of the $k-\varepsilon$ turbulence model given above is a modification of the typically implemented variant of the $k-\varepsilon$ turbulence model $(C_1 = 1.44, C_2 = 1.92)$ to take account of the round jet/plane jet anomaly, Pope [168] where the spreading rate of round jets tends to be over-predicted by the standard version of the turbulence model. This is a well known limitation of most two equation turbulence models and second moment closure models unless some modifications is brought in to account for the reduced spreading rate. The modification to the $k-\varepsilon$ model introduced above is due to Morse [173], and has been used successfully in previous rim stabilised fire simulations, Moss et al. [174]. The axisymmetric correction is used here as it gives an appropriate balance between model complexity and predictive capability. The boundary layer form of the mixture fraction transport equation and mixture fraction variance transport equation are stated below

$$\bar{\rho}\tilde{u}\frac{\partial \tilde{f}}{\partial x} + \tilde{v}\frac{\partial \tilde{f}}{\partial r} = -\frac{1}{r}\frac{\partial}{\partial r}\left(r\frac{\mu_t}{\sigma_f}\frac{\partial \tilde{f}}{\partial r}\right) \tag{3.58}$$

$$\bar{\rho}\tilde{u}\frac{\partial \widetilde{f''^2}}{\partial x} + \bar{\rho}\tilde{v}\frac{\partial \widetilde{f''^2}}{\partial r} = \frac{1}{r}\frac{\partial}{\partial r}\left(r\frac{\mu_t}{\sigma_f}\frac{\partial \widetilde{f''^2}}{\partial r}\right) + C\,f_1\mu_t\left(\frac{\partial \widetilde{f''^2}}{\partial r}\right)^2 - C\,f_2\bar{\rho}\frac{\tilde{\varepsilon}}{\tilde{k}}\widetilde{f''^2} \tag{3.59}$$

3.6 Thermal radiation modelling

The calculation of the external radiation field of a hydrogen jet fire is on the whole a challenging task, as a jet fire is highly directional with source momentum dominating the fire dynamics in the near field compared with further downstream where the buoyancy of the fire becomes influential [175]. The mathematical modelling of high temperature processes calls for an ability to predict the thermal radiation fields with confidence. The primary quantity of interest, the spectral intensity, depends in a multifaceted way on the temperature and participating species distribution such as H_2O. This, together with the fact that the spectral intensity is a function of location, orientation and wavelength, makes the simulation of combusting flows a challenging scientific computation. Inspite of today's computer hardware and the usual use of parallel computing facilities, alternatives have to be made regarding the balance between the levels of sophistication of the radiation model relative to other sub-models that form the composite flame or fire model.

The influence of turbulence on the total radiative heat transfer emitted by a hot medium was theoretically analysed by Cox [3]. The radiative energy emitted per unit area by a grey homogeneous and isothermal hot gaseous layer is equal to $\varepsilon\sigma T^4$. The emissivity of the gaseous layer ε, is defined as the ratio of the energy emitted by a volume of gas compared to that emitted by a blackbody at the same temperature. Expressing the instantaneous temperature, *T*, and the emissivity, ε, as a sum of the mean value and a fluctuation yields

$$\overline{\varepsilon T^4} = \overline{\left(\bar{\varepsilon}+\varepsilon'\right)\left(\bar{T}+T'\right)^4} = \bar{\varepsilon}\bar{T}^4\left(1+6\frac{\overline{T'^2}}{\bar{T}^2}+4\frac{\overline{T'^3}}{\bar{T}^3}+\frac{\overline{T'^4}}{\bar{T}^4}+4\frac{\overline{\varepsilon'T'}}{\bar{\varepsilon}\bar{T}}+6\frac{\overline{\varepsilon'T'^2}}{\bar{\varepsilon}\bar{T}^2}+4\frac{\overline{\varepsilon'T'^3}}{\bar{\varepsilon}\bar{T}^3}+\frac{\overline{\varepsilon'T'^4}}{\bar{\varepsilon}\bar{T}^4}\right) \quad (3.60)$$

The first four terms in the parenthesis on the right side of Equation (3.60) constitute the temperature self-correlation, while the last four terms represent the emissivity-temperature correlation. Hence, ignoring the correlations of odd order, equation (3.60) is simplified to

$$\overline{\varepsilon T^4} \approx \bar{\varepsilon}\bar{T}^4\left(1+6\frac{\overline{T'^2}}{\bar{T}^2}+\frac{\overline{T'^4}}{\bar{T}^4}+4\frac{\overline{\varepsilon'T'}}{\bar{\varepsilon}\bar{T}}+4\frac{\overline{\varepsilon'T'^3}}{\bar{\varepsilon}\bar{T}^3}\right) \quad (3.61)$$

Experimental data [176] show that

$$\overline{T'^4}/\bar{T}^4 << 6\overline{T'^2}/\bar{T}^2, \quad (3.62)$$

but no data are available for the cross-correlation between temperature and emissivity. The ratio $\overline{T'^4}/\bar{T}^4$ was evaluated assuming the PDF of the temperature. A truncated-Gaussian PDF shape was used with different parameters that closely approximate PDFs of temperature experimentally observed in the axial and radial regions of turbulent non-premixed flames.

3.6.1 Radiative source term

The equation of radiative transfer describes the effects of emission, absorption and scattering on a monochromatic beam of intensity I_λ, passing through a medium of known spectral absorption and scattering coefficients, K_λ and Y_λ. If I_λ is the energy

emitted at wavelength λ per unit time per unit solid angle per unit area normal to the beam, then the change in I_λ on passing through a fluid element of width *ds* is given by

$$\frac{dI_\lambda}{ds} = -\beta_\lambda I_\lambda(s) + \frac{k_\lambda}{\pi} e_{b\lambda}(s) + \frac{Y_\lambda}{4\pi} G_\lambda(s) \tag{3.63}$$

where *s* denotes the position along an arbitrary path within the radiating fluid. β_λ is the spectral extinction coefficient, equal to the sum of K_λ and Y_λ and $G_\lambda(s)$ denotes the incident energy per unit area within the medium. $e_{b\lambda}$ is the spectral blackbody emissive power as described by Planck's law.

$$e_{b\lambda} = \frac{c_1}{\lambda^5}(e^{c_2/\lambda T} - 1) \tag{3.64}$$

where c_1 and c_2 are the first and second radiation constants. The source term appearing in equation (3.63) represent extinction by absorption and scattering, emission from and scattering into the fluid element respectively. The emission term is a function of position owing to the dependence of the Planck function on temperature, $T(s)$.

In a hydrogen jet fire the scattering term can be ignored as there is no soot present. In this case, the equation of transfer is simplified considerably to become

$$\frac{dI_\lambda}{ds} = k_\lambda(s)\left(\frac{e_{b\lambda}}{\pi}(s) - I_\lambda(s)\right) \tag{3.65}$$

If the direction of the radiative path, s, makes an angle θ with the coordinate direction x, it can be shown that

$$\mu \frac{dI_\lambda}{dx} = k_\lambda(x)\left(\frac{e_{b\lambda}}{\pi}(x) - I_\lambda(x,\mu)\right) \tag{3.66}$$

where $\mu = \cos\theta$

This is readily integrated along the radiation path to give the spectral intensity.

$$I_\lambda(x,\mu) = I_\lambda(0,\mu)e^{-\tau_\lambda/\mu} + \int_0^x k_\lambda \frac{e_{b\lambda}}{\pi} e^{(\tau_\lambda(x')-\tau_\lambda(x))/\mu} \frac{dx'}{\mu} \tag{3.67}$$

where τ_λ is the optical depth at wavelength λ defined by

$$\tau_\lambda(x) = \int_0^x k_\lambda(x')dx' \tag{3.68}$$

It is often useful to employ the optical depth as the independent coordinate so that I_λ becomes

$$I_\lambda(\tau_\lambda, \mu) = I_\lambda(0, \mu)e^{-\tau_\lambda/\mu} + \int_0^{\tau_\lambda} k_\lambda \frac{e_{b\lambda}}{\pi} e^{-(\tau_\lambda - t)/\mu} \frac{dt}{\mu} \tag{3.69}$$

In order to find the heat flux at wavelength λ, $q_{R\lambda}$, in the direction of x(or τ), it is necessary to integrate over all solid angles forming the hemisphere above the fluid element. It can be shown that Sparrow and Cess [177]

$$q_{R\lambda}(\tau_\lambda) = 2\pi \int_0^1 I_\lambda(\tau_\lambda, \mu)\mu d\mu \tag{3.70}$$

such that

$$q_{R\lambda}(\tau_\lambda) = 2\pi\int_0^1 I_\lambda(0,\mu)e^{-\tau_\lambda/\mu}\mu d\mu + 2\int_0^{\tau_\lambda} e_{b\lambda}(t)E_2(\tau_\lambda - t)dt \tag{3.71}$$

where $E_n(v)$ is the exponential integral Abramowitz and Stegun [178]

$$E_n(v) = \int_0^1 t^{n-2}e^{-v/t}dt \tag{3.72}$$

The total heat flux, q_R, in the direction of x is then found by integrating over all wavelengths to give,

$$q_R(\tau) = \int_0^\infty q_\lambda(\tau_\lambda)d\lambda \tag{3.73}$$

There will also be a radiative heat flux in the negative x-direction, found by integrating over the second hemisphere surrounding the fluid element, which can be similarly specified. Subtraction of these two quantities then gives the heat flux vector, $\tilde{Q}$, appearing in the energy conservation equation (3.39)

The energy equation is thus an integro-differential equation and highly non-linear due to the dependence of the Planck function on temperature. To solve this energy balance, together with the remaining flowfield equations, it is necessary to specify the spectral absorption coefficient, k_λ. In general, this is a strongly varying function of temperature, chemical composition and pressure as well as wavelength. The following sub-section considers ways in which the complexity of the energy equation may be reduced and the applicability of such approximations in the calculation of radiative transfer in turbulence diffusion flames.

3.6.2 Radiation from hydrogen diffusion flames

So far we have described the formulation of the radiative heat flux vector, identifying its dependence on local thermodynamic quantities and the spectral absorption coefficient, κ_λ. It is the aim of this investigation to describe the sources of gaseous emission in hydrogen diffusion flames and their relative contributions to the absorption coefficient.

The primary contribution to the radiant emission from hydrogen combustion gases is from the combustion product, H_2O (water vapour), and to a lesser extent from the fuel itself. Energy is emitted from discrete wavelength ranges the most significant of these ranges are centred on 1.8µm, 2.7µm and 6.3 µm (water vapour). Many other sources occur but their contribution is considered negligible in comparison to the H_2O bands already noted.

Experimental investigations of the spectra emitted by combustion gases indicate that the spectral emissivity

$$\varepsilon_\lambda = 1 - e^{-\kappa_\lambda} \tag{3.74}$$

is strongly dependent on wavelength. Energy is emitted from specific wavelength ranges or bands, and the shape of these bands varies with both temperature and pressure of the radiating gases: elevated pressures cause the wavelength domain of the band to broaden while higher temperatures increase its strength or intensity. Each of these bands consists of many spectral lines of varying strengths which arise from energy emission associated with transitions between energy levels within the gas molecules. Hottel and Sarofim [128] give detailed descriptions of the shape and size of the spectral

lines and the models used to quantify the effects of temperature, pressure and pathlength upon them.

The detailed line description is too cumbersome for the calculation of radiating flows and so models have been developed which describe the average spectral emissivity over a narrow wavelength range. The emissivity of the *i*-th radiation band is then found by integrating over all these narrow bands. These narrow band models, although accurate, must be provided with many empirically obtained parameters and, moreover, require considerable computational effort. Edwards and Balakrishnan [179] proposed a method by which the computational efficiency is increased, although the process remains lengthy especially for highly inhomogeneous paths requiring the use of Curtis-Godson scaling techniques (Goody [127]). Leckner [180] also developed an approximation to the narrow band model for homogeneous CO_2 - H_2O mixtures but this is inapplicable for temperatures below 1000K. Simpler models have therefore been developed which describe the spectral emissivity over the whole band. The wide band models, such as the exponential model derived by Edwards and Menard [130], are frequently used in engineering calculations and provide an acceptable compromise between accuracy and efficiency. Several researchers have extended the exponential wide band model, originally developed for homogeneous paths, to include scaling techniques for inhomogeneous flows [123].

Both the narrow and wide band models may require modification, however, when considering emission from mixtures of radiating gases. If the emission bands of the constituent gases do not coincide, the total gas emissivity is simply the weighted sum of the band emissivities, ε_i

$$\varepsilon = \frac{1}{\sigma T^4} \sum_i e_{b\lambda_i} \varepsilon_i \tag{3.75}$$

where $e_{b\lambda_i}$ is the spectral blackbody emission evaluated at the band centre, λ_i. If the emission bands overlap, as does the H_2O bands at 2.7μm, then a correction term, accounting for the mutual absorption, must be applied to the total emissivity.

3.7 Time-averaged and instantaneous forms of the RTE in reactive flows

3.7.1 Radiative transfer equation

The Radiative Transfer Equation (RTE) may be written as follows for an emitting-absorbing-scattering medium [181]:

$$\frac{dI_\lambda(r,s)}{ds} = -\beta_\lambda(r) I_\lambda(r,s) + \kappa_\lambda(r) I_{b\lambda}(r) + \frac{\sigma_{s\lambda}(r)}{4\pi}\int_{4\pi} I_\lambda(r,s^*)\Phi(s^*,s)\,d\Omega^* \quad (3.76)$$

In this equation $I_\lambda(r,s)$ is the spectral radiation intensity at point r and direction s, $I_{b\lambda}$ is the spectral blackbody radiation intensity, $\kappa_\lambda, \beta_\lambda$ and $\sigma_{s\lambda}$ are the spectral absorption, extinction and scattering coefficients of the medium, respectively, and $\Phi(s^*,s)$ is the scattering phase function. The subscripts λ and b denote wave number and blackbody properties respectively. The ratio $\Phi(s^*,s)/4\pi$ represents the probability that radiation propagating in direction s^* and confined within solid angle $d\Omega^*$ is scattered through the angle $s^* \cdot s$ into the direction s confined within solid angle $d\Omega$.

The boundary condition for a grey surface that emits and reflects diffusively is given by

$$I_{w\lambda}(s) = \varepsilon_w I_{b\lambda} + \frac{1-\varepsilon}{\pi}\int_{n\cdot s^*<0} |n\cdot s^*| I_\lambda(s^*)\,d\Omega^* \quad (3.77)$$

where ε_w is the emissivity of the surface, $\boldsymbol{n}$ is the unit normal vector, $\boldsymbol{s}$ is the direction of the outgoing radiation intensity, and $\boldsymbol{s^*}$ is the incoming direction associated with the elementary solid angle $d\Omega$.

Scattering is neglected here as hydrogen flames do not produce any particles. The RTE in an emitting-absorbing medium may be written as

$$\frac{dI_\lambda(s)}{ds} = -\kappa_\lambda I_\lambda(s) + \kappa_\lambda I_{b\lambda} \quad (3.78)$$

where the dependence on the spatial coordinate has been omitted for simplification. Conservation of radiative energy may be expressed as [181]

$$\nabla \cdot q = \int_0^{+\infty} \kappa_\lambda \left(4\pi I_{b\lambda} - G_\lambda\right) d\lambda = \kappa\left(4\pi I_b - G\right) \tag{3.79}$$

where the second equality only holds in the case of a grey medium. Here, q is the radiative heat flux vector, and G is the incident radiation given by

$$G = \int_0^{\infty} \int_{4\pi} I_\lambda \, d\Omega \, d\lambda = \int_{4\pi} I \, d\Omega \tag{3.80}$$

Whenever the temperature field is unknown, the energy conservation equation needs to be solved with the RTE.

3.7.2 Time-average integral form of the RTE

The RTE for an emitting-absorbing medium, equation (3.78), may be integrated along a line of sight yielding [181]

$$I_\lambda(s,t) = I_\lambda(0)\exp\left[-\int_0^s \kappa_\lambda\left(s^*,t\right)ds^*\right] + \int_0^s \kappa_\lambda\left(s^*,t\right) I_{b\lambda}\left(s^*,t\right)\exp\left[-\int_{s^*}^s \kappa_\lambda\left(s^{**},t\right)ds^{**}\right]ds^* \tag{3.81}$$

where the coordinate ***s*** along the line of sight, in direction ***s***, and the time, ***t***, have been explicitly indicated as arguments of the radiation intensity and absorption coefficient, to remind us that these quantities change in time as a result of the fluctuations of temperature and participating species concentrations.

The radiation intensity at the boundary $s = 0$ is either prescribed or obtained from the boundary condition. The first term on the right hand side of equation (3.81) represents the radiation intensity coming from the boundary and transmitted throughout the medium without being absorbed. The second term stands for the contribution from the radiation emitted by the medium, and attenuated by reabsorption. It is often convenient, for calculation purposes, to rearrange equation (3.81) as follows:

$$I_\lambda\left(s,t\right) = I_\lambda\left(0\right)\tau_\lambda\left(0 \to s,t\right) + \int_0^s I_{b\lambda}\left(s^*,t\right)\frac{\partial \tau_\lambda\left(s^* \to s,t\right)}{\partial s^*} ds^* \tag{3.82}$$

where the spectral transmissivity τ_λ is defined as

$$\tau_\lambda \left(s^* \rightarrow s \right) = \exp\left[-\int_{s^*}^{s} \kappa_\lambda \left(s^{**}, t \right) ds^{**} \right]. \tag{3.83}$$

In the case of a mixture of absorbing species, and using the usual assumption of statistical independence between the absorption coefficients of the different species [182], the absorption coefficient of the mixture is given by

$$\kappa_\lambda = \sum_i \kappa_{\lambda,i} \tag{3.84}$$

where the summation extends over all the absorbing species, and the spectral absorption coefficient of the *i*th species, $\kappa_{\lambda,i}$ depends on the temperature and concentration of species i.

The rate of emission from a volume element will be proportional to the magnitude of the volume. Consequently, the emitted intensity (which is the rate of emitted energy per unit area) along any path again must be proportional to the length of the path, and it must be proportional to the local energy content in the medium. Since, at thermodynamic equilibrium, the intensity everywhere must be equal to the blackbody intensity

$$(dI_\lambda)_{em} = \kappa_\lambda I_{b\lambda} ds \tag{3.85}$$

that is, the proportionality constant for emission is the same as for absorption.

As discussed previously there are two kinds of time averaging procedures commonly employed for the flow fields: Reynolds averaging and mass weighted averaging, also called Favre averaging [165]. However, both averaging procedures require the Reynolds average of the radiative source term of the energy conservation equation [165]. Hence, applying this procedure to equation (3.81) gives

$$\bar{I}_\lambda(s) = I_\lambda(0)\exp\left[-\int_0^s \bar{\kappa}_\lambda(s^*)ds^*\right]\underbrace{\overline{\exp\left[-\int_0^s \kappa'_\lambda(s^*,t)ds^*\right]}}_{A_1}$$
$$+\int_0^s \underbrace{\overline{\kappa_\lambda(s^*)I_{b\lambda}(s^*)}}_{B}\exp\left[-\int_{s^*}^s \bar{\kappa}_\lambda(s^{**},t)ds^{**}\right]\underbrace{\overline{\exp\left[-\int_{s^*}^s \kappa'_\lambda(s^{**},t)ds^{**}\right]}}_{A_2}ds^*$$
$$+\underbrace{\int_0^s \exp\left[-\int_{s^*}^s \bar{\kappa}_\lambda(s^{**})ds^{**}\right]\overline{\left[\kappa_\lambda(s^*,t)I_{b\lambda}(s^*,t)\right]'\exp\left[-\int_{s^*}^s \kappa'_\lambda(s^{**},t)ds^{**}\right]}ds^*}_{C}$$

(3.86)

If the PDFs of the temperature and spectral absorption coefficient are Gaussian, this equation may be rearranged and expressed in terms of two-point correlation coefficients [183]. The factor

$$\exp\left[-\int_0^s \bar{\kappa}_\lambda(s^*)ds^*\right] \tag{3.87}$$

in equation (3.86) represents the spectral transmissivity of the medium (see equation(3.83)) if there are no fluctuations of the radiative properties. In the presence of such fluctuations, the exponential term is multiplied by factor A_1 in equation(3.86), which is generally greater than unity. In particular, it is easy to demonstrate that $A_1 > 1$ if the PDF of the absorption coefficient of the medium is Gaussian. Accordingly, the first term on the right of equation (3.86) shows that the turbulence fluctuations of the absorption coefficient increase the transmissivity of the medium to the radiation coming from the boundary by the factor A_1. This observation is in agreement with the experimental findings of Foster [184], that is, the medium becomes more transparent to radiation due to turbulence fluctuations. Similarly, the transmissivity to radiation emitted from the medium (factor B in equation(3.86)) is increased by turbulence fluctuations, as given by the factor A_2 in the second term of equation(3.86).

Term B represents the correlation between the spectral absorption coefficient and the spectral blackbody radiation intensity, the Planck function. The Taylor series expansion of the Planck function about $\bar{T}$ yields

$$I_{b\lambda}(T) = I_{b\lambda}(\bar{T}) + T'\left(\frac{\partial I_{b\lambda}}{\partial T}\right)_{T-\bar{T}} + \frac{T'^2}{2}\left(\frac{\partial^2 I_{b\lambda}}{\partial T^2}\right)_{T-\bar{T}} + \ldots \tag{3.88}$$

If the terms of order higher than two in this Taylor series expansion are neglected, then the evaluation of $\overline{I}_{b\lambda}$ only requires the calculation of the variance of the temperature, which may be carried out using an appropriate turbulence model. Such a simple approach, which was used in [185], would fully account for TRI if the fluctuations of the radiative properties of the medium were negligible. This is not usually the case.

The fluctuating component of the Planck function is obtained as follows:

$$I'_{b\lambda}(T) = I_{b\lambda}(T) - \overline{I}_{b\lambda}(T) = T'\left(\frac{\partial I_{b\lambda}}{\partial T}\right)_{T-\overline{T}} + \frac{T'^2}{2}\left(\frac{\partial^2 I_{b\lambda}}{\partial T^2}\right)_{T-\overline{T}} - \frac{\overline{T'^2}}{2}\left(\frac{\partial^2 I_{b\lambda}}{\partial T^2}\right)_{T-\overline{T}} + \ldots \tag{3.89}$$

Therefore, term B in equation (3.86) may be written as

$$\overline{\kappa_\lambda I_{b\lambda}} = \overline{\kappa}_\lambda \overline{I}_{b\lambda} + \overline{\kappa'_\lambda I'_{b\lambda}} = \overline{\kappa}_\lambda \overline{I}_{b\lambda} + \overline{\kappa'_\lambda T'}\left(\frac{\partial I_{b\lambda}}{\partial T}\right)_{T-\overline{T}} - \frac{\overline{\kappa'_\lambda T'^2}}{2}\left(\frac{\partial^2 I_{b\lambda}}{\partial T^2}\right)_{T-\overline{T}} + \ldots \tag{3.90}$$

Neglecting higher order terms, and realising that the third term on the right of this equation involves an odd order correlation, which is also small (or zero in the case of a Gaussian PDF of the spectral absorption coefficient), it follows that

$$\overline{\kappa_\lambda I_{b\lambda}} \approx \overline{\kappa}_\lambda \overline{I}_{b\lambda} + \overline{\kappa'_\lambda T'}\left(\frac{\partial I_{b\lambda}}{\partial T}\right)_{T-\overline{T}}. \tag{3.91}$$

Notice that $\overline{\kappa}_\lambda \neq \kappa_\lambda\left(\overline{T}, \overline{x}_s\right)$, where x_s is the mole fraction of the participating species, and that $\overline{I}_{b\lambda} \neq I_{b\lambda}\left(\overline{T}\right)$. The absorption coefficient self-correlation, $\overline{\kappa}_\lambda$, will be ignored for the time being, that is, $\overline{\kappa}_\lambda$ will be assumed equal to $\kappa_\lambda\left(\overline{T}, \overline{x}_s\right)$, while $\overline{I}_{b\lambda}$ must be accounted for due to the strong non-linearity of the Planck function on temperature. Evaluating $\overline{I}_{b\lambda}$ from equation (3.88) and inserting into equation (3.91) gives

$$\overline{\kappa_\lambda I_{b\lambda}} \approx \bar{\kappa}_\lambda \bar{I}_{b\lambda}\left(\bar{T}\right) + \bar{\kappa}_\lambda \frac{\overline{T'^2}}{2}\left(\frac{\partial^2 I_{b\lambda}}{\partial T^2}\right)_{T-\bar{T}} + \overline{\kappa'_\lambda T'}\left(\frac{\partial I_{b\lambda}}{\partial T}\right)_{T-\bar{T}} \qquad (3.92)$$

The first and second term derivatives of the Planck function on the right of this equation are both positive, as it can be illustrated analytically. Consequently, the temperature fluctuations contribute to enhance the radiation that would be emitted by the medium if there were no fluctuations of the absorption coefficient of the medium, that is, if the last term were zero.

The influence of the correlation between the fluctuations of the spectral absorption coefficient and fluctuations of the temperature in equation (3.92) is not so evident. The spectral absorption coefficient of the medium is proportional to the mole fraction of the participating species. In general, in the case of gaseous radiation, the most significant participating species in combustions systems, namely CO_2 and H_2O, are positively correlated with temperature [149]. In fact, a fluctuation that locally increases the concentration of CO_2 and H_2O implies a greater conversion of reactants into products, and a corresponding increase of temperature. The reverse occurs in the case of a fluctuation that locally decreases the concentration of CO_2 and H_2O. This trend is confirmed by the state relationships [186], which are on the basis of several widely used combustion models for non-premixed flames such as the laminar flamelet model.

However, the spectral absorption coefficient of the medium is also a function of temperature, and decreases with the increase of temperature. It turns out that the influence of the mole fraction of the species on the absorption coefficient is greater than that of temperature, except at high temperatures, i.e., close to the stoichiometric mixture fraction. Therefore, the correlation between fluctuations of the spectral absorption coefficient and temperature fluctuations contributes to increase the radiation emitted by the medium above the level observed without fluctuations, with the possible exception of the flame front region, where the correlation may be negative [149]. However, even if the correlation is negative, it must compensate the positive contribution of the 2nd term on the right of Equation (3.92) to decrease the emitted radiation below the level observed without fluctuations.

If the total radiation intensity is considered, rather than the spectral radiation intensity, term B of equation (3.86) may be rearranged by Reynolds decomposition of the instantaneous absorption coefficient and blackbody radiation intensity into mean and fluctuating components. Proceeding as illustrated in (3.60) leads to

$$\overline{\kappa I_b} = \bar{\kappa}\frac{\sigma \bar{T}^4}{\pi}\left(1+6\frac{\overline{T'^2}}{\bar{T}^2}+4\frac{\overline{T'^3}}{\bar{T}^3}+\frac{\overline{T'^4}}{\bar{T}^4}+4\frac{\overline{\kappa' T'}}{\bar{\kappa}\bar{T}}+6\frac{\overline{\kappa' T'^2}}{\bar{\kappa}\bar{T}^2}+4\frac{\overline{\kappa' T'^3}}{\bar{\kappa}\bar{T}^3}+\frac{\overline{\kappa' T'^4}}{\bar{\kappa}\bar{T}^4}\right) \quad (3.93)$$

Ignoring correlations of order higher than two gives

$$\overline{\kappa I_b} = \bar{\kappa} I_b\left(\bar{T}\right)\left(1+6\frac{\overline{T'^2}}{\bar{T}^2}+4\frac{\overline{\kappa' T'}}{\bar{\kappa}\bar{T}}\right) \quad (3.94)$$

This equation confirms that the radiation emitted by the medium is augmented by temperature fluctuations and influenced by the correlation between the fluctuations of temperature and fluctuations of the absorption coefficient. If this correlation is positive, it reinforces the role of the temperature fluctuations and vice-versa.

The last term of equation (3.86), term C, accounts for the contribution to the transmissivity of the medium of the two-point correlation between fluctuations of the emission rate (product of the spectral absorption coefficient by the Planck function) and fluctuations of the transmissivity of the medium. There are no experimental data for this two point correlation, and as a result this term is rather difficult to calculate.

The TRI may be handled in a clear-cut way by solving the exact governing equations for flow, combustion and radiative transfer, since the exact equations account for this interaction. However, this DNS approach is not feasible in turbulence flows, except for simple geometries and low Reynolds numbers. Still, many studies have taken a similar approach to study the influence of turbulence on radiation, decoupling the flow field simulation from the radiative transfer calculation. These studies are generally limited to the propagation of radiation along a line of sight, and require as input the temporal and spatial distributions of temperature and absorbing species concentrations along that line [40]. If such information is available, then Equation (3.76) may be solved for a sufficiently large number of time instants, and averaged in time to provide the required mean and statistical data on the radiation intensity at the end of the line of sight. The approach outlined above is the most accurate one to study the influence of turbulence on

radiation, apart from DNS, but it has two main disadvantages. First, the RTE needs to be solved many times for every line of sight to achieve small statistical errors. This implies that the method is too time consuming for most practical applications, and becomes prohibitively expensive for coupled or uncoupled fluid flow/radiative transfer problems. Second, the spatial and temporal distributions of instantaneous temperature and species concentration are not available. These data need to be generated somehow, but care is needed to satisfy the mean values and variance of the temperature and species concentration, as well as spatial and temporal correlations.

The solution of the RTE for instantaneous scalar data has mainly been applied to determine the radiation intensity and corresponding statistical information along a line of sight, rather than for the complete solution of radiative transfer in an uncoupled fluid flow / radiative transfer problems. These more realistic problems are generally solved using the time-averaged form of the RTE, as described above.

3.8 Basis of the mathematical model

3.8.1 Flow model

The first step in our study is to calculate the fire structure. For free jet fires it has been shown that the boundary layer equations formulated for high-speed shear flows give a reasonable representation of the fire structure. The basis of the model used in this study is the parabolised Favre averaged Navier–Stokes equations in an axisymmetric co-ordinate system.

The system is closed using a variant of the $k-\varepsilon$ turbulence model (see equation(3.45)). The version of the $k-\varepsilon$ turbulence model implemented includes a modification to take account of the round jet/plane jet anomaly [168], where the spreading rate of round jets tends to be over predicted by the 'standard' version of the turbulence model. This is a well-known limitation of most two equation turbulence models and 2nd moment closure models unless some modification is introduced to account for the reduced spreading rate. Indeed the 2nd moment closure model of Jones and Musonge [187] was also applied to the jet fires considered here with little or no improvement. See Appendix A for a statement of the model.

The modification to the $k-\varepsilon$ model introduced is due to Morse [174], and has been used successfully in previous rim-stabilised fire simulations [174]. The axisymmetric correction is used here as it gives an appropriate balance between model complexity and predictive capability. In addition, a further modification to the turbulence model to account for buoyancy-induced turbulence was implemented [188], but ultimately was rejected as the improvement in the mean temperature field was marginal at best.

3.8.2 Turbulence combustion model

The turbulence combustion model is a laminar flamelet combustion model, with two flamelet libraries, one for combustion and the other for isothermal mixing. Combustion is assumed to be infinitely fast with a prescribed probability density function, Fairweather et al [189]. Two different probability density function have been investigated a beta PDF and a truncated Gaussian PDF. The shape of the probability density function at any spatial location is determined by a conserved scalar, the mixture fraction f and its variance f''^2, which are calculated using modelled transport equations, Fairweather et al [189]. The combusting flamelet is derived by calculating the adiabatic flame temperature at stoichiometric conditions, based on the sum of the chemical and sensible enthalpies which are conserved during the reaction.

$$H_{fu} - \sum_{i=1}^{N_{react}} x_i \left(h_i \left(T_{amb} \right) - h_i \left(T_{ref} \right) \right) + \sum_{i=1}^{N_{prod}} x_i \left(h_i \left(T_{adia} \right) - h_i \left(T_{ref} \right) \right) = 0 \qquad (3.95)$$

The flamelet for equivalence ratios other than the stoichiometric ratio is specified by assuming fast chemistry. This gives a flamelet similar to one calculated by assuming equilibrium. The equilibrium assumption for the hydrogen reaction is a reasonable assumption given the reactivity of hydrogen in air.

To account for radiation heat loss a transport equation for a specific enthalpy perturbation is solved,

$$\frac{\partial \bar{\rho} \tilde{U} \Delta h}{\partial z} + \frac{1}{r} \frac{\partial r \bar{\rho} \tilde{V} \Delta h}{\partial r} = \frac{1}{r} \frac{\partial}{\partial r} \left(r \frac{\mu_{eff}}{\sigma_{\Delta h}} \frac{\partial \Delta h}{\partial r} \right) + 4 K_a \sigma \left(\bar{T}^4 - T_{amb}^4 \right) \qquad (3.96)$$

where radiation heat loss is introduced using the optically thin approximation, [125]. The absorption coefficient, K_a is adjusted to gain agreement between the model and laboratory scale jet fire temperature measurements. The optically thin approximation is valid for hydrogen jet fires. This approach has been used successfully in other computational studies [190, 191]. The mean temperature is then calculated as,

$$\overline{T}_{adia} = \int_0^1 T(f) pdf(f)\, df$$
$$\tilde{T} = \overline{T}_{adia} - \frac{\triangle h}{C_{p,mix}\left(\overline{T}_{adia}\right)} \tag{3.97}$$

The use of the mean adiabatic temperature to evaluate the specific heat capacity of the mixture introduces a small error as $C_{p,mix}$ is a relatively weak function of temperature. This approximation makes the mean temperature an explicit function, easily evaluated compared to finding a solution to the non-linear function

$$f\left(\tilde{T}\right) = \overline{T}_{adia} - \tilde{T} - \frac{\triangle h}{C_{p,mix}\left(\overline{T}\right)} \tag{3.98}$$

3.8.3 Radiation model

A wide range of different radiation models have been used for jet fire simulation over the years. The models mainly differ from each other in the way they solve the spatial and angular field of intensity. The ray tracing models such as Discrete Transfer Method (DTM) [96] are theoretically good for fires but may become computationally expensive. In DTM, the RTE is integrated along the lines of sight, or rays, starting from the boundaries of the domain. The flux models such as the Discrete Ordinates Method (DOM) [95] and Finite Volume Method (FVM) [57] are currently receiving the most attention in new commercial CFD models. In these models, the solid angle is first divided into small control angles or directions, and the flux of intensity for each direction is solved separately in space. The DOM and FVM are very similar techniques. In the DOM, the angular distributions are defined by generalized moment matching quadratures schemes such as S_N and T_N quadratures. In the FVM, the polar/azimuthal discretisation is code specific but the angular integration is performed exactly. The most general technique is the Monte Carlo Method (MCM) [125] where

the radiative emission and absorption processes are modelled by sending photons with random energy and direction.

Another feature of the RTE that needs modelling is the calculation of the absorption coefficient, which depends on the local gas concentrations. In a typical jet fire, a grey gas is assumed, which means that a single value is used for the whole spectrum. Some aspects of the spectral resolution can be captured by dividing the spectrum to a relatively small number of bands, and solving a separate RTE for each band. In the combustion literature, a large number of wide-band models have been developed to account for the band-structure of the emission spectra of the most important combustion gases. The most accurate results using band models is obtained by using a narrow-band model, where separate RTEs are solved for hundreds of wavelengths. This is computationally expensive for practical fires.

Some of the challenges of radiation modelling are discussed:

- **Inhomogeneity**: The strong inhomogeneity of the optical properties and temperature field makes the simplest and fastest models such as the P-1 and six flux models attractive even though they are inaccurate. The presence of large optically thin areas aggravates the ray effect [192] for all the models dealing with discrete directions, especially ray tracing methods.

- **Emission source term**: For the spectrally integrated Radiative Transfer Equation, the emission source term is $kI_b = kT^4$ where T is the local temperature. Due to the T^4 - dependence, it is extremely sensitive to errors in temperature. For example, a 10% underestimation of temperature would lead to a source term that is 32% too small. In a large-scale simulation, this kind of error in the flame region can rarely be avoided. The problem is typically solved by modelling the emission source term as a linear function of heat release rate [193].

- **Spectral dependence**: Ways to handle the spectral dependence of the radiation are currently being studied to find computationally efficient ways to include both the smooth emission spectrum from soot and solid surfaces, and the spectral bands of gaseous combustion products.

- **Time dependence:** The inherent time dependence of the fires sets strong requirements for the computational efficiency. In Reynolds Averaged Navier-stokes codes, the radiation field must be updated within the internal iterations of the time step, but the computational cost can be relaxed by solving Radiative Transfer Equation only every N^{th} iteration.

- **Scattering:** The solution to a radiation problem is greatly simplified if the medium does not scatter which is the case with our flame structure. Due to no soot production in hydrogen flames, scattering has been neglected in our jet fire model. In this case the equation of transfer reduces to a relatively simpler integral equation as radiative equilibrium prevails.

Little work has been done on the influence of radiation on the turbulence fields. Radiative transfer enhances the dissipation of large thermal eddies and tends to smooth temperature fluctuations. This effect is especially significant if turbulence dissipation due to molecular diffusion is small compared to the radiative dissipation. Gas and particle radiation may significantly influence the structure of the spectrum of temperatures in the boundary layer. The effects of radiation increase with temperature, but decrease with the dissipation rate of turbulence kinetic energy.

3.8.4 Discrete transfer method

The radiation model considered in our study is the discrete transfer method (DTM) developed by Lockwood and Shah [194]. The method is numerically exact, geometrically flexible and easily coupled to a computational fluid dynamics solver. The DTM can be implemented with emissivity models such as the narrow band models [132] and exponential wide band models [195]. These models are discussed in detail in subsequent section.

A number of numerical techniques exist for solving the equation (3.81) governing the transfer of thermal radiation, examples being Hottel's zone method [196], Monte Carlo techniques [196] and flux models [194]. Each of the above methods have their merits and demerits, a comprehensive discourse of which can be found in [194]. The DTM algorithm has resemblances to all three numerical methods referred above, utilising the

merits of each without many of the demerits. The DTM will be implemented with one emissivity models in this work namely a narrow band model, RADCAL [132].

The discrete transfer method of calculating radiation heat transfer involves the tracing of representative rays from one surface to another through the domain of interest. The intensity distribution along each ray is calculated by solving a discretisation of the equation of radiative heat transfer. Essentially, the more rays traced, the more accurate the prediction of radiative heat distribution obtained. There are many situations where accurate prediction of radiative heat flux requires a large number of rays, particularly where the view factor from the high temperature emitting regions is small [197].

In the DTM the domain of interest is overlaid with a computational mesh and representative rays are traced from one surface to another, through the intervening control volumes defined by the mesh. From equation (3.78) for an emitting absorbing medium the transfer equation for thermal radiation along a ray, can be expressed in the form,

$$\frac{dI}{ds} = -K_a I + \frac{K_a \sigma T^4}{\pi} \tag{3.99}$$

For any representative ray the intensity distribution can be calculated by assuming each control volume is homogeneous. Under this assumption equation (3.99) can be integrated to give the recurrence relation

$$I_{n+1} = \frac{\sigma T^4}{\pi}\left(1 - e^{-k_a \Delta s}\right) + I_n e^{-K_a \Delta s} \tag{3.100}$$

where I_n and I_{n+1} are the intensity of the ray on entry and exit respectively and Δs is the distance travelled in the control volume. Consequently, given the initial intensity at a point on an emitting surface, the change in intensity along the ray can be calculated using equation (3.100). The initial intensity is specified by taking the walls to be Lambert surfaces or if the ray intersects an opening it is treated as a cold black surface emitting at the ambient temperature.

For grey walls the emitted intensity is dependent on the incident flux q^-

$$q^{-} = \int_{2\pi} I_w^{-}(\Omega)\cos\theta d\Omega \tag{3.101}$$

Where $I_w^{-}$is the incident intensity. In the DTM the incident flux integral is replaced by a numerical quadrature

$$q^{-} = \sum I_w^{-}(\Omega)\cos\theta d\Omega \tag{3.102}$$

The values of incident intensity I_w^{-} at a point on a wall are calculated by tracing rays from the point and backtracking from the walls intercepted, applying equation (3.100) through each control volume. Therefore for grey walled enclosures the coupling between the incident flux and emitted intensity make the DTM a guess and correct procedure in which an estimate of the incident flux distribution is iteratively improved. A number of improvements have been suggested over the years Cumber [198], Malalasekera and Henson[199].

In my model the radiation fields are decoupled from the fluid flow model. As our focus is on the free jet fires the boundary conditions for all rays are prescribed using cold black boundary conditions. This simplifies the DTM to require a single iteration to converge.

3.8.5 Narrow-band statistical model

This model has been used extensively in modelling radiative properties of atmospheric gases. They provide a function for the transmissivity average over a spectral band, typically $10cm^{-1}$ to $100cm^{-1}$ wider. This bandwidth is chosen because it is typically large enough to include many rotational lines of approximately uniform statistical properties, but small enough so that the Planck function is approximately constant. By assuming uniform statistical properties over each band, analytical expressions can be derived for the transmissivity as a function of pressure and path-length. These expressions can be fitted to experimental data for homogeneous paths of a given species, yielding the necessary narrow band parameters.

When calculating spectral radiative fluxes from a molecular gas one finds that the gas absorption coefficient and with it, the radiative intensity varies much more rapidly

across the spectrum than other quantities, such as blackbody intensity, etc. It is, therefore, in principle possible to replace the actual absorption coefficient (and intensity) by smoothened values appropriately averaged over a narrow spectral range. In principle, narrow band calculations can be as accurate as line-by-line calculations, provided an "exact" narrow band average can be found [181].

Examination of the formal solution of the radiative transfer equation (3.81) demonstrates that all spectral integrations may be reduced to

$$\int_0^\infty \kappa_\lambda I_{(b)\lambda} d\lambda \quad \text{and} \quad \int_0^\infty \kappa_\lambda I_{(b)\lambda} \left[1 - \exp\left(-\int_0^s \kappa_\lambda ds\right)\right] d\lambda, \tag{3.103}$$

where $I_{(b)\lambda}$ denotes that either $I_{b\lambda}$ or I_λ can occur. The Planck function will never vary appreciably over the spectral range of a few lines, considering that adjacent lines are very closely spaced (measured in fraction of cm^{-1}) [181]. Local radiation intensity I_λ, on the other hand, may vary just as strongly as the absorption coefficient, since emission within the gas takes place at those wave-numbers where κ_λ is large [see equation(3.85)]. However, we limit our consideration to non-scattering media, the formal solution of the radiative equation of transfer, equation(3.81), demonstrates that all spectral integrations involve only the Planck function, and not the local intensity. For such a constrained circumstance we may simplify expressions(3.103), with extremely good accuracy, to

$$\int_0^\infty I_{b\lambda} \left\{ \frac{1}{\Delta\lambda} \int_{\lambda - \Delta\lambda/2}^{\lambda + \Delta\lambda/2} \kappa_\lambda \, d\lambda' \right\} d\lambda \tag{3.104}$$

and

$$\int_0^\infty I_{b\lambda} \left\{ \frac{1}{\Delta\lambda} \int_{\lambda - \Delta\lambda/2}^{\lambda + \Delta\lambda/2} \left[1 - \exp\left(-\int_0^s \kappa_\lambda ds\right)\right] d\lambda' \right\} d\lambda. \tag{3.105}$$

The expressions within the large braces are local averages of the spectral absorption coefficient and of the spectral emittance, respectively, indicated by an overbar.

$$\overline{\kappa}_\lambda (\lambda) = \frac{1}{\Delta\lambda} \int_{\lambda - \Delta\lambda/2}^{\lambda + \Delta\lambda/2} \kappa_\lambda \, d\lambda', \tag{3.106}$$

$$\bar{\varepsilon}_{\lambda}(\lambda)=\frac{1}{\Delta\lambda}\int_{\lambda-\Delta\lambda/2}^{\lambda+\Delta\lambda/2}\left[1-\exp\left(-\int_{0}^{s}\kappa_{\lambda}ds\right)\right]d\lambda'. \qquad (3.107)$$

For clarity, it is worth mentioning that the definition of $\bar{\kappa}$ in equation (3.106) is not sufficient since $\bar{\varepsilon}\neq 1-\exp(-\bar{\kappa}s)$. Nevertheless, one can anticipate that the spectral variation of $\bar{\kappa}$ and $\bar{\varepsilon}$ is relatively smooth over the band, making spectral integration of the radiative heat flux feasible. For our investigation we have implemented Grosshandler's narrow band radiation model, RADCAL [132].

3.8.6 Wide-band models

Where we are only interested in finding heat fluxes or divergences of heat fluxes integrated over the entire spectrum, it is attractive to have models that can readily predict the total absorption or emission from an entire band. These models are known as wide band models since they treat the spectral range of the entire band. Wide band permits us to determine the radiative emission (or the absorption of incoming radiation) from a volume of gas over an entire vibration-rotation band with a single calculation except they are inherently less accurate than narrow band models.

Wide-band models provide correlations for the absorptivity from an entire absorption band in terms of the physical state of the gas. The absorptivity is usually expressed in terms of the effective bandwidth $\bar{A}_1$ define as,

$$\bar{A}_1=\int_{bandwidth}\left(1-\exp\left(-a_w L\right)\right)dw \qquad (3.108)$$

where L is the path-length through the gas.

The effective bandwidth can be used to characterise the radiative properties of a given absorption band and allows for the calculation of radiative exchange within that region of the spectrum. The total radiative exchange problem then involves summing the contributions from each spectral region. Water has only four significant absorption bands at flame temperatures; hence this method provides great computational savings.

Use of this method requires correlations of the effective bandwidth for each significant band of the radiating gases as a function of a number of parameters; the path-length, temperature, total pressure, and mole fraction of participating species. Correlation data, such as wide band, comes from theory, experiments, or a combination of both. Wide-band models have been used extensively in atmospheric science [125] and combustion applications [179] and data have been compiled for a range of gases at the required temperature and pressure ranges. They provide greater computational savings, approximately an order of magnitude over narrow-band statistical models, at the expense of less accuracy. Initially wide band models were considered as an alternative to the narrow band model implemented but were ultimately rejected because of the accuracy issues.

3.9 Concluding remarks

We have presented and developed the transport equations for our jet fire model and by extension the thermal radiation model. In Chapter Four we use the transport equation developed to investigate lifted hydrogen jet fires. The lift-off model was originally proposed by Sanders and Lamers [48] and modified by Cumber and Spearpoint [49]. In this study the model has been extended to predict lifted hydrogen jet fires. The model is based on the laminar flamelet quenching concept which is extended to predict lifted hydrogen jet fires. The original model was applied to lifted methane jet fires, Cumber and Spearpoint [49] demonstrating that for a lifted methane jet fires the large scale strain rate, the eddy strain rate was the important parameter in determining the liftoff height rather than the strain rate at the smaller scales nearer the molecular scale. The lift-off model presented in the next chapter is based on a parabolic flow model and as such the use of the laminar flamelet quenching is a convenient lift-off model and it yields reasonably accurate predictions of the mean lift-off heights.

Chapter 4

Lifted hydrogen jet flames

A vehicle fuelled by hydrogen is likely to have a pressure relief system in case of accident. Should the relief valve lift then a jet of hydrogen will form. If the jet of hydrogen finds a source of ignition it will form a lifted jet fire based on the typical valve diameters and source velocities encountered. Therefore the understanding of lifted jet fires is of interest to industrial combustion engineers. Turbulence jet flames occur in many areas of industry either by accident such as following the ignition of a leak from a high pressure plant processing hydrocarbons or in a controlled environment such as a furnace or industrial burner. In a turbulent jet the flow is characterised by the diameter of the nozzle or pipe, the fuel composition and the speed of the fuel at the nozzle exit. For a given fuel and nozzle diameter, if the jet speed is sufficiently low the flame is attached or rim-stabilised. If the jet speed is gradually increased then at some critical velocity the jet lifts off and the flame structure fundamentally changes. Immediately downstream of the nozzle the flow is non-reacting, further downstream combustion is initiated at a fluctuating flame base followed by the main body of the jet flame. Figure 4.1 shows a schematic diagram of the lift-off region of a lifted flame with the mean lift-off height labelled.

Lifted flames are found in practical applications such as burners in commercial boilers, where the lifted jet flame is utilised to reduce the damage to nozzle material by minimising contact between the flame and the nozzle. Elevated flares also involve lifted flame phenomena. Combustion of stratified mixtures, such as those witnessed in turbines as well as diesel and direct fuel-injection gasoline engines and even mine fires, have elements of their reaction zone structures that prompt comparisons to the edge of the laboratory lifted flame.

Fundamentally, lifted flames are of interest since they are simple systems which exhibit important characteristics of finite-rate chemistry, turbulence-chemistry interaction, effects of heat release, local extinction of combustion as well as a host of other effects. In addition, lifted flames are interesting from a scientific point of view because many of the flame stabilisation and extinction controlling mechanisms are involved. This

simplicity lends them to joint modelling and experimental efforts in ongoing investigation to develop predictive codes in turbulence combustion.

For most fuels lift-off of the flame occurs at fairly low fuel exit velocities, and as a result lift-off is an important phenomenon. A lifted turbulence diffusion flame consists of a cold flow near field region and a non-equilibrium flame region, separated by the fluctuating flame base. The distance from the nozzle to the flame base is called the lift-off height. As stated in chapter two the mechanism for flame lift-off is a competition between chemical and mixing processes characterised by a chemical reaction time and a flow residence time. The ratio of these time-scales is defined as the Damköhler number. As the jet velocity increases the flow residence time decreases. At the critical velocity or Damköhler number there is insufficient time for the chemical reaction to take place and lift-off occurs, Sanders and Lamers [48]. This regime is the primary focus of this chapter.

4.1 Investigation of lift-off flames

Two main problems characterise the calculation of a lifted turbulence diffusion flame. Firstly the mean lift-off height has to be determined and secondly the fluctuating behaviour of the flame base must be taken into account. The lift-off model developed in this investigation is described below.

4.1.1 Modelling of lift-off height

If lift-off occurs through laminar diffusion flamelet quenching, then the topology of the lifted flame is a disconnected surface of instantaneous stoichiometry. Local quenching of the flame occurs through the disconnectedness. This is caused by local values of the stretch or non equilibrium parameter, higher than the quenching value. At these points no flame can exist, and these positions are called holes [82]. The fraction of burnable flamelets, which is equal to one minus the probability that a hole is present at a certain position, can be estimated by integrating the probability density function of the relevant stretch parameter up to the quenching value of a laminar diffusion flame. This fraction of burnable flamelets is also called the probability of burning.

$$P_b = \int_0^{\Omega_q} P(\Omega)\, d\Omega, \tag{4.1}$$

in which Ω is the stretch parameter, which can be the scalar dissipation rate χ or the strain rate s. The quenching value Ω_q is determined from laminar diffusion flamelet calculation [52] or from experiments [82]. The form of the probability density functions $P(\Omega)$ are a lognormal distribution for the scalar dissipation [51] and a quasi Gaussian probability density function for the strain rate [200]. The latter is written as

$$P(s) = \frac{2}{(2\pi\sigma_s)^{1/2}} \exp\left(-\frac{s^2}{2\sigma_s{}^2}\right). \tag{4.2}$$

Here σ_s denotes the variance. The mean and variance are coupled by the equation

$$\tilde{s} = \left(\frac{2}{\pi}\right)^{1/2} \sigma_s. \tag{4.3}$$

If too many holes are present, or the probability of burning is too low, on the contour of the stoichiometric mixture where the flame is located instantaneously, the flame cannot be stabilised at the burner rim and lift-off occurs. The fraction of holes which is allowed until the lift-off can be roughly estimated with percolation theory. This theory can be used to describe the threshold behaviour of the lift-off of the flame by means of the probability of burning [82]. This idea leads to a lift-off condition involving both a percolation threshold P_c and a probability of burning P_b [51].

$$P_b = P_c \tag{4.4}$$

at a radial position where the mean mixture fraction $\tilde{f}$ is at the stoichiometric value $\tilde{f} = f_{st}$. If equation (4.4) is used at the mentioned radial position, with the probability density function $P(\Omega)$ inserted into equation (4.1) for P_b, then a relationship is obtained between Ω_q and the mean $\tilde{\Omega}$, with the variance of Ω as a parameter. The mean and the variance of Ω are supposed to completely determine the probability density function $P(\Omega)$. The above procedure leads to the following lift-off condition if the strain rate is used for Ω

$$P_c = erf\left(\frac{s_q}{\tilde{s}\,(r = r_{st})\,\pi^{1/2}}\right), \tag{4.5}$$

where r is the radial distance from the symmetry axis. If the value of P_c is about 0.63 [51], then this equation can be simplified to approximately

$$\tilde{s}\left(r = r_{st}\right) = \frac{s_q}{P_c \pi^{1/2}} \tag{4.6}$$

If the scalar dissipation rate is used, then the lift-off condition

$$\tilde{\chi}\left(r = r_{st}\right) \approx \chi_q \tag{4.7}$$

is obtained with $P_c = 0.63$ and $\sigma_\chi = 0.5$ [51]. In the following several opinions are given to support the choice of the strain rate for Ω, and the practical justification of this choice is demonstrated with the results obtained in this investigation in which the slope of the $z_L\left(U_0\right)$ curve (lift-off height, z_L as a function of source velocity, U_0) is the primary important parameter and has been published [201]. In [48] four arguments are presented in favour of the strain rate as the stretch parameter rather than the scalar dissipation rate.

Firstly, laminar counter-flow diffusion flames are considered. They are the cornerstone for laminar flamelet models in turbulent combustion [52]. In these counter-flow diffusion flames the strain rate imposed on the flame gives rise to stretch effects, leading to non-equilibrium chemistry. The scalar dissipation rate is just the consequence of this strain rate. Additionally, the scalar dissipation rate should be evaluated. Often the scalar dissipation rate at stoichiometric conditions χ_{st} is chosen [52], but conditioning of the scalar dissipation rate on a specific value of the mixture fraction leads to a fundamental problem. The flamelet concept leads to the following general expression for the mean of a scalar

$$\overline{\phi} = \int_0^1 \int_0^\infty P\left(f, \Omega\right) \phi\left(f, \Omega\right) d\Omega \, df, \tag{4.8}$$

in which $P\left(f, \Omega\right)$ is the joint probability density function for the mixture fraction and the stretch parameter Ω and $\phi\left(f, \Omega\right)$ is a scalar and a function of the mixture fraction with Ω as a parameter. If Ω is chosen to be the scalar dissipation rate conditioned on stoichiometry $\left(\Omega = \chi\left(f = f_{st}\right)\right)$ then $P\left(f, \chi_{st}\right)$ has no meaning other than $P\left(\chi_{st}\right)$. This

is not realistic because no account would be taken of the mixture fraction fluctuations. In practical calculations this inconsistency has been solved by simply stating that there is no satisfactory model for the conditioned scalar dissipation rate, and so the unconditioned model $\tilde{\chi} = 2\varepsilon g/k$ was used, with g the scalar variance and k is the turbulence kinetic energy. In that case, assuming statistical independence, $P(f,\Omega) = P(f)P(\Omega)$, the integral in equation (4.8) can be evaluated. The strain rate, however, need not be conditioned on any particular mixture fraction value because it is a boundary condition in a counter-flow diffusion flamelet, so this problem does not arise.

Secondly, a more serious problem is the increase of the quenching value of the scalar dissipation rate at quenching of a laminar counter-flow diffusion flamelet if the mass fraction at the fuel boundary is decreased. This is contrary to the value of the strain rate at quenching, which decreases with decreasing fuel mass fraction, as it ought to be. As a result, if the scalar dissipation rate is used as the stretch parameter, then the application of the lift-off condition as stated above, would yield shorter lift-off heights if the fuel stream is diluted, which is unphysical.

Thirdly, Peters [51, 202] used a lift-off condition similar to equation (4.7). The gradients of the predicted $z_L(U_0)$ curves were not in agreement with the experiments. The differences might be clarified by the different scaling properties of the scalar dissipation rate and the strain rate. The scalar dissipation rate on the axis of an isothermal axisymmetric jet scales with x^{-4} while the strain rate with x^{-2}. Although the points where the mean mixture fraction is stoichiometric are not located on the axis, it is fair to say that there is a large difference between these two variables regarding their scaling properties. Owing to the slower decrease of the strain rate in axial direction, the lift-off condition, equation (4.6) will be met at higher x-values leading generally to higher lift-off heights in better agreement with experiments.

Lastly, if the scalar dissipation rate is preserved as the descriptor of stretch effects, it is still basically a strain rate. This is due to the fact that the flame thickness in mixture fraction space is constant, independent of the stretch imposed on the flamelet. Ultimately the scalar variance g is replaced by the flame thickness, leading to a scalar dissipation rate at the position of the flame

$$\tilde{\chi}_F \sim \varepsilon/k\,, \tag{4.9}$$

which essentially is the strain rate of the large eddies.

4.1.2 Modelling of the fluctuating base

The fluctuating flame base will be handled by initiating a probability density function for the location of the flame base $P(x_L)$ where x_L denotes the axial distance from the nozzle to the flame base. The mean scalar quantities such as density and temperature can now be written as

$$\begin{aligned}\overline{\phi}(x) = \int_0^\infty P(x > x_L)\,dx_L \times \int_0^\infty \int_0^1 P(f,s)\phi(f,s)\,df\,ds \\ + \left(1 - \int_0^\infty P(x > x_L)\,dx_L\right) \times \int_0^\infty P(f)\,\phi(f)\,df\,.\end{aligned} \tag{4.10}$$

In equation (4.10) the last term is the isothermal value of the scalar, and the factor in front of it is the probability that the flame base is located downstream of *x*. The probability that the instantaneous flame base is upstream of *x* is denoted by $P(x > x_L)$. The first term in equation (4.10) is valid in the burning part of the jet, and is due to both burning and non-burning flamelets, where the average must be calculated over the mixture fraction and the strain rate must be assumed if no transport equations for the probability density functions are to be solved, so $P(f,s) = P(f)\,P(s)$

For a lifted flame any mean property can be calculated as a weighted average of the burning and isothermal mixing flamelet weighted by the PDF and integrated over instantaneous mixture fraction,

$$\tilde{\varphi} = P_d P_b \int_0^1 P(f)\,\varphi_b(f)\,df + (1 - P_d P_b) \int_0^1 P(f)\,\varphi_m(f)\,df \tag{4.11}$$

where P_b is a probability of burning defined in equation (4.1) and P_d is a probability that the axial location is above the fluctuating flame base.

$$P_d = \int_0^\infty P_{base}(z > z_L)\,d\,z_L \tag{4.12}$$

Sanders and Lamers prescribe the PDF for the location of the instantaneous flame base, z_L to have a triangular shape, the apex located at the mean lift-off height and the base of the triangle is taken to be five nozzle diameters. It should be noted that this is an assumption of convenience rather than one based on observation, however a sensitivity study has shown that the overall flame structure is insensitive to this aspect of the model. The mean density and mean adiabatic temperature are given by the relations,

$$\bar{\rho} = \left[\frac{P_d P_b}{\int_0^1 P(f)\rho_b(f)df} + \frac{1-P_d P_b}{\int_0^1 P(f)\rho_m(f)df} \right]^{-1}$$
$$\bar{T}_{adia} = P_d P_b \bar{\rho}_b \int_0^1 P(f)\frac{T_b(f)}{\rho_b(f)}df + (1-P_d P_b)\bar{\rho}_m \int_0^1 P(f)\frac{T_m(f)}{\rho_m(f)}df \tag{4.13}$$

To close the system the probability of burning and the mean lift-off height must be modelled. The probability of burning is given by,

$$P_b = \int_0^{s_q} P(s)\,ds \tag{4.14}$$

s is the strain rate, s_q is the quenching strain rate and $P(s)$ is a quasi Gaussian probability density function for the strain rate. Sanders and Lamers [48] give a quench strain rate of $565s^{-1}$ derived from an analysis of diluted methane–air counter flow diffusion flames. However a sensitivity study indicates that lift-off predictions are fairly insensitive to the quench value used, Cumber and Spearpoint [49]. The strain rate can either be taken to be the strain rate of the small-scale turbulence,

$$s = C_{s,1}\left(\frac{\varepsilon}{2\nu_l}\right)^{1/2} \tag{4.15}$$

or the strain rate of the large-scale turbulence.

$$s = C_{s,2}\frac{\varepsilon}{k} \tag{4.16}$$

where $C_{s,1}$ and $C_{s,2}$ are calibration constants. The laminar dynamic viscosity is given by Sutherland's law. The mean lift-off height is prescribed using percolation theory, Peters and Williams [51] and the probability of burning on the stoichiometric contour,

$$z_L \left(P_b = P_c \right)$$
$$s\big|_{r=r_{st}} = \frac{s_q}{P_c \pi^{1/2}} \tag{4.17}$$

the above equation is an approximation to the error function and implicitly gives the percolation threshold, P_c, see Cumber and Spearpoint [49] for more details of the lift-off model.

A third lift-off model is considered based on a correlation for lift-off height using a turbulence time-scale threshold.

$$z_L \left(\frac{k}{\varepsilon} = t_{thresh} \right) \tag{4.18}$$

The turbulence time-scale is evaluated on the jet axis. For methane jets t_{thresh} is $5\times10^{-3}s$. In this study it will be fixed by calibrating against one of Kalghatgi's jet fires [39]. This lift-off model is considered here as it is consistent with a parabolic flow model without modification and has been used in the past to predict the lift-off height of methane jet fires in a cross-flow, Fairweather et al. [189]. In this model the transition from no reaction to combustion is instantaneous at the lift-off height.

4.2 Boundary conditions and numerical parameters

In all of the simulations presented in Figure 4.6 the bulk inlet conditions are given by the nozzle diameter and the average source velocity. The mean stream-wise velocity distribution and radial velocity distribution are taken to be consistent with fully developed pipe flow that is a $1/7^{th}$ power law is prescribed for the stream-wise velocity distribution and zero for the radial velocity component. Nozzle exit turbulence profiles are prescribed to be given by equilibrium profiles for fully developed turbulence pipe flow. Our choice of fuel considered is hydrogen and Figure 4.2 shows a schematic representation of the jet flame in air. For some of the jets considered the source velocity is above the local sound speed. To accommodate the compressibility of the flow the source condition is modelled as a nozzle and the jet expanded isentropically to atmospheric pressure. For all simulations in this study 80 control volumes in the radial co-ordinate direction spanning the jet radius are used to calculate the flame structure,

with a maximum fractional step in the axial direction of less than 1% of the radial control volume spacing. A number of simulations using 160 control volumes were also completed to confirm that the predictions presented are independent of further mesh refinement. It is estimated that the predicted lift-off heights are within 2% of the fully mesh converged values.

4.3 Description of numerical algorithm

When considering how a lifted flame differs from a rim-stabilised flame in the context of the mathematical model described above, the key difference is the composite probability of burning field,

$$P_{burn} = P_b P_d \tag{4.19}$$

In a rim-stabilised flame P_{burn} is one everywhere, whereas in a lifted flame this takes a value between zero and one. Zero below the lift-off region, between zero and one in the lift-off region and one above it. Therefore an algorithm based on a ‘‘guess and correct” approach for the composite probability of burning field suggests itself as one way of extending a parabolic flow model suitable for simulating rim-stabilised jet fires to simulate lifted jet fires. An overview of the algorithm in the form of a flow chart is given in Figure 4.3. To initialise the process some estimate of the composite probability of burning field must be prescribed. There are a number of possibilities, for example the fire could start off as being rim-stabilised, and hence the initial composite probability of burning field could be set to one everywhere. An alternative choice is to prescribe the jet to be isothermal, with a composite probability of burning of zero everywhere. Both options have some appeal as in the initial rim-stabilised fire approach $\left(P_{burn,0} = 1\right)$, this is how a lifted jet fire would initiate, alternatively the analysis of Pitts [46] work on isothermal jets indicates that the non-reacting isothermal region upstream of the flame base is important in the flame stabilisation process, favouring the second approach $\left(P_{burn,0} = 0\right)$. In Cumber and Spearpoint [49] both approaches were evaluated and taking the initial lift-off height to be zero, i.e., a rim-stabilised fire gave a marginal improvement in convergence rate compared to starting with a non-combusting isothermal simulation of the jet. Once the composite probability of burning field is prescribed, an estimate of the flame structure can be calculated by running the parabolic flow model. As the flame structure is calculated flow fields required to estimate the lift-

off height and the composite probability of burning field, such as the mean mixture fraction, mean temperature, turbulence kinetic energy, and the dissipation rate of the turbulence kinetic energy, are stored. Once the flame structure is complete, a new estimate of the lift-off height is calculated and the composite probability of burning field recalculated. If the change in lift-off height is small the algorithm is terminated otherwise the flame structure is recalculated and the process continues.

4.3.1 Large and small-scale rates

An iterative procedure poses the important question of 'how fast does the algorithm converge and what is an appropriate convergence criterion? To illustrate the convergence behaviour of the algorithm a typical jet fire is used. The jet fire simulated is the same in each case, (a nozzle diameter of d = 2.95 mm, a source velocity of U_0 = 1190 m/s). Figure 4.4a shows the convergence history for two simulations using the two different strain rate models. The relative change in mean lift-off height is plotted against the iteration number. Considering the simulation using the large-scale strain rate sub-model convergence is monotonic for the first twenty iterations after which round-off error prevents further convergence, however the differences in predicted lift-off heights for successive iterations using the large-scale strain rate model is less than 10^{-5} % and changes of less than 1% is sufficient for the lift-off height to be converged to the visual resolution of Figure 4.4b. In Figure 4.4b the lift-off height as a function of iteration number is shown for the two simulations. Figure 4.4a and b taken together suggest for the large-scale strain rate model the algorithm takes around 5–6 iterations to converge.

Considering the convergence history for the small-scale strain rate simulation, the situation is less satisfactory. The convergence rate is slower than the large-scale strain model simulation and round-off error has a larger effect on the convergence history. Oscillations in the relative difference occur with peak relative differences of the order of 10^{-3} % although a relative difference of 0.5% is sufficient for the methodology to have converged to the resolution of Figure 4.4b. The slower convergence means that for the small-scale strain rate model the flame structure takes of the order of 10 iterations to converge. The relatively poor convergence behaviour of the simulations using the small-scale strain rate sub-model is believed to be due to its dependence on the dissipation rate of turbulence and the kinematic viscosity. These two properties are

weakly correlated and when the lift-off height changes these two properties respond differently to the change in the mean temperature field. This convergence problem is lessened when more control volumes are introduced in the radial co-ordinate direction, with of course an increase in computational cost. The large-scale strain rate sub-model does not suffer from this problem as its dependency on turbulence parameters alone means that it responds in a consistent way to changes in the mean temperature field brought about by changes in the predicted mean lift-off height.

4.3.2 Lift-off height model calibration

The three lift-off models are calibrated for lifted hydrogen jet fires, using one of Kalghatgi's [39] experiments, d = 2.95 mm and U_0 = 1190 m/s. This particular jet was chosen as it had one of the highest source velocities that were still subsonic. This has the advantage that the isentropic nozzle approximation does not influence the calibration. Fitting the models to this data gives values of

$$C_{s,1} = 0.0023 \quad and \quad C_{s,2} = 0.0073 \quad and \quad t_{thresh} = 7.9 \times 10^{-5} s \tag{4.20}$$

for the calibration constants in the strain rate sub-models and the turbulence time-scale sub-model respectively.

4.4 Lifted Jet Flame Model Predictions

Before presenting the validation of the model for lifted jets it is of interest to explore how the lift-off models influence the local flame structure in the lift-off region. Figure 4.5 shows the predicted temperature field in the lift-off region. Three simulations are shown, each differing in the sub-model used to predict lift-off. This jet fire (d = 2.95 mm, U_0 = 1190 m/s) is used for illustrative purposes as it is the jet fire used for calibrating the models and so in each simulation the lift-off height is the same. For each temperature field five equi-spaced contours are shown, starting at 600 K increasing in increments of 300 K, the lowest temperature nominally defining the boundary of the jet. To aid interpretation an arrow on each of the predicted temperature fields indicates where the mean temperature is increasing. The main points of note are that the temperature fields predicted using the two strain rate models are remarkably similar. This is different to previous simulations of lifted methane jets, Cumber and Spearpoint

[49]. Another point of note is the flame structure in both simulations is physically plausible as the combusting region is initiated off axis where the stoichiometric contour is located and the mean temperature increases relatively smoothly with increasing axial distance. Considering the predicted temperature field calculated using the turbulence time-scale to predict lift-off the predictions are not physically plausible as combustion is initiated as a step change in flow conditions at the lift-off height across the width of the jet. Taking this analysis one stage further would result in an over prediction of the received radiation field in the near field. However considering all three simulations someway downstream of the lift-off region, the predicted temperature field is insensitive to how the lift-off region is modelled.

Figure 4.6 shows the lift-off height as a function of source velocity for six different nozzle diameters. The lift-off height for a given fuel is primarily dependent on the source velocity with the nozzle diameter having a much weaker influence on the lift-off height. As discussed above, to make a fair comparison of the three lift-off models they were all calibrated against a single datum, d = 2.95 mm, U_0 = 1190 m/s, see Figure 4.6c. Considering the small-scale strain rate model predictions of lift-off height, this model gives the overall best agreement with the measured lift-off height measurements as the lift-off measurements for nozzle diameters of 1.74, 2.95 and 4.06 mm are predicted reasonably well. For the smallest nozzle diameter, 1.08 mm there is a tendency to under-predict the lift-off height for the intermediate and high source velocities. This discrepancy in the model will be considered further below. Considering the predicted lift-off heights calculated with the large-scale strain rate although some of the predicted lift-off heights are in close agreement with the measurements, particularly for the nozzle diameter of 2.95 mm, for the most part the gradient

$$\frac{dz_L}{dU_0} \tag{4.21}$$

is under-predicted making it a poor choice for application to jet fires outside the envelope of Kalghatgi's experiments. The turbulence time-scale model exhibits the worst performance of all three lift-off models, as for each nozzle diameter it predicts the lift-off height for one source velocity. Overall all models tend to under-predict the lift-off height for small diameters and tend to over-predict the lift-off height for larger diameter nozzles.

The superiority of the small-scale strain rate model compared to the large-scale strain rate model for lifted hydrogen jet fires is particularly interesting given previous experience of simulating lifted methane jet fires, Cumber and Spearpoint [49] where the opposite was the case. The major difference between the methane and the hydrogen jet fires is that the mean strain rate for the hydrogen jet fires is much higher.

Considering how the lift-off height predictions could be improved, the most obvious weakness is the isentropic nozzle approximation used to account for compressibility effects for sonic source conditions. For the smaller diameter nozzles where the higher source velocities are possible, combining the flame structure model with a compressible flow solver, [18] to resolve the shock structure downstream of the nozzle should improve model performance. As well as resolving the shocks this will also introduce compressibility effects on the turbulence field as turbulence mixing tends to be reduced in high Mach number flows. The mechanism for this is believed to be shocks in the instantaneous flow fields, so called 'eddy shocklets'. This effect would tend to increase the predicted lift-off height. Note this would improve the agreement for the smaller diameter nozzle jets for source velocities above 1200 m/s. For the larger nozzle jets most measured lift-off heights are for source velocities below Mach one where significant compressibility effects on turbulence mixing would occur.

4.5 Concluding remarks

An important characteristic of the lifted jet fire methodology is the flame structure is calculated using the boundary layer approximation. The advantage of this is finite volume mesh independent predictions of the mean flow fields can be calculated on readily available computer resources. The simulations presented here typically required of the order of 5 minutes run-time on a PC with a 450MHz Pentium III processor. This has allowed a rigorous calibration of the lift-off models considered.

The major difference between Sanders and Lamers analysis and our study is the turbulence model implemented. The use of an axisymmetric correction to the turbulence model proved critical in evaluating the capabilities of the lift-off models. The turbulence model has been validated for lifted jets and can predict lift-off heights reasonably accurately.

The predicted mean temperature fields downstream of the lift-off region are similar for all three simulations. Therefore, the flame structure downstream of the lift-off region is fairly insensitive to the lift-off region see Figure 4.5. In chapter five we will validate the flame structure downstream of the lift-off region using a wider range of measurement. Detailed predictions of the mean temperature, RMS temperature and chemical species will be presented.

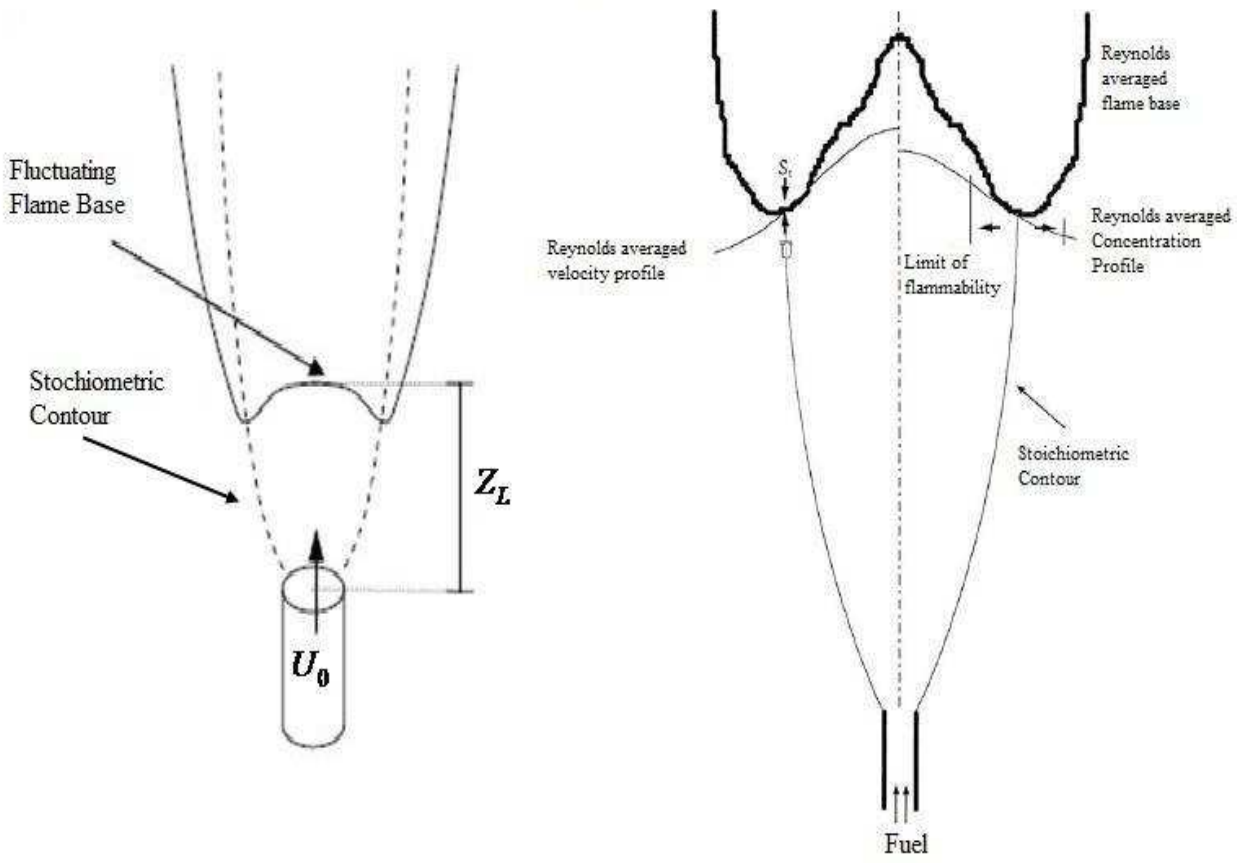

Figure 4. 1: Schematic diagram of a lifted flame in a lift-off region.

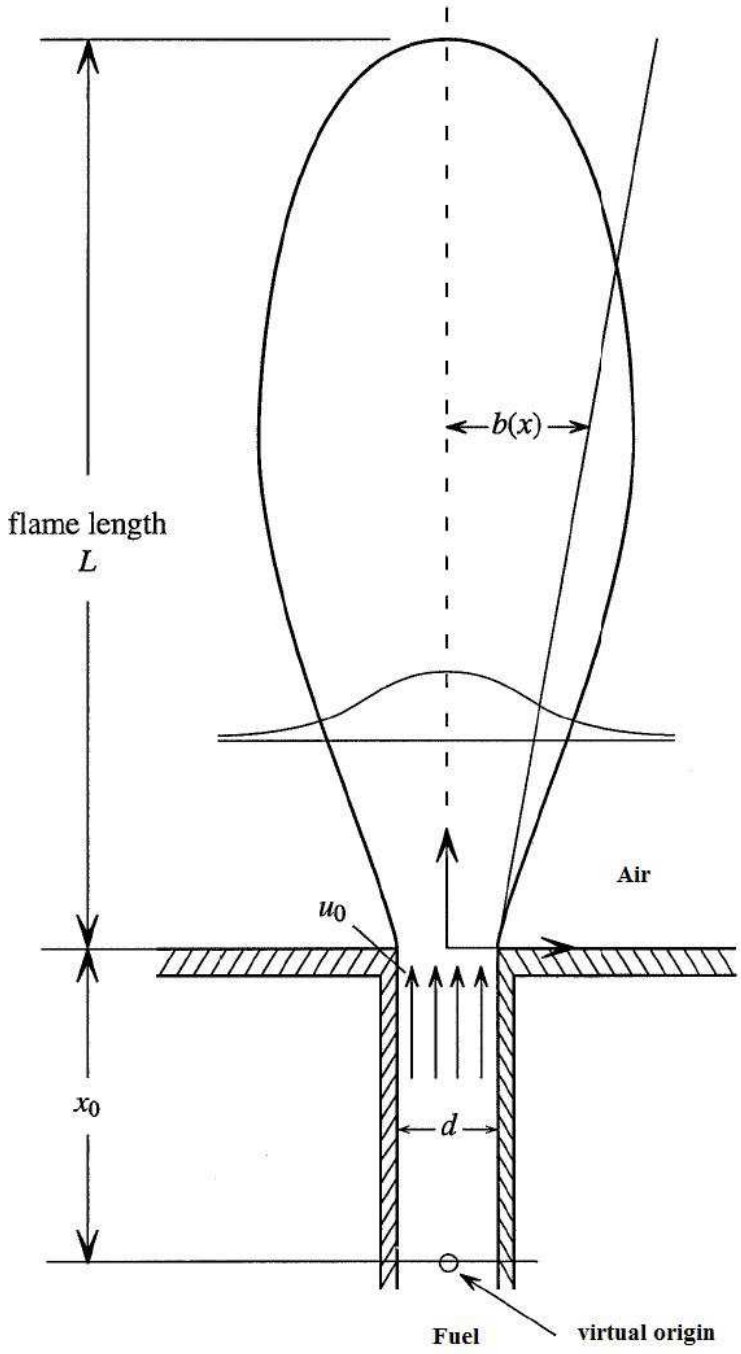

Figure 4. 2: Schematic representation of a vertical jet flame into quiescent air

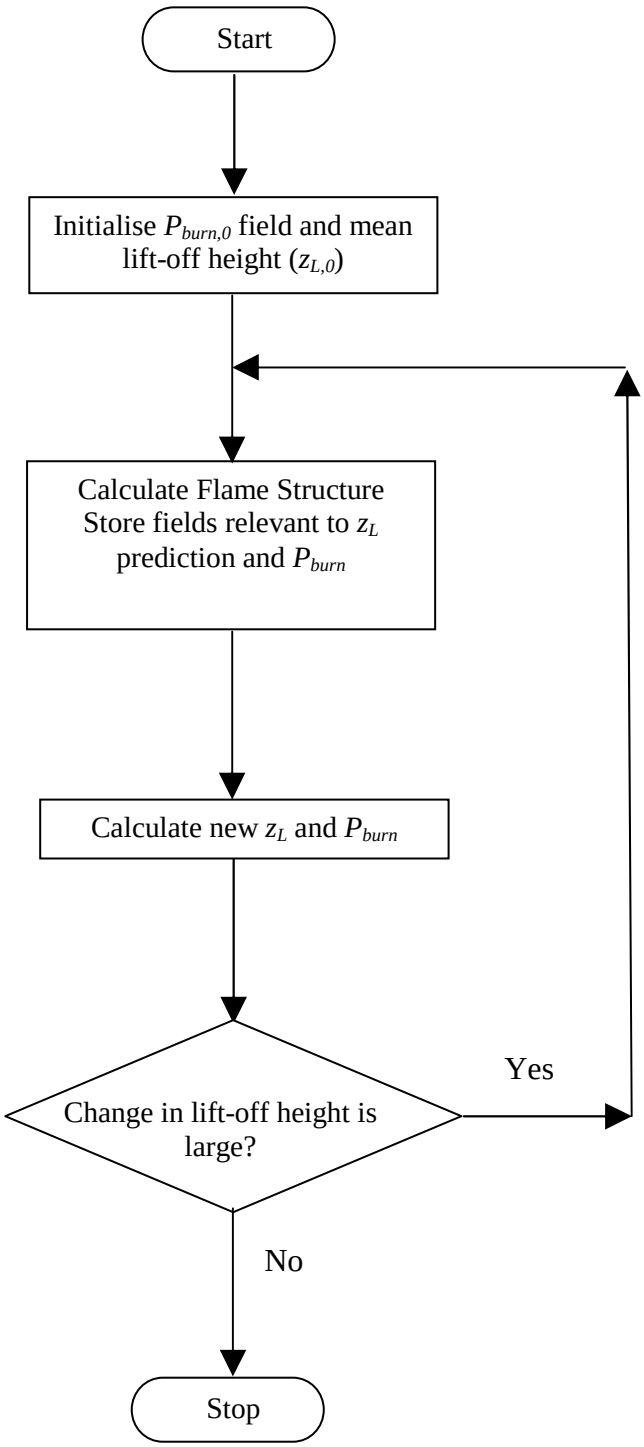

Figure 4. 3 Flow chart of the lifted jet flame methodology

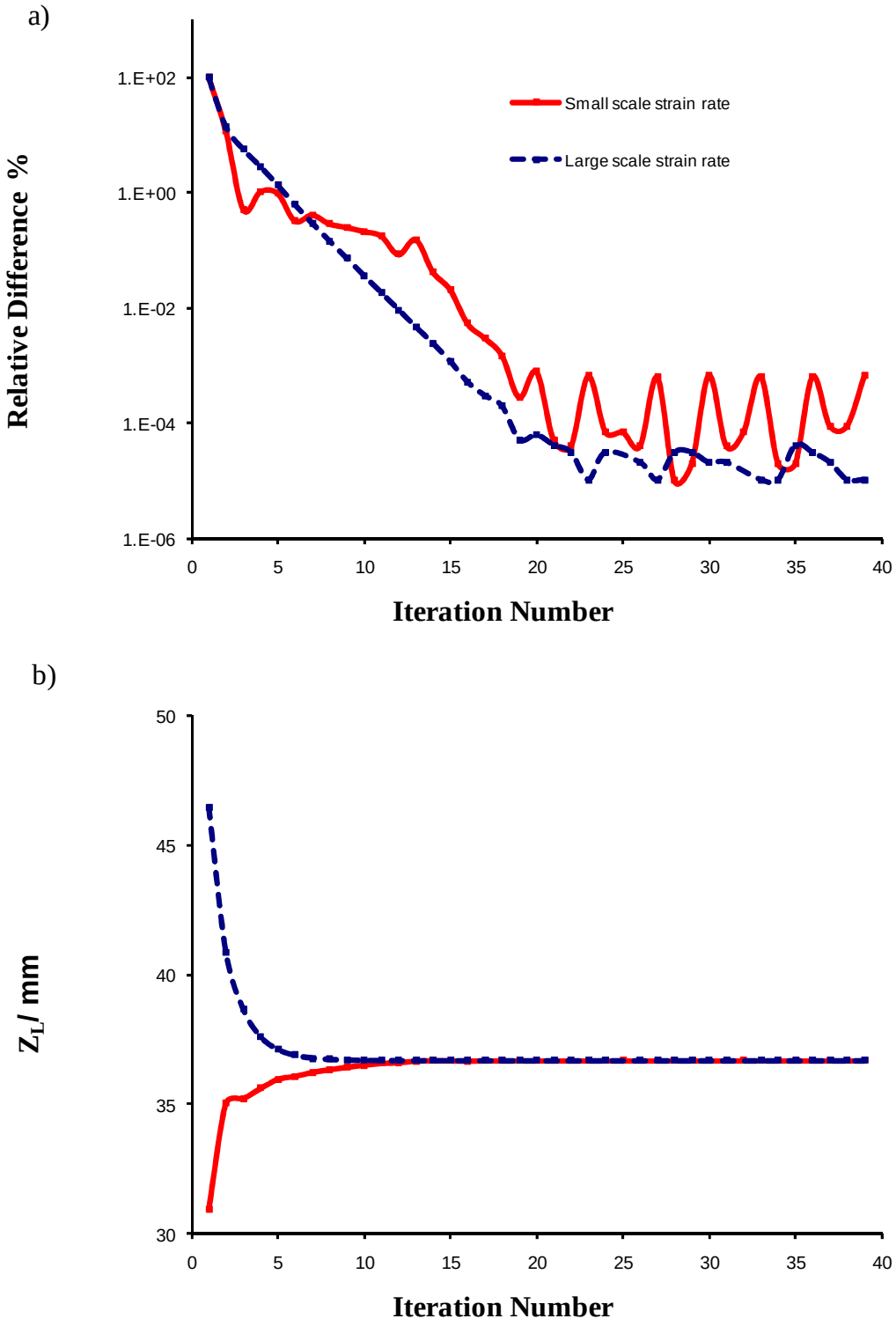

Figure 4. 4: Typical convergence histories of a lifted jet flame simulation
a) Relative difference in lift-off height b) Predicted lift-off height

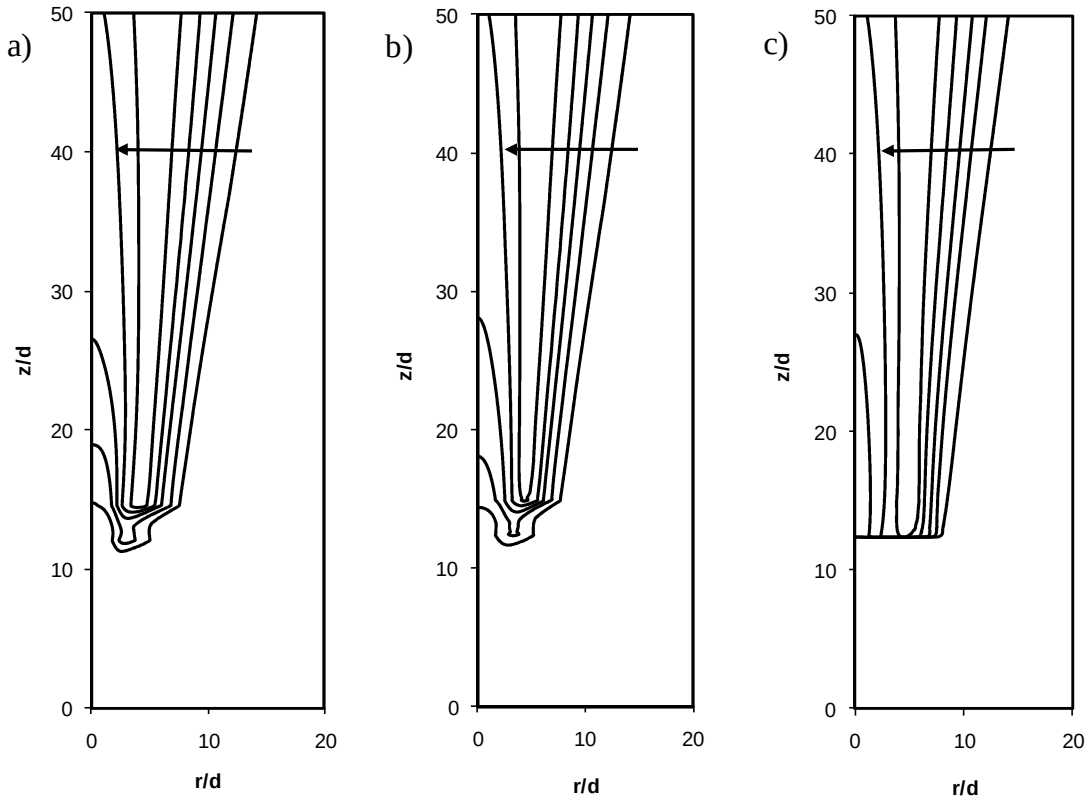

Figure 4. 5: Predicted temperature field in the lift-off region, ($U_0 = 1190 m/s, d = 2.95 mm$). (a) Small-scale strain rate, (b) Large-scale strain rate and (c) Turbulence time scale model. (Arrow indicating increasing temperature)

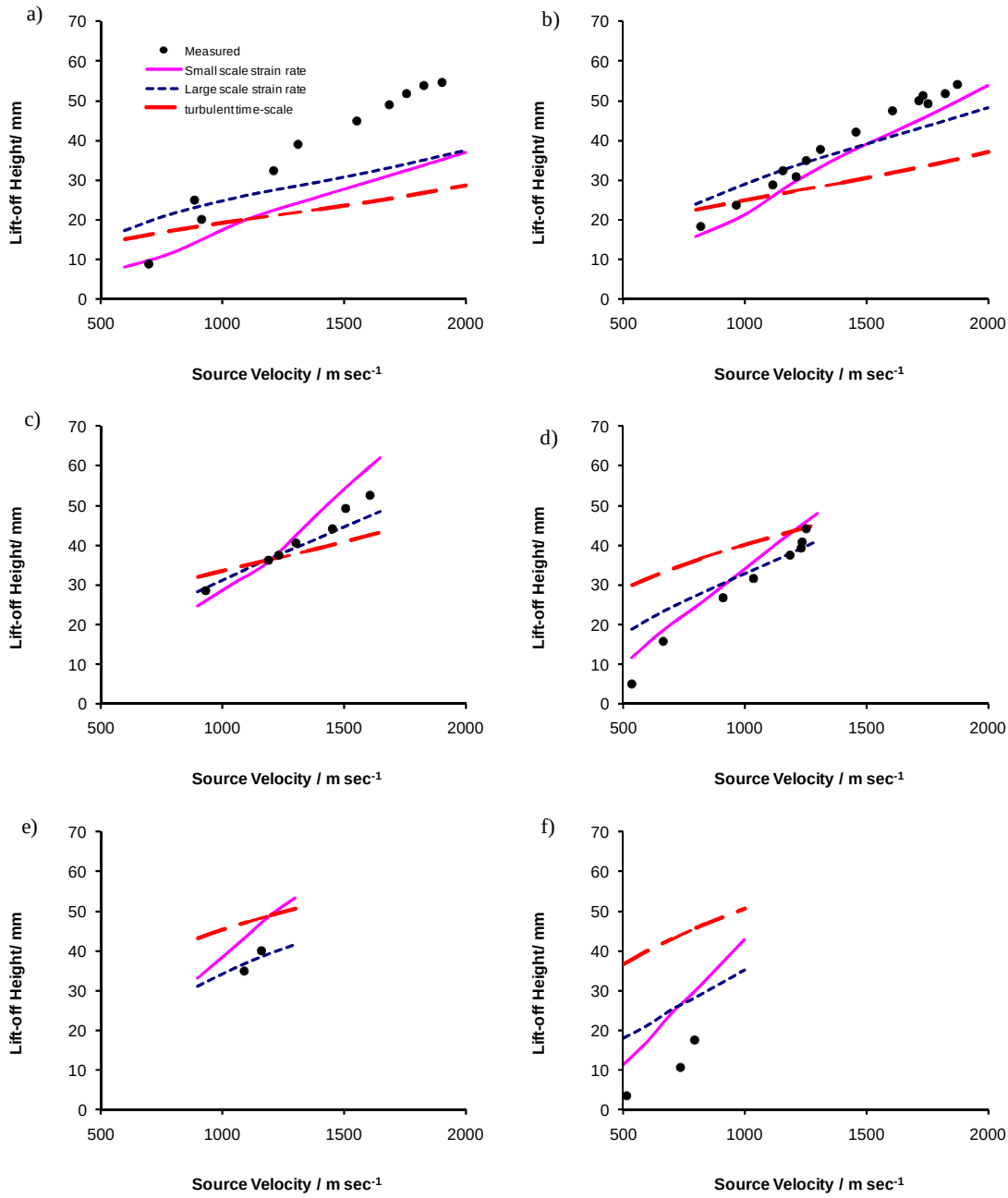

Figure 4. 6: Lift-off height versus source velocity for (a) d=1.08mm (b) d=1.74mm (c) d=2.95mm (d) d= 4.06mm (e) d=5.03mm (f) d=6.10mm.

Chapter 5

Flame Structure

Radiation tends to dominate the heat transfer process in many high-temperature applications, such as turbulent flames. In such cases radiation and turbulence are coupled processes. As discussed in chapter three turbulence fluctuations of temperature and species concentrations tend to enhance emission and heat loss, which have an influence on the temperature and density fields. The density field may further affect the turbulence flow field. The treatment of turbulence-radiation interactions (TRIs) is a challenging task because of the non-linear coupling between the temperature, species concentrations and radiative intensities. In traditional combustion simulations radiation and turbulence are treated as decoupled processes, using mean temperature and species concentration fields. However, many experimental and numerical results have shown that such treatment may result in under-estimation of heat loss by a factor of up to three [149]. Consequently, TRIs must be taken into account in most combustion calculations.

Previous jet fire models development has focussed on the accurate prediction of the mean scalar fields and evolution of intermediate chemical species. This chapter 5 focus is the extension of a conventional Reynolds averaged reacting flow model to predict the root mean square (RMS) fields of the scalars important in predicting the radiation fields that is RMS temperature ($\sqrt{T''^2}$) and RMS H_2O concentration ($\sqrt{X''^2_{H_2O}}$).

As stated previously two classes of PDF approaches exist for dealing with the chemical closure problem. The first approach involves assuming a form for the PDF to close the chemical source terms using information from a finite number of moments. The second approach consists of solving an evolution equation for the PDF [95, 203]. This approach is more elaborate, and consequently, computationally expensive. The emphasis of this investigation is on the advancement of the assumed PDF approach using a truncated Gaussian PDF and Beta PDF methodologies for turbulent diffusion jet flames to predict the RMS scalar fields important in a radiation analysis of hydrogen jet fires.

5.1 Transport equation and the PDF used in the jet flame model

5.1.1 Moments of scalar quantities

In chapter three the basis of the laminar flamelet combustion model was presented. We considered the turbulent flame to be composed of an ensemble of laminar flamelets. The conserved scalar is the mixture fraction confined to values between zero and unity. The relationship between the dependant scalars and the conserved scalar are called flamelets. As these flamelets are usually non-linear functions of the conserved scalar the statistics of this conserved scalar must be known at a point in a turbulent flame for the determination of the local statistics of the dependent scalars. Clearly, for a complete statistical description of local flame properties the probability density function (PDF) of the conserved scalar must be known. The method used in this investigation, is to assume a simple function for this PDF. The exact shape of the assumed PDF at each location of the flame is determined from a limited number of moments, each moment obtained by the solution of its own transport equation.

In this section this analysis is progressed further to demonstrate how mean and second moment properties can be calculated. Assuming that a relationship of the form $\phi_i = \phi_i (f)$ is available through an equilibrium assumption or the laminar flamelet concept, this sub-section illustrates the evaluation of the first and second moments of any accompanying scalar in turbulence non-premixed flames. The determination of the first and second moments of species concentration and temperature involves the specification of a PDF of f. The most widely employed shape is either a Beta function or a clipped Gaussian distribution. In this chapter we investigate the beta function PDF or a truncated Gaussian PDF. A truncated Gaussian PDF is similar to a clipped Gaussian PDF but simpler to implement. The problem is formulated for both these shapes in subsequent sub-sections.

Here, we concern ourselves with modelling the turbulence terms in their Favre averaged form. $\tilde{P}(f)$ for the mixture fraction is

$$\tilde{P} (f) = \frac{1}{\overline{\rho}} \int_0^{\infty} \rho \; P (\rho , f) d \rho \qquad (5.1)$$

Where $\overline{\rho}$ is the Reynolds average of the density, ρ is the instantaneous density and $P(\rho, f)$ is the conventional joint PDF of ρ and f. Conventionally defined mean density, Favre variance and conventional variance of a scalar are respectively

$$\frac{1}{\overline{\rho}} = \int_0^1 \frac{1}{\rho(f)} \tilde{P}(f)\, df \tag{5.2}$$

$$\tilde{\phi}_i = \int_0^1 \phi_i(f)\, \tilde{P}(f)\, df \tag{5.3}$$

$$\overline{\phi_i} = \overline{\rho} \int_0^1 \frac{\phi_i(f)}{\rho(f)} \tilde{P}(f)\, df \tag{5.4}$$

$$\tilde{\phi}_i''^2 = \int_0^1 \left(\phi_i(f) - \tilde{\phi}_i(f)\right)^2 \tilde{P}(f)\, df \tag{5.5}$$

$$\overline{\phi_i'^2} = \overline{\rho} \int_0^1 \frac{\left(\phi_i(f) - \overline{\phi_i(f)}\right)^2}{\rho(f)} \tilde{P}(f)\, df \tag{5.6}$$

with similar results for any other thermodynamic variables. For either chemical equilibrium or the laminar flamelet model the $\phi_i(f)$'s are known. This leaves the question of modelling $\tilde{P}(f)$ unresolved.

5.1.2 Probability density function (PDF)

The Probability Density Function (PDF) of the mixture fraction was modelled by two methods: the truncated Gaussian PDF and the beta PDF. These PDF models are a function of mean mixture fraction $\tilde{f}$ and mixture fraction variance, $\widetilde{f''^2}$ and are valid only for bimodal mixtures, which is fine for our purposes since the mixture fraction f is limited to be in the range

$$0 \le f \le 1. \tag{5.7}$$

Let us consider the truncated Gaussian distribution first. The truncated Gaussian PDF may be written as

$$\tilde{P}(f)=\frac{\int_0^f \exp\left(-(f-\tilde{f})^2/\left(2\widetilde{f''^2}\right)\right)df}{\int_0^1 \exp\left(-(f-\tilde{f})^2/\left(2\widetilde{f''^2}\right)\right)df}. \tag{5.8}$$

The clipped Gaussian PDF is presented below

$$\begin{aligned}\tilde{P}(f)=&\frac{1}{2}erfc\left(\frac{\tilde{f}}{\sqrt{2\pi\widetilde{f''^2}}}\right)\delta(f)+\frac{1}{2}erfc\left(\frac{1-\tilde{f}}{\sqrt{2\pi\widetilde{f''^2}}}\right)\delta(1-f)\\&+\left(H(f)-H(f-1)\right)\frac{1}{\sqrt{2\pi\widetilde{f''^2}}}erfc\left(\frac{-(f-f_0)^2}{2\widetilde{f''^2}}\right)\end{aligned} \tag{5.9}$$

Clearly the truncated Gaussian PDF (5.8) is mathematically much simpler than the clipped Gaussian PDF (5.9) and for mid range $\tilde{f}$ gives similar results. In our study the physically unattainable tails, $(-\infty,0)$ and $(1,\infty)$ of the normal distribution, having mean $\tilde{f}$ and variance $\widetilde{f''^2}$ are truncated and redistributed uniformly across the unit interval hence we called this distribution the "Truncated Gaussian PDF". Mean and variance can be obtained in terms of the values of $\tilde{f}$ and $\widetilde{f''^2}$, that is

$$\tilde{P}(f)=\frac{1}{\sqrt{2\pi\widetilde{f''^2}}}\exp\left(\frac{-(f-\tilde{f})^2}{2\widetilde{f''^2}}\right) \tag{5.10}$$

$$\tilde{f}=\int_0^1 f\ \tilde{P}(f)\,df \tag{5.11}$$

$$\widetilde{f''^2}=\int_0^1 (f-\tilde{f})^2\,\tilde{P}(f)\,df \tag{5.12}$$

$$\tilde{P}(f)=\frac{\int_0^f \exp\left(-(f-\tilde{f})/\left(2\widetilde{f''^2}\right)\right)}{\int_0^1 \exp\left(-(f-\tilde{f})/\left(2\widetilde{f''^2}\right)\right)} \tag{5.13}$$

In general, the values of $\tilde{f}$ and $\widetilde{f''^2}$ are calculated from the solution of their transport equations. It is then possible to deduce $\tilde{f}$ and $\widetilde{f''^2}$ from transport equation (5.13) and so to specify the PDF. Nevertheless, it is not possible to get detail expressions for $\tilde{f}$ and $\widetilde{f''^2}$ even though the two integrals in (equations (5.11) and(5.12)) can be reduced to analytical forms, and so their values must be gotten by an iterative technique. Lockwood and Naguib [204] in their prediction of turbulence diffusion flames stored a "look-up" table of mean and variance in terms of $\tilde{f}$ and $\widetilde{f''^2}$ and consulted this at each grid node. The iterative evaluation of mean and variance is relevantly rather tedious and hence is not suggested for use in a complete flow field computation using finite-difference techniques.

Turning to the Beta function PDF and following Richardson et al [205], the Beta function can be written as

$$\tilde{P}(f)=\frac{f^{\alpha-1}(1-f)^{\beta-1}}{\int_0^1 f^{\alpha-1}(1-f)^{\beta-1}\,df} \qquad 0\le f\le 1 \tag{5.14}$$

Where the values of the exponents α and β are given by

$$\alpha=\tilde{f}\left[\frac{\tilde{f}(1-\tilde{f})}{\widetilde{f''^2}}-1\right] \text{ and } \beta=\frac{(1-\tilde{f})\alpha}{\tilde{f}} \tag{5.15}$$

The PDF equation (5.14) is specified simply if $\tilde{f}$ and $\widetilde{f''^2}$ is known. $\tilde{f}$ and $\widetilde{f''^2}$ can be calculated via their respective transport equations. $\tilde{f}$ is given by equation (3.51). The transport equation for $\widetilde{f''^2}$ is formulated and modelled see equation (3.53). The PDF formulations above are based on Favre averaging. If conventional PDF's are employed the tildes are replaced by overbars in equations (5.8) to (5.15).

5.2 RMS Temperature Predictions

It is possible to accurately predict the mean temperature in flames but there is little work in the open literature where the focus is the prediction of the root mean square (RMS)

temperature $\sqrt{\widetilde{T''^2}}$. However, previous studies [18, 206] include radiative heat loss and can predict mean temperature but very few researcher consider $\sqrt{\widetilde{T''^2}}$ let alone predict it well.

5.2.1 RMS Temperature field based on a PDF Method

In most if not all fires a significant fraction of heat is lost to the surroundings through radiation, and since the radiative heat loss is usually not taken into consideration in the simulations temperature prediction tends to over-predict the temperature levels within the flame. Using the adiabatic flame temperature $\tilde{T}_{adia}$ and from the equation (5.5) established for the Favre variance we can write an equation of a general flow variable for the variance of the adiabatic temperature

$$\widetilde{T''^2_{adia}} = \int_0^1 \left(\tilde{T}(f) - \tilde{T}_{adia}(f)\right)^2 \, pdf\,(f)\, df \tag{5.16}$$

where $\tilde{T}$ is the mean temperature.

It is possible to calculate the RMS temperature by assuming the ratio of the RMS temperature to the mean temperature is conserved when considering the temperature with a radiative heat loss and the adiabatic temperature.

$$\frac{\sqrt{\widetilde{T''^2}}}{\tilde{T}} = \frac{\sqrt{\widetilde{T''^2_{adia}}}}{\tilde{T}_{adia}} \tag{5.17}$$

$$\sqrt{\widetilde{T''^2}} = \sqrt{\widetilde{T''^2_{adia}}} \left(\frac{\tilde{T}}{\tilde{T}_{adia}}\right) \tag{5.18}$$

5.2.2 RMS Temperature based on a Transport equation

An alternative approach for predicting the RMS temperature field is to use a modelled transport equation for the temperature variance similar to how the mixture fraction variance is predicted. The modelled transport equation in an axisymmetric co-ordinate system consistent with the boundary layer equation is stated below

$$\rho\tilde{u}\frac{\partial\widetilde{T''^2}}{\partial x}+\rho\tilde{u}\frac{\partial\widetilde{T''^2}}{\partial r}=\frac{1}{r}\frac{\partial}{\partial r}\left(r\frac{\mu_t}{\sigma_{\widetilde{T''^2}}}\frac{\partial\widetilde{T''^2}}{\partial r}\right)+C_{T_1}\mu_t\left(\frac{\partial\tilde{T}}{\partial r}\right)^2-C_{T_2}\rho\frac{\varepsilon}{k}\widetilde{T''^2} \quad (5.19)$$

The values for the constants in the model C_{T_1}, C_{T_2} and $\sigma_{\widetilde{T''^2}}$ have not been optimised so are assigned the same values as those used in the mixture fraction variance transport equation.

5.3 General description of the flames

A primary goal of this numerical investigation is to provide detailed information on prediction of the scalar fields important in predicting the radiation field in turbulent hydrogen jet flames that is the mean and RMS of the temperature field and the mean and RMS of the H_2O concentration field. The logic being that a flame structure model that can predict the RMS fields of flow fields of relevance to radiative heat transfer is more likely to be of use in studying turbulence radiation interactions. The experimental jet fires considered are those reported by Barlow [41], who made experimental measurements of three flames and Faeth [40] who made experimental measurements of two flames. The present data set includes radial profiles at several streamwise locations along the visible flame length for each of the flames [41]: undiluted H_2, 20% Helium dilution, and 40% Helium dilution. Dilution reduces the radiative fraction to low levels. Faeth's measurements represent axial profiles of the flames he considered.

We have made extensive predictions against Barlow's data consisting of radial profiles at several streamwise locations in an undiluted hydrogen jet flame with a Reynolds number of 10,000 and in two helium-diluted hydrogen flames with Reynolds numbers of 9,800 for flames with 20% Helium and 8,300 for flames with 40% Helium. Our major interest in this investigation is to validate our jet fire model for the flame structure with a view to ultimately accurately predicting the radiation field. Flow conditions and measurement locations are given in Table 5.1. In Table 5.1 Barlow only carried out measurements for two radial locations for the flames with 40% helium. L_vis is the approximate visible flame length, L_stoic is the stoichiometric flame length based upon interpolation of results for the Favre average mixture fraction along the jet centreline. The source velocity for the 40% helium flame was reduced to avoid lift-off.

5.4 Boundary conditions

5.4.1 Faeth Jet Flames

Faeth et al. [40] studied two turbulent hydrogen air diffusion flames using a nozzle diameter of 5mm and relatively low burner exit velocities 108.4 m/s for the flame with Reynolds number (Re=5,722) and 66.3m/s for the flame with Reynolds number (Re=3,000). Starting Richardson numbers were somewhat small; yet, effects of buoyancy were still substantial, mostly near the ends of the visible flame zone. Faeth et al. [40] attributed the visible flame zone to be due to low levels of impurities in the hydrogen fuel for the flame with Reynolds number (Re=3,000). These test conditions were selected to predict mean temperature and species concentrations against measured experimental data of Faeth et al. [40].

5.4.2 Barlow's Jet Flames

The three flames Barlow studied had a nozzle diameter of 3.75mm. Table 5.1 summarises the flow conditions and measurement locations for the predicted flames. In all cases the coflow air velocity was 1.0m/s, and the flames were attached and unconfined. Ranges of temperature and humidity in the coflowing air were 294-296 K and 0.006 – 0.008 kg/kg-air respectively. In Table 5.1, Re_d is the cold jet exit Reynolds number, and L is the approximate visible flame length. These flame conditions were chosen to match the conditions for which Barlow [41] reported his experimental data.

H_2:He (by vol)	u_j (m/s)	Re_d	L_vis/d	Streamwise Locations (x/L_vis)	*L_Stoic (mm)*
100:0	296	10,000	180	1/8,1/4,3/8, 1/2,5/8,3/4,1	*475*
80:20	294	9,800	150	1/8,1/4,3/8, 1/2,5/8,3/4,1	*375*
60:40	256	8,300	100	1/2, 3/4 and 1	*270*

Table 5.1 Fuel flow Conditions and Measurement Locations Barlow [41].

5.5 Grid Independence

For all simulations in this chapter, 80 control volumes in the radial co-ordinate direction spanning the jet radius are used to calculate the flame structure, with a maximum fractional step in the axial direction of less than 2% of the radial control volume spacing. A number of simulations using 40 and 160 control volumes were also completed to confirm that the predictions presented are independent of further mesh refinement. It is estimated that the predicted mean temperature (Figure 5.1) and RMS temperature (Figure 5.2) are within 2% of the fully mesh converged values.

The choice of fuel in this investigation is hydrogen and its by-product when it burns in air is water (H_2O). Prediction of mean temperature and mean H_2O as well as their fluctuations within the flames are of paramount concern in our investigation. Consequently we need to validate our jet fire model by predicting accurately the RMS temperature and RMS H_2O which will be sufficient to characterise the radiation model. However, for completeness we use as much of Barlow's data as possible for validation purposes.

5.6 The Jet Flame Structure Predictions.

5.6.1 Faeth Jet Flames [40]

To gain confidence in the model two rim-stabilised hydrogen fires are considered first as for the lifted jets the lift-off height alone is used for validation. The two jet fires considered are presented in Faeth et al.[40], for both the nozzle diameter is 5 mm and the source velocities are 66.3 m/s (Re = 3,000) and 108.4 m/s (Re = 5,722). Figure 5.3 shows the predicted and measured axial temperature distribution on the jet axis for the two jet fires. For the Re = 5,722 jet fire the agreement between the model and the measured temperature distribution is very good. For the lower Reynolds number, Re = 3,000 there is a tendency to over-predict the temperature field by approximately 10%. This level of agreement is marginally superior to that reported by Gore et al.[40]. This is not surprising as for rim-stabilised fires the models are similar, differing in the mesh resolution, a finer mesh is used here; the turbulence model implemented and the temperature flamelet are also different. All of these differences are points of detail that do not radically change the performance of the model.

Figure 5.3 shows predictions of the mean temperature with Faeth's [40] measured experimental data. In Figure 5.3 (a) where the flame Reynolds number is low we over-predict the measured data by a margin of 5-10% with both PDFs but have good agreement with the high Reynolds number as seen in Figure 5.3 (b). However, it should be noted that Faeth's temperature measurements are uncorrected for radiative heat loss. This suggests that in reality the predicted mean temperature for the Re=3,000 jet fire is closer to reality than the Re=5,722 although both predictions are in good agreement with the measurements with or without the radiation heat loss correction. A further conclusion is that if the radiative heat loss correction in the measurements is taken into account the predicted mean temperature based on the truncated Gaussian PDF is likely to be marginally superior to the beta PDF prediction.

The model over-predicts X_{H_2O} as shown in Figure 5.4 in the near field but asymptotes to the correct value. The reason for the discrepancy in the near field is unclear. Where the reaction is not quenched within the measurement probe you would expect an under-prediction of H_2O in the near field, the opposite to what we have found. Similar to Figure 5.5 the far field mole fraction H_2 is well predicted but surprisingly the near field H_2 is over-predicted. The model conserve mass and the fact that H_2 and H_2O mole fractions are both over-predicted is indicative of there being a discrepancy in the experimental measurements.

The measured and predicted oxygen mole fractions (see Figure 5.6) along the jet axis are in reasonable accord although there is a tendency to under-predict the measurements. Considering the measured O_2 mole fraction and the H_2 mole fraction in the near field imply the oxygen and hydrogen exist together in significant concentrations invalidating the fast chemistry assumption in the model. Faeth et al [40] along the axis in the near field is consistent with Barlow's measurements [41].

In Figure 5.7 the trends in N_2 mole fraction distribution along the axis for Faeth's jet fires are similar to that reported for the other species. The agreement in the near field is poor but accuracy in the far field improves. There are some discrepancies in the measured concentration data but this is clearly not the whole story. This will be considered further once Barlow's jet fires have been presented.

5.6.2 Barlow Jet Flames [41]

Predicted and measured profiles of f, T and X_{H_2O} at the centreline are shown in Figures 5.8, 5.10, and 5.12. The solid and dash lines are results from the simulations with truncated Gaussian PDF and beta PDF respectively. The points are measured experimental data taken by Barlow [41]. The temperature-mixture fraction relationship is obtained from the temperature laminar flamelet. The predicted mean temperatures are then calculated by integrating the instantaneous temperature and PDF over instantaneous mixture fraction as defined in equation (5.20). The PDF's shape is dependent on the mean and variance of mixture fraction. The mean temperature is then calculated using the enthalpy perturbation

$$\overline{T}_{adia} = \int_0^1 T(f)\, pdf\, df \quad \text{and} \quad \overline{T} = \overline{T}_{adia} - \frac{\triangle h}{C_{p,mix}\left(\overline{T}_{adia}\right)} \tag{5.20}$$

Everything depends on the mean and variance of the mixture fraction. For 100% hydrogen jet fires in Figure 5.8 the jet width is well predicted. Overall agreement between predicted and measured mean mixture fraction f is excellent. The truncated Gaussian PDF is marginally better than the beta PDF. From Figure 5.9 similar conclusions to the mean mixture fraction f comparison that is excellent agreement for the predictions of mixture fraction variance $\sqrt{\widetilde{f''^2}}$ and the truncated Gaussian PDF is better than the beta PDF. Model predictions with Barlow's second jet fires (80:20) are excellent in the far field for the mixture fraction as shown in Figure 5.17. However, the model under-predicts in the near field. This may be due to too much turbulence as this promotes mixing. From Figure 5.18 the model tends to under-predict the mixture fraction variance $\sqrt{\widetilde{f''^2}}$ and the mixture fraction variance is insensitive to the PDF used. Barlow's third jet fire (60:40) illustrates in Figure 5.26 that the model under-predicts the mean mixture fraction f but the predicted jet width is similar to the measured jet width. Furthermore in Figure 5.27, model prediction of the mixture fraction variance is quantitatively correct but tends to under-predict the measurements.

A valuable approach to quantifying the effects of turbulent mixing on thermochemical states in these flames is to consider the conserved scalar in mixture fraction coordinates and verify the instantaneous value of the mixture fraction. It would be convenient to include all predicted mixture fraction against Barlow's [41] measured data from a radial

profile as shown in Figures 5.8, 5.17 and 5.26. Figure 5.8 shows mean mixture fraction at six radial locations in the undiluted flame. The truncated Gaussian PDF gives very good predictions to measured data at all locations except near the flame base where it under-predicts by about 10% and the beta PDF had a better prediction. For the diluted flame with 20% helium, predictions were very good at locations *r/d=75*, *r/d=93.75* and *r/d=112.5* as illustrated in Figure 5.17. However, both PDF under-predicted the third flame diluted with 40% helium by approximately 15% near the flame base which gets worse with increasing streamwise distance, such that the spread in the curves at *r/d=75* is about 30% less than the measured data. Despite the poor prediction in the diluted flame with 40%, the truncated Gaussian PDF still gave a better prediction than the beta PDF by about 6%.

Figures 5.9, 5.18 and 5.27 shows the radial profile evolution of the Reynolds-averaged and Favre-averaged mixture fraction variance statistics as a function of downstream distance for the undiluted, 20% helium and 40% helium flames respectively. The trend shown in the mixture fraction variance profiles in the jet inlet and farther downstream is consistent with the RMS temperature profiles along the axis with a relatively more rapid decay in the near field and a subsequently slower decay in the far-stream. These figures also demonstrate relatively higher fluctuations in the predicted near field radial RMS mixture fraction variance profiles. The agreement between the predicted and measured data mixture fraction variance is better in the far-field in all three flames.

Figure 5.10 (100% hydrogen jet fire) shows the radial profiles of measured and predicted mean temperature. For the mean temperature fields in Figure 5.10, as the probe volume moves out radially, our predictions were much better at locations *r/d=90*, *r/d=112.5* and *r/d=135* as shown in Figure 5.10(d), 5.10(e) and 5.10(f). Initially, just downstream of the burner exit plane, agreement between the predictions and measurements is very good. The mean temperature is fairly insensitive to the PDF used and tends to over-predict temperature slightly but agreement is good.

However, in Figure 5.19 (80:20) and Figure 5.28 (60:40) helium is used to dilute the fuel so as to reduce radiative loss. In Figure 5.19 same locations as above relative to the visible flame length predictions of the mean temperature showed excellent agreement even though the flame was diluted with 20% helium. Nevertheless, with 40% helium in Figure 5.28 at two locations namely *r/d=50* and *r/d=75* prediction of Barlow's [41]

measurements is in good agreement though not as excellent as the 100% hydrogen jet and the 80:20 jet fires. This could be due to the presence of significant amount of helium that reduces radiative fraction to a very low level. The truncated Gaussian PDF is marginally better than the beta PDF.

Figures 5.11, 5.20 and 5.29 shows the measured and predicted RMS temperature profiles at six radial locations. A number of predictions are shown, two based on the truncated Gaussian PDF and the beta PDF and two based on the transport equation for temperature variance. The width of the temperature profile is in good agreement with the experiments, while the predictions are lower for $r/d \geq 10$ in the diluted flame with 40% Helium. In the undiluted flame as shown in Figure 5.11 our predictions were in very good agreement with measured data however the transport equation model prediction under-predicted the measured temperature variance by approximately 35% in all six locations. Consequently, the PDF method is better than transport equation method. RMS temperature production in the shear layer is predicted well by the PDF methods. Overall, the PDF method demonstrates excellent agreement with Barlow's measurements [41].

The second case of Barlow's jet fire measurement (80:20) investigation as shown in Figure 5.20 the transport equation model tends to under-predict the measurements while prediction using the PDF models are in excellent agreement with Barlow's measurement. Comparing the prediction of the RMS temperature in Figure 5.20 to the mixture fraction variance $\sqrt{\widetilde{f''^2}}$ you would expect to under-predict measured RMS temperature. In this second case (80:20) no real difference between the truncated Gaussian PDF and the beta PDF predictions is evident.

The third case of RMS temperature (60:40) investigation with Barlow's measurement [41] it is difficult to analyse trends based on two measurement stations. From Figure 5.29 the shape of the predicted profile is in acceptable agreement with the experiments, but the predicted RMS temperature is some 30% higher than the experimental data in the near field. The prediction of the RMS temperature is consistent with poor prediction of the mixture fraction variance $\sqrt{\widetilde{f''^2}}$. The predicted peak of RMS temperature is closer to the axis which implies turbulence has smoothed out the gradients in the RMS

field. Agreement overall is not acceptable in that the RMS fields are of the correct order but quantitatively incorrect.

Radial profiles of Favre-averaged H_2O mole fraction, for the three flames are shown in Figures 5.12, 5.21 and 5.30. These data quantify the spreading rate of the flame and the shape of the mean stoichiometric contour. Note that the mean mixture fraction (Figure 5.8) on the centreline reaches the stoichiometric value at something less than three-quarter of the visible flame length in each case. Any model for H_2O formation in non-premixed flames should, at the first level, predict these mean quantities accurately, as they reflect the entrainment and mixing process and determine the global residence time for H_2O formation.

In Figure 5.12 we use the model to predict the mean H_2O in the case where we have 100% hydrogen jet fire Barlow's measurements [41]. In the near field there is a tendency to over-predict water vapour probably due to the fast chemistry assumption. Further downstream there is a tendency to under-predict but agreement is acceptable. The truncated Gaussian PDF gives marginally better agreement with the measurements than the beta PDF. From Figure 5.21 (80:20) similar to 100% (Figure 5.12) prediction that is over-predict in the near field on the axis maybe due to fast chemistry assumption and under-predicts in the far field but agreement is acceptable. Our investigation of the third jet (60:40) as shown in Figure 5.30 agreement is poor in the near field. Further downstream when the jet is becoming self-similar the agreement is reasonable.

In hydrogen jet flames, radiant losses are assumed to consist solely of the energy emission from H_2O molecules in the gas phase. RMS values of H_2O mole fraction $\sqrt{\widetilde{X''^2_{H_2O}}}$ are presented in Figures 5.13, 5.22 and 5.31 for the undiluted, 20% helium and 40% helium flames respectively. In all cases the H_2O levels increase gradually along the length of the flame. The peak H_2O levels occur near the stoichiometric mixture fraction in the undiluted flames and appear to be shifted slightly to the lean side of the stoichiometric mixture fraction in the helium diluted flames. Large fluctuations of scalar dissipation in the thin reaction layers contribute to large fluctuations in X_{H_2O} near the flame base. Toward the flame tip, scalar dissipation and its fluctuations decrease, radical concentrations approach equilibrium, and H_2O production rates at a given mixture fraction are expected to become more uniform. Furthermore, as fluid is

convected downstream, turbulence mixing tends to average out the large H_2O fluctuations that were generated near the flame base. The highest fluctuations at a given streamwise location occur near the stoichiometric mixture fraction in each case. H_2O forms at near-stoichiometric conditions and then mixes to leaner or richer conditions as a relatively stable product. Therefore, one would expect $\sqrt{\widetilde{X''^2_{H_2O}}}$ to be greatest near the stoichiometric mixture fraction and lower elsewhere, due to the moderating influence of the mixing process.

Considering Figure 5.13 we see excellent agreement is achieved with the prediction of the RMS H_2O for the undiluted case potentially considering the level of agreement in the X_{H_2O} field which the RMS H_2O field depends on. Again the truncated Gaussian PDF has slightly better agreement than the beta PDF. For the 80:20 case (Figure 5.22) the prediction of RMS H_2O agreement is excellent. Predictions using both PDF approaches are similar. However, for the diluted case of 40% helium (60:40) as shown in Figure 5.31 prediction in the near field is qualitatively acceptable but the predicted peak is too close to the axis. This discrepancy has developed further by *r/d=75*.

The profiles for the undiluted case and the 20% helium case (Figures 5.13 and 5.22) show that near the nozzle (*r/d=22.5* and *r/d=18.75* respectively) the mixture fraction gradients are steep, even in the mean and the zones of high temperature and high H_2O concentration are narrow. H_2O production rates near the flame base are expected to be sensitive to local scalar dissipation rates (local strain) in these thin reaction layers, due to the influence of strain on temperature depression and O-atom superequilibrium. H_2O concentrations are doubly sensitive to local strain rates because of the combined effects of non-equilibrium chemistry and residence time. A high local strain rate means low temperature (relative to equilibrium) and short residence time at the H_2O forming conditions. Further downstream (*r/d=135*) scalar dissipation decreases, temperature and radical concentration approach equilibrium, the high-temperature zones become broad, and instantaneous H_2O production rates at a given mixture fraction can be anticipated to approach the rate corresponding to equilibrium temperature and species concentrations. This streamwise evolution of reaction zone structure will be a significant consideration as we investigate mean and fluctuations of H_2O mole fraction and temperature in the radiation model.

Considering H_2, O_2 and N_2 together shown in Figures 5.14, 5.15 and 5.16 for undiluted flame (100%) respectively. Agreement of prediction with Barlow's measurement is excellent. The truncated Gaussian PDF in some cases is a significant improvement to the beta PDF predictions particularly when considering the N_2 field. Similarly, considering H_2, O_2 and N_2 (see Figures 5.23, 5.24 and 5.25 respectively) for the diluted case with 20% helium (80:20) agreement with Barlow's measurement is excellent. However, prediction is insensitive to the PDF used. Again considering H_2, O_2 and N_2 together (see Figures 5.32, 5.33 and 5.34 respectively) for the third jet with 40% dilution of helium (60:40) predictions are consistent with other fields that is overall qualitatively correct but near the axis quantitatively the predictions are not acceptable.

5.7 Concluding remarks

We carried out complete predictions of the hydrogen jet diffusion flames in this investigation providing a benchmark for the validation of the flame structure. The agreements between the predicted and measured data are good along the radial profiles particularly the undiluted flame from Barlow's [41] measurements. It can be seen from the figures that the predicted results compare much better along the radial direction at the downstream of the flame than upstream near the jet nozzle. The radial temperature and species profiles become wider and flatter with increasing axial distance. In all cases, the peak mean temperature appears at the same position where the maximum mole fraction of X_{H_2O} occurs and the species O_2 and H_2 are almost consumed.

A significant body of results from this investigation is based on the mixture fraction and temperature. We focussed on the relationships among species, mixture fraction and temperature by considering averages and root mean square (RMS) fluctuations of the species mole fraction based on: 1) the mixture fraction alone and 2) both mixture fraction and the temperature. Our predictions provides useful tool for investigating the influence of turbulence mixing on thermochemical states in flames. Processing the data based on the instantaneous mixture fraction yields quantitative information on turbulence-chemistry interactions that cannot be extracted from time-averaging or Favre-averaging approaches.

The truncated Gaussian PDF delivers a better modelling quantity than the beta PDF for the flames investigated even though a simple laminar flamelet is used. Chemistry takes

place in thin layers where the chemical source term and the molecular transport are the leading terms, while outside the strongly-reactive zone the turbulent mixing dominates the flow-field. The fast chemistry mechanism is a sound assumption in hydrogen/air diffusion flames where the major chemical species are of interest.

The temperature field of Faeth jets is well predicted but the chemistry fields are poorly predicted, particularly in the near field. Considering Barlow's jets the 100% and the 20% helium diluted (80:20), predictions are very good. The PDF method is superior to using a transport equation in the $\sqrt{\widetilde{T''^2}}$ for predicting the RMS temperature field. The truncated Gaussian PDF is the better PDF method with a marginal improvement in accuracy for some jets. Considering the 40% helium diluted (60:40) jet the agreement is not as encouraging, why this might be is difficult to say. There is some evidence for too much turbulence generating in the model. Considering the excellent agreement with Barlow's measurements in the 100% and 20% helium diluted (80:20) jet fires the poor agreement with Faeth measurements of the chemistry fields is likely to be due to the probes used for the measurements compared to the laser diagnostic techniques employed by Barlow.

Overall the model predictions of the participating species and the temperature are well predicted indicating that any radiative model can be evaluated rigorously, confident in the knowledge that the flame structure is well predicted. The validation of the flame structure model will make it possible to evaluate the radiation fields to be discussed in Chapter Six secure in the knowledge that any discrepancies between the measured and predicted radiation fields is a function of the radiation modelling methodology alone.

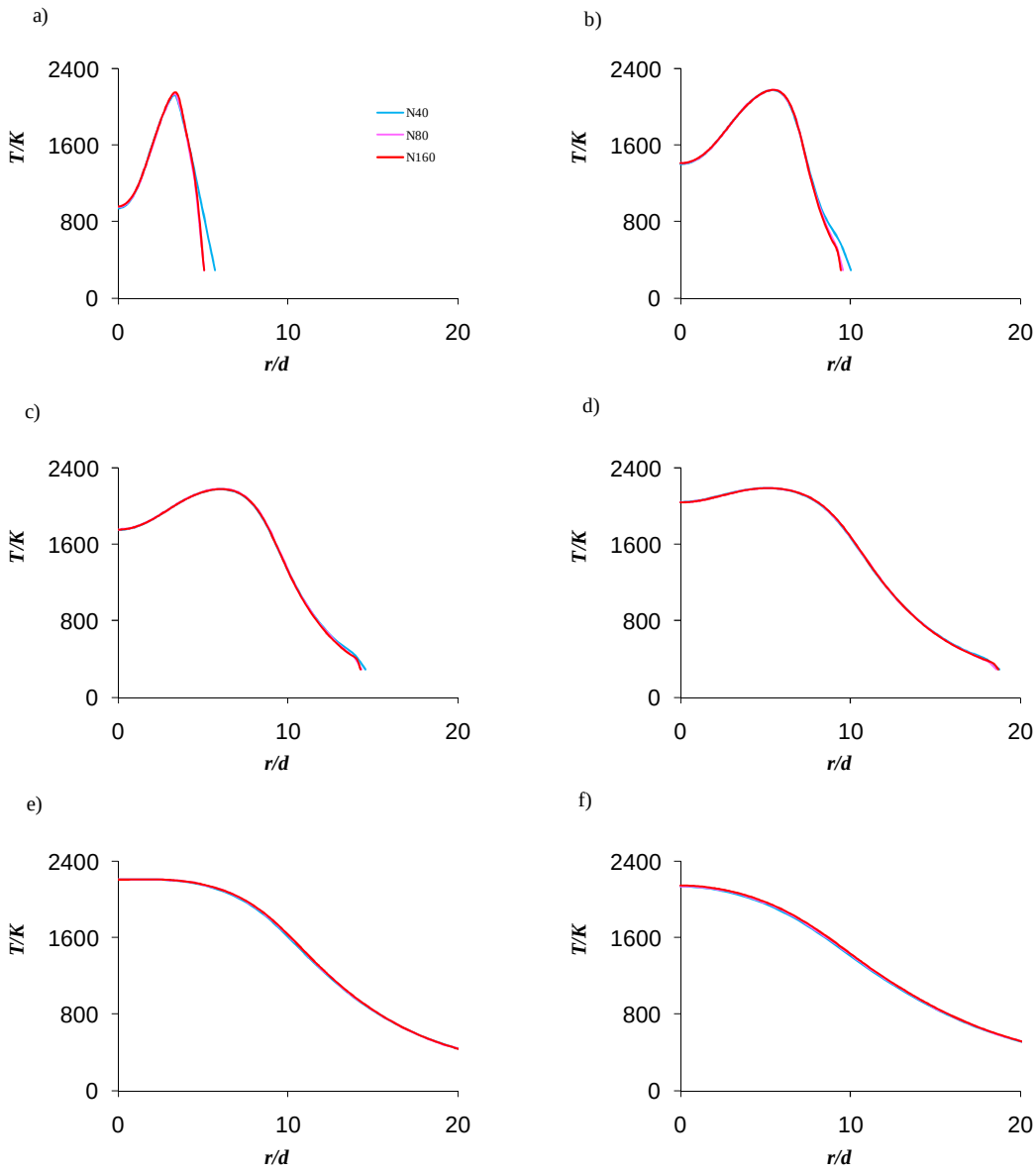

Figure 5. 1: Radial profiles of mean temperature in turbulent hydrogen air diffusion flame using different control volumes to validate the grid independence.
a) *r/d=22.5*, b) *r/d =45*, c) *r/d =67.5* d) *r/d =90*, e) *r/d =112.5* and f) *r/d =135*.

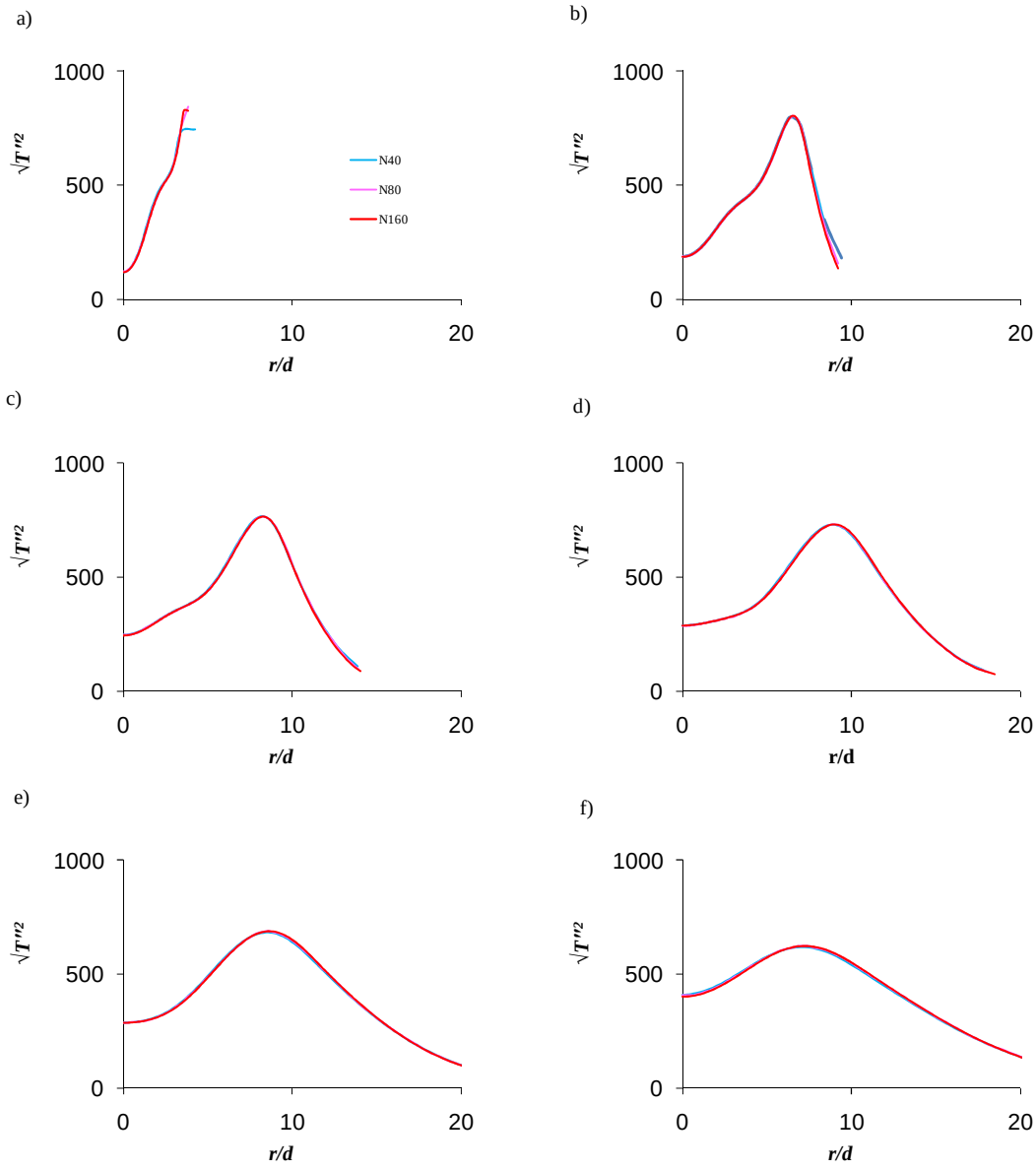

Figure 5. 2: Radial profiles of RMS temperature in turbulent hydrogen air diffusion flame using different control volumes to validate the grid independence.
a) *r/d=22.5*, b) *r/d =45*, c) *r/d =67.5* d) *r/d =90*, e) *r/d =112.5* and f) *r/d =135*.

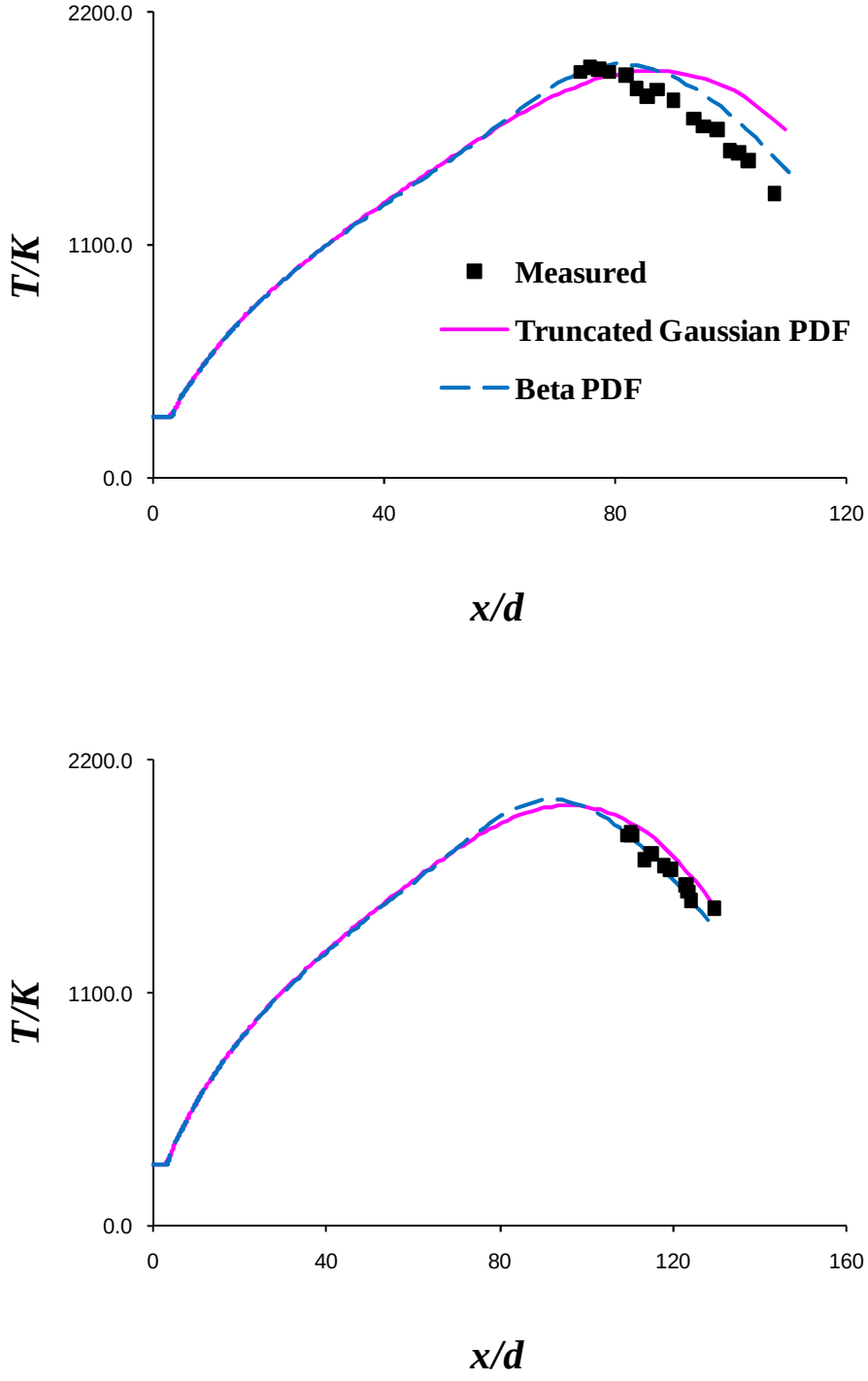

Figure 5. 3: Axial profiles of mean temperature in turbulent hydrogen air diffusion flame with Reynolds number a) Re = 3,000 b) Re = 5,722.

a)

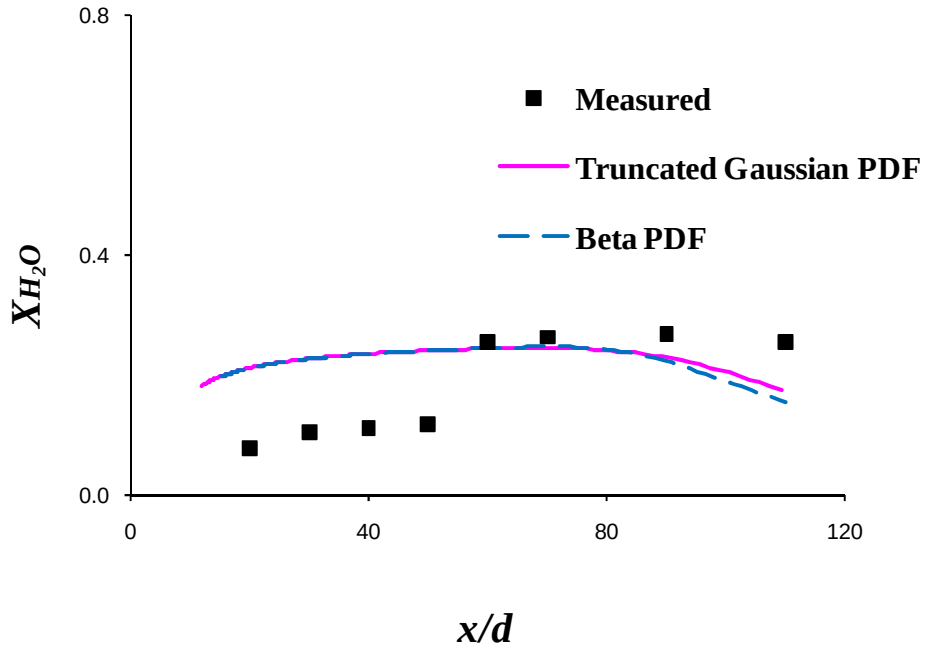

b)

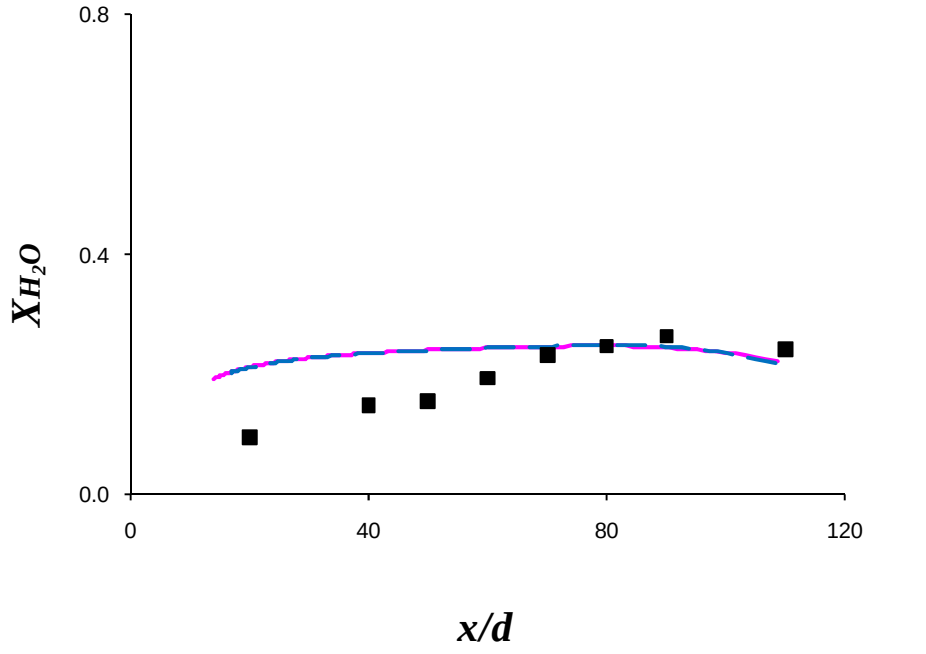

Figure 5. 4: Axial profiles of H_2O (X_{H_2O}) mole fraction in turbulent hydrogen air diffusion flame with Reynolds number a) Re = 3,000 b) Re = 5,722.

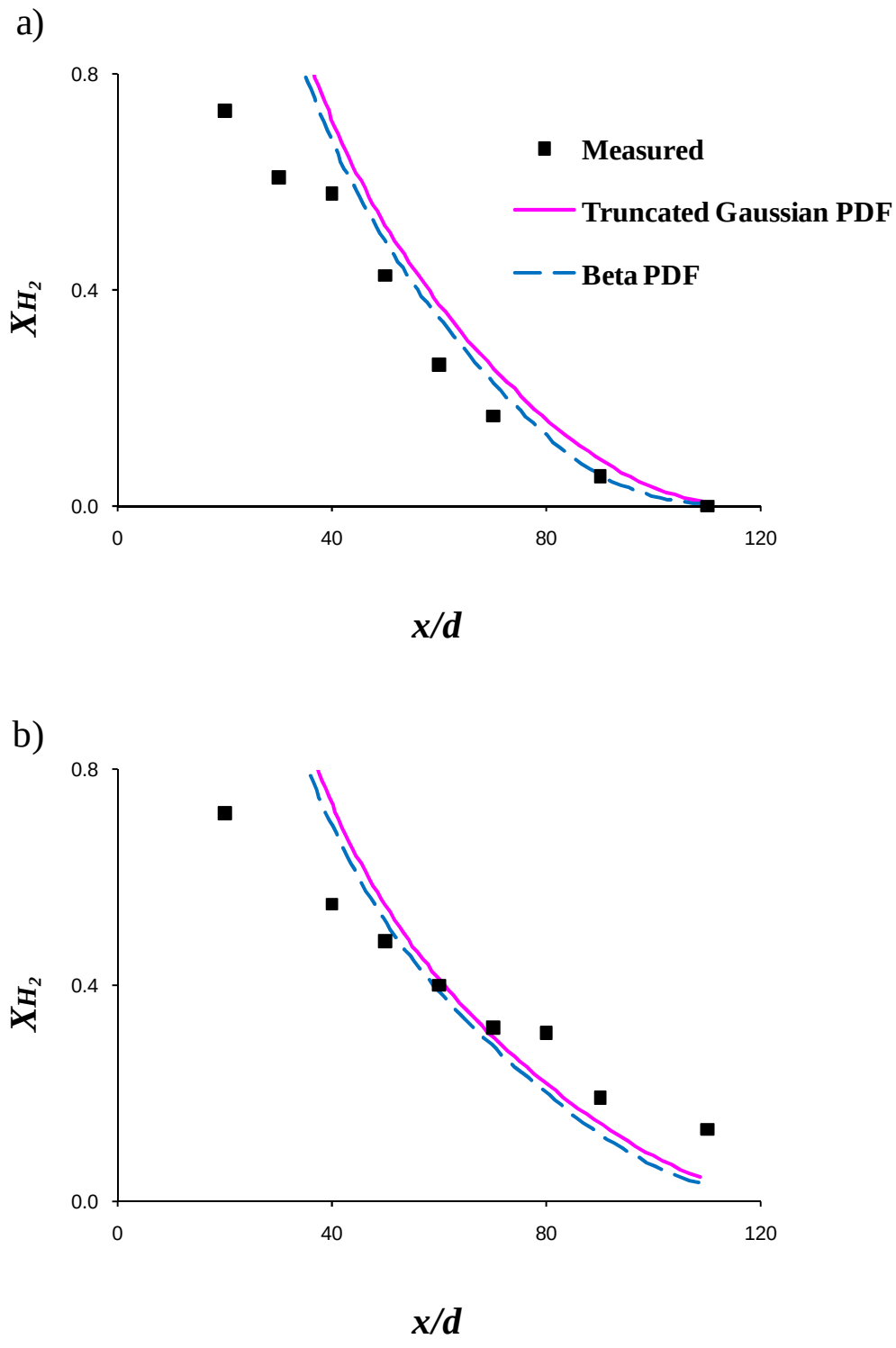

Figure 5. 5: Axial profiles of hydrogen mole fraction in turbulent hydrogen air diffusion with Reynolds number a) Re = 3,000 b) Re = 5,722.

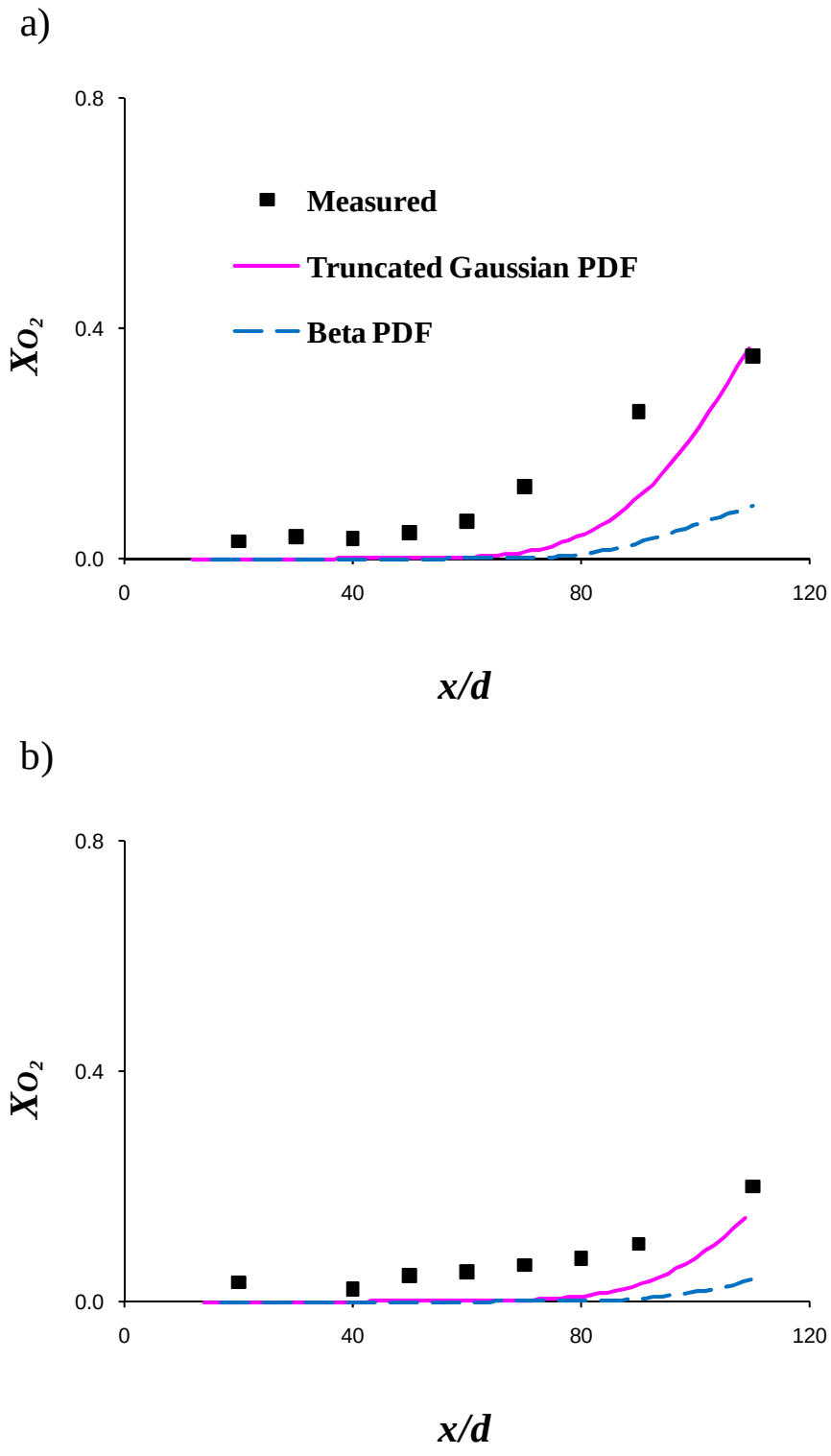

Figure 5. 6: Axial profiles of oxygen mole fraction in turbulent hydrogen air diffusion flame with Reynolds number a) Re = 3,000 b) Re = 5,722.

a)

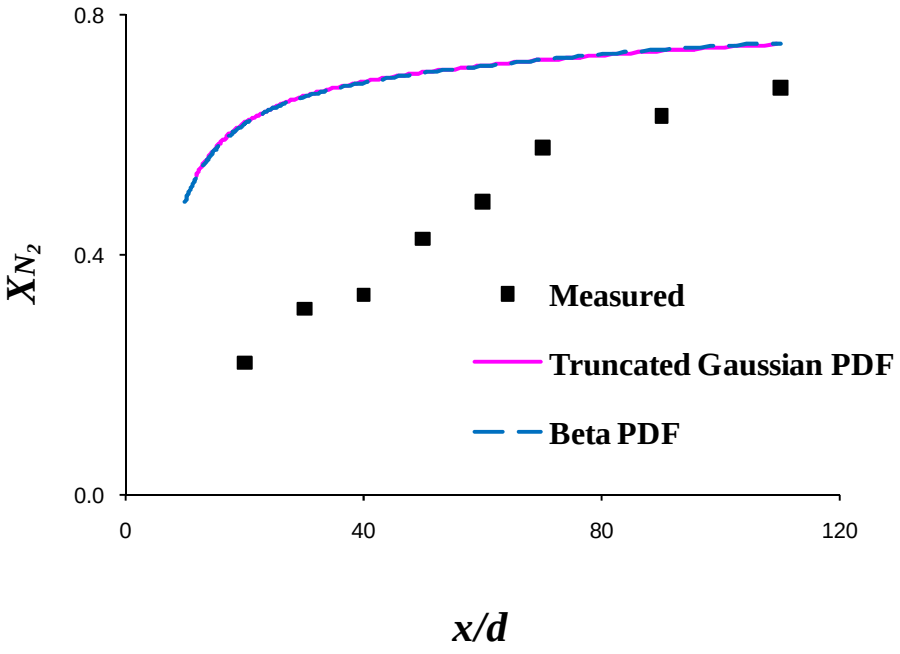

b)

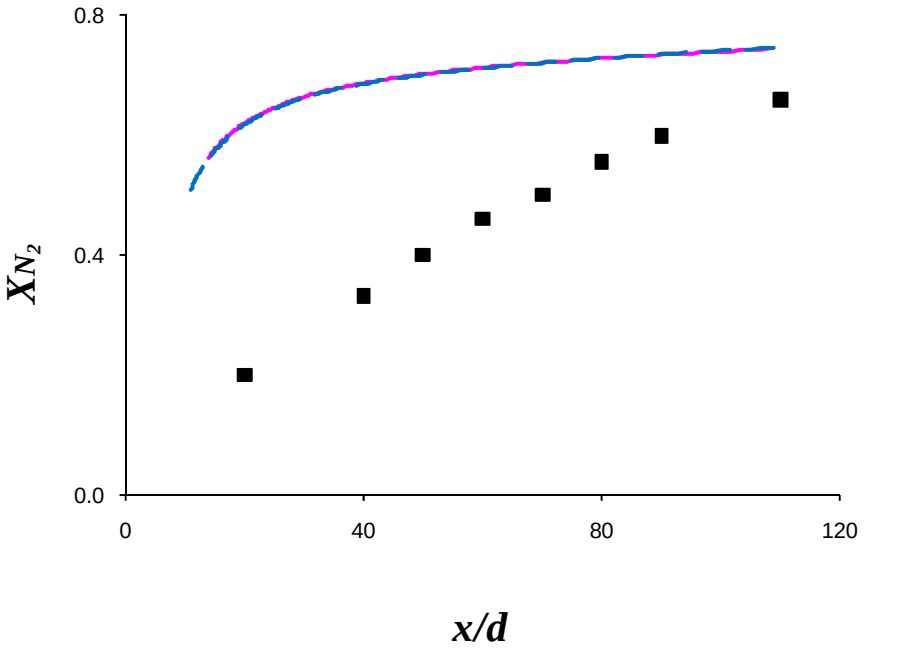

Figure 5. 7: Axial profiles of nitrogen mole fraction in turbulent hydrogen air diffusion flame with Reynolds number a) Re = 3,000 b) Re = 5,722.

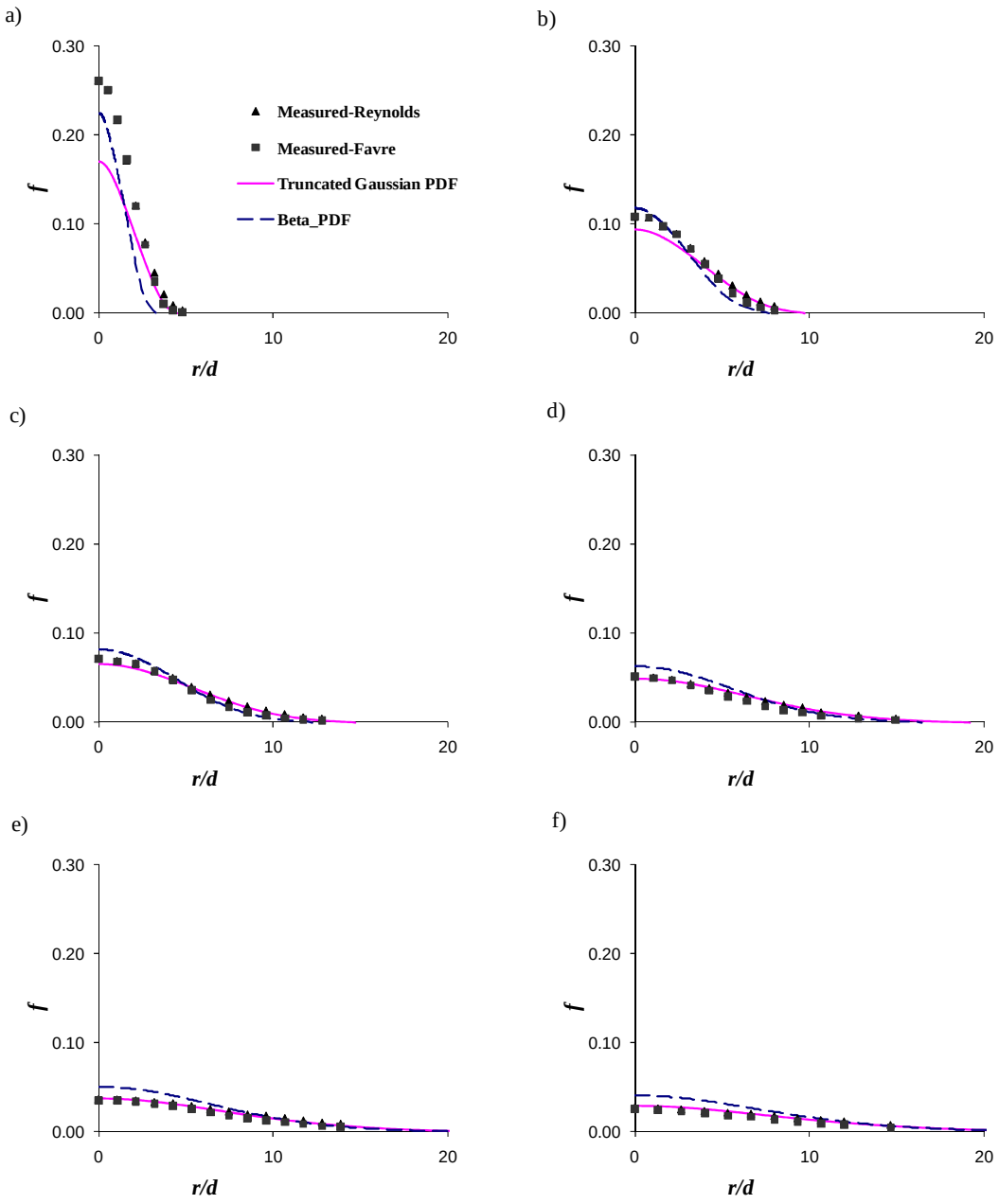

Figure 5. 8: Radial profiles of mean mixture fraction in turbulent hydrogen air diffusion using 100% hydrogen.
a) *r/d=22.5*, b) *r/d =45*, c) *r/d =67.5* d) *r/d =90*, e) *r/d =112.5* and f) *r/d =135*.

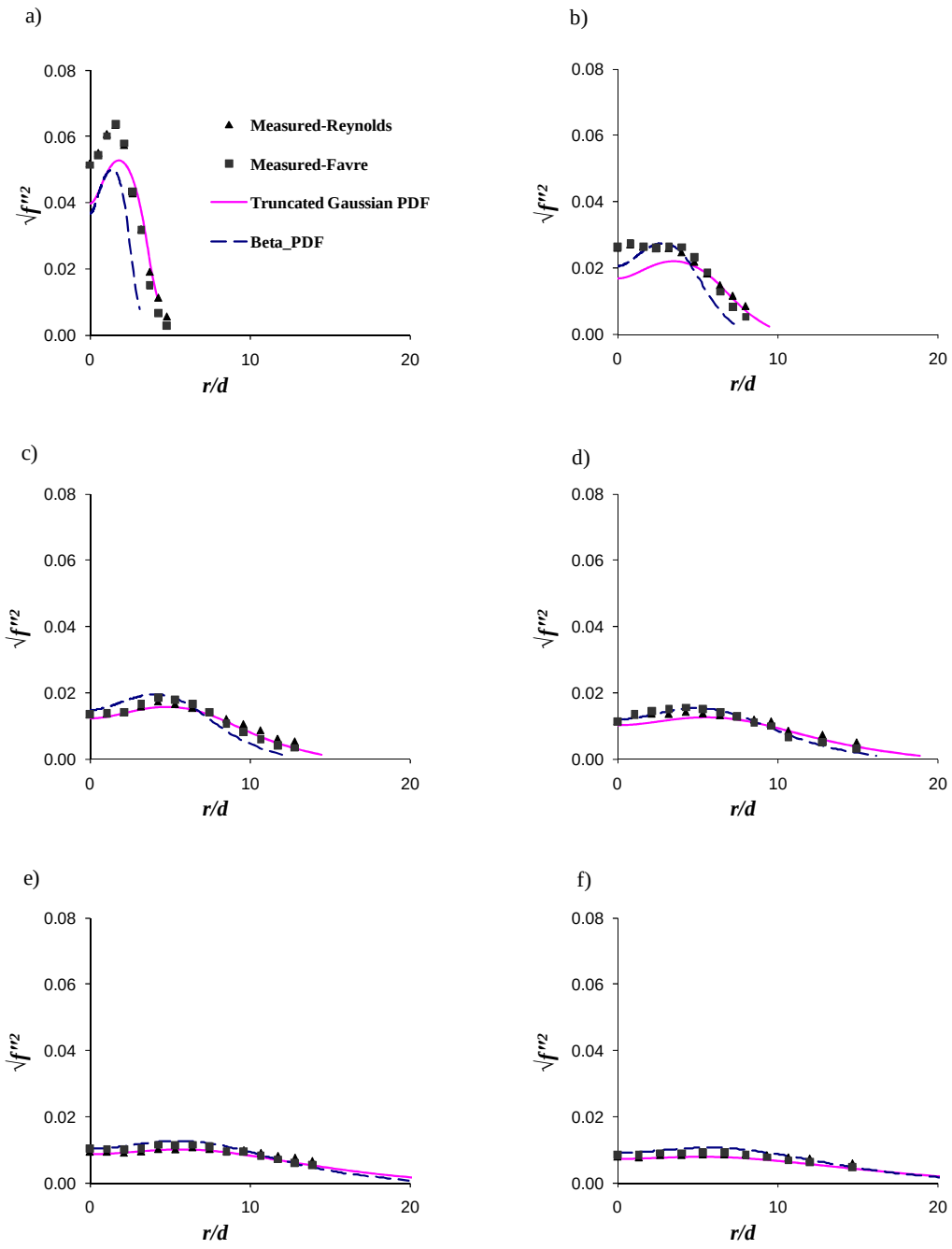

Figure 5. 9: Radial profiles of RMS mixture fraction in turbulent hydrogen air diffusion using 100% hydrogen.
a) *r/d=22.5*, b) *r/d =45*, c) *r/d =67.5* d) *r/d =90*, e) *r/d =112.5* and f) *r/d =135*.

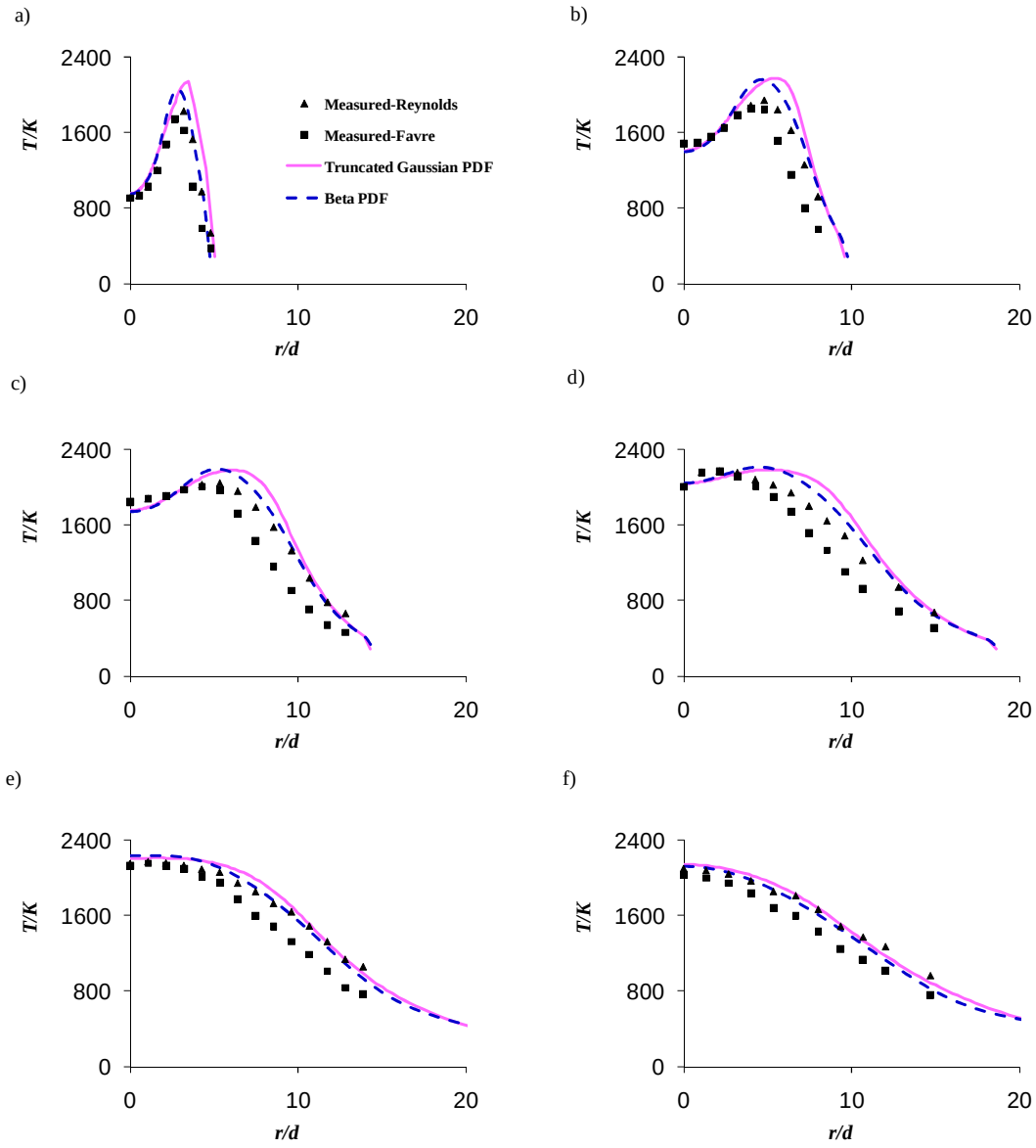

Figure 5. 10: Radial profiles of mean temperature in turbulent hydrogen air diffusion using 100% hydrogen.
a) *r/d=22.5*, b) *r/d =45*, c) *r/d =67.5* d) *r/d =90*, e) *r/d =112.5* and f) *r/d =135*.

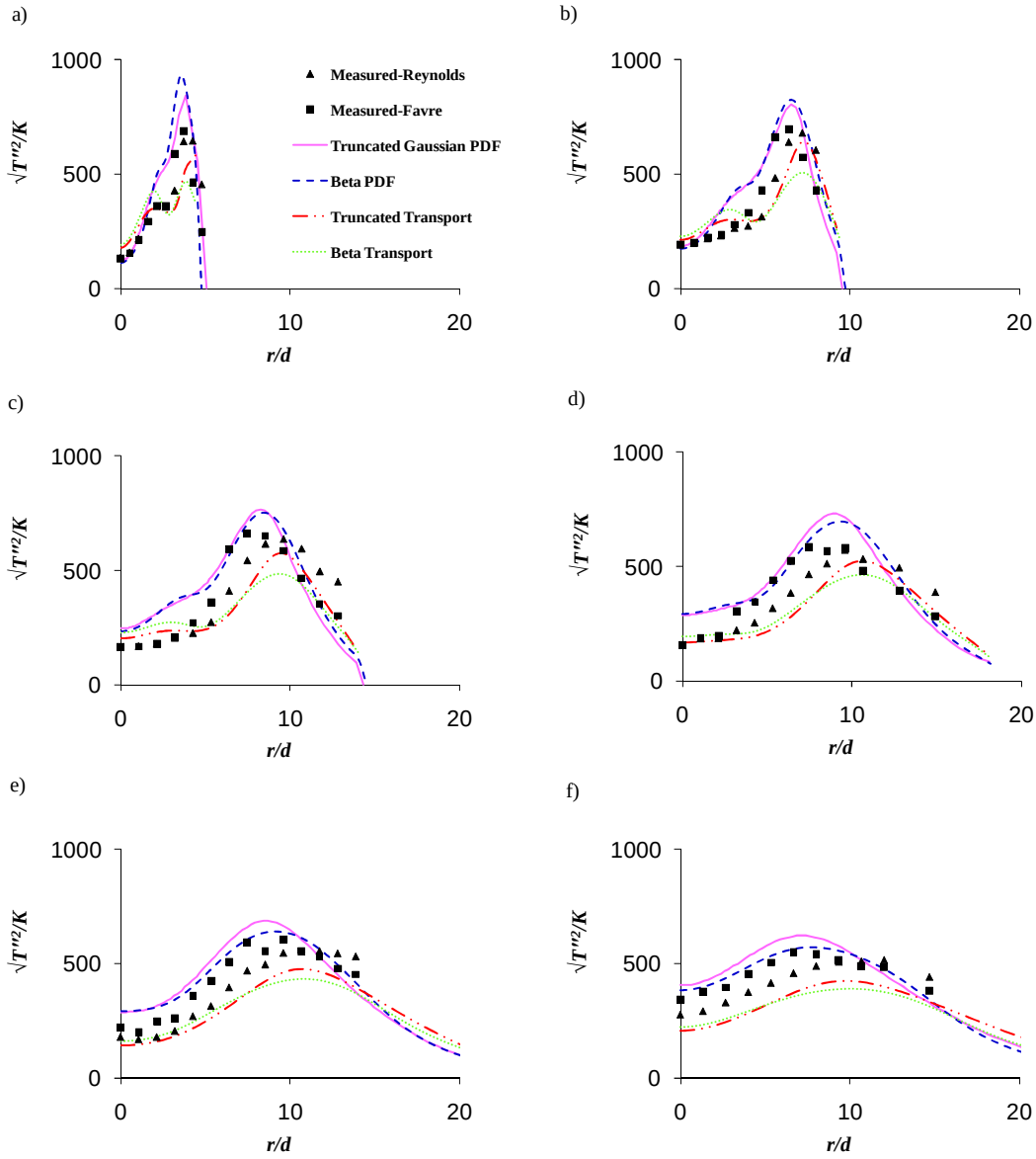

Figure 5. 11: Radial profiles of RMS temperature in turbulent hydrogen air diffusion using 100% hydrogen.
a) *r/d=22.5*, b) *r/d =45*, c) *r/d =67.5* d) *r/d =90*, e) *r/d =112.5* and f) *r/d =135*.

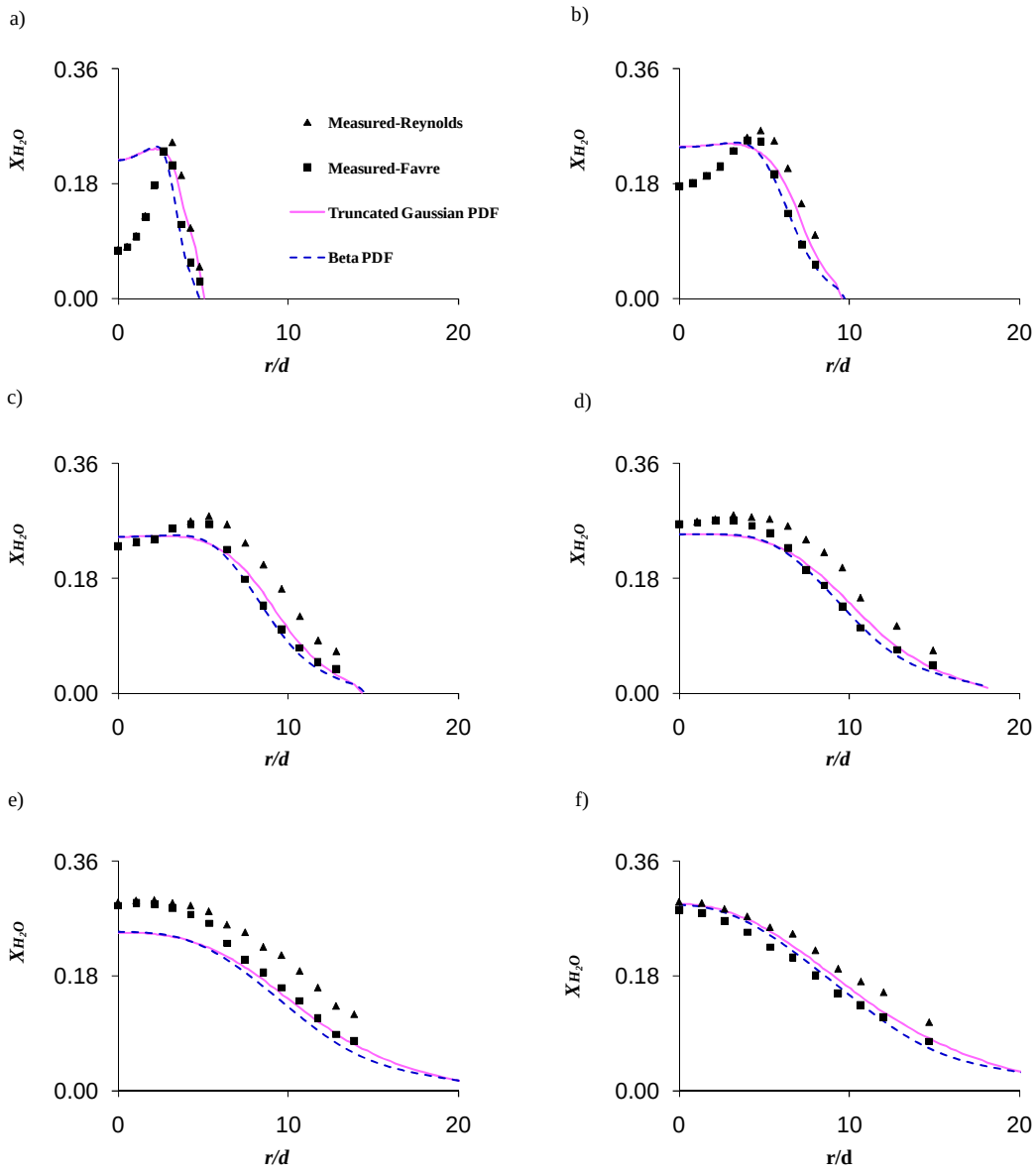

Figure 5. 12: Radial profiles of mean H_2O mole fraction in turbulent hydrogen air diffusion flame using 100% hydrogen.
a) *r/d=22.5*, b) *r/d =45*, c) *r/d =67.5* d) *r/d =90*, e) *r/d =112.5* and f) *r/d =135*.

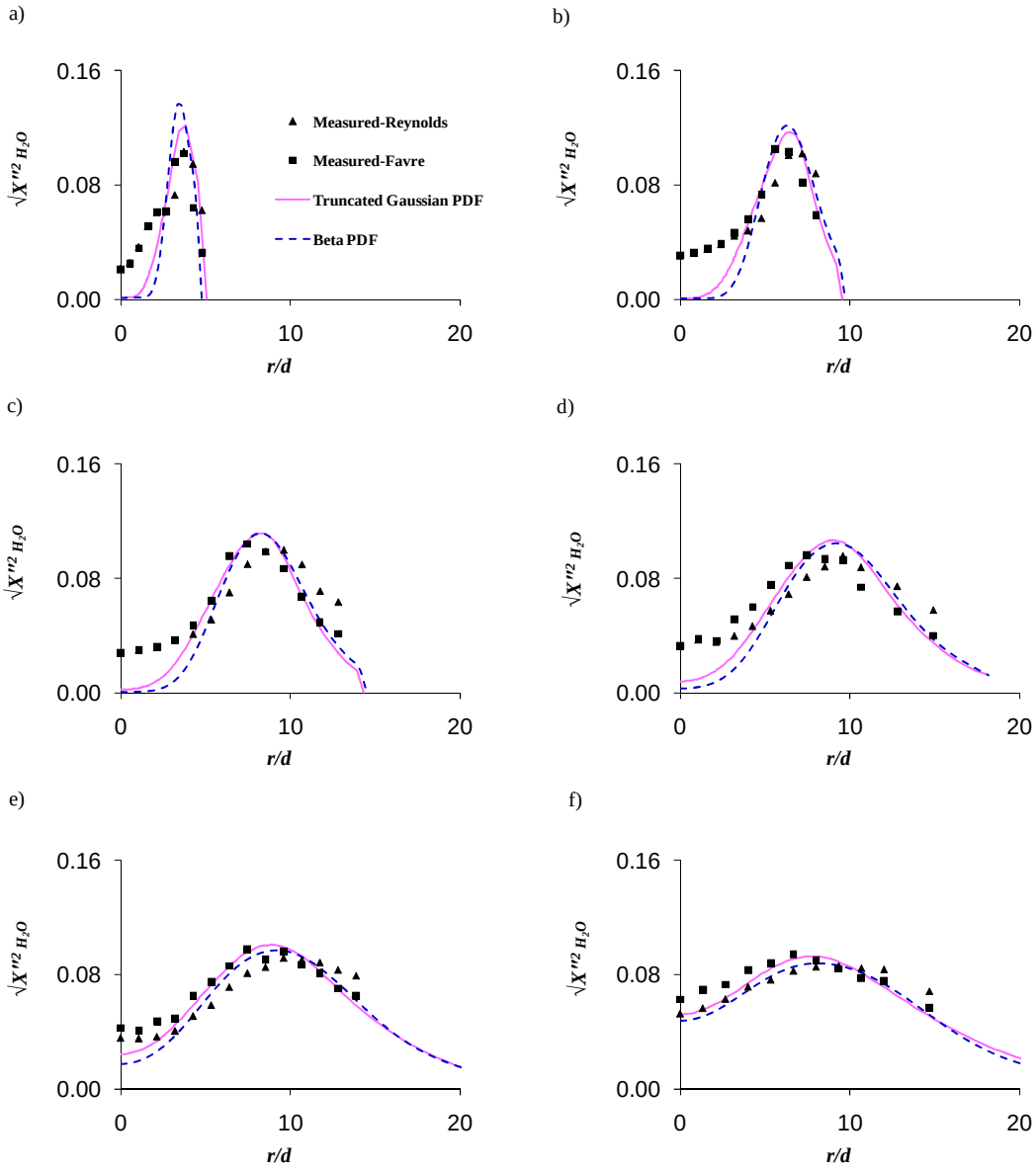

Figure 5. 13: Radial profiles of RMS H_2O mole fraction in turbulent hydrogen air diffusion flame using 100% hydrogen.
a) *r/d=22.5*, b) *r/d =45*, c) *r/d =67.5* d) *r/d =90*, e) *r/d =112.5* and f) *r/d =135*.

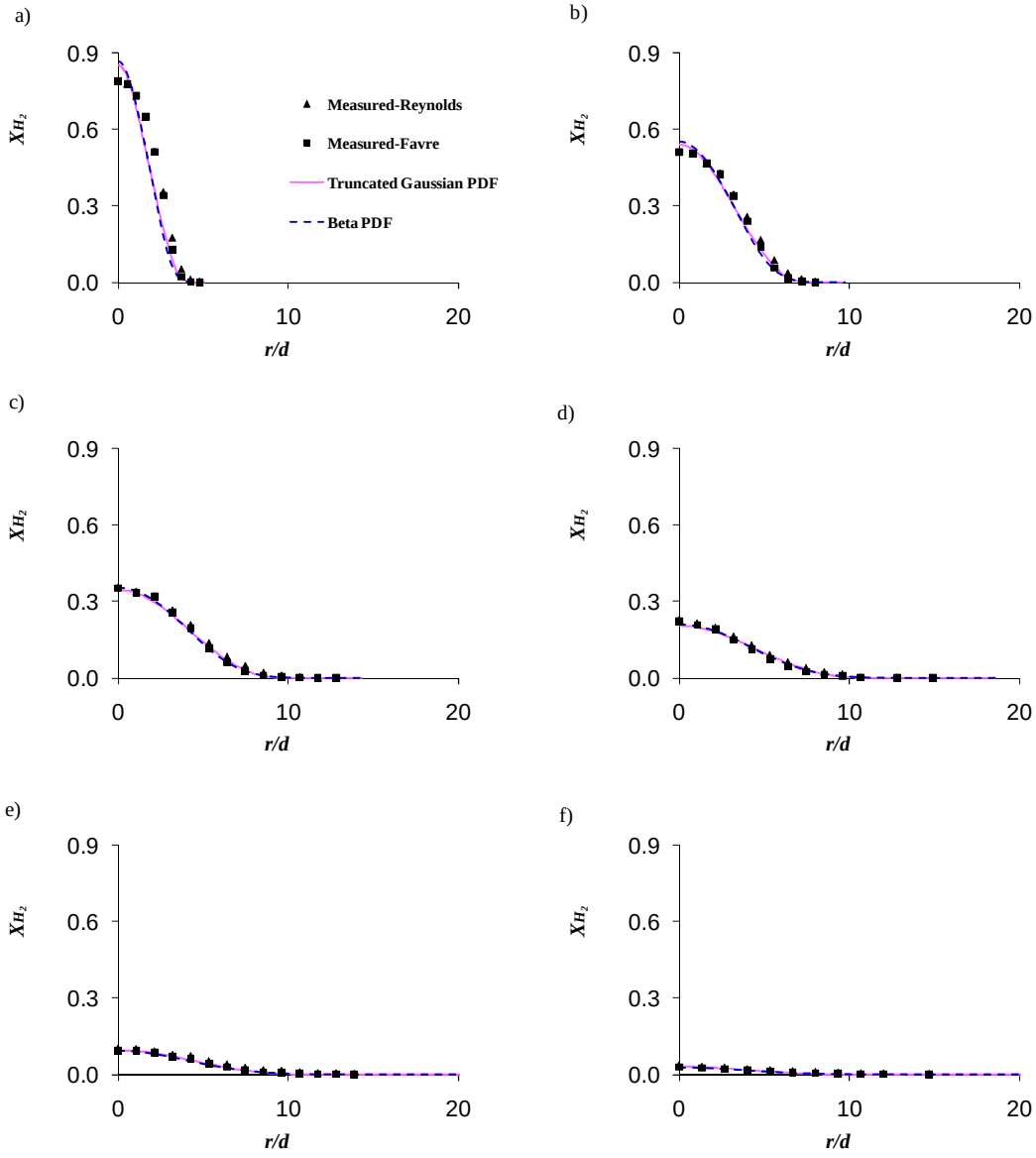

Figure 5. 14: Radial profiles of hydrogen mole fraction in turbulent hydrogen air diffusion flame using 100% hydrogen.
a) *r/d=22.5*, b) *r/d =45*, c) *r/d =67.5* d) *r/d =90*, e) *r/d =112.5* and f) *r/d =135*.

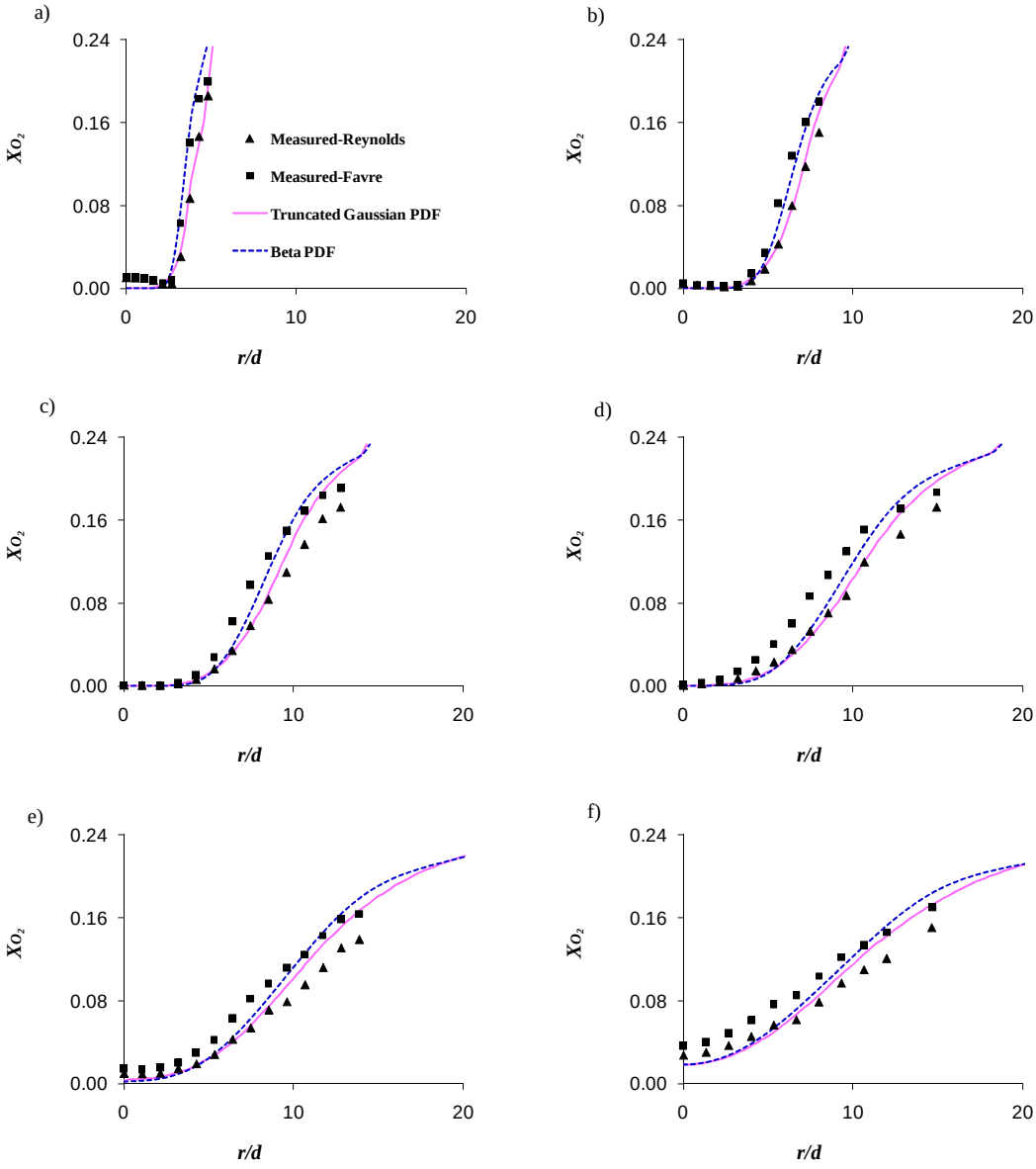

Figure 5. 15: Radial profiles of oxygen mole fraction in turbulent hydrogen air diffusion flame using 100% hydrogen.
a) *r/d=22.5*, b) *r/d =45*, c) *r/d =67.5* d) *r/d =90*, e) *r/d =112.5* and f) *r/d =135*.

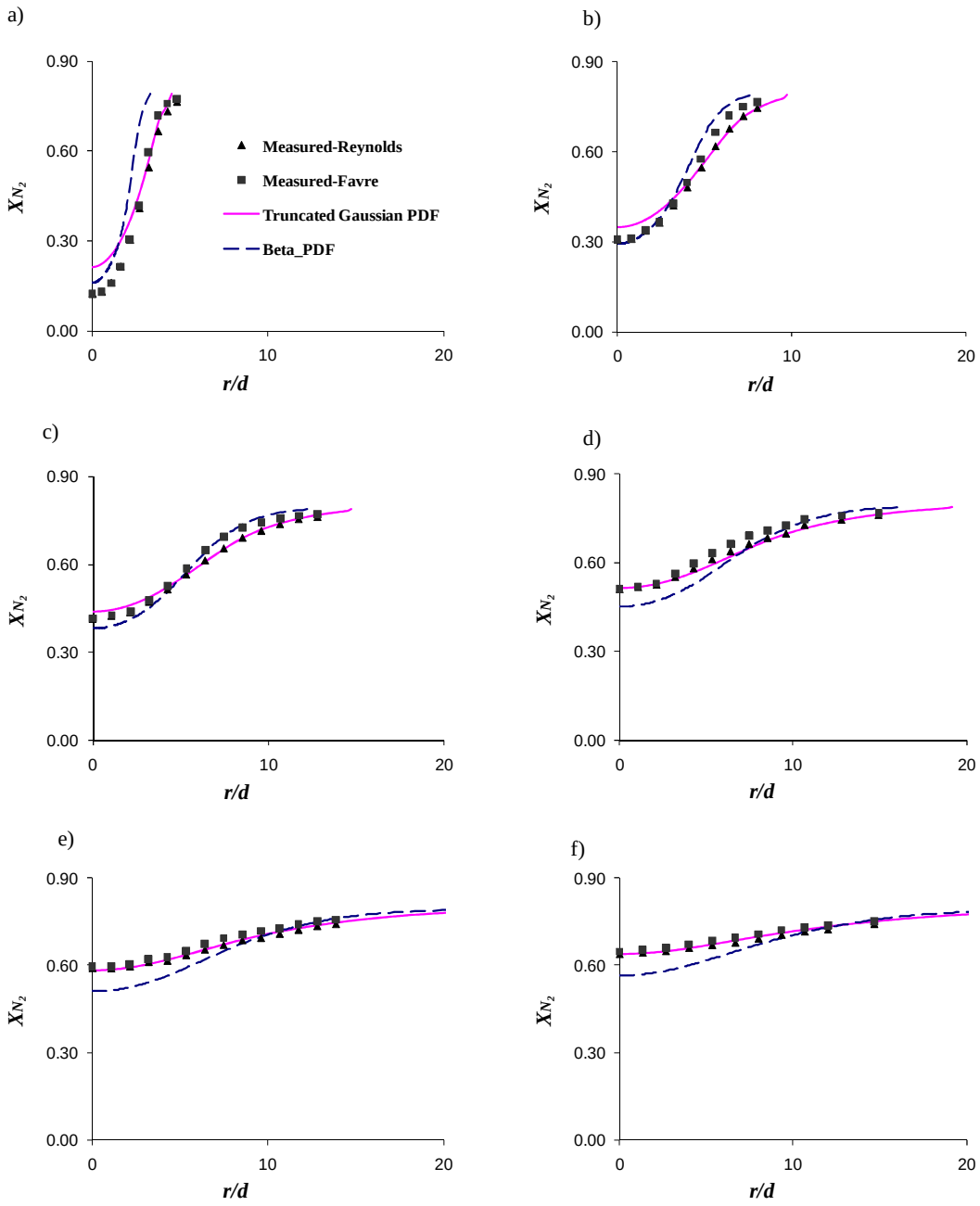

Figure 5. 16: Radial profiles of nitrogen mole fraction in turbulent hydrogen air diffusion flame using 100% hydrogen.
a) *r/d=22.5*, b) *r/d =45*, c) *r/d =67.5* d) *r/d =90*, e) *r/d =112.5* and f) *r/d =135*.

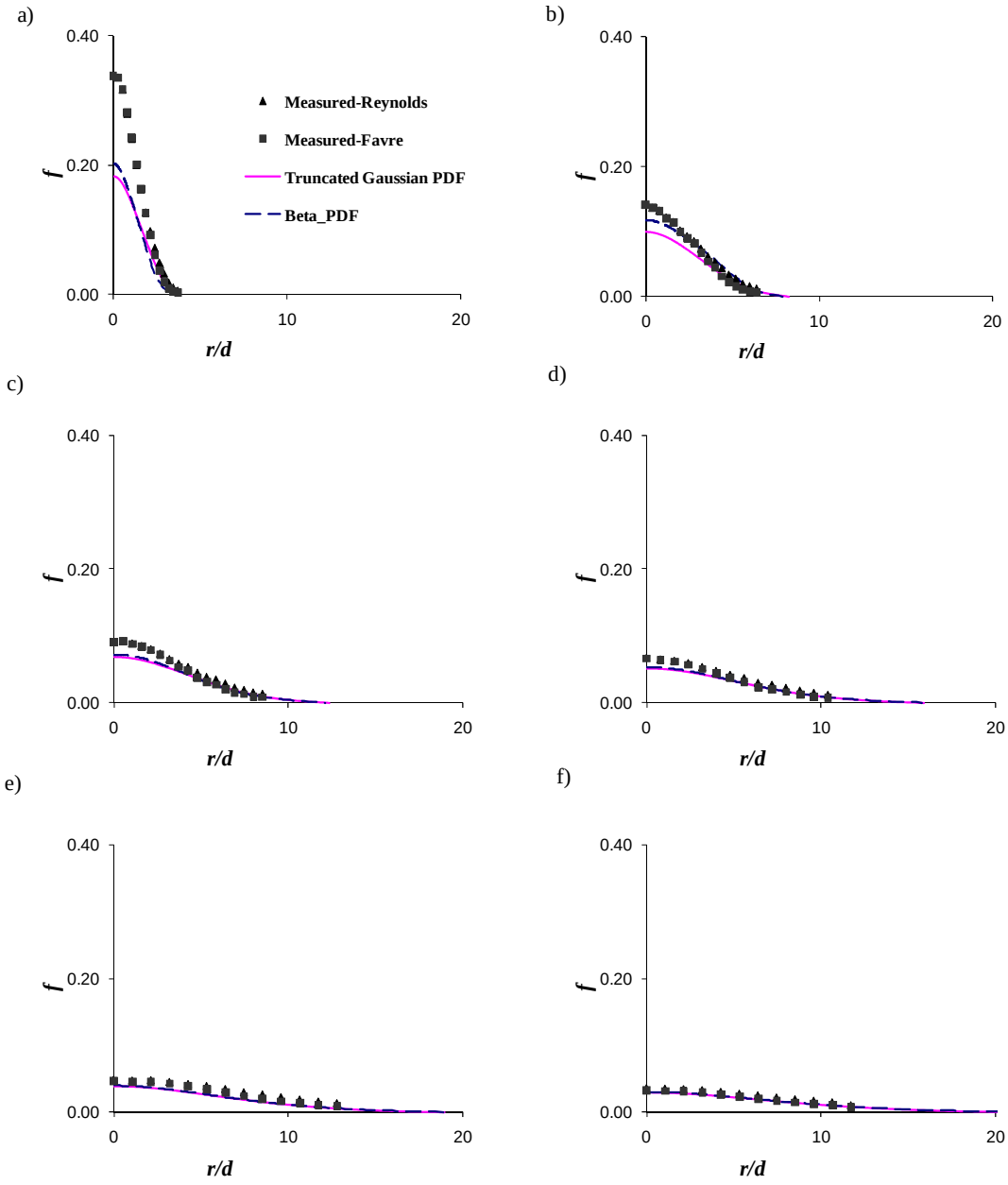

Figure 5. 17: Radial profiles of mean mixture fraction in turbulent hydrogen air diffusion flame using 80% hydrogen and 20% helium fuel.
a) *r/d =18.75*, b) *r/d =37.5*, c) *r/d =56.25*, d) *r/d =75*, e) *r/d =93.75* and f) *r/d =112.5*.

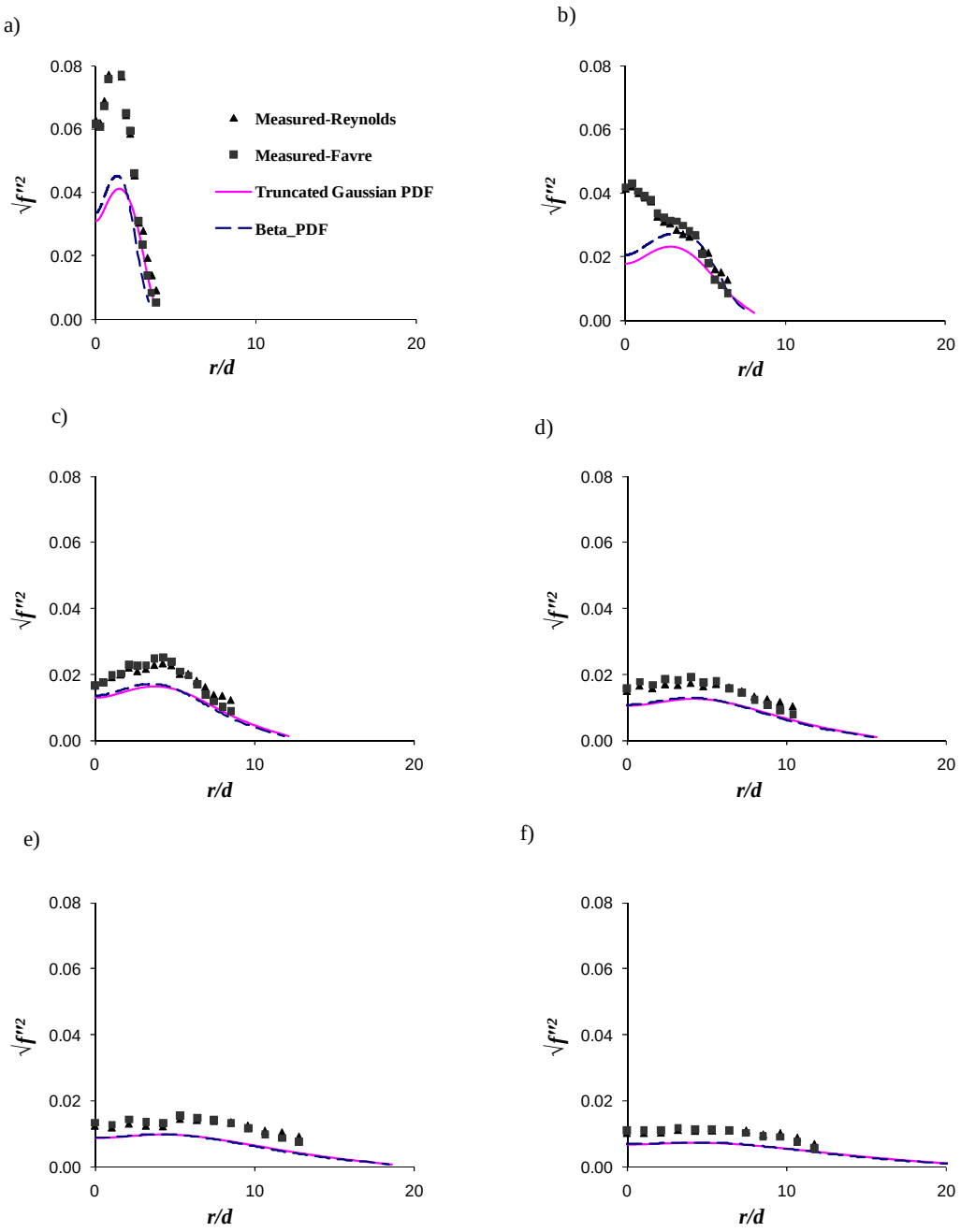

Figure 5. 18: Radial profiles of RMS mixture fraction in turbulent hydrogen air diffusion flame using 80% hydrogen and 20% helium in the flame.
a) *r/d =18.75*, b) *r/d =37.5*, c) *r/d =56.25*, d) *r/d =75*, e) *r/d =93.75* and f) *r/d =112.5*.

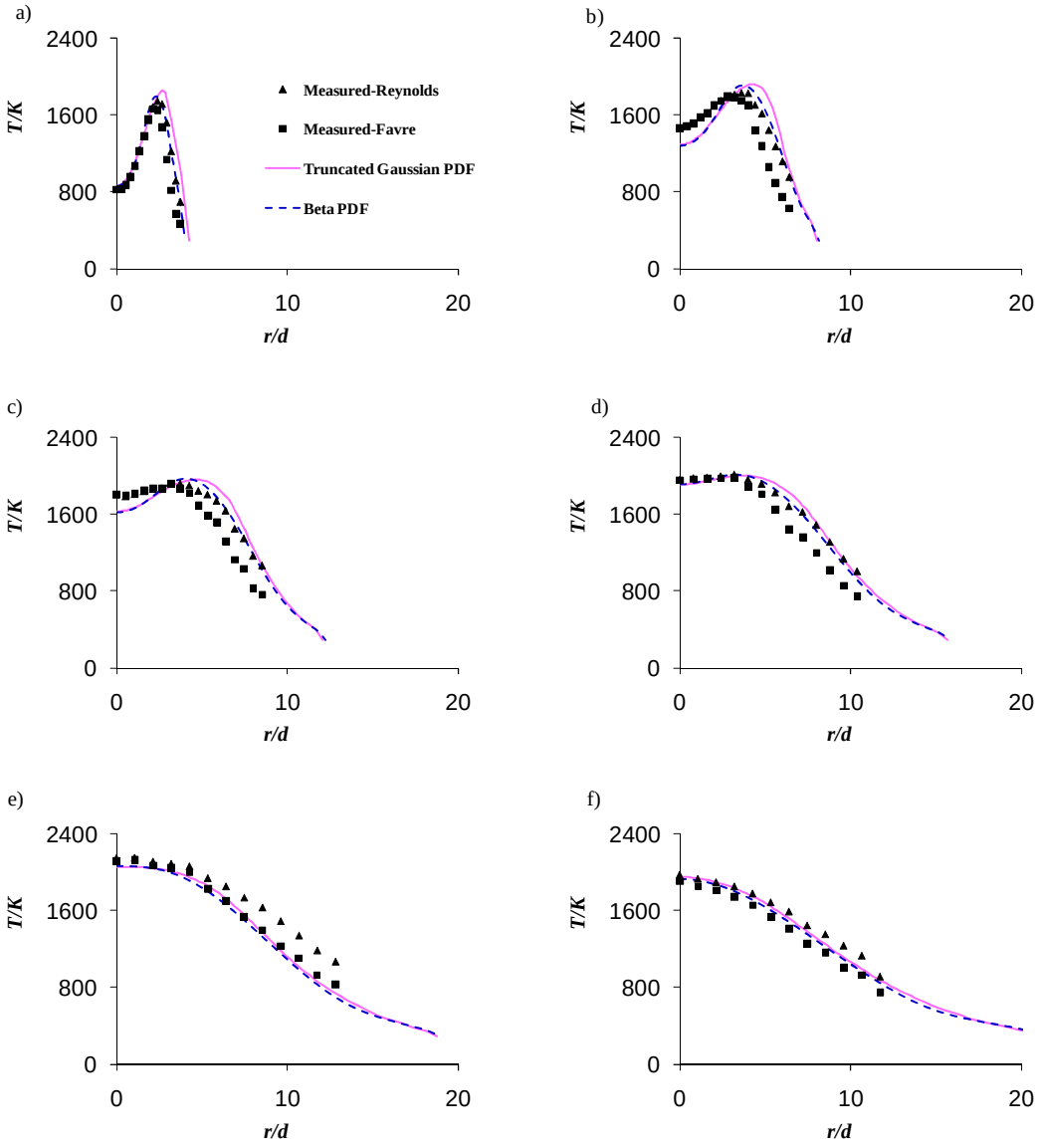

Figure 5. 19: Radial profiles of mean temperature T in turbulent hydrogen air diffusion flame using 80% hydrogen and 20% helium fuel.
a) *r/d =18.75*, b) *r/d =37.5*, c) *r/d =56.25*, d) *r/d =75*, e) *r/d =93.75* and f) *r/d =112.5*.

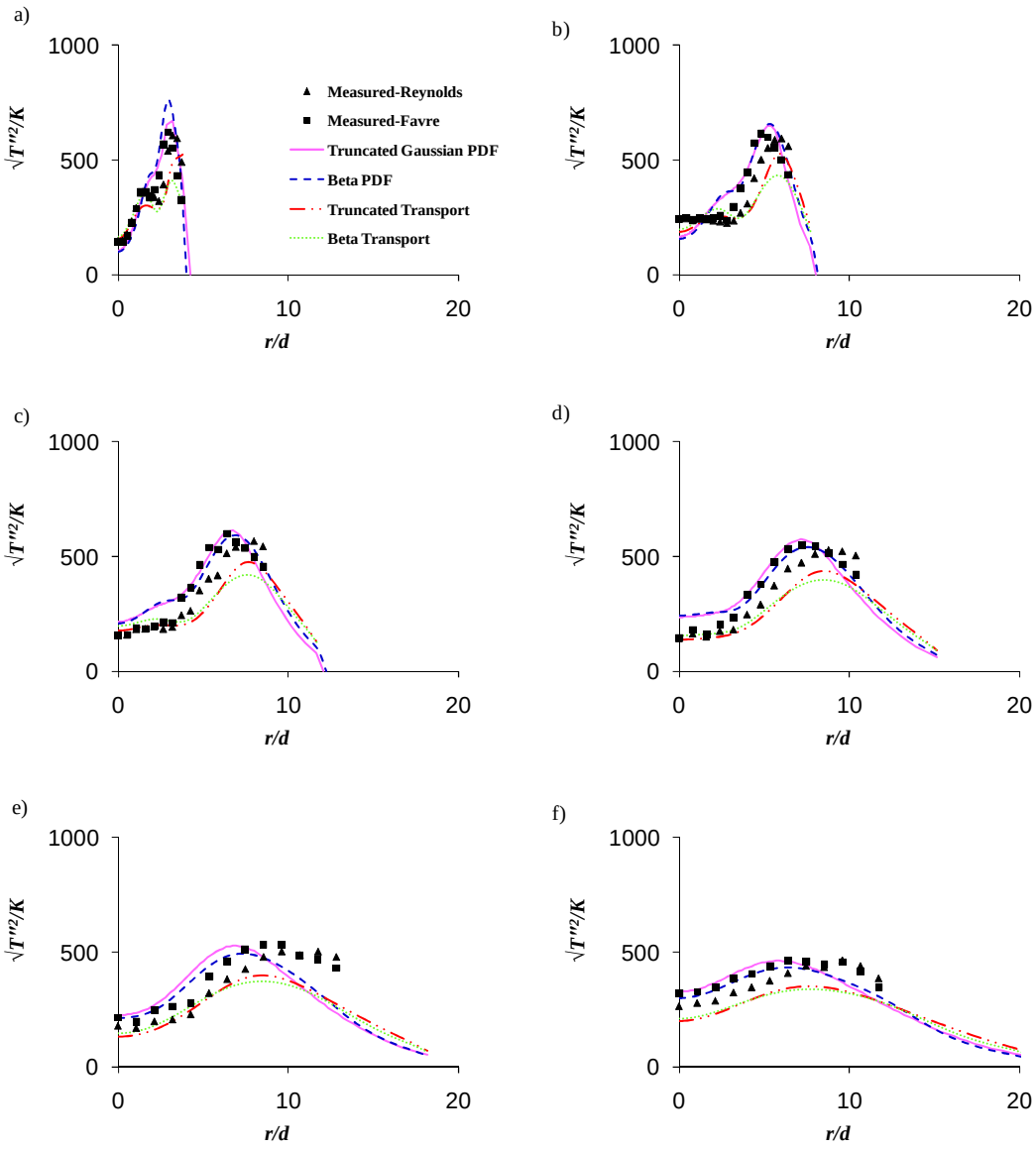

Figure 5. 20: Radial profiles of RMS temperature in turbulent hydrogen air diffusion flame using 80% hydrogen and 20% helium fuel.
a) *r/d =18.75*, b) *r/d =37.5*, c) *r/d =56.25*, d) *r/d =75*, e) *r/d =93.75* and f) *r/d =112.5*.

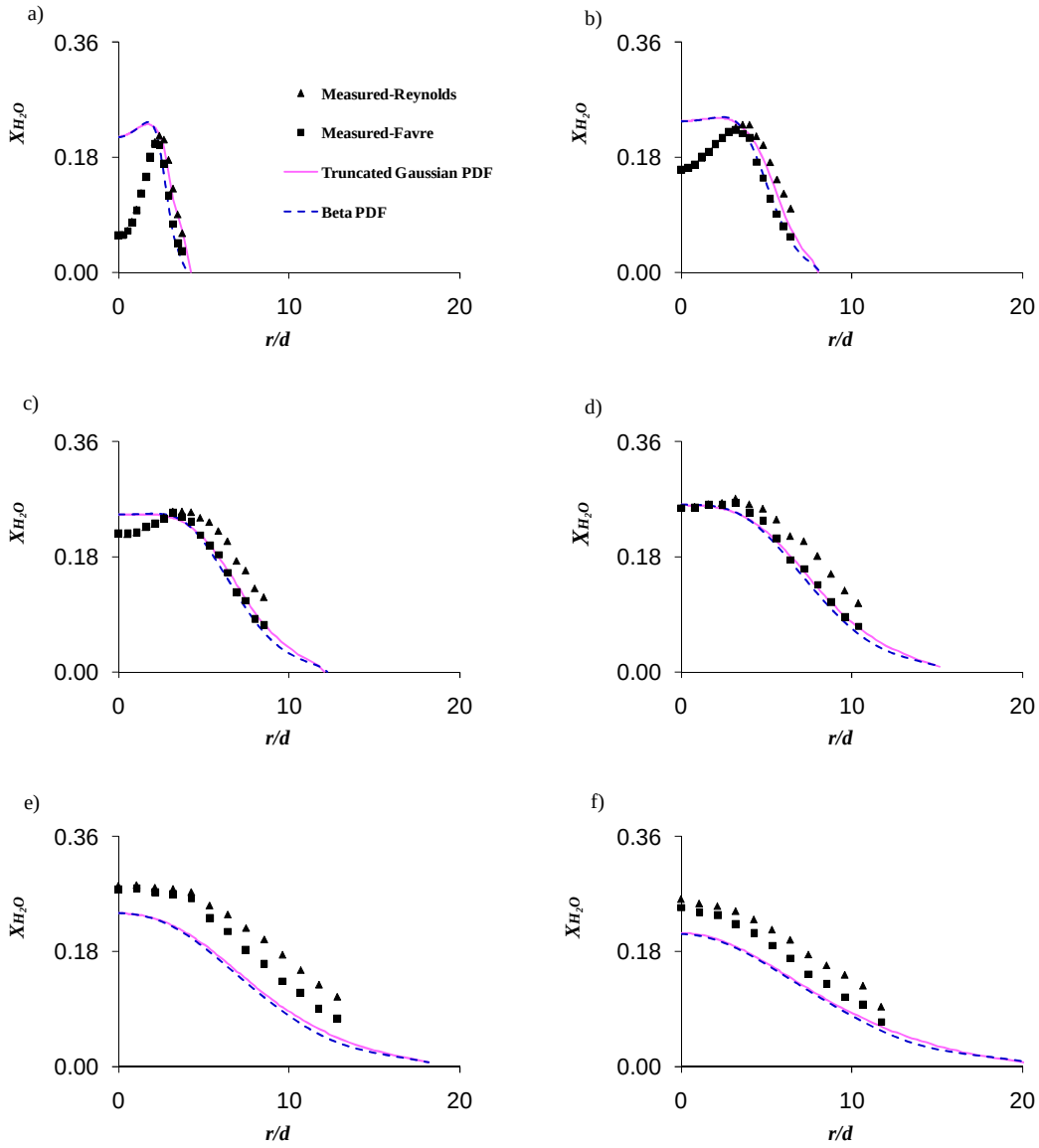

Figure 5. 21: Radial profiles of mean H_2O mole fraction in turbulent hydrogen air diffusion flame using 80% hydrogen and 20% helium fuel.
a) *r/d =18.75*, b) *r/d =37.5*, c) *r/d =56.25*, d) *r/d =75*, e) *r/d =93.75* and f) *r/d =112.5*.

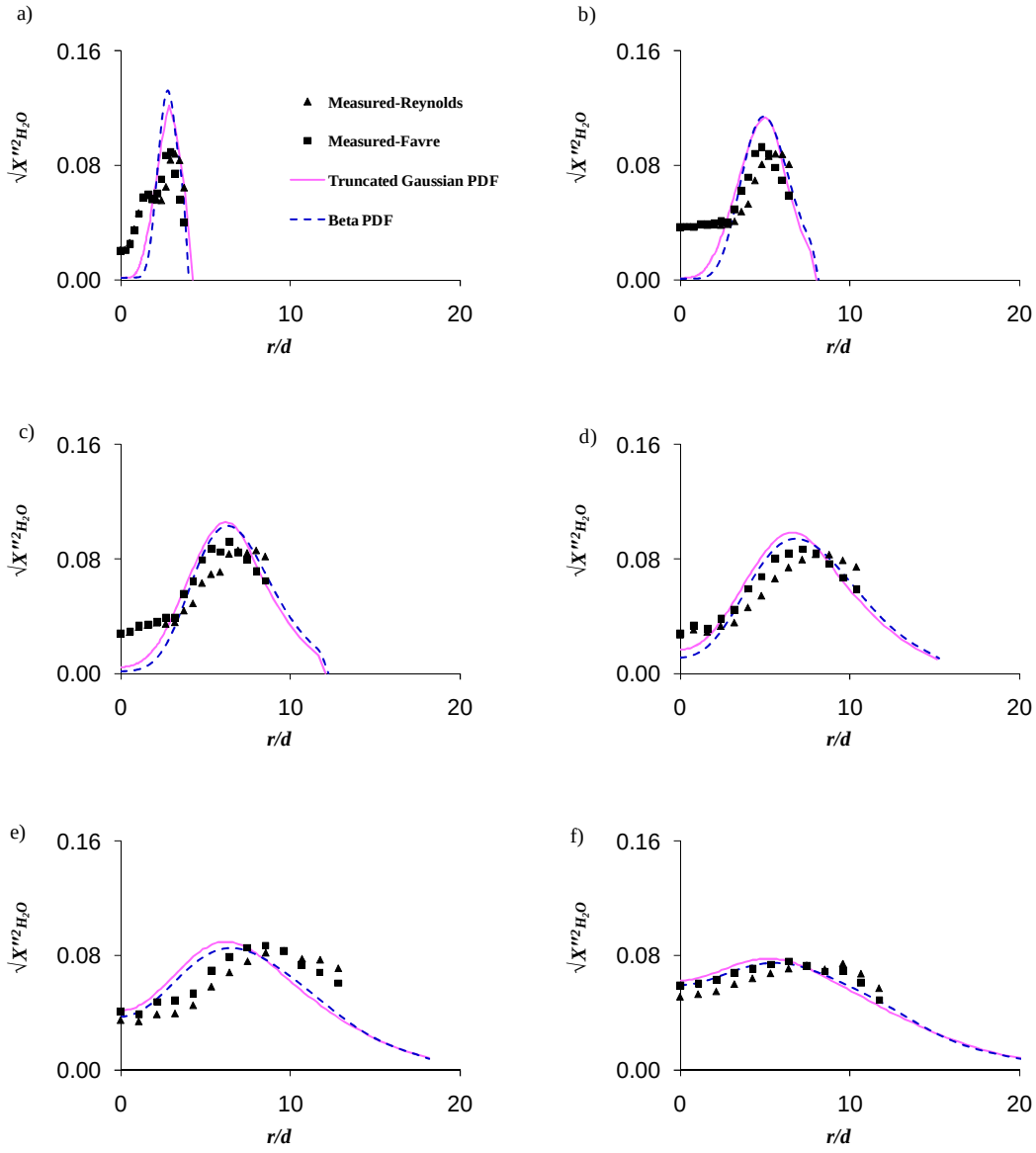

Figure 5. 22: Radial profiles of RMS H_2O mole fraction in turbulent hydrogen air diffusion flame using 80% hydrogen and 20% helium fuel.
a) *r/d =18.75*, b) *r/d =37.5*, c) *r/d =56.25*, d) *r/d =75*, e) *r/d =93.75* and f) *r/d =112.5*.

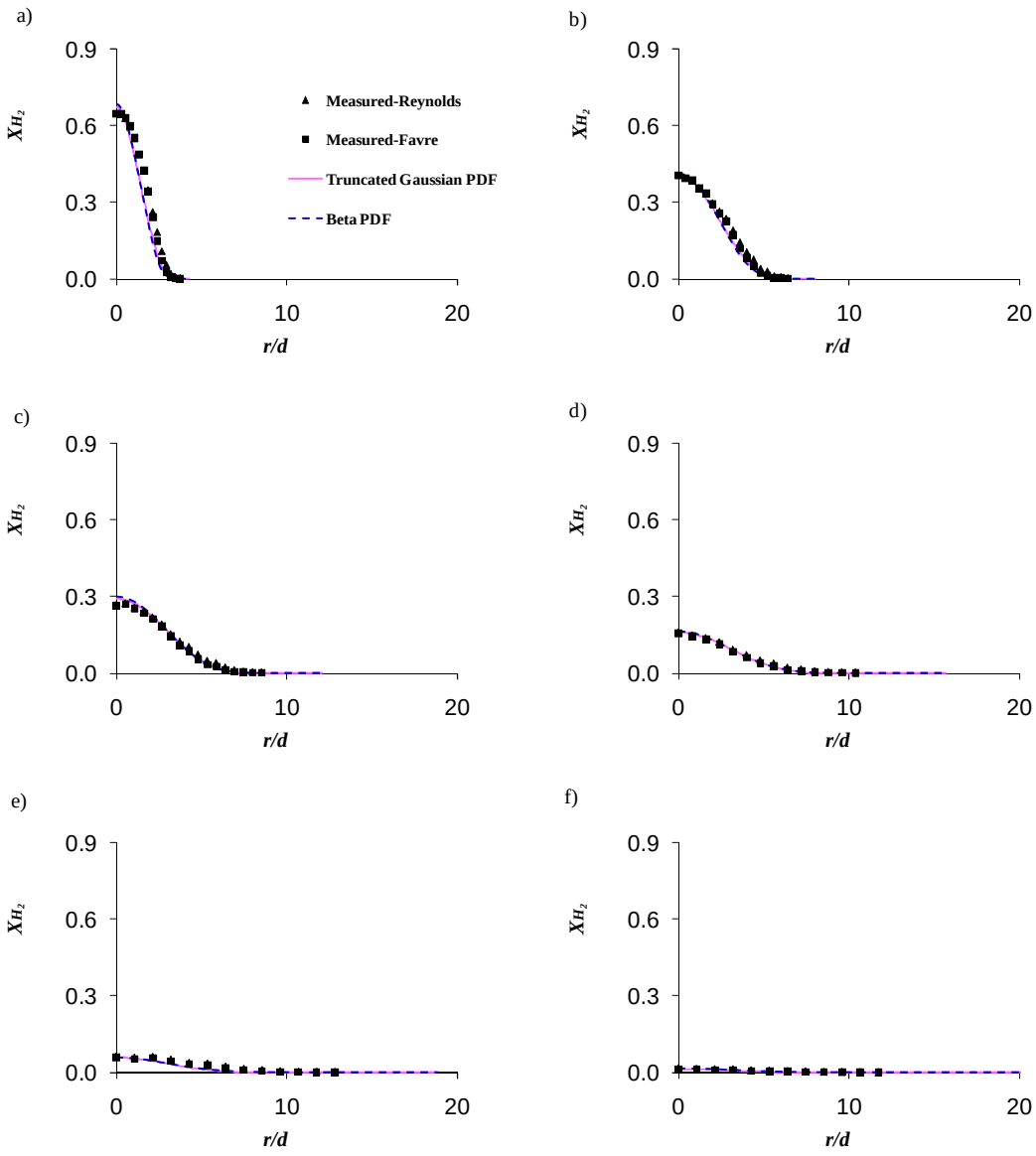

Figure 5. 23: Radial profiles of hydrogen mole fraction in turbulent hydrogen air diffusion flame using 80% hydrogen and 20% helium fuel.
a) *r/d =18.75*, b) *r/d =37.5*, c) *r/d =56.25*, d) *r/d =75*, e) *r/d =93.75* and f) *r/d =112.5*.

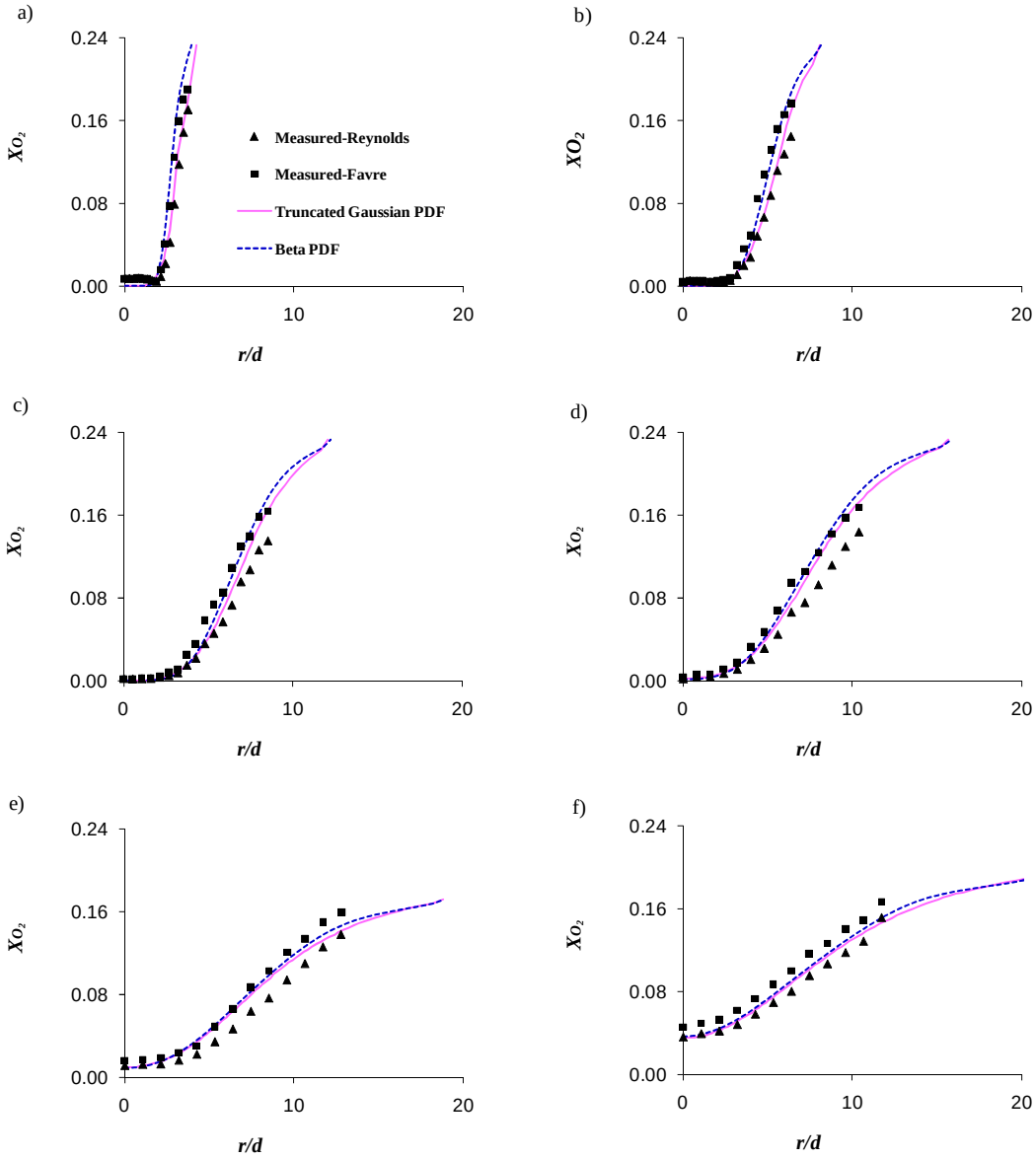

Figure 5. 24: Radial profiles of oxygen mole fraction in turbulent hydrogen air diffusion flame using 80% hydrogen and 20% helium fuel.
a) *r/d =18.75*, b) *r/d =37.5*, c) *r/d =56.25*, d) *r/d =75*, e) *r/d =93.75* and f) *r/d =112.5*.

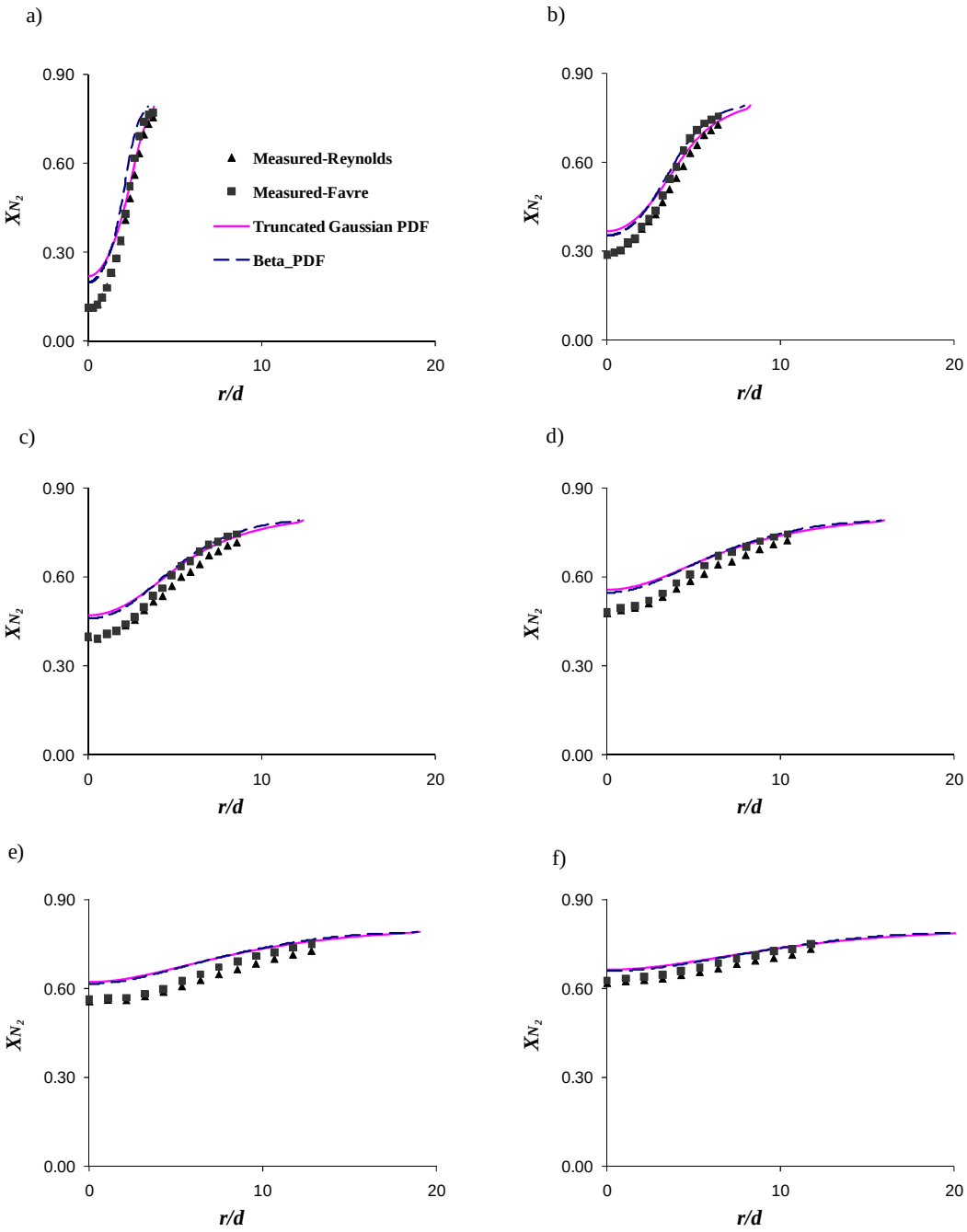

Figure 5. 25: Radial profiles of Nitrogen mole fraction in turbulent hydrogen air diffusion flame using 80% hydrogen and 20% helium fuel.
a) *r/d =18.75*, b) *r/d =37.5*, c) *r/d =56.25*, d) *r/d =75*, e) *r/d =93.75* and f) *r/d =112.5*.

a)

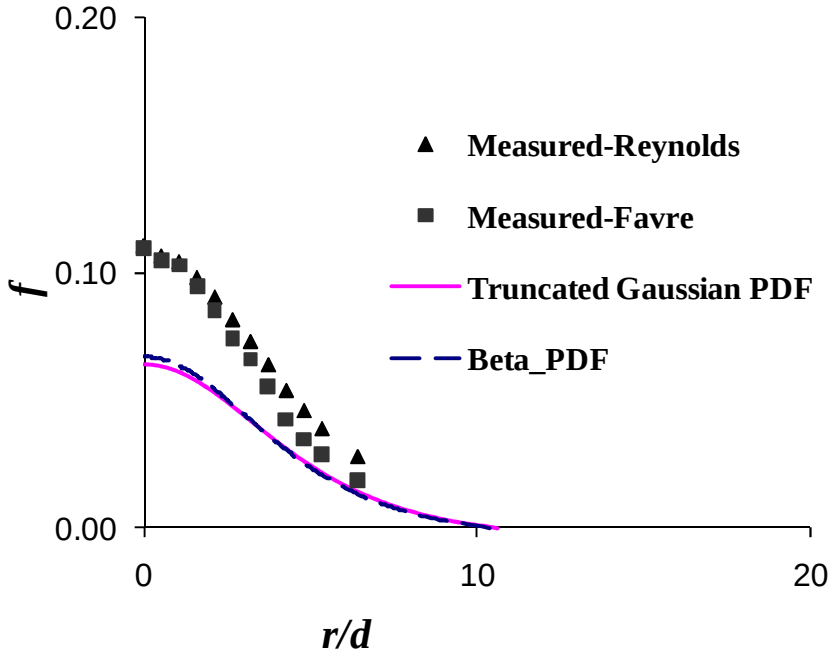

b)

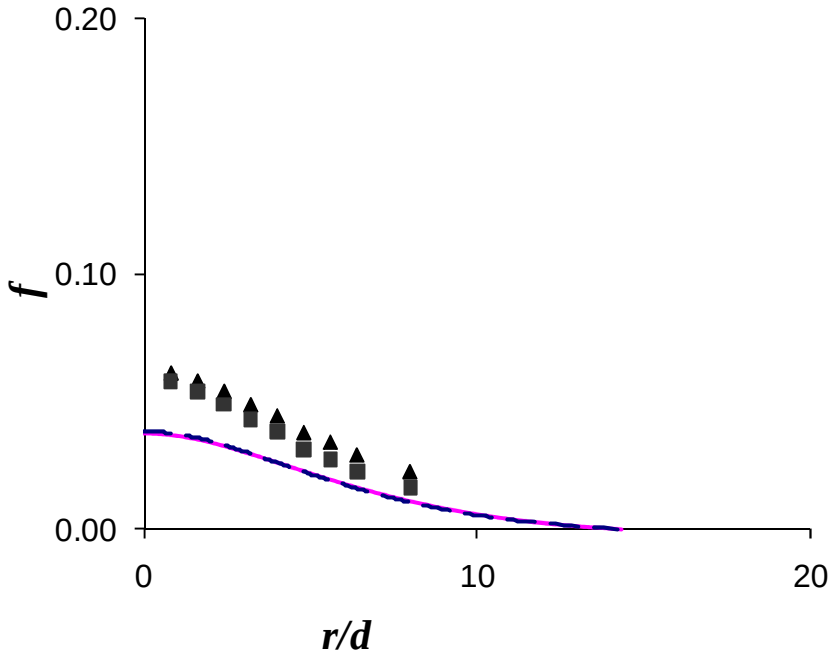

Figure 5. 26: Radial profiles of mean mixture fraction in turbulent hydrogen air diffusion flame using 60% hydrogen and 40% helium fuel.
a) *r/d =50* and b) *r/d =75*.

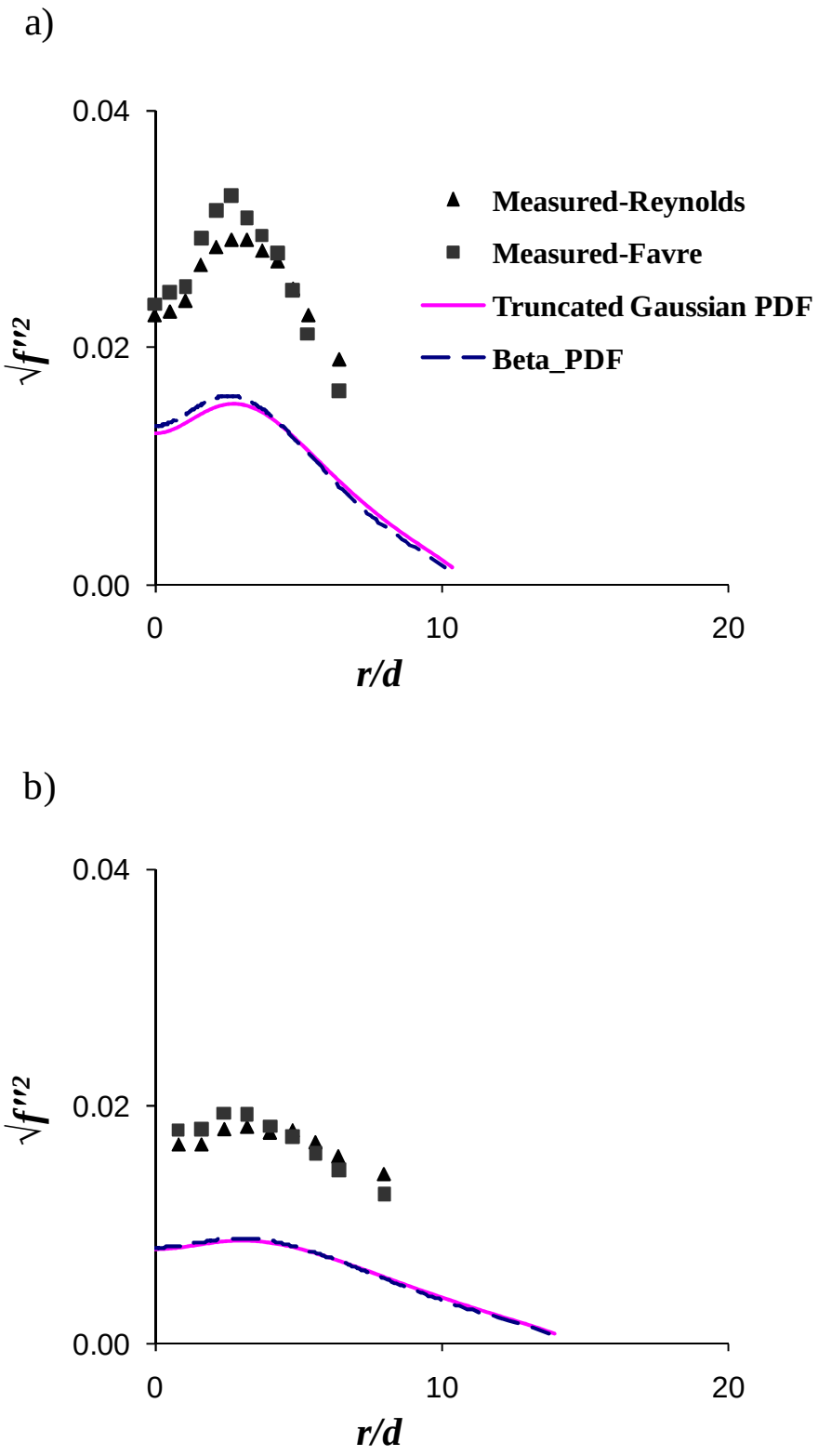

Figure 5. 27: Radial profiles of RMS mixture fraction in turbulent hydrogen air diffusion flame using 60% hydrogen and 40% helium fuel.
a) *r/d =50* and b) *r/d =75*.

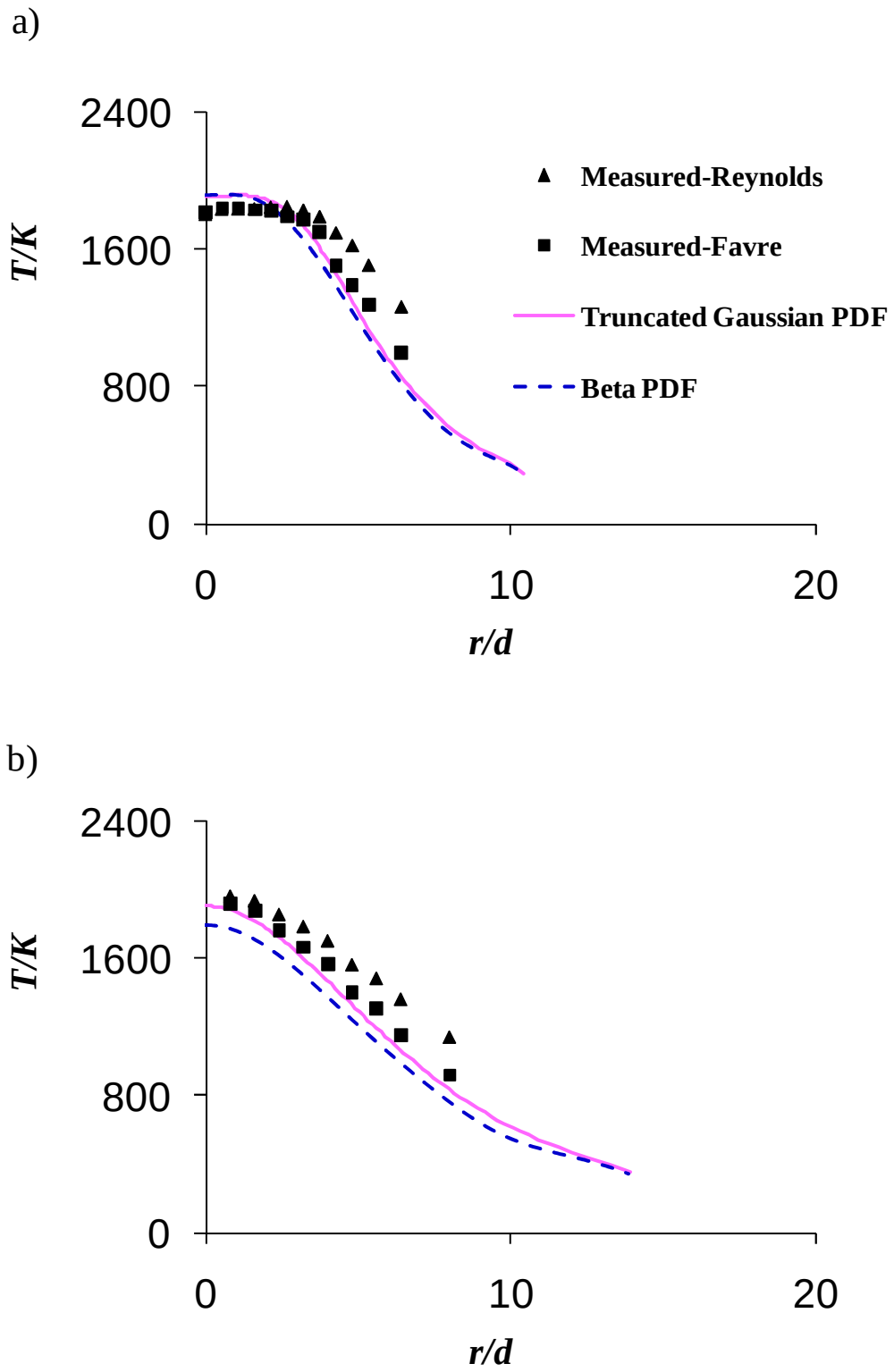

Figure 5. 28: Radial profiles of mean temperature in turbulent hydrogen air diffusion using 60% hydrogen and 40% helium in the flame.
a) *r/d =50* and b) *r/d =75*.

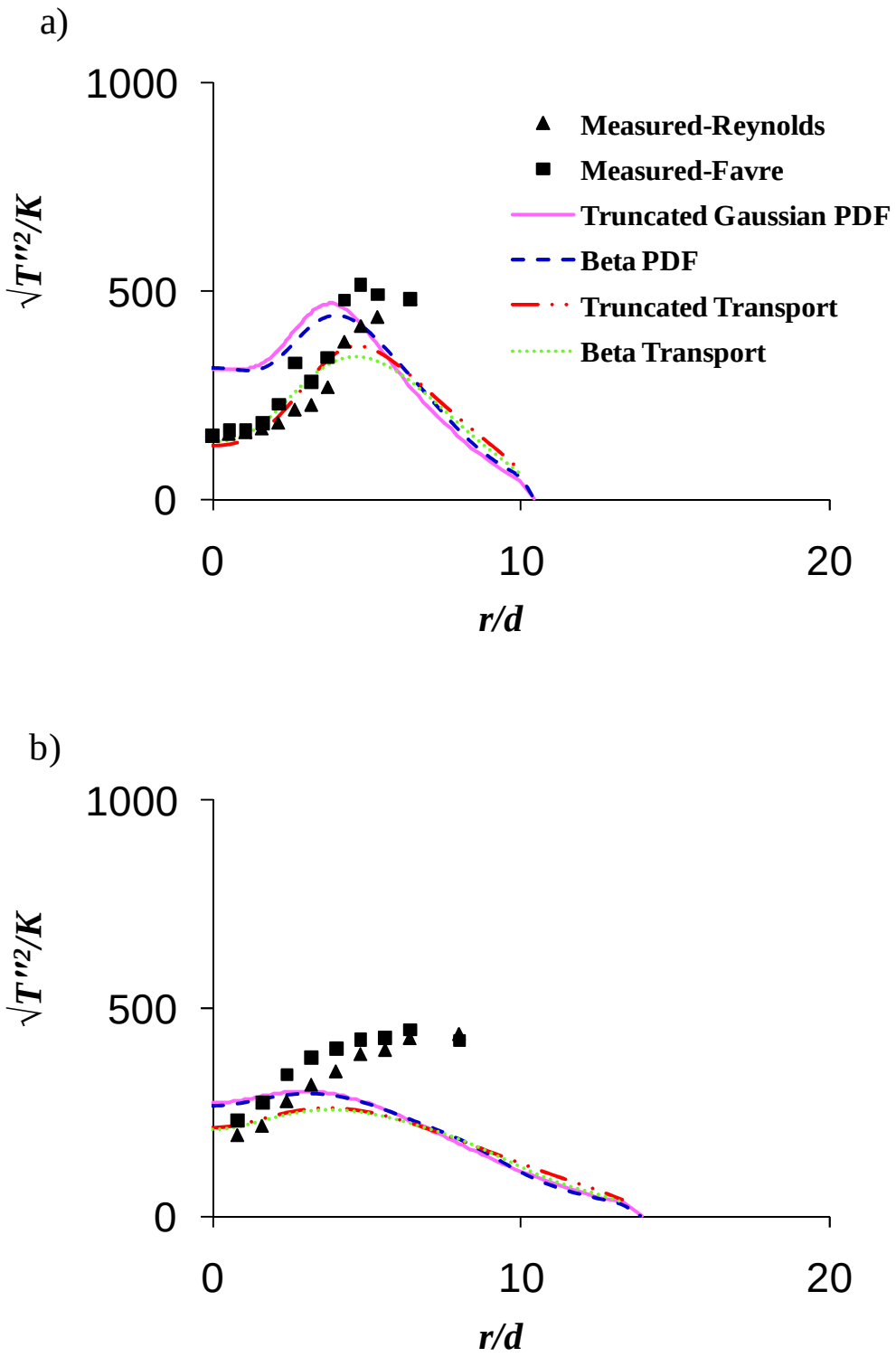

Figure 5. 29: Radial profiles of RMS temperature in turbulent hydrogen air diffusion flame using 60% hydrogen and 40% helium fuel.
a) *r/d =50* and b) *r/d =75*.

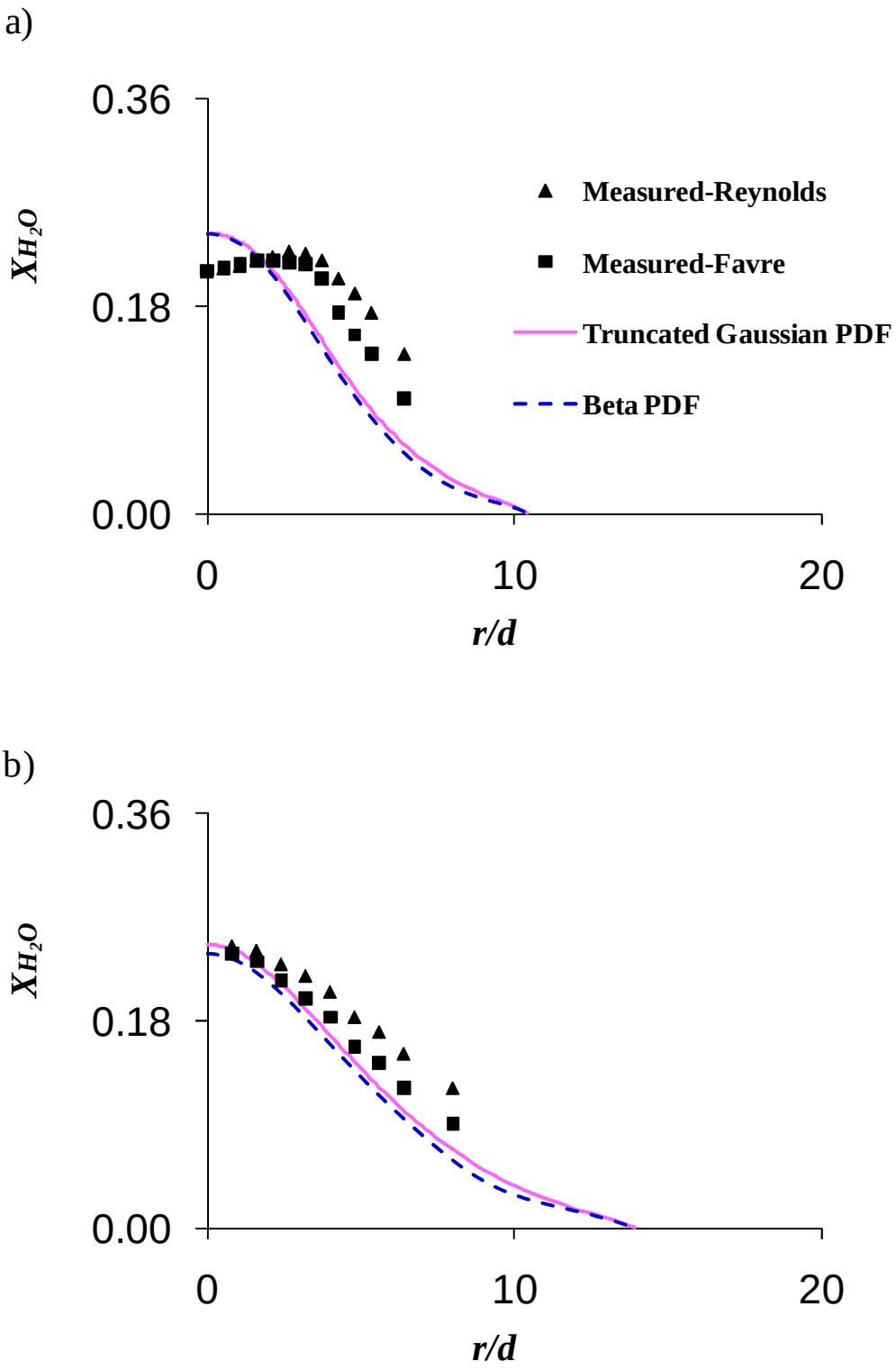

Figure 5. 30: Radial profiles of H_2O mole fraction in turbulent hydrogen air diffusion using 60% hydrogen and 40% helium fuel.
a) *r/d =50* and b) *r/d =75*.

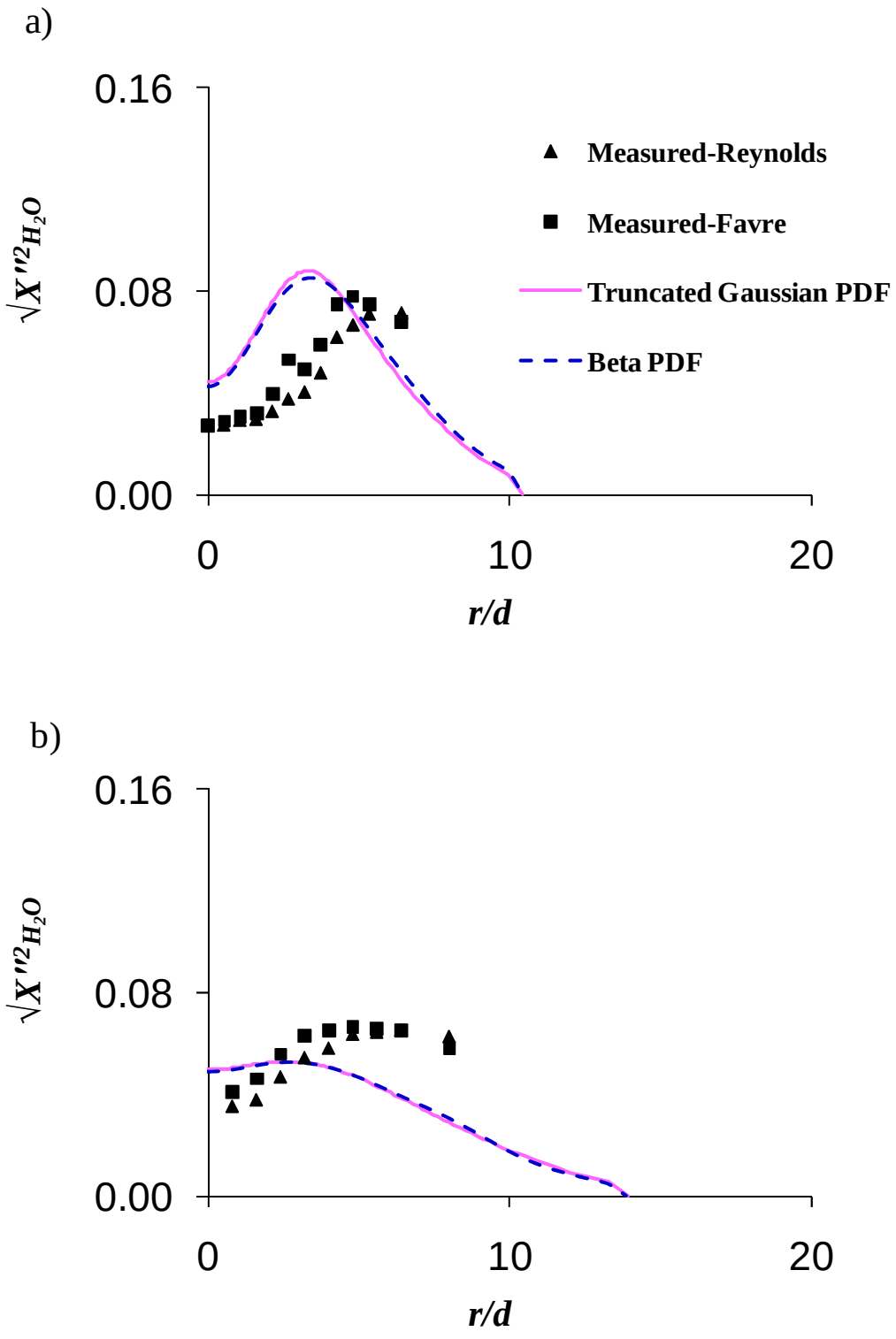

Figure 5. 31: Radial profiles of RMS H_2O mole fraction in turbulent hydrogen air diffusion flame using 60% hydrogen and 40% helium fuel.
a) *r/d =50* and b) *r/d =75*.

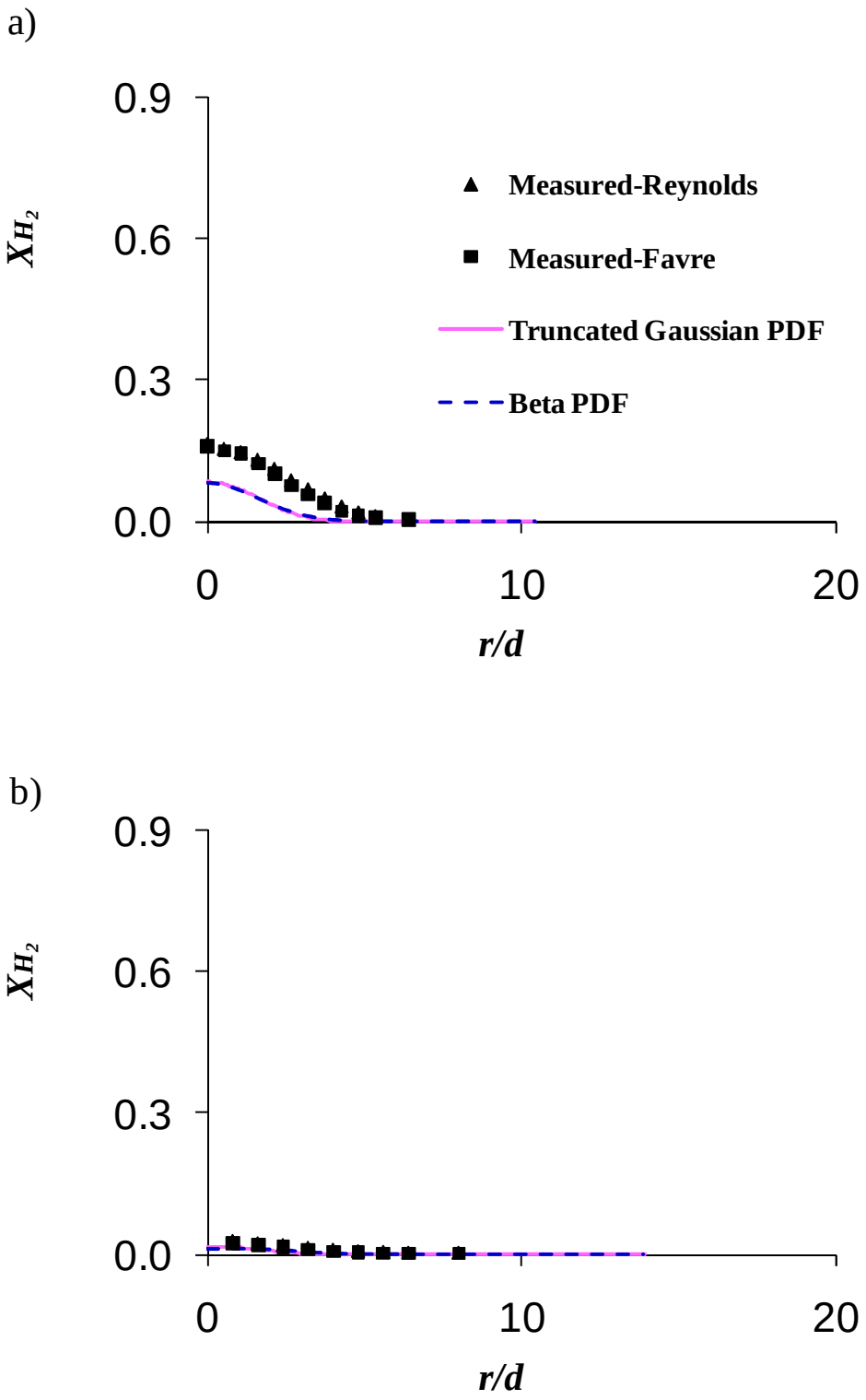

Figure 5. 32: Radial profiles of hydrogen mole fraction in turbulent hydrogen air diffusion flame using 60% hydrogen and 40% helium fuel.
a) *r/d =50* and b) *r/d =75*.

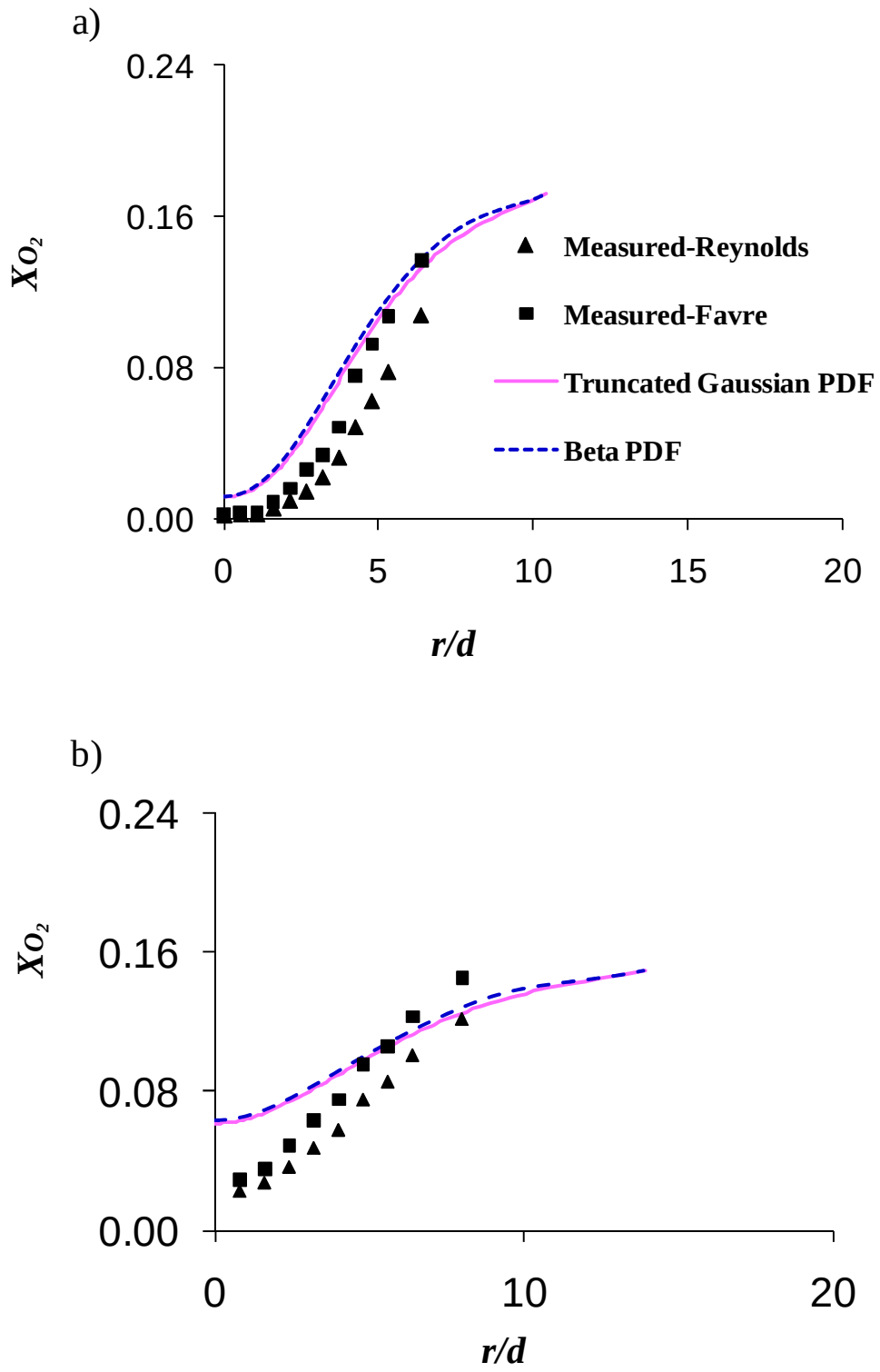

Figure 5. 33: Radial profiles of Oxygen mole fraction in turbulent hydrogen air diffusion flame using 60% hydrogen and 40% helium fuel.
a) *r/d =50* and b) *r/d =75*.

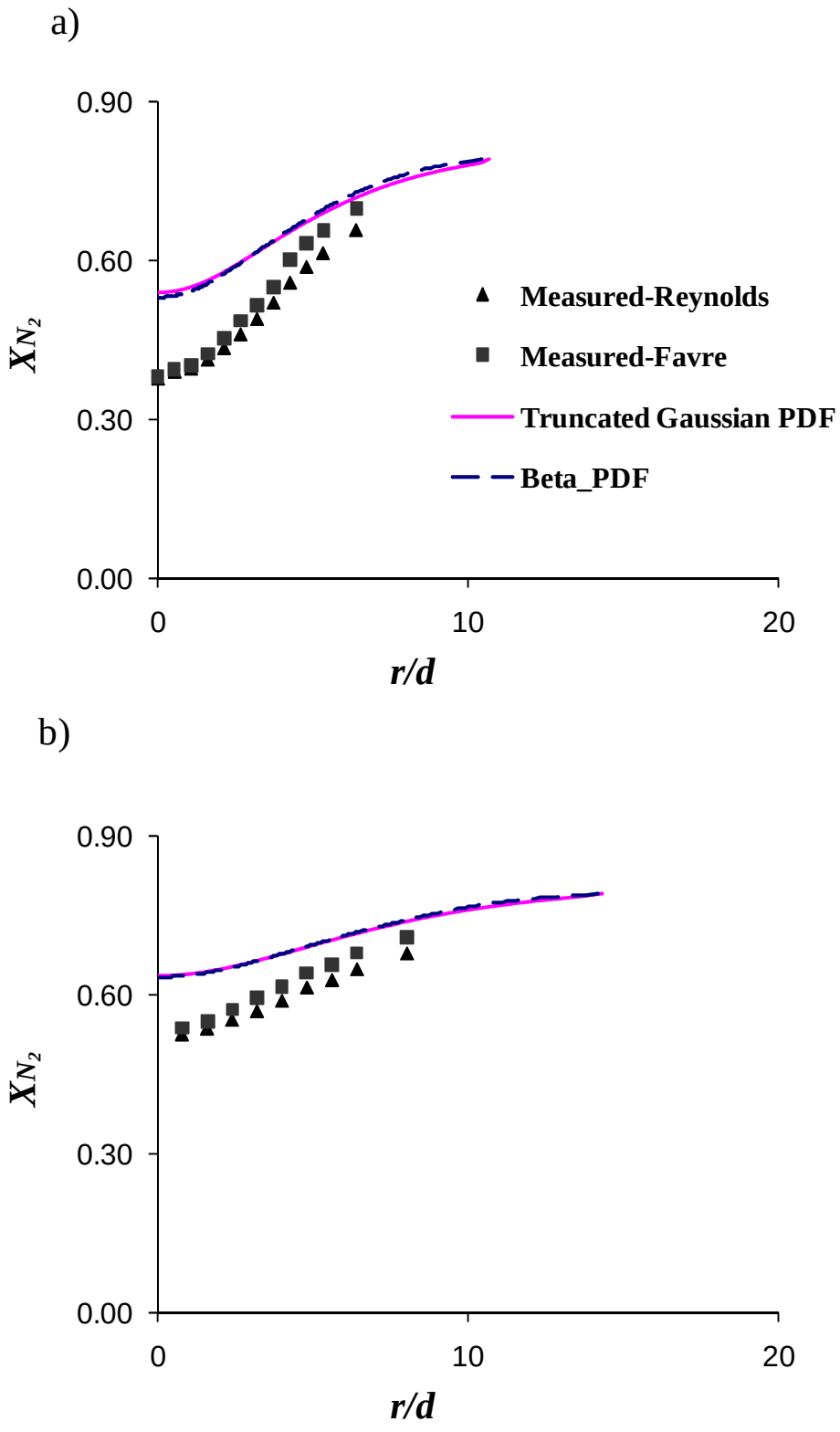

Figure 5. 34: Radial profiles of Nitrogen mole fraction in turbulent hydrogen air diffusion flame using 60% hydrogen and 40% helium fuel.
a) *r/d =50* and b) *r/d =75*.

Chapter 6

Radiation analysis of hydrogen flames

In chapter five we confirmed the flame structure model can predict $\overline{T}$, $\sqrt{\widetilde{T''^2}}$, $\overline{X}_{H_2O}$ and $\sqrt{\widetilde{X''^2_{H_2O}}}$ accurately, in this chapter we move on to consider the prediction of the radiation field. The scalar fields obtained from the flame structure model show generally good agreement with the measured experimental data. This allows the information from these calculations to be confidently passed to a detailed calculation, of the spectrally resolved radiative properties. This chapter focuses on thermal radiation modelling in hydrogen jet fires, a challenging task. The radiation field is highly anisotropic in nature with a relatively small volume of gas dominating the field of view of the receivers external to the fire. The anisotropy means that the direction cosine dependence of the intensity field must be modelled using an approach that allows the evaluation of the heat flux integral from the intensity field to be as accurate as required by the user. This means that a model based on a differential approximation such as the six flux model [196] is not appropriate.

One approach that is numerically exact for anisotropic radiation fields is one that includes ray tracing as a component of the solution strategy such as that used in the discrete transfer method [194, 198]. Ray tracing can be a potentially time consuming process, the computational time being sensitive to the number of rays used and the fineness of representation of the flame structure on the finite volume mesh. An additional difficulty arises from our choice of fuel and the scale of the jet fire as the spectral intensity distribution for a pencil of radiation is banded in nature making the grey gas approximation invalid adding to the computational cost. This occurs as there is no soot present in a hydrogen jet fire. Thermal emission is sensitive to the fluctuations in the temperature and participating H_2O concentration field as the jet fires used in this investigation are turbulent. The non-linear dependence of the Planck distribution on temperature means that there is a tendency for more radiation to be emitted from a turbulent fire than an analysis based on the mean flow fields would imply as discussed in previous chapters. Thermal radiation measurements and predictions may be useful

for evaluating turbulent combustion models because of their strong sensitivity to fluctuating scalar properties.

6.1 Hydrogen Jet Fire Experiments

Two jets studied by Faeth et al [40] are considered to predict the spectral radiation intensity and radiative heat flux. In each case the nozzle diameter is 5mm. The jet fires differ in the source mean stream-wise velocity prescribed. A low speed jet fire with a source velocity of 66.3 ms^{-1} and a high speed jet fire with a source velocity of 108.4 ms^{-1} are considered. For convenience we will refer to the jet fires by the source Reynolds numbers, Re=3,000 and Re=5,722. Faeth et al. [40] studied rim-stabilised jet fires as they used a coflow of hydrogen to anchor their flames onto the burner nozzle. The jet fire model can simulate both lifted and rim stabilised jet fire. As a result, the spectral radiation intensity and incident heat flux distribution for the two different types of jet fire are similar in the far field, potentially making it possible to use Faeth's [40] measurement to validate the radiation models in this investigation.

6.2 TRI methodologies

The radiation computations in this investigation were performed using a modified version of the computer code RADCAL developed by Grosshandler [207], which employs a narrow band model considering both collision and Doppler broadening for an inhomogeneous path length. The radiation model used in this investigation considers molecular emission from H_2O. Although N_2, O_2, and H_2 are present in the mixture, they are transparent to infrared radiation and do not directly enter into the investigation. The present approach takes the assumption that the equation of transfer along a line of sight, with negligible intensity at the far boundary, can be integrated to obtain the spectral intensity along the path length.

Mean properties are usually used to calculate radiation from the flames. However, the effects of turbulent fluctuations must be considered since radiation is a non-linear function of flame properties such as temperature as illustrated in Figure 6.1. The mean temperature (*Tmean*) which is seen in Figure 6.1 varies smoothly whereas the instantaneous temperature (*Tinst*) fluctuates as it traverses the ray path and is difficult to

characterise. We have developed a radiation model to adequately compute radiation heat transfer from a fluctuating source.

Three methods are investigated to predict the spectral radiation intensity and radiative heat flux external to the fire using the turbulent flow fields of flames accurately predicted in chapter five: namely,

- The mean property method,
- Stochastic simulation
- The mean emission method.

All three methods used DTM to evaluate the incident radiation flux integral.

6.2.1 The mean property method

The mean property fields were calculated by integrating the PDF combined with the appropriate flamelet over the instantaneous mixture fraction. For convenience we present the RTE where scattering is ignored again, taken from chapter three. The spectral radiant heat flux along a line of sight can be determined from the equation of transfer.

$$\frac{\partial I_\lambda}{\partial s} + \kappa_\lambda \rho I_\lambda = \kappa_\lambda \rho \frac{e_{\lambda,b}}{\pi} \tag{6.1}$$

Where $e_{\lambda b}$ is the blackbody spectral emissive power. After integration, assuming that the radiance is small at $s = 0$, the equation can be rewritten as:

$$I_\lambda(s) = \int_0^s \frac{e_{\lambda,b}(s')}{\pi} \frac{\partial}{\partial s'} \tau_\lambda(s, s') ds' \tag{6.2}$$

where τ_λ is the spectral transmittance.

$$\tau_\lambda(s,s') = \exp\left[-\int_{s'}^{s} \kappa_\lambda(s'')\rho(s'')ds''\right] \tag{6.3}$$

The total intensity in a given direction at the sensor is evaluated by integrating with respect to wavelength

$$I(s) = \int_0^\infty I_\lambda(s)d\lambda \tag{6.4}$$

The radiative heat flux at a sensor is given by the integral

$$H = \int_{\Delta\theta} I(s)\cos\theta d\Omega \tag{6.5}$$

Where the integration is over the field of view of the sensor, Ω represents the solid angle and $\cos\theta$ is introduced to account for Lambert Cosine Law. θ is the angle a ray makes with the normal vector of the sensor.

In the DTM equation (6.5) simplifies to the radiative heat flux at the surface of the sensor, H is then given by summing over all paths j

$$H = \sum_{j=1}^{n} \left(I\cos\theta\,\Delta\Omega\right)_j \tag{6.6}$$

Where the path of ray j passes through the centroid of the portion of solid angle with solid angle area $\Delta\Omega$.

We evaluated the incident flux integral as it is expressed in spherical co-ordinates and the field of view discretised with a uniform spacing in the angle of rotation (φ) and angle of incidence (θ). The incident intensity distribution is assumed piece-wise constant over the field of view of the receiver, with each element of the discretisation taking the value of the incident intensity at its centroid as being representative of the whole element. The incident intensity over an element is calculated by tracing the ray with orientation defined by the centroid, through the computational domain, noting the control volumes of the finite volume grid traversed. In each control volume traversed the length of ray segment and local thermo-chemical quantities are noted. The ray trace is terminated at the computational boundary.

Using the temperature flamelet in conjunction with the instantaneous mixture fraction f we can determine the adiabatic temperature $\tilde{T}_{adia}$ defined as

$$\tilde{T}_{adia} = \int_0^1 T(f)\, pdf(\tilde{f}, \tilde{f}''^2) df . \tag{6.7}$$

The mean temperature can then be evaluated using the enthalpy perturbation

$$\tilde{T} = \tilde{T}_{adia} - \frac{\triangle h}{C_{p,mix}\left(\bar{T}_{adia}\right)} \tag{6.8}$$

It is assumed that turbulence fluctuations have no effect on radiation properties in the mean property method. The properties needed for the calculation are taken to be average scalar quantities such as temperature and species concentrations, which are supplied from predictions of the flame structure model discussed comprehensively in Chapter 5. For hydrogen jet fires previous studies Faeth et al [40] using the mean prediction method suggest this approach tends to under-predict radiation fields. In Figures 6.2 and 6.3 using the mean property method predictions were carried out at three axial locations and with two different flow configurations. In all locations the mean property method under-predicts the radiation field by approximately 20%. However, the truncated Gaussian PDF shows better agreement than the beta PDF predictions compared to Faeth measurements. The mean property method is computationally less expensive than other methods but; the drawback with this method is its inability to account for the fluctuations that occur in turbulent jet flames.

6.2.2 Stochastic method

If radiation properties and scalar properties were linearly dependent on mixture fraction, the mean property method is exact. However, this is not correct for flames. As a result, turbulence fluctuations can have a significant effect on radiative transfer. The stochastic method seeks to provide insight concerning the effect of turbulence radiation interactions using a model of turbulence. Consequently, this method is in contrast to the mean property method as it does consider the interaction between turbulent fluctuations and radiation.

The radiation intensities leaving a turbulent flame depend on the instantaneous scalar properties at all points along a radiation path. For optically thick wavelengths, the properties beyond a certain distance do not have a significant effect on the radiation field as the energy emitted is reabsorbed. The hydrogen/air flames studied are optically thin so the entire infrared spectrum is considered; the effects of fluctuations from all parts of the flame have an impact on turbulent radiation interactions. Consequently, a suitable scheme for the inverse interpretation of turbulent radiation interactions in terms of the multipoint scalar statistics may present valuable insights.

The instantaneous values of scalar required to solve the RTE along a line of sight, such as temperature and mole fractions of participating species, may be pseudo randomly generated assuming the shape of the PDF of these scalars. Using the results from the predictions of the flame structure, described earlier we will use the truncated Gaussian PDF and beta PDF for the distribution function of scalar quantities such as temperature and mole fraction of absorbing specie H_2O for all our radiation predictions.

The instantaneous values of a scalar, typically the mixture fraction, was generated from a presumed PDF such as a truncated Gaussian or beta PDF, while the instantaneous temperature and mole fractions of the absorbing species are related to the scalar through the laminar flamelet. Once the scalars distribution along the line of sight is known, the RTE may be solved to obtain the instantaneous spectral and total radiation intensity at the end of the optical path. This procedure is repeated for a sufficiently large number of samples to compute statistically significant mean intensity values.

For example

$$T_{inst,adia} = T_{flamelet}\left(f_{inst}\right) \tag{6.9}$$

strictly speaking this gives the instantaneous temperature without radiative heat loss. The radiative heat loss is incorporated into the stochastic method by assuming the ratio of the mean temperature to the mean adiabatic temperature is preserved in the instantaneous fields, so

$$T_{inst} = T_{inst,adia}\left(\frac{\tilde{T}}{\tilde{T}_{adia}}\right) \tag{6.10}$$

Implementing the stochastic method we defined the instantaneous mixture fraction f_{inst} implicitly using a cumulative probability density function (CPDF) as

$$z = \int_0^{f_{inst}} pdf\left(\tilde{f}, \widetilde{f''^2}\right) df \tag{6.11}$$

where z is a random number, $0 \le z \le 1$. The stochastic method relies on the efficient calculation of the instantaneous mixture fraction given a pseudo random number z. To this end for each control volume the CPDF (6.11) was evaluated numerically and an appropriate curve fit calculated using the least square fit algorithm embedded in the radiation software. A number of functions were investigated such as quadratic and cubic polynomials before deciding on quartic polynomials as being sufficiently accurate and simple to evaluate.

Figure (6.4) using equation (6.12) shows a comparison of the curve fits to the CPDF for two pairs of mean mixture fraction and mixture fraction variance using quadratic, cubic and quartic polynomial curve fits. The accuracy of the quartic fit is clear.

$$f_{inst}(z) = C_0 + C_1 z + C_2 z^2 + C_3 z^3 + C_4 z^4 \tag{6.12}$$

where C_0, C_1, C_2, C_3 and C_4 are coefficient constants determined by the curve fitting software. Examples of the curve fits (see Figures 6.5 and 6.6) showing the relationship between instantaneous mixture fraction and pseudo random number z for a number of values of mean mixture fraction and mean mixture fraction variance pairs.

Once the instantaneous mixture fraction is modelled the instantaneous temperature and instantaneous H_2O mole fraction follow from the laminar flamelet library as discussed above. In Figures 6.7 and 6.8 the instantaneous temperature and instantaneous H_2O mole fraction are shown as a function of the original pseudo random number variable z. Figures 6.4 – 6.8 justified the choice of the quartic polynomial as the fittings are satisfactory.

Having established the curve fitting algorithm implemented we now consider its application in the stochastic simulation of the instantaneous radiation field. For a characteristic ray passing through the fire starting from a receiver an instantaneous

profile of the temperature and H_2O mole fraction field can be calculated. These can then be input to the radiation model, RADCAL [207]. This will give one realisation of the spectral intensity distribution at the receiver for the characteristic ray.

The mean spectral intensity can be calculated from a sample of instantaneous realisations

$$\tilde{I}_{\lambda} = \frac{1}{N_{sample}} \sum_{\substack{i=1 \\ N_{sample}}}^{N_{sample}} \tilde{I}_{\lambda,i} \tag{6.13}$$

This procedure allows for non-linear effects along the optical path. As a result, there is a convergence to the mean intensity with respect to the number of realisations in a given ray direction used in the stochastic method as showed in Figure 6.9. This was carried out at various wavelength bands where emission from water vapour is significant to yield the mean spectral radiation intensity. From Figure 6.9 it can be seen that 32 samples were sufficient for convergence to the mean

Figures 6.10 and 6.11 plots the instantaneous temperature across the shear layer for the two flames investigated at downstream location $\frac{z}{d} = 90$. For convenience we also have the distribution of the instantaneous H_2O and instantaneous mixture fraction variance shown in the figures. It presents a clear illustration of the non-linearity of the scalar properties and it is highly inhomogeneous. Both the temperature fluctuations and H_2O concentration have several peaks and the peak locations for the several profiles are nearly the same roughly at the centre of the flame path. The maximum temperature fluctuation is just less than 12% of the mean while the H_2O concentration is more than 30% of the mean, indicating that a relative small temperature fluctuation can occur when a large fluctuation in chemical composition occurs.

The stochastic method accounts for the fluctuations in the flame structure fields of relevance to the radiation fields. It seems reasonable to expect that with TRI modelled the spectral intensity distribution should be predicted more accurately. The calculation of the instantaneous profiles using pseudo random numbers is a significant computational overhead. However, when calculating the radiation heat flux distribution

this is still relatively small compared to the computational cost of tracing rays through the flow domain.

To calculate the spectral radiation intensity, the non-homogeneous radiation paths were divided into several homogeneous control volumes (CV). Given the CV length and the instantaneous scalar distributions, emission and transmittance of each CV and the spectral radiation intensities leaving the path can be calculated using RADCAL, (see appendix D for a detail description of the code) a narrow-band radiation model.

Predictions of spectral radiation intensity using the truncated Gaussian PDF and Beta PDF are shown in Figures 6.12 and 6.13 together with Faeth's [40] measured distribution. The predictions show that fluctuating temperature components higher than 30%, produces radiance values which are at least twice those predicted using the mean temperature. The truncated Gaussian PDF achieves better agreement with the measured distribution than the Beta PDF.

The stochastic method presented here is similar to Faeth's [40] stochastic method. It differs in a number of key aspects.

- In this investigation two PDFs are considered, one of them, the truncated Gaussian is a new PDF that has yielded more accurate prediction of the spectral intensity than the "standard" beta PDF.

- The radiative heat loss is incorporated in a more sophisticated way.

- The CPDF curve fit algorithm used to derive the functional relationship

$$f_{inst} = g\left(z, \tilde{f}, \widetilde{f''^2}\right) \tag{6.14}$$

  is very efficient making the calculation of the instantaneous temperature and H_2O mole fraction fields sufficiently computationally frugal to calculate the radiative heat flux distribution, accounting for the TRI.

The first two points means the predicted spectral intensity fields are more accurate than Faeth et al [40] prediction. The third point means TRI can be included in the calculation of the radiative heat flux distributions, something Faeth et al [40] never attempted. This will be presented in a later section.

6.2.3 Mean emission method

One last method of calculating the spectral intensity distribution that can in some way incorporate TRI is considered. The stochastic method requires many realisations to achieve a convergent mean spectral intensity. To overcome this disadvantage a methodology that can be thought of as a hybrid between the mean property method and the stochastic method is considered. The basis of the new method is that fundamentally the stochastic method produces accurate predictions because the PDF is sufficiently accurate. All of the statistics of the flow fields are characterised by the PDF. Therefore, we make the assumption that the mean black body emission for a turbulent homogeneous isothermal flow is characterised as

$$\int I_{b,\lambda}\left(T\right) d\lambda = \sigma \overline{T^4} \tag{6.15}$$

and

$$\overline{T_{adia}^4} = \int_0^1 T^4\left(f\right) pdf\, df \tag{6.16}$$

From this, we can calculate the "emission temperature".

$$\overline{T}_{emission} = \left(\overline{T_{adia}^4}\right)^{0.25} \tag{6.17}$$

Clearly this does not include radiative heat loss. Similar to the approach for calculating the RMS temperature $\sqrt{\widetilde{T''^2}}$ we account for radiative heat loss as

$$\frac{\overline{T_{emission}^4}}{\overline{T_{adia}^4}} = \left(\frac{\overline{T}_{mean}}{\overline{T}_{adia}}\right)^4 \Rightarrow \overline{T}_{emission} = \left(\frac{\overline{T}_{mean}}{\overline{T}_{adia}}\right)\left(\overline{T_{adia}^4}\right)^{0.25} \tag{6.18}$$

In the radiation model, RADCAL it follow that the narrow band absorption coefficient and Planck spectral intensity are evaluated at the mean emission temperature

$$\frac{K_{H_2O}\left(\overline{T}_{emission}\right)}{I_{b,\lambda}\left(\overline{T}_{emission}\right)} \tag{6.19}$$

Thus the mean emission temperature method follows the same algorithm as the mean property method that is it is a deterministic methodology but TRI is included.

Using the mean emission temperature and the RTE described in connection with the mean property method is then solved once to yield the spectral radiation intensity distribution shown in Figures 6.14 and 6.15. In Figures 6.14 and 6.15 the predictions are as good as the stochastic method at axial location $x/d = 50$. However, this method under-predicts at axial location $x/d = 90$ yet yielded better predictions than the mean property method. The mean emission method implies that chemical reactions affect the calculations of the temperature fluctuations only through the energy equation. Furthermore at $x/d = 130$ the mean emission method prediction is poor. The possible reason for this behaviour could be lack of eddies present at higher flame length. In all predictions the truncated Gaussian PDF gave higher intensities than the Beta PDF. Unfortunately, overall, the mean emission method prediction is poor.

6.3 Presentation of predictions/measurement comparison

We have established from the previous section that the truncated Gaussian PDF yields better predictions of the spectral radiation distribution than the Beta PDF. For the remainder of this thesis we will use the truncated Gaussian PDF in our analysis.

6.3.1 Prediction of Faeth radiation measurements

The variations of spectral intensity along radial paths crossing the vertical axis of the two hydrogen-fuelled flames are shown in Figures 6.16 and 6.17. Measurements were undertaken at two axial positions, *x/d=50* and *90* for *Re=3,000* jet fire and three axial positions, *x/d=50, 90* and *130* for *Re=5,722* jet fire. Results for *x/d=130* are not illustrated for the lower Reynolds Number flame, as this position is well beyond the flame tip and spectral intensities measured data are unavailable for this position. Predictions using the mean property, stochastic and mean emission methods are given in these figures. All predictions of the flame structure model use the laminar flamelet model for state relationships.

Considering the spectral intensity distribution in Figures 6.16 and 6.17 the dominated bands are centred on 1.38, 1.87, and 2.7µm bands of water vapour. Intensities also increase gradually beyond 4µm, as the broad 6.3µm band of water vapour is approached. In summary the stochastic method generally yields higher values of spectral radiation intensities than the mean property method. This suggests greater effects of turbulence radiation interactions for hydrogen-air diffusion flames than either carbon monoxide-air or methane-air diffusion flames where differences between the two methods were generally less than 30 percent [115]. This behaviour is caused by the rapid variation of radiation properties (that is, temperature and water vapour concentration) with instantaneous mixture fraction near stoichiometric conditions.

Use of predicted mean properties always yield lower spectral intensity than the stochastic method as this is crucially evident near the 2.7 µm band of water vapour as shown in Figure 6.17c. The population of molecules at higher energy levels increases with increasing temperature, causing the radiation properties, such as the spectral absorption coefficient κ_λ, to be highly dependent on temperature. For the 2.7 µm band of water vapour, κ_λ increases as temperature increases. Taking into account the temperature dependence of κ_λ, in combination with blackbody radiance, the temperature fluctuations have a great effects on the predictions of radiative transfer in that band, so the value from the stochastic method is higher than the mean property and mean emission method. It is noteworthy to point out the irregular behaviour of the mean emission method as it does have higher spectral intensity predictions in the near field, compared to the measurements such as at *x/d =50* as shown in Figure 6.17a and under-predicts the measured spectral intensity at *x/d=130* as shown in Figure 6.17c.

6.3.2 Radiative heat fluxes

Computations of radiative heat fluxes are a straightforward extension of the spectral radiation intensity computations using the discrete transfer method of Lockwood and Shah [194]. Cumber [115, 198] successfully applied this method to the calculation of heat-fluxes surrounding natural gas flames and Faeth et al [40, 208, 209] calculated the heat flux for a number of different jet fires including hydrogen jet fire although he did not include TRI. This involves determining the spectral intensity for various wavelengths and paths passing through the receiver in question and then summing over both the wavelengths and paths to find the total radiative heat flux. The present study

calculations were based on all three radiation methods; the mean property method, the stochastic method and the mean emission method.

In the results shown in Figures 6.18 and 6.19 the spectral narrowband model was applied to predicting radiation intensities received from line-of-sight measurements taken both along radial and axial paths through the flame, and total radiation fluxes received at various locations around the flame obtained using radiometers with a 150^{o}, circular field of view and a spectral window of 1 - 6.5μm. In making these predictions line-of-sight results were derived from radial and axial temperatures and compositions calculated by the flame structure model, with the number of control volumes used to represent the non-homogeneous profiles through the flame being increased until received intensities were invariant to further refinement.

Predictions of total radiative fluxes to points surrounding hydrogen turbulence flames are illustrated in Figures 6.18 and 6.19 where the spectral response of the heat flux sensor used for the total radiative heat flux predictions (denoted 1 - 6.5 μm). In Figure 6.18 the heat flux receiver is facing the flame axis and is traversed in the vertical direction at a distance of 575mm from the axis. Figure 6.19 is an illustration of the results for a sensor orientated to be vertically upward in the plane of the burner exit and is traversed radially outward. In this scenario, the radiative heat flux diminishes monotonically with increasing radial distance. Although flame tip mean temperatures and compositions are alike for both flames of Faeth's hydrogen jet fires (*Re=3,000* and *Re=5,722*), radiative heat fluxes are smaller for the lower Reynolds number flame due to the flame's smaller dimension. Buoyancy caused the flames to be shorter and narrower at lower Reynolds numbers for the current test range. This effect would wane at higher Reynolds numbers, where flame structure is relatively insensitive to Reynolds number. The turbulence model was developed for high Reynolds number flows and the agreement between the predictions and measured data were reasonable using the stochastic method in the higher Reynolds number fire.

For the total radiative heat flux distribution parallel to the flame axis as shown in Figure 6.18 the axial radiative heat flux distribution is more difficult to predict than the radial distribution (see Figure 6.19) as it is more sensitive to the flame shape. The stochastic method tends to slightly over-predict the measured distribution in the far field but the

agreement is acceptable. In the near field the agreement is excellent for the stochastic method.

Considering the mean property method as shown in Figure 6.18 this tends to under-predict the measured distribution as expected as TRI is not included. Our prediction using the mean property method is similar to Faeth's prediction [40] as they roughly under-predicted the measured axial heat flux distribution by 20%. However, the mean emission method is very poor as qualitatively the distribution is incorrect and the under-prediction is worse than the mean property.

Looking at the radial heat flux distribution presented in Figure 6.19 the model prediction using the stochastic method is in excellent agreement with the measured distribution. The mean property method under-predicts the measured distribution as TRI is not accounted for but our prediction is marginally better than that of Faeth's prediction [40]. However, the mean emission method is qualitatively correct but quantitative accuracy is poor.

The predicted heat flux distributions shown in Figures 6.18 and 6.19 were calculated with 3072 rays per receiver. This was determined to be sufficiently accurate as further ray mesh refinement does not change the predicted distribution to the resolution of the figure. Figure 6.20 shows the predicted incident heat flux distribution for the vertical line of receivers calculated using four different ray distributions. A coarse ray mesh of 48 rays and three further ray distributions calculated by successively quadrupling the number of rays as the incident intensity hemisphere is a two-dimensional manifold. The 48 ray and 192 ray predicted heat flux distributions are physically incorrect with multiple local maxima present. This is typical behaviour where the heat flux distribution is dominated by a small hot volume of emitting gas, i.e. the ray effect is significant. The 3072 ray prediction of the incident heat flux distribution was confirmed to be insensitive to further ray refinement by comparing it to a predicted heat flux distribution calculated with 12,288 rays. In the simulations presented in Figures 6.18 and 6.19 the ray meshes in the θ and ϕ directions are maintained at a 1:3 ratio.

All these predictions were made on the basis of Reynolds-averaged mean temperatures and Favre-averaged mean gaseous species mass fraction [40]. The actual intensity of

radiation emitted from a fluctuating turbulence flame can, however, exceed values estimated using the mean scalar properties since the physical parameters controlling radiative heat transfer interact in a highly non-linear manner [3]. The amplification of radiative heat transfer by fluctuations of the temperature field does, conversely, depend significantly on the root mean square (RMS) of the fluctuating temperatures [185]. Soufiani et al [185] studied turbulence radiation interactions in a homogeneous turbulence medium and demonstrated that for the configuration examined a relative RMS temperature of 10% meant that the relative difference in band intensity calculated using the mean temperature and a stochastic simulation, which took the effects of turbulence fluctuations into account, was of the order 8%.

The radiative heat loss is not a fixed fraction of the heat release rate, as observed by Marstein [210], but reaches a maximum for intermediate Reynolds number jets. At high Reynolds number, when buoyancy is insignificant, flame structure and thus radiation properties tend to be independent of the jet nozzle flow rate. In this region, the radiative heat loss fraction would be inversely proportional to jet nozzle flow rate which possibly explains the insignificant reduction in radiative fraction for the higher flow rate of the present investigation. On the whole, thus, predictions of the radiant heat flux with the narrow-band model using the stochastic approach are in very good accord with measured data.

6.4 Concluding remarks

In this chapter we have evaluated three methods of calculating the radiation fields surrounding hydrogen jet fires. The three radiation methods either ignore turbulence radiation interactions, the mean property method or TRI is accounted for using a stochastic method or through the PDF based on the mean emission method. The methods have been evaluated by comparison with Faeth's measured spectral intensity distribution and measured radiative heat flux distribution. Of the three methods the stochastic method is demonstrated to be very accurate, able to predict the spectral intensity distribution and radiative heat flux distributions. The mean property method does not include TRI so is not acceptable. The mean emission method numerically includes TRI through the PDF but is shown to produce poor quality prediction of the spectral intensity distribution and radiative heat flux distribution.

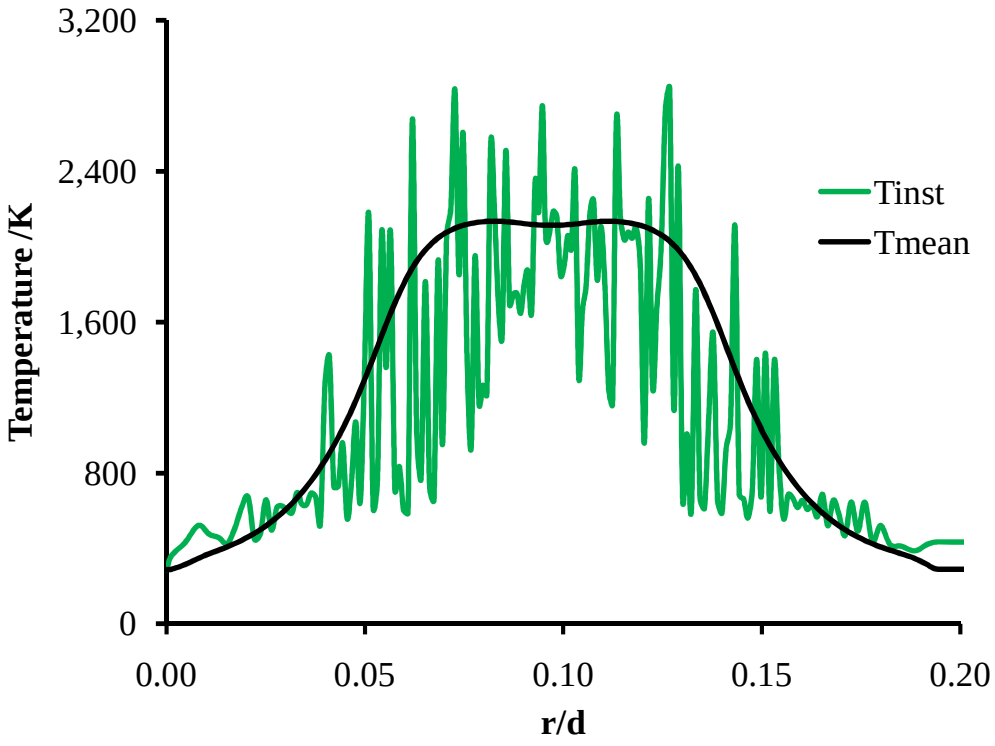

Figure 6.1: Temperature distribution in the radial direction at $z/d = 90$ for the Re=5,722 jet fire.

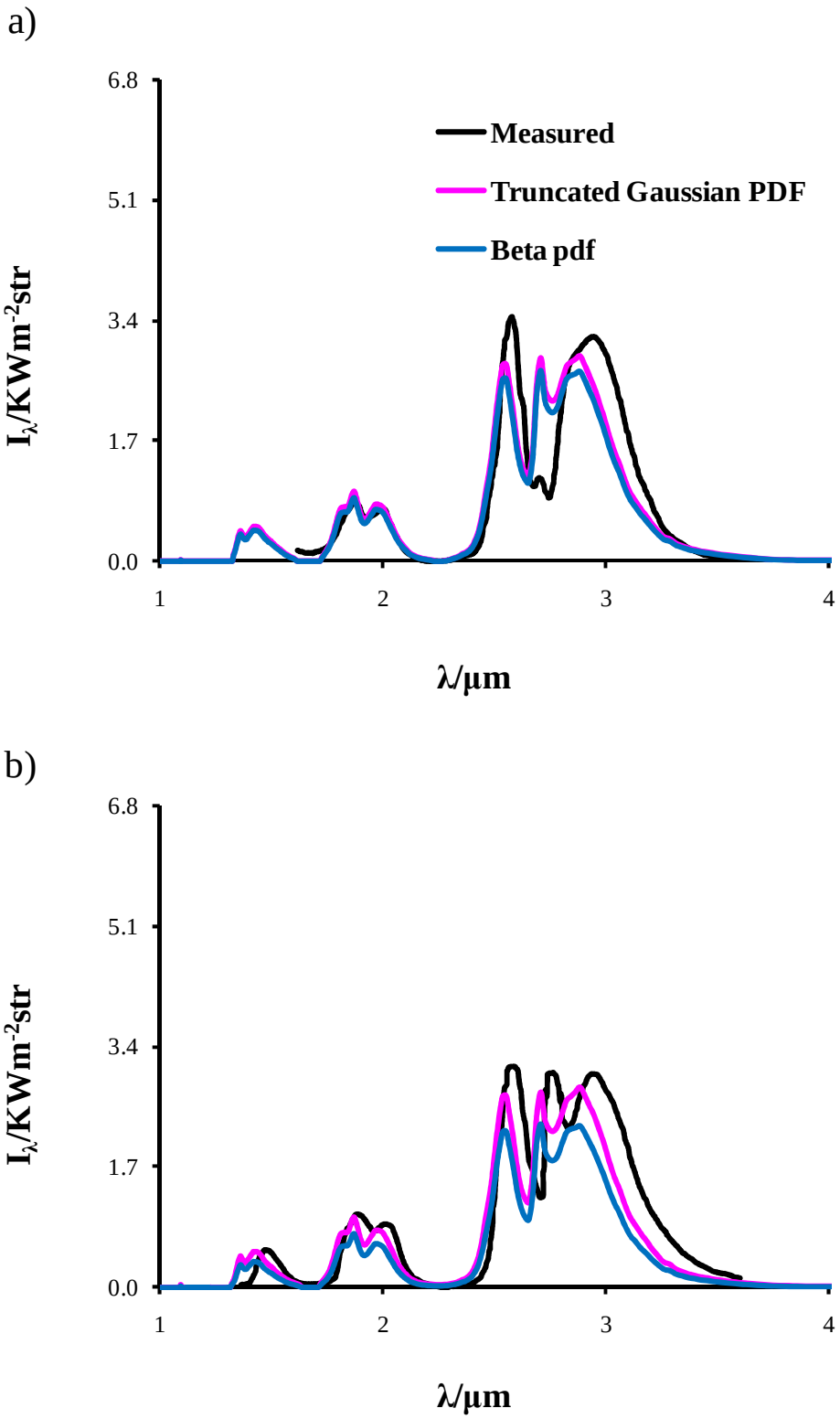

Figure 6.2: Using the Mean property method to predict spectral radiation intensity with the Truncated Gaussian PDF and the Beta PDF. (a) x/d=50 and (b) x/d=90 for the Re=3,000 jet fire.

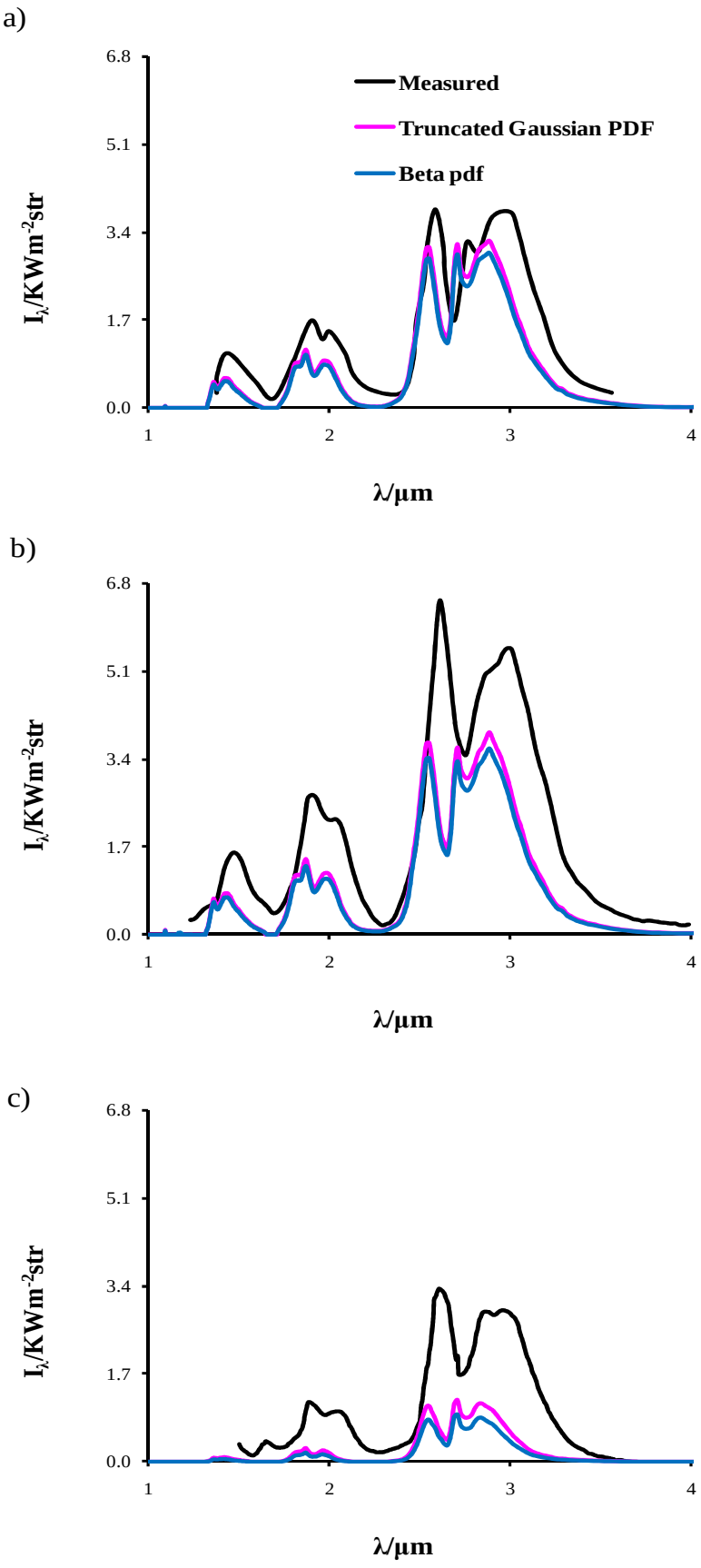

Figure 6.3: Using the Mean property method to predict spectral radiation intensity with the Truncated Gaussian PDF and the Beta PDF for (a) x/d=50 (b) x/d=90 and (c) x/d=130 for the Re=5,722 jet fire.

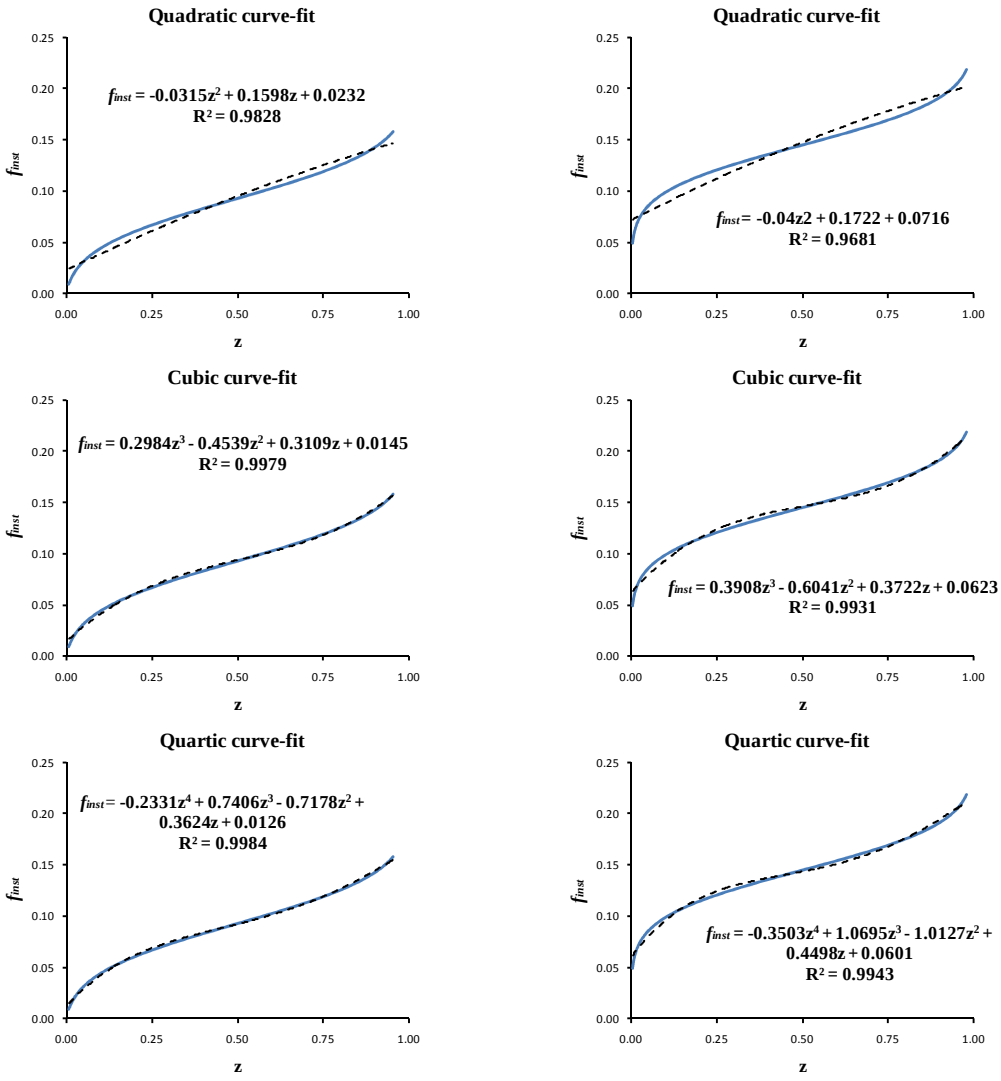

Figure 6.4: Comparison of polynomial curve fits to equation (6.11).

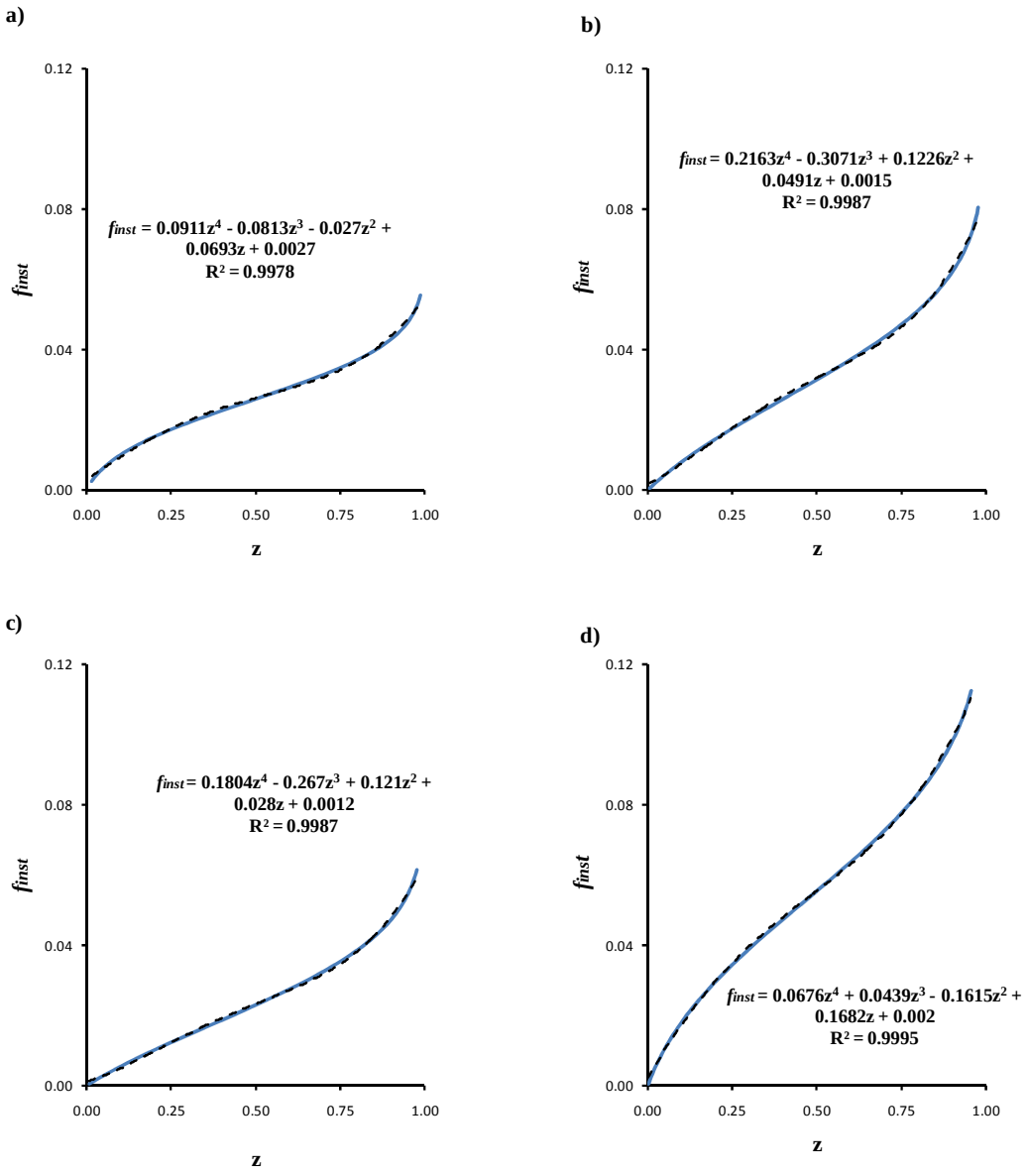

Figure 6.5: Curve-fit of the instantaneous mixture fraction plotted against the random number z for a) ($\tilde{f}$ = 1.75E-02, $\sqrt{\widetilde{f''^2}}$ = 2.11E-2); b) ($\tilde{f}$ = 3.41E-02, $\sqrt{\widetilde{f''^2}}$ = 2.9E-02); c) ($\tilde{f}$ = 5.28E-02, $\sqrt{\widetilde{f''^2}}$ = 3.43E-02) and d) ($\tilde{f}$ =8.29E-02, $\sqrt{\widetilde{f''^2}}$ = 3.86E-02).

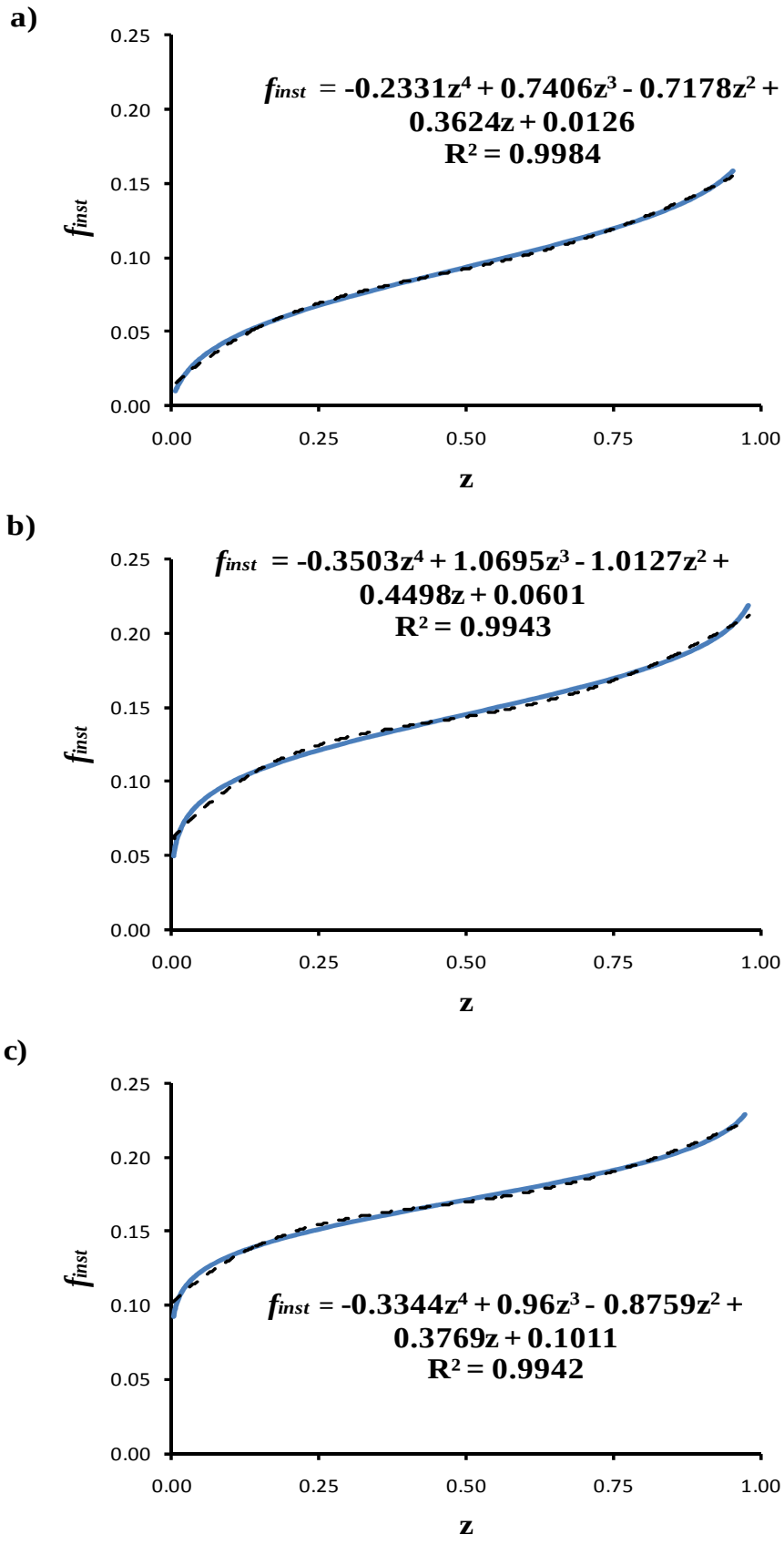

Figure 6.6: Curve-fit of the instantaneous mixture fraction plotted against the random number z for a) ($\tilde{f}$ = 9.28E-02, $\sqrt{\widetilde{f''^2}}$ = 3.91E-02); b) ($\tilde{f}$ = 1.45E-01, $\sqrt{\widetilde{f''^2}}$ = 3.59E-02) and c) ($\tilde{f}$ = 1.7E-01, $\sqrt{\widetilde{f''^2}}$ = 2.94E-02).

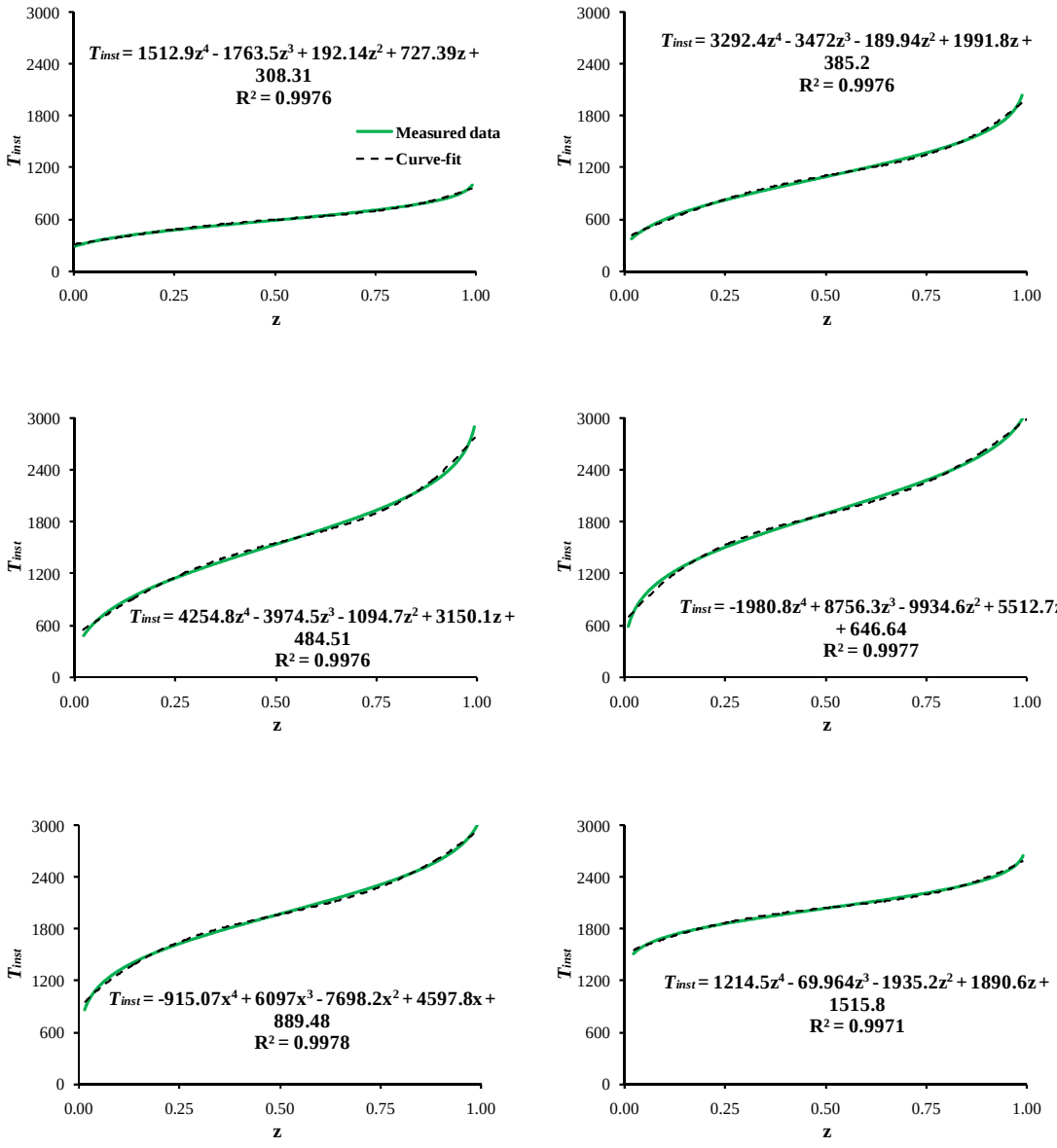

Figure 6.7: The instantaneous temperature calculated using the flamelet $T_{inst}\left(f_{inst}(z)\right)$ and plotted against the random number z.

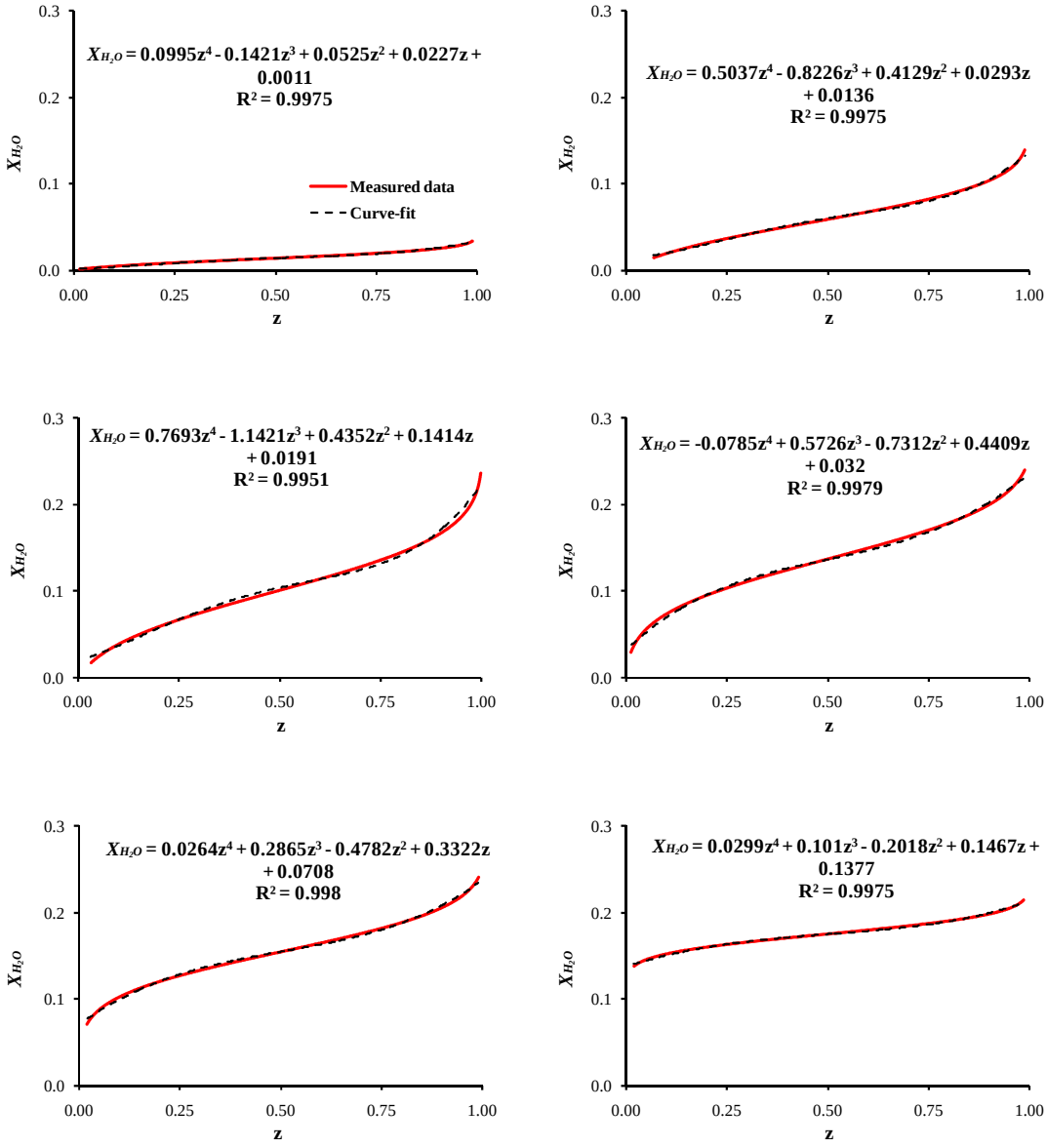

Figure 6.8: The instantaneous H_2O concentration calculated using the flamelet $X_{H_2O\,inst}\left(f_{inst}(z)\right)$ and plotted against the random number z.

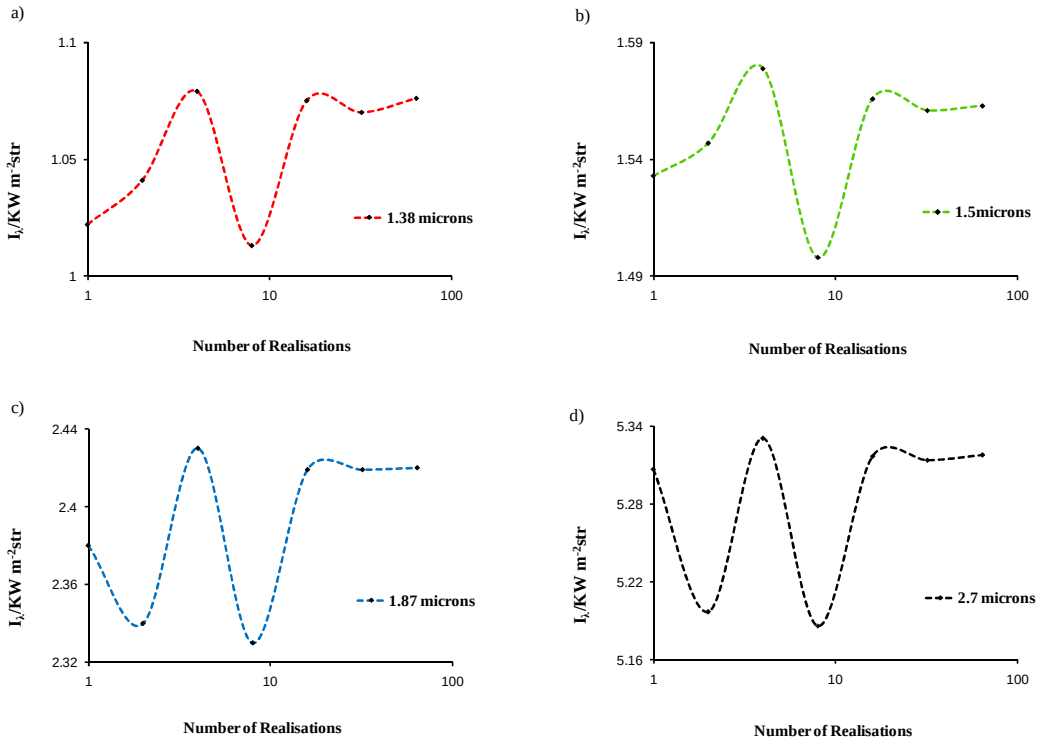

Figure 6.9: Stochastic method showing the plot of spectral radiation intensity against number of rays, $x/d = 90$ and Re=5,722 jet fire.

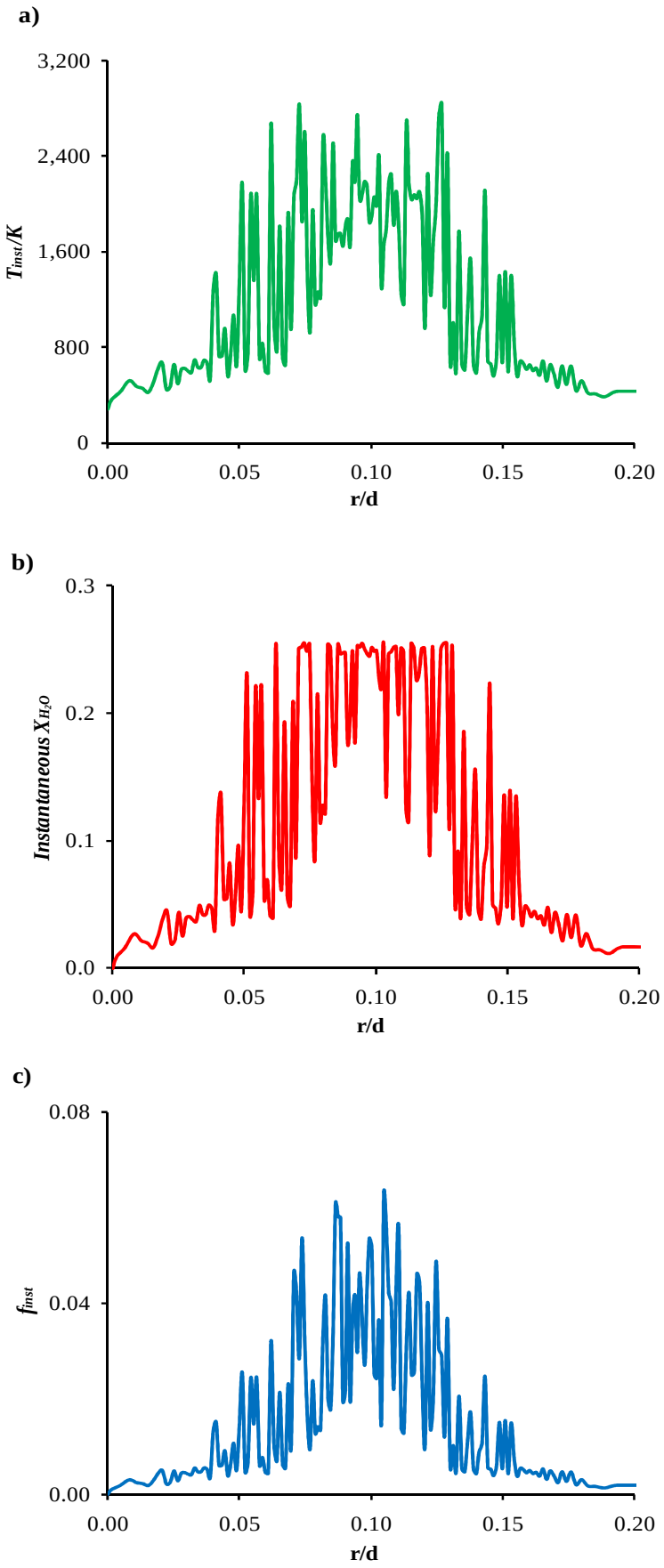

Figure 6.10: Instantaneous profiles across the shear layer a) Temperature b) Water vapour and c) Mixture fraction at $z/d = 90$ for the Re=5,722 jet fire.

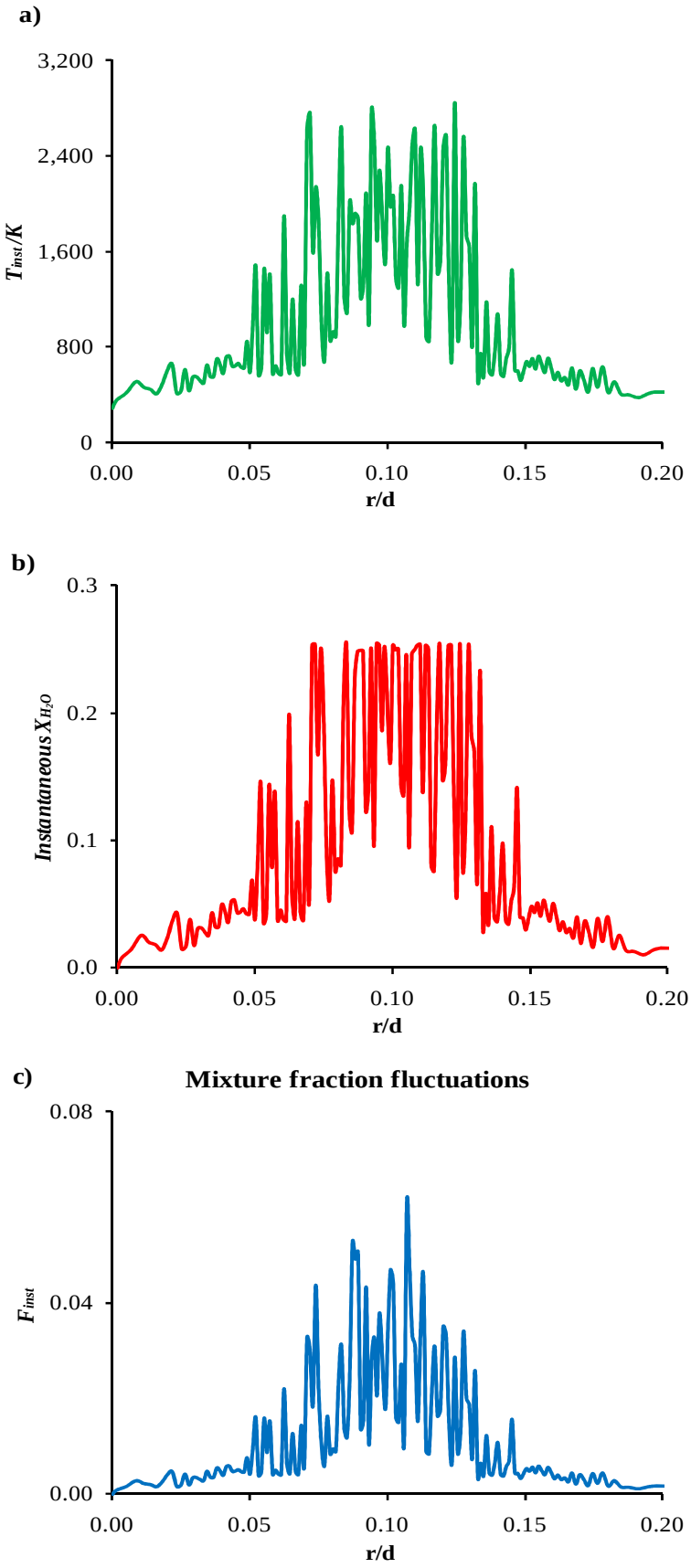

Figure 6.11: Instantaneous profiles across the shear layer a) Temperature b) Water vapour and c) Mixture fraction at $z/d = 90$ for the Re=3,000 jet fire.

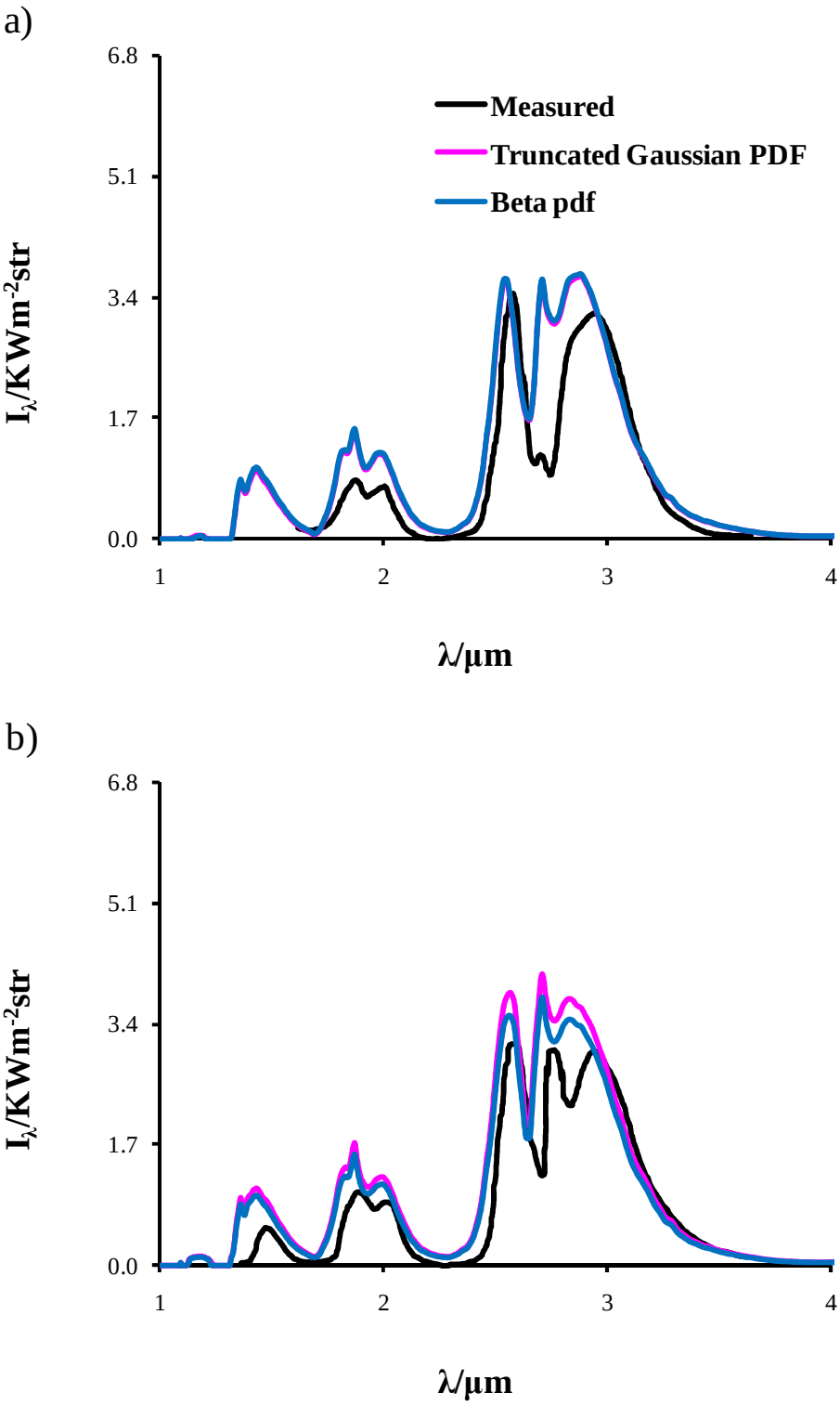

Figure 6.12: Using the Stochastic method to predict the spectral radiation intensity with the Truncated Gaussian PDF and the Beta PDF for (a) x/d=50 and (b) x/d=90 for the Re=3,000 jet fire.

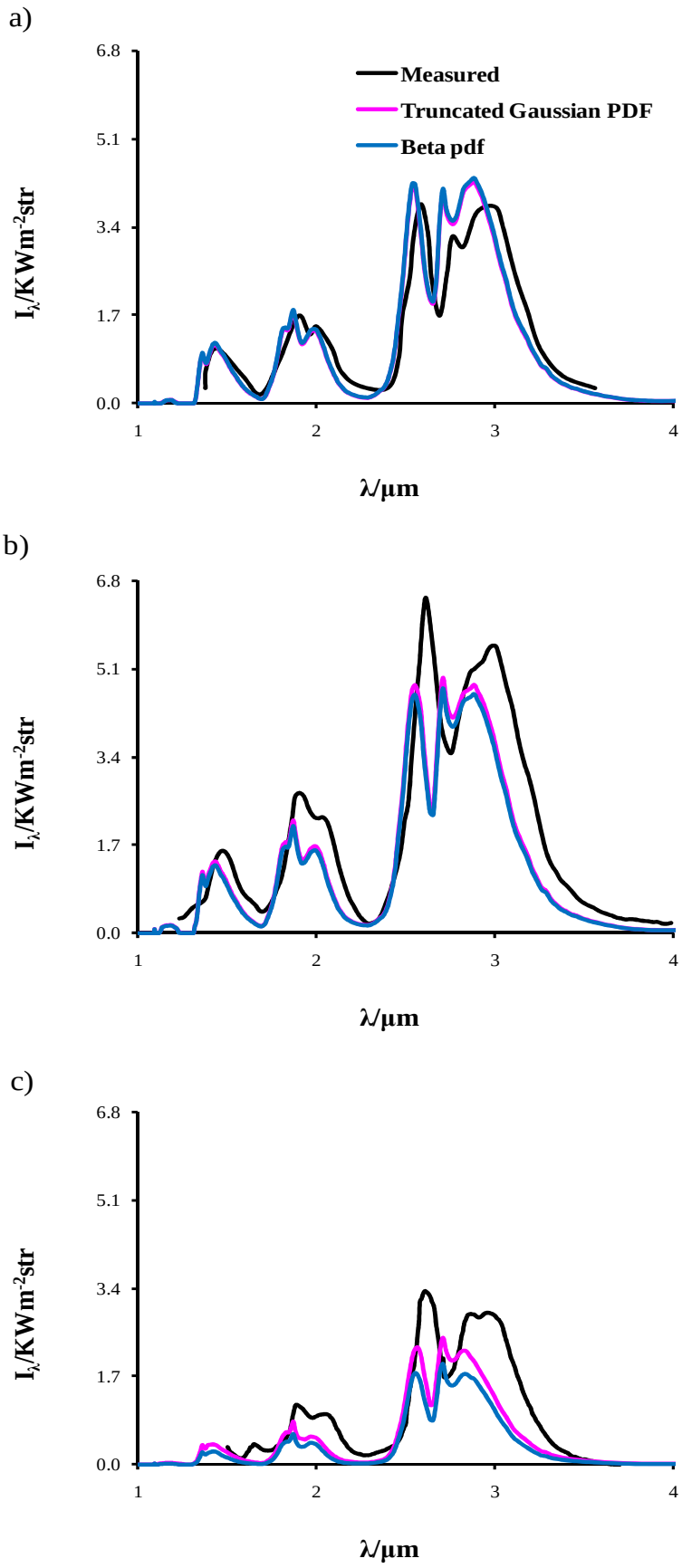

Figure 6.13**:** Using the Stochastic method to predict the spectral radiation intensity with the Truncated Gaussian PDF and the Beta PDF for (a) x/d=50 (b) x/d=90 and (c) x/d=130 for the Re =5,722 jet fire.

.

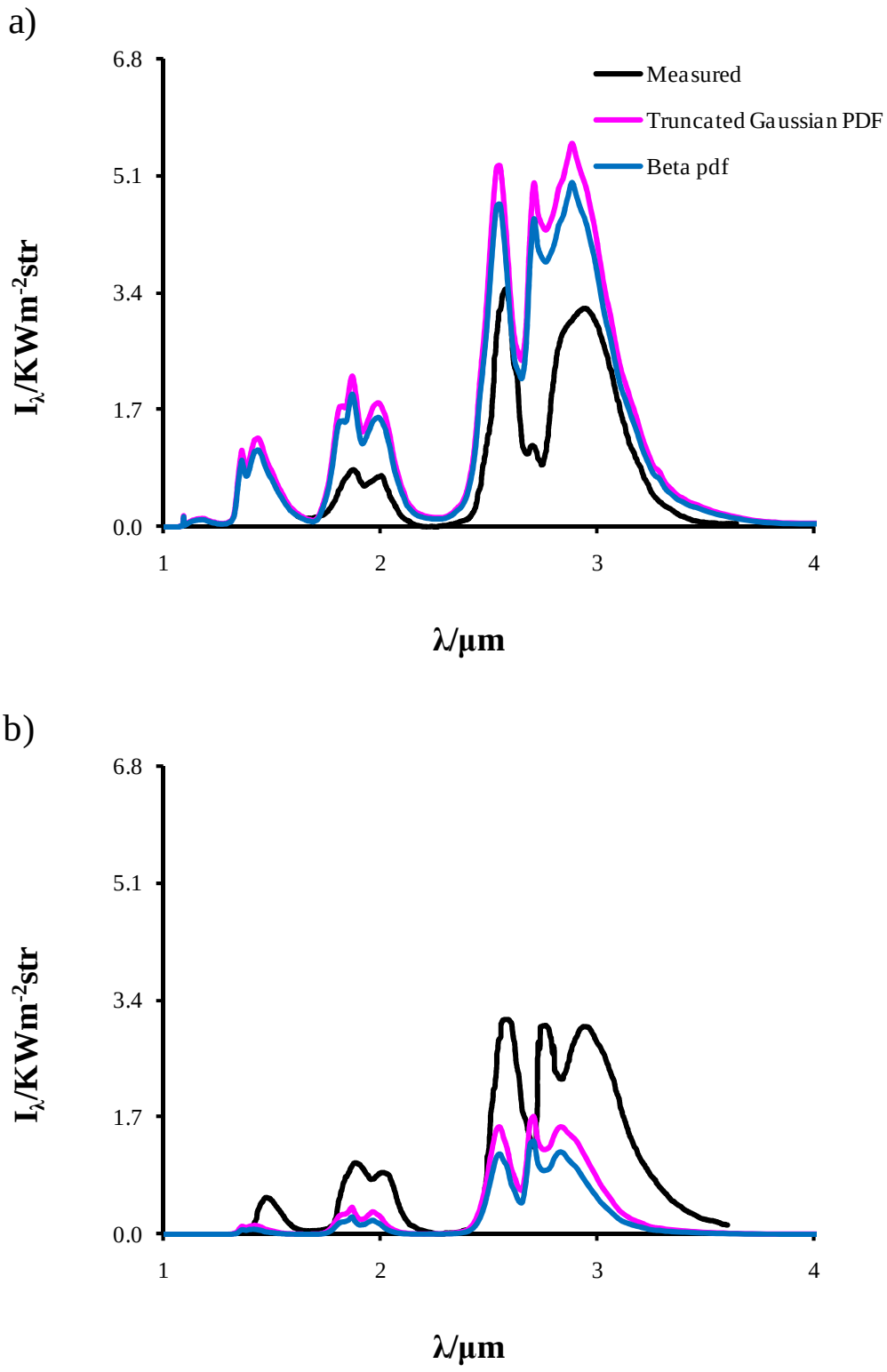

Figure 6.14: Using the mean emission method to predict the spectral radiation intensity with the Truncated Gaussian PDF and the Beta PDF for (a) x/d=50 and (b) x/d=90 for the Re=3,000 jet fire.

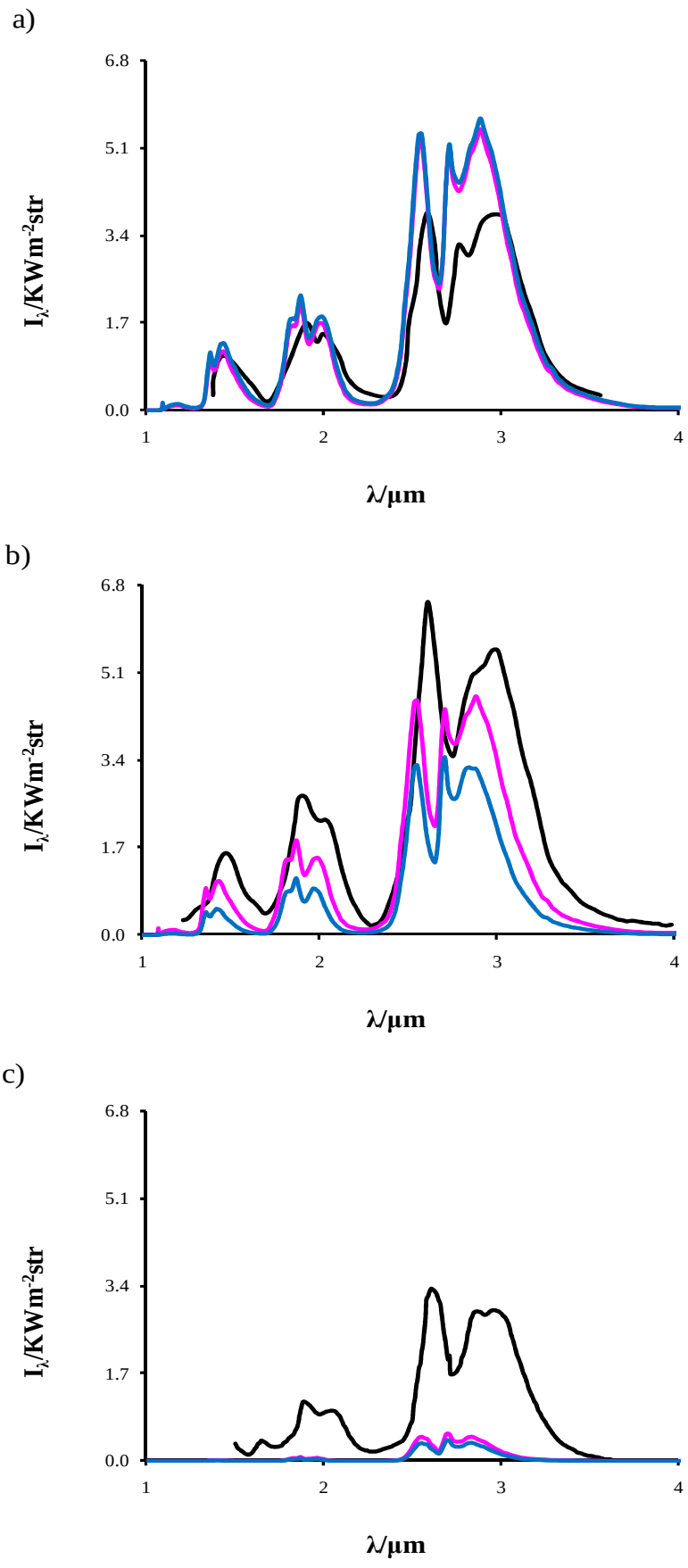

Figure 6.15: Using the mean emission method to predict the spectral radiation intensity with the Truncated Gaussian PDF and the Beta PDF for (a) x/d=50 (b) x/d=90 and (c) x/d=130 for the Re=5,722 jet fire.

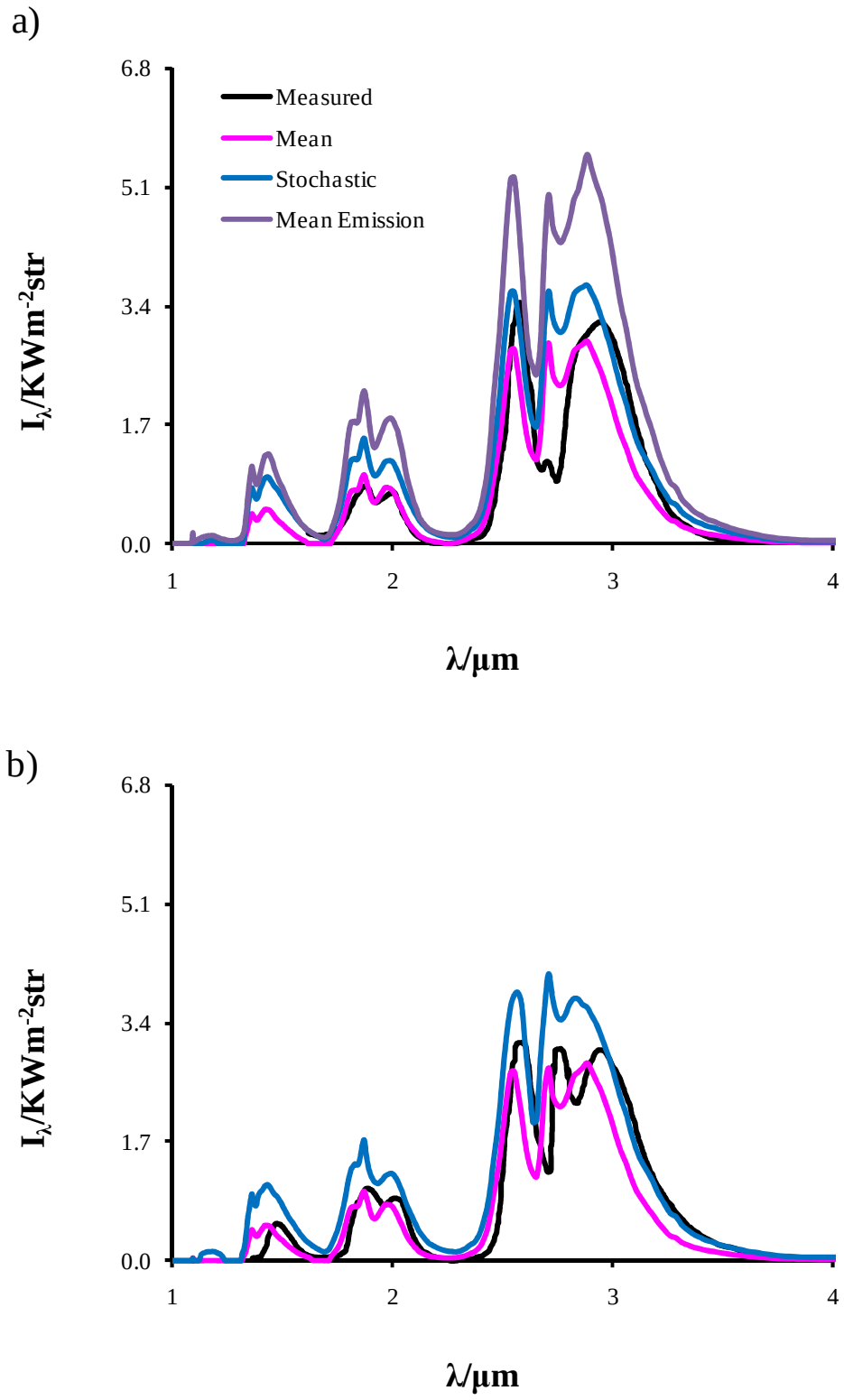

Figure 6.16 : Spectral radiation intensities for radial paths through the axis: a) *x/d=50* and b) *x/d=90* for the Re=3,000 jet fire.

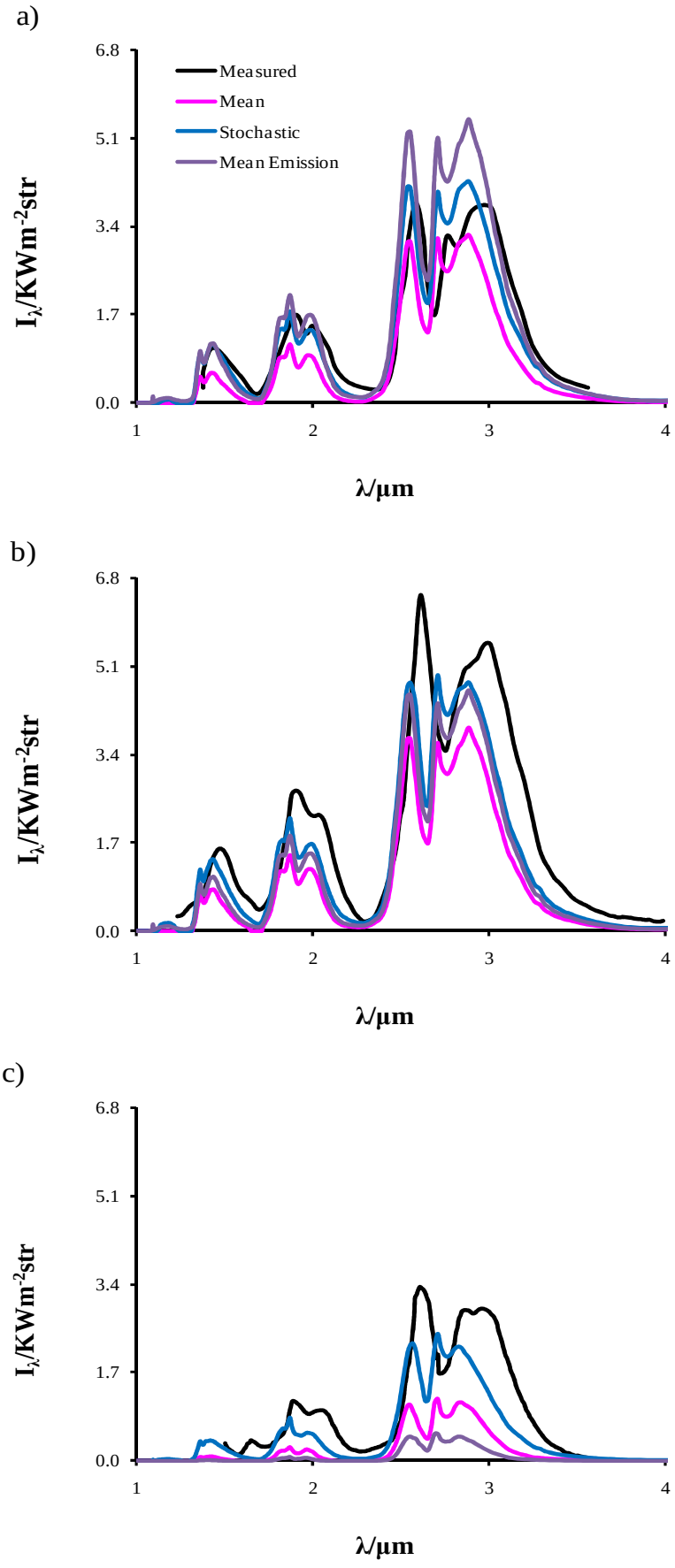

Figure 6.17 : Spectral radiation intensities for radial paths through the axis: a) *x/d=50* b) *x/d=90* and c) *x/d=130* for the Re=5,722 jet fire.

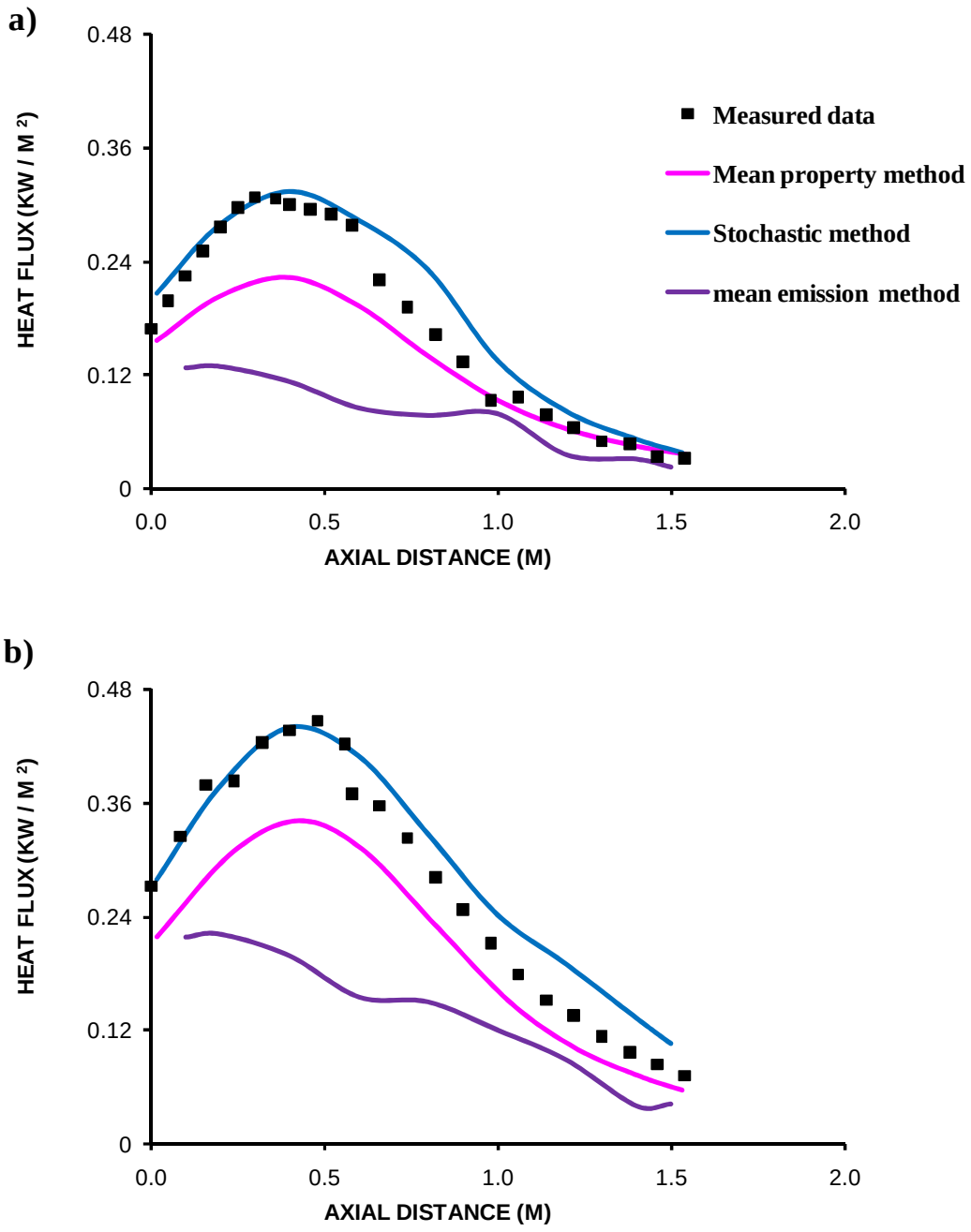

Figure 6.18: Total radiative heat flux distribution parallel to the flame axis at a distance of 0.575m. For a) Re=3,000 and b) Re=5,722 jet fires.

a)

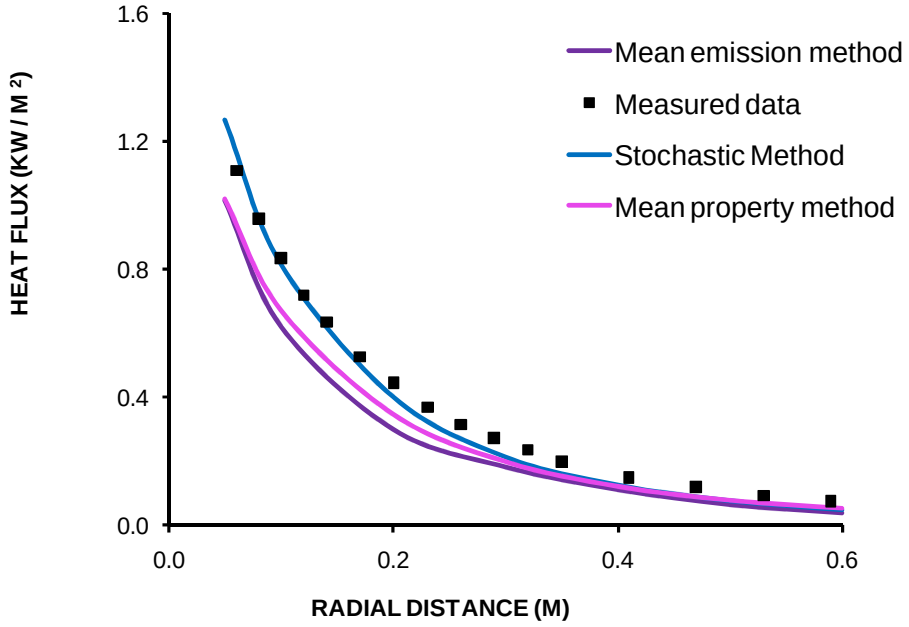

b)

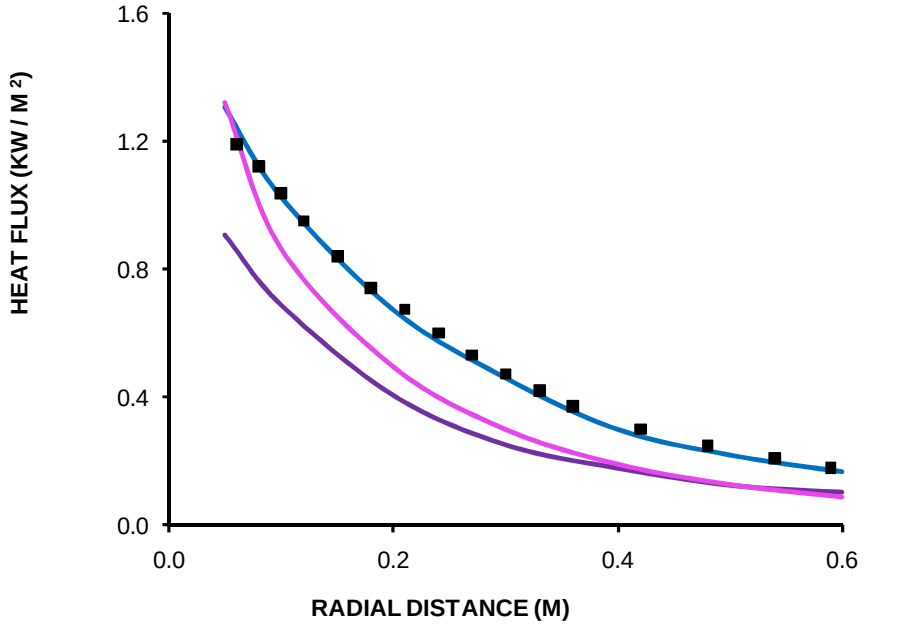

Figure 6. 19: Total radiative heat flux distribution in the plane of the nozzle for receivers with a vertical orientation. For a) Re=3,000 and b) Re=5,722 jet fires.

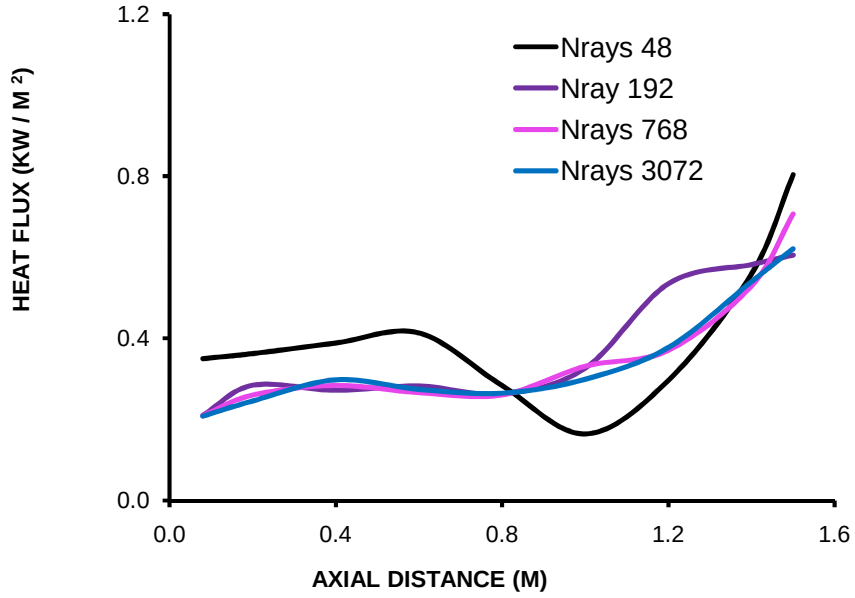

Figure 6.20: A ray refinement investigation of the incident heat flux distribution parallel to the flame axis at a distance of 0.575m for the Re=5,722 jet fire.

Chapter 7

Mathematically modelling of physical phenomena plays an ever more significant part in industry. Computational Fluid Dynamics, CFD, the modelling approach used in this investigation, is predominantly fitting for fluid flow problems which cannot be tested at full-scale. In fire risk analysis, the probabilities of fire consequences are computed using deterministic models for fire phenomena, taking into account the statistical variation or uncertainty of the initial and boundary conditions. The development of the computational resources has allowed the use of stochastic simulation, the most general approach where the space of possible answers is covered in a statistically satisfactory manner.

In general, the present work demonstrates a comprehensive approach for the simulation of turbulent hydrogen jet fires. In particular, it focussed on the modelling of detailed chemistry of relevance to the radiation fields and the modelling of detailed radiative heat transfer in gas-phase turbulent flames. In addition, the present work centres on numerical investigations of turbulent hydrogen-air non-premixed flames.

7.1 Conclusion

We have developed a model for a turbulent hydrogen jet fire. The starting point is the development of a lift-off model. The lift-off model is an extension of Sanders and Lamers [48] flame quenching model calibrated by Cumber and Spearpoint [49] for methane jet fires. For lifted hydrogen jet fires the small scale strain rate model gives the best agreement with Kalghatgi's [39] lift-off measurements across the range of source velocities and diameters considered.

Having established the ability to predict the lift-off region the thesis then moves onto the prediction of the flame structure further downstream. The model is based on the boundary layer equations and is fairly standard. The main work of investigation is the prediction of the RMS temperature and RMS H_2O mole fraction fields as this has not been investigated in any great depth before and is key to being able to predict TRI. Two PDFs were considered namely a beta PDF and a truncated Gaussian PDF. The RMS fields were calculated through the integration of the PDF and using a modelled transport

equation similar to the mixture fraction variance. Of these two approaches the integration of the PDF was far superior. The transport equation for the RMS temperature tends to under-predict the measurements of Barlow [41]. The truncated Gaussian PDF gave marginally better agreement with the measurements of Barlow [41] than the beta PDF predictions of the RMS fields.

Having established the accuracy of the flame structure model the final component of the model is the modelling of TRI. Three approaches were considered neglecting TRI, the mean property method to give a baseline for quantifying TRI. Two other methods were considered, the stochastic method where TRI is modelled by generating instantaneous realisations of the spectral intensity distribution and the mean emission method where TRI is modelled using the PDF to calculate the mean emission temperature. Of these approaches the stochastic method proved able to predict the spectral intensity distribution and the radiative heat flux distribution.

The stochastic method presented in this study is similar to Faeth's [40] stochastic method. It differs in a number of key aspects.

- In this investigation two PDFs are considered, one of them, the truncated Gaussian is a new PDF that has yielded more accurate prediction of the spectral intensity than the "standard" beta PDF.

- The radiative heat loss is incorporated in a more sophisticated way.

- The CPDF curve fit algorithm used to derive the functional relationship is very efficient making the calculation of the instantaneous temperature and H_2O mole fraction fields sufficiently computationally frugal to calculate the radiative heat flux distribution, accounting for the TRI.

In this investigation there are a number of novel components of the model development and challenges encountered as stated below:

- The extension of the lift-off model to hydrogen jet fires.

- Accurate prediction of the RMS fields.

- The prediction of the radiative heat flux distribution with excellent accuracy using a stochastic method.

The present calculations have helped to clarify several qualitative features of turbulence flame radiation. The difficulties of incorporating a time-averaged radiative source term in turbulence flow field calculations can be overcome by employing a radiating rather than adiabatic, laminar flamelet description. Overall the agreement with the experiments was not entirely satisfactory. Nevertheless, the results of the simulations compare favourably with other computational studies reported in the literature. The models employed once implemented are easy to use and robust. In light of this there are certainly situations where the level of accuracy of the solutions achieved with the models is satisfactory. The calculation of radiative heat flux to external targets, of importance to burning rates and fire spread, is relatively straightforward using the radiation model advocated in this investigation and involves integrating the emitted intensity over all lines of sight from the target through the flame. Its application is again reliant on details of flame structure along each of these paths; it is the necessity to predict the turbulent flame geometry which again forms the most imperative undertaking in fire radiation modelling.

7.2 Proposals for future research

The radiating laminar flamelet is fundamental to both numerical computations of turbulence flame scalar structure and to the calculations of flame radiative emission using the jet fire model. The present investigation has uncovered many areas where research is needed in order to enhance our understanding of radiation from turbulent flames. The important areas are:

- Measurements of species concentration and temperature fluctuations in hydrogen/air flames are required to study the effects of turbulence radiation interactions and also to appraise temperature predictions based on existing analyses and extensions.

- All the flows considered in the present study are axisymmetric, which simplifies matters a great deal. It is only crucial to consider a section of the flow, a two dimensional manifold which is desirable from a computational

point of view. Nonetheless, in most if not all industrial large scale fires, at least if they occur outdoors, in windy conditions or in confinements, are three dimensional in nature. Even fires which are not influenced by cross winds show three-dimensional characteristics, such as induced swirling motion around the perimeter of the flame. Consequently, predictions in three dimensional reacting flows are desirable.

- Predictions of turbulence flame structure need some measure of the magnitude of radiative heat losses within the flow in order to choose an appropriate radiating flamelet description. In the present study a simple model, but with a realistic T^4 dependence, was used to account for radiative heat loss. Despite the crudity of the model it performs well for all flows considered in our investigation. A systematic experimental programme is required to identify the range and type of turbulent flame for which radiative heat losses are significant and to develop suitable criteria for incorporating radiative transfer into computational flame calculations.

- Compressible flow solution to model shock containing region similar to Cumber et al [18] such that a model for all accidental hydrogen jet fires can be produced. Numerically this is a very challenging task as it requires the resolution of shocks. A further complication is the reverse Joule Thomson effect could be important.

- The emission temperature model has some theoretical basis but ultimately proved disappointing. However, further investigation of this approach may yield fruit. For example, it is not clear if the emission temperature is the correct temperature to use when calculating the narrow band absorption coefficient. This has potential benefit as the emission temperature method is a deterministic method and therefore computationally more efficient than the stochastic method of modelling TRI.

- Similarly, the stochastic method could be made more efficient by incorporating variance reduction techniques such as incorporating Sobol

sequences [211] Cumber. These would tend to accelerate convergence to the mean spectral intensity.

References

1. Dunn, S. *Hydrogen futures: towards a sustainable energy system*, in *Worldwatch paper*. 2001, WorldWatch Institute: Washington D.C.

2. Gummer, J.H. and Head, C.R. *Hydrogen, hydropower and World Poverty.* The International Journal of Hydropower and Dams, 2003. **5**.

3. Cox, G. *On Radiant Heat Transfer from Turbulent Flames.* Combustion Science and Technology, 1977. **17**: p. 75-78.

4. Nelson, D.A. *Band radiation from a fluctuating medium.* Journal of Heat Transfer, 1989. **111**: p. 131-134.

5. Modest, M.F. and Li, G. *Importance of turbulence-radiation interactions in turbulent diffusion jet flames.* Journal of Heat Transfer, 2003. **125**: p. 831-838.

6. Mazumder, S. and Modest, M.F. *A probability density function approach to modelling turbulence-radiation interactions in nonluminous flames.* Journal of Heat and Mass Transfer, 1999. **42**: p. 971-991.

7. Wolanski, P. and Wojcicki, S. *Investigation into the Mechanism of the Diffusion Ignition of a Combustible Gas flowing into an oxidizing atmosphere.* The Combustion Institute, Pittsburgh, 1972. **14th Symposium (Int.) on Combustion**: p. 1217-1223.

8. Hawksworth, S.J. and Astbury, G.R. *Spontaneous ignition of hydrogen leaks: a review of postulated mechanisms.* International Journal of Hydrogen Energy, 2007. **32**: p. 2178-2185.

9. Wen, J.X., Dembele, S., Tam, V.H.Y., Xu, B.P. and Hawksworth, S.J. *The effect of pressure boundary rupture rate on spontaneous ignition of pressurized hydrogen release* Journal of Loss Prevention in the Process Industries, 2009. **22**: p. 279-287.

10. Wen, J.X., Dembele, S., Tam, V.H.Y. and Xu, B.P. *Effects of the accuracy order of numerical schemes on spontaneous ignition of high-pressure hydrogen release.*, in **32nd (Int.) Symposium on Combustion.** 2008: Montreal, Canada.

11. Wen, J.X., Dembele, S., Hima, L.E.L., Tam, V.H.Y., Xu, B.P. and Donchev, T. *Numerical study of spontaneous ignition of pressurized hydrogen release through a tube into air.* Journal of Loss Prevention in the Process Industries, 2007. **21**: p. 205-221.

12. Drikakis, D. *Advances in turbulent flow computations using high-resolution methods.* Progress in Aerospace Sciences, 2003. **39**: p. 405-452.

13. Larminie, J. and Dicks, A. *Fuel Cell Systems Explained*. 2003, John Wiley and Sons: Chichester, United Kingdom.

14. Ogden, J. *Hydrogen: The fuel of the future?* Physics Today, 2002. **55**: p. 69-75.

15. Venetsanos, A.G., Adam, P., Huld, T. and Bartzis, J.G. *Source, dispersion and combustion modelling of an accidental release of hydrogen in an urban environment.* Journal of Hazardous Materials, 2003. **A105**.

16. Lewis, B. and Elbe, G.V. *Combustion, Flames, and Explosion of Gases*. 3rd edition, 1987, Orlando, Florida: Academic Press.

17. Lees, F.P. *Loss Prevention in the Process Industries*. 2nd edition, **3:** 1996. Butterworth Heinemann.

18. Cleaver, R.P., Cumber, P.S. and Fairweather, M. *Predictions of free jet fires from high pressure, sonic releases.* Combustion and Flame, 2003. **132**: p. 463-474.

19. Roberts, T.A. *Effectiveness of an enhanced deluge system to protect LPG tanks and sensitivity to blocked nozzles and delayed deluged initiation.* J. Loss Prevention Process Ind., 2004. **17**: p. 151-158.

20. Toland, J. *The Great Dirigibles, their triumphs and disasters*. 1972, New York: Dover publications. Chapter 17.

21. Andrew, R. and Carpenter, P.E. *System safety analysis of hydrogen and methanol vehicles fuels.* Loss Prevention Symposium AIChE, 2003. **37** p. 465-482.

22. Fristrom, R.M. and Westerberg, A.A. *Flame Structure*. 1965, New York: McGraw-Hill.

23. Weinberg, F.J. *The first half-million years of combustion research and today's burning problem.* Proceedings of the Combustion Institute, 1974. **15th (Int.) Symposium on Combustion:** p. 1-17

24. Chomiak, J. *Combustion, A study in theory, fact and application*. 1990, New York: Gordon and Breach.

25. Kanury, A.M. *Introduction to Combustion Phenomena*. 1975, London: Gordon and Breach.

26. Gaydon, A.G. and Wolfhard, H.G. *Flames: Their Structure, Radiation and Temperature* 4th edition 1979, London: Chapman and Hall.

27. Toong, T.Y. *Combustion Dynamics: the dynamics of chemically Reacting Fluids*. 1983, New York: McGraw-Hill.

28. Strehlow, R.A. *Combustion Fundamentals*. 1984, New York: McGraw-Hill.

29. Glassman, I., *Combustion*. 3rd edition 1996, San Diego: Academic Press.

30. Albini, F.A. A *physical model for firespread in brush.* The Combustion Institute, 1967. **11th Symposium (Int.) on Combustion:** p. 553-560.

31. Thomas, P.H. *On the development of urban fires from multiple ignitions*. 1968, Fire Research Station: Borehamwood, England.

32. Walton, W.D. and Budnick, E.K. *Deterministic computer fire models*, in *the SFPE Handbook of Fire Protection Engineering*, Cote, A.E. et al Editor. 1997, National Fire Protection Association: Quincy, MA. p. **11**-52 - **11**-59.

33. Stroup, D.W., *Using field modelling to simulate enclosure fires*, in *The SFPE Handbook of Fire Protection Engineering*, DiNenno, P.J. Editor. 1995, National Fire Protection Association: Quincy, MA. p. **3**-152 - **3**-159.

34. El-Amin, M.F. and Kanayama, H. *Boundary layer theory approach to the concentration layer adjacent to a ceiling wall at impinging region of a hydrogen leakage.* International Journal of Hydrogen Energy, 2008. **33**: p. 6393-6400.

35. El-Amin, M.F., Kanayama, H. and Inoue, M. *Boundary layer theory approach to the concentration layer adjacent to a ceiling wall of a hydrogen leakage: far region.* International Journal of Hydrogen Energy, 2008. **33**: p. 7642-7647.

36. Houf, W. and Schefer, R. *Analytical and Experimental investigation of small-scale unintended releases of hydrogen.* International Journal of Hydrogen Energy, 2008. **33**: p. 1435-1444.

37. Houf, W.G., Schefer, R.W. and Williams, T.C. *Investigation of small-scale unintended releases of hydrogen momentum-dominated regime.* International Journal of Hydrogen Energy, 2008. **33**: p. 6373-84.

38. Agrawal, A. and Prasad, A.K. *Integral solution for the mean flow profiles of turbulent jets, plumes, and wakes.* ASME Journal of Fluids Energy, 2003. **125**: p. 813-22.

39. Kalghatgi, G.T. *Lift-off heights and visible lengths of vertical turbulent jet diffusion flames in still air.* Combustion Science and Technology, 1984. **41**: p. 17-29.

40. Faeth, G.M., Jeng, S.M. and Gore, J.P. *Spectral and Total Radiation properties of turbulent hydrogen/air diffusion flames.* ASME Journal of Heat Transfer, 1987. **109**: p. 165-171.

41. Barlow, R.S. *Sandia H_2/He Flame data - Release 2.0*. 2003; Available from: http://www.ca.sandia.gov/TNF.

42. Pitts, W.M. *Assessment of theories for the behaviour and blowout of lifted turbulent diffusion flame.* The Combustion Institute, Pittsburgh, 1989. **22nd Symposium (Int.) on Combustion**: p. 809-816

43. Peters, N. *Laminar flamelet concepts in turbulent combustion.* The Combustion Institute, Pittsburgh, 1986. **Proceedings of the 21st Symposium (Int.) on Combustion**: p. 1231-1250.

44. Ferraris, S.A. and Wen, J.X. *Large eddy simulation of a lifted turbulent jet flame.* Combustion and Flame, 2007. **150**: p. 320-339.

45. Fiorina, B., Gicquel, O., Vervisch, L., Carpentier, S. and Darabiha, N. *Approximating the chemical structure of partially premixed and diffusion*

counterflow flames using FPI flamelet tabulation. Combustion and Flame, 2005. **140**: p. 147-160.

46. Pitts, W.M. *Importance of isothermal mixing processes to the understanding of lift-off and blowout of turbulent jet diffusion flames.* Combustion and Flame, 1989. **76**: p. 197-212.

47. Birch, A.D. and Hargrave, G.K. *Lift-off heights in underexpanded natural gas jet fires.* The Combustion Institute, Pittsburgh, 1980. **22nd Symposium (Int.) on Combustion**: p. 1463-1471.

48. Sanders, J.P.H. and Lamers, A.P.G. *Modelling and calculation of turbulent lifted diffusion flames.* Combustion and Flame, 1994. **96**: p. 22-33.

49. Cumber, P.S. and Spearpoint, M. *Modelling lifted methane jet fires using the boundary layer equations.* J. Numerical Heat Transfer, 2006. **49**: p. 239-258.

50. Vanquickenborne, L. and Van Tiggelen, A. *The stabilization mechanism of lifted diffusion flames.* Combustion and Flame 1966. **10**: p. 59-68.

51. Peters, N. and Williams, F.A. *Lift-off characteristics of turbulent jet diffusion flames.* AIAA 1983. **24**: p. 423-429.

52. Peters, N. *Laminar diffusion flamelet models in non-premixed turbulent combustion.* Progress in Energy and Combustion Science 1984. **10**: p. 319-339.

53. Muller, C.M., Breitbach, H. and Peters, N. *Partially premixed turbulent flame propagation in jet flames.* The Combustion Institute, Pittsburgh, 1994. **25th Symposium (Int.) on Combustion**: p. 1099-1106.

54. Upatnicks, A., Driscoll, J.F., Ramussen, C.C. and Ceccio, S.L. *Lift-off turbulent jet flames-assessment of edge flame and other concepts using cinema-PIV.* Combustion and Flame, 2004. **138**: p. 259-272.

55. Bradley, D., Gaskell, P.H. and Lau, A.K.C. *A mixedness-reactedness flamelet model for turbulent diffusion flames.* The Combustion Institute, Pittsburgh, 1990. **23rd Symposium (Int.) on Combustion**: p. 685-692.

56. Hawthorne, W.R., Weddell, D.S. and Hottel, H.C. *Mixing and combustion in turbulent gas jets.* 1949. **3rd Symposium (Int.) on Combustion and Flame, and Explosion Phenomena**: p. 266-288.

57. Burke, S.P. and Schumann, T.E.W. Proceedings of the Combustion Institute, 1928. **1st Symposium (Int.) on Combustion**: p. 2-11.

58. Turns, S.R. *An Introduction to Combustion: Concepts and Applications*. 1996, New York: McGraw-Hill.

59. Longwell, J.P. and Weiss, M.A. *High temperature reaction rates in hydrocarbon combustion.* Ind. Eng. Chem., 1955. **47**: p. 1634-1643.

60. Hottel, H.C. *Models in Fire research,* in *International Symposium on Models in Fire research,* Berl, W.G. Editor. 1961, National Academy of Sciences-National Research Council: Washington D.C.

61. Homsy, C.A. *Similitude in turbulent free-jet diffusion flames,* in *Chemical Engineering*. 1959.

62. R.W.Bilger and Beck, R.E. *Further experiments on turbulent jet diffusion flames.* Proceedings of the Combustion Institute, 1974. **15th Symposium (Int.) on Combustion**: p. 541-552.

63. Driscoll, J.F., Chen, R.H. and Yoon, Y. *Nitric oxide levels of turbulent jet diffusion flames: Effects of residence time and Damköhler number.* Combustion and Flame, 1992. **88**: p. 37-49.

64. Gunther, R. *Turbulence properties of flames and their measurements.* Progress in Energy and Combustion Science, 1983. **9**: p. 105-154.

65. Kent, J.H. and Bilger, R.W. *Turbulent diffusion flames.* Proceedings of the Combustion Institute, 1972. **14th Symposium (Int.) on Combustion**: p. 615-625.

66. Launder, B.E. and Spalding, D.B. *Mathematical models of Turbulence*. 1972, New York: Academic Press.

67. Bray, K.N.C. *AASU Report No. 330,* 1973, Department of Aeronautics and Astronautics, University of Southampton.

68. Bilger, R.W. *A note on Favre averaging in variable density flows.* Combustion, Science and Technology, 1975. **11**: p. 215-217.

69. Dibble, R.W., Kollman, W., Farshchi, M. and Schefer, R.W. *Second-order closure for turbulent nonpremixed flames: scalar dissipation and heat release effects.* Proceedings of the Combustion Institute, 1988. **21st Symposium (Int.) on Combustion**: p. 1329-1340.

70. Kent, J.H. and Bilger, R.W. *The prediction of turbulent diffusion flame fields and nitric oxide formation.* Proceedings of the Combustion Institute, 1977. **16th Symposium (Int.) on Combustion** p. 1643-1656.

71. Bowman, C.T. *Control of combustion-generated nitrogen oxides emissions: Technology driven by regulation.* Proceedings of the Combustion Institute, 1992. **24th Symposium (Int.) on Combustion**: p. 859-878.

72. Bilger, R.W. *The structure of diffusion flames.* Combustion Science and Technology, 1976. **13**: p. 155-170.

73. Tsuji, H. and Yamaoka, I. *The structure of counterflow diffusion flames in the forward stagnation region of a porous cylinder.* Proceedings of the Combustion Institute, 1968. **12th Symposium (Int.) on Combustion**: p. 997-1005.

74. Laboratory, S.N. *TNF Workshop*. 2006; Available from: www.ca.sandia.gov/TNF.

75. Barlow, R.S. and Frank, J.H. *Effects of turbulence on species mass fractions in methane/air jet flames.* Proceedings of the Combustion Institute, 1998. **27th Symposium (Int.) on Combustion**: p. 1087-1095.

76. Starner, S.H. and Bilger, R.W. *Characteristics of a piloted diffusion flame designed for study of combustion turbulence interactions.* Combustion and Flame, 1985. **61**: p. 29-38.

77. Dibble, R.W., Masri, A.R. and Bilger, R.W. *The spontaneous Raman scattering technique applied to nonpremixed flames of methane.* Combustion and Flame, 1987. **67**: p. 189-206.

78. Masri, A.R., Dibble, R.W. and Bilger, R.W. *Conditional probability density functions measured in turbulent nonpremixed flames of methane near extinction.* Combustion and Flame, 1988. **74**: p. 267-284.

79. Masri, A.R., Dibble, R.W and Bilger, R.W. *The structure of turbulent nonpremixed flames revealed by Raman-Rayleigh-LIF measurements.* Progress in Energy and Combustion Science, 1996. **22**: p. 307-362.

80. Mansour, M.S., Dibble, R.W. and Bilger, R.W. *Raman/Rayleigh and mie-scattering measurements in a reverse flow reactor close to extinctions.* Proceedings of the Combustion Institute, 1988. **22nd Symposium (Int.) on Combustion**: p. 711-719.

81. Dally, B.B., Masri, A.R., Barlow, R.S. and Fiechtner, G.J. *Instantaneous and mean composition structure of bluff-body stabilised nonpremixed flames.* Combustion and Flame, 1998. **114**: p. 119-148.

82. Peters, N. *Local quenching due to flame stretch and nonpremixed turbulent combustion.* Combustion Science and Technology, 1983. **30**: p. 1-17.

83. Liew, S.K., Bray, K.N.C. and Moss, J.B. *A flamelet model of turbulent nonpremixed combustion.* Combustion Science and Technology, 1981. **27**: p. 69-73.

84. Bilger, R.W. *Future progress in turbulent combustion research.* Progress in Energy and Combustion Science, 2000. **26**: p. 367-380.

85. Favier, V. and Vervisch, L. *Edge flames and partially premixed combustion in diffusion flame quenching.* Combustion and Flame, 2001. **125**: p. 788-803.

86. Maus, F., Keller, D. and Peters, N. *A Lagrangian simulation of flamelet extinction and re-ignition in turbulent jet diffusion flame.* Proceedings of the Combustion Institute, 1990. **23rd Symposium (Int.) on Combustion**: p. 693-698.

87. Peters, N. *Turbulent Combustion*. 2000: Cambridge University Press

88. Pitsch, H. *Improved pollutant predictions in large-eddy simulations of turbulent nonpremixed combustion by considering scalar dissipation rate fluctuations.* Proceedings of the Combustion Institute, 2002. **29th Symposium (Int.) on Combustion**: p. 1971-1978.

89. Bilger, R.W. *The structure of turbulent nonpremixed flames.* Proceedings of the Combustion Institute, 1988. **22nd Symposium (Int.) on Combustion**: p. 475-488.

90. Ratner, A., Mullin, J.A., Carter, C.D., Donbar, J.M. and Driscoll, J.F. *Reaction zone structure of nonpremixed turbulent flames in the "intensity wrinkle" regime.* Proceedings of the Combustion Institute, 2000. **28th Symposium (Int.) on Combustion**: p. 245-252

91. Chen, J.Y. and Dibble, R.W. *Reduced kinetic mechanisms and asymptotic approximations for methane-air flames*, editor Smooke. M.D. 1991, London: Springer. Chapter 9.

92. Dopazo, C. and O'Brien, E.E. *An approach to the auto-ignition of a turbulent mixture.* Acta Astronautica, 1974. **1**: p. 1239-1266.

93. Frost, V.A., Emelianov, V.M. and Nedoroob, S.A. *Analysis of joint PDF equation in turbulent flow with density variations.* Proceedings of the Combustion Institute, 1992. **24th Symposium (Int.) on Combustion**: p. 435-442

94. Pope, S.B. *The probability approach to the modelling of turbulent reacting flows.* Combustion and Flame, 1976. **27**: p. 299-312.

95. Pope, S.B. *PDF methods for turbulent reacting flows.* Progress in Energy and Combustion Science, 1985. **11**: p. 119-192.

96. Pope, S.B. *Computations of turbulent combustion: progress and challenges.* Proceedings of the Combustion Institute, 1990. **23rd Symposium (Int.) on Combustion**: p. 591-612.

97. Dopazo, C. *Turbulent Reacting Flows*, F.A.W.E., P.A. Libby, Editor. 1994, Academic Press: New York.

98. Pope, S.B. *Turbulent Flows*. 2000, Cambridge: Cambridge University Press.

99. Fox, R.O. *Computational Models for Turbulent Reactive Flows.* 2003, Cambridge: Cambridge University Press.

100. Pope, S.B. *Computationally efficient implementation of combustion chemistry using in situ adaptive tabulation.* Combustion Theory Modelling, 1997. **1**: p. 41-63.

101. Chen, J.Y. *Analysis of in situ adaptive tabulation performance for combustion chemistry and improvement with a modified search algorithm.* Combustion Science and Technology, 2004. **176**: p. 1153-1169.

102. Sung, C.J., Law, C.K. and Chen, J.Y. *An augmented reduced mechanism for methane oxidation with comprehensive global parametric validation.* Proceedings of the Combustion Institute, 1998. **27th Symposium (Int.) on Combustion**: p. 295-304.

103. Tang, Q., Xu, J. and Pope, S.B. *Probability density function calculations of local extinction and no production in piloted-jet of turbulent methane/air flames.* Proceedings of the Combustion Institute, 2000. **28th Symposium (Int.) on Combustion**: p. 133-139.

104. Lindstedt, R.P., Louloudi, S.A. and Vaos, E.M. *Joint scalar probability density function modelling of pollutant formation in piloted turbulent jet diffusion flames with comprehensive chemistry.* Proceedings of the Combustion Institute, 2000. **28th Symposium (Int.) on Combustion**: p. 149-156.

105. Xu, J. and Pope, S.B. *PDF calculations of turbulent nonpremixed flames with local extinction.* Combustion and Flame, 2000. **123**: p. 281-307.

106. Lindstedt, R.P. and Louloudi, S.A. *Joint scalar probability density function modelling of turbulent methanol jet diffusion flames.* Proceedings of the Combustion Institute, 2002. **29th Symposium (Int.) on Combustion**: p. 2147-2154.

107. Villermaux, J. and Devillon, J.C. Proceedings of the 2nd International Symposium on Chemical Reaction Engineering 1972: p. 1-13.

108. Janicka, J., Kolbe, W. and Kollmann, W. *Closure of the transport equation for the probability density function of turbulent scalar fields.* Journal of Non-Equilibrium Thermodynamics., 1977. **4**: p. 47-66.

109. Curl, R.L. *Disperse phase mixing: 1. Theory and effects in simple reactors.* AIChE J., 1963. **9**: p. 175-181.

110. Subramaniam, S. and Pope, S.B. *A mixing model for turbulent reactive flows based on Euclidean minimum spanning trees.* Combustion and Flame, 1998. **115**: p. 487-514.

111. Ren, Z. and Pope, S.B. *An investigation of the performance of turbulent mixing models.* Combustion and Flame, 2004. **136**: p. 208-216.

112. Subramaniam, S. and Pope, S.B. *Comparison of mixing model performance for nonpremixed turbulent reacting flow.* Combustion and Flame, 1999. **117**: p. 732-754.

113. Norris, A.T. and Pope, S.B. *Turbulent mixing model based on order pairing.* Combustion and Flame, 1990. **83**: p. 37-42.

114. Borghi, R. *Turbulent Combustion Modelling.* Progress in Energy and Combustion Science, 1988. **14**: p. 245-292.

115. Faeth, G.M., Jeng, S.M. and Lai, M.C. *Non Luminous Radiation in Turbulent Bouyant Axisymmetric Flames.* Combustion Science and Technology, 1984. **40**: p. 41-53.

116. DesJardin, P.E. and Frankel, S.H. *Large eddy simulation of a nonpremixed reacting jet: application and assessment of subgrid-scale combustion models.* Physic of Fluids, 1998. **10**: p. 1-17.

117. Muradoglu, M., Liu, K. and Pope, S.B. *PDF modelling of a bluff-body stabilized turbulent flame.* Combustion and Flame, 2003. **132**: p. 115-137.

118. Libby, P.A. and Williams, F.A. *Turbulent Reacting Flows.* Vol. 44. 1980: Springer.

119. Bilger, R.W. ed. *Turbulent flows in nonpremixed reactants*. Turbulent Reacting flows, ed. Libby, P.A. and Williams, F.A.. 1980, Springer. 65.

120. Bilger, R.W. *Turbulent Jet Diffusion Flames.* Progress in Energy and Combustion Science, 1976. **1**: p. 87-109.

121. Williams, F.A. *Combustion Theory*, 2nd edition. 1994: Addison-Wesley.

122. Gordon, S. and McBride, B.J. *Computer program for calculation of complex chemical equilibrium compositions, rocket performance incident and reflected shocks, and Chapman-Jouguet detonations*. 1971.

123. Tien, C.L. and Lee, S.C. *Flame Radiation.* Progress in Energy and Combustion Science, 1982. **8**: p. 41-59

124. John deRis *Fire Radiation.* The Combustion Institute, Pittsburgh, 1979. **17th Symposium (Int.) on Combustion**: p. 1003-1016.

125. Seigel, R. and Howell, J.R. *Thermal Radiation Heat Transfer*. 3rd edition 1992, Washington D.C.: Hemisphere Publishing Corporation.

126. Ludwig, C.B., Malkmus, W., Reardon, J.E. and Thomson, J.A. *A handbook of Infrared Radiation from combustion gases*. 1973.

127. Goody, R.M. *Atmospheric radiation theoretical base*. Vol. **1**. 1964, Oxford: Clarendon Press.

128. Hottel, H.C. and Sarofim, A.F. *Radiative Transfer*. 1967, New York: McGraw-Hill.

129. Negrelli, D.E., Lloyd, J.R. and Novotny, J.L. *A Theoretical and Experimental Study of Radiation convection interaction in a diffusion flame.* Journal of Heat Transfer, 1977. **99**: p. 212-220

130. Edwards, D.K. and Menard, W.A. *Comparison of Models for Correlation of Total Band Absorption.* Appl. Optics, 1964. **3**.

131. Grosshandler, W.L. and Sawyer, R.F. *Radiation from a methanol furnace.* Journal of Heat Transfer-Transactions of the ASME, 1978. **100**: p. 247-252.

132. Grosshandler, W.L. *Radiative Heat-Transfer in Non-homogeneous Gases - A Simplified Approach.* International Journal of Heat and Mass Transfer, 1980. **23**: p. 1447-1459.

133. Grosshandler, W.L. and Nguyen, H.D. *Application of the total transmittance non-homogeneous radiation model to methane combustion.* Journal of Heat Transfer-Transactions of the ASME, 1985. **107**: p. 445-450.

134. Karman, D. and Steward, F.R. *The radiation spectrum from a test furnace.* International Journal of Heat and Mass Transfer, 1984. **27**: p. 1357-1364.

135. Steward, F.R. and Guruz, K.H. *Effects of solid particles on radiative transfer in a cylindrical test furnace.* The Combustion Institute, Pittsburgh, 1974. **15th Symposium (Int.) on Combustion**: p. 1271-1283.

136. Souil, J.M., Most, J.M. and Joulain, P. *Diffusion flame radiative properties in gas-solid combustion.* Combustion Science and Technology, 1980. **24**: p. 93-105.

137. Gengembre, E., Joulain, P. and Souil, J.M. *Experimental and Theoretical Study of Thermal Radiation from Turbulent Diffusion Flames to Vertical Target Surface.* Combustion Science and Technology, 1984. **41**.

138. Syed, J.K. *Soot and radiation modelling in buoyant fires*. 1990, **PhD Thesis:** Cranfield University, United Kingdom.

139. Crauford, N.L. *The structure of an unconfined buoyant turbulent diffusion flames.* 1984, **PhD Thesis:** University of Southampton, Southampton, UK.

140. Wilcox, D.C. *Model for fires with low initial momentum and nongray thermal-radiation.* AIAA Journal, 1975. **13**: p. 381-386.

141. Shackelford, W. *Results of Spectroscopic Measurements on Six Foot Diameter LNG Pool Fires at Capistrano test site*. 1972, TRW Systems Group: Redondo beach, California.

142. Fishburne, E.S. and Pergament, H.S. *The dynamics and radiant intensity of large hydrogen flames.* The Combustion Institute, Pittsburgh, 1979. **17th Symposium (Int.) on Combustion**: p. 1063.-1073

143. Williams, F. and Fuhs, A.E. *Apparent emission intensities from a turbulent flame composed of wrinkled laminar flames.* Jet propulsion, 1957. **27**.

144. Kmit, G.I. and Kabashnikov, V.P. *Influence of turbulent fluctuations on thermal radiation.* J. Applied Spectroscopy, 1979. **31**.

145. Grosshandler, W.L. and Joulain, P. *The effects of large-scale fluctuations on flame radiation*, in *dynamics of reactive systems part 2: Modelling and heterogeneous combustion*. 1986, AIAA progress series. p. 123-152.

146. Portscht, R. *Studies on characteristic fluctuations of flame radiation emitted by fires.* Combustion Science and Technology, 1975. **10**: p. 73-84.

147. Grosshandler, W.L. and Sawyer, R.F. *Radiation from a methanol Furnace.* Journal of Heat Transfer, 1978. **100**: p. 247-252.

148. Faeth, G.M. and Jeng, S.M. *Predictions of mean scalar properties in turbulent propane diffusion flames.* Journal of Heat Transfer, 1984. **106**: p. 891-893

149. Mazumder, S. and Modest, M.F. *Turbulence-radiation interactions in non-reactive flow of combustion gases.* Journal of Heat Transfer, 1999. **121**: p. 726-729.

150. Burns, S.P. *Turbulence radiation interaction modelling in hydrocarbon pool fire simulations*. 1999, Sandia.

151. Spiegel, E.A. *The smoothing of temperature fluctuations by radiative transfer.* Astrophysical, 1957. **126**: p. 202-207.

152. Townsend, A.A. *The effects of radiative transfer on turbulent flow of a stratified fluid.* Journal of Fluid Mechanics, 1958. **4**: p. 361-375.

153. Coelho, P.J., Teerling, O.J. and Roekaerts, D. *Spectral radiative effects and turbulence/radiation interaction in a non-luminous turbulent jet diffusion flames.* Combustion and Flame, 2003. **133**: p. 75-91.

154. Soufiani, A. *Temperature turbulence spectrum for high-temperature radiating gases.* Journal of Thermophysics, 1991. **5**: p. 489-494.

155. Janicka, J., Hassel, E.P., Tacke, M.M., Krieger, G. and Neuber, A. *Finite rate chemistry and no mole fraction in non-premixed turbulent flames.* Combustion and Flame, 1998. **113**: p. 198-211.

156. Janicka, J., Neuber, A., Fruechtel, G., Hassel, E.P. and Pfuderer, D.G. *Turbulence modulation in jet diffusion flames: Modelling and Experiments.* Combustion and Flame, 1998. **106**: p. 301-317.

157. Janicka, J., Tacke, M.M., Hassel, E.P., Chen, J.Y., Linow, S. and Geiss, S. *Experimental and Numerical Study of a Highly Diluted Turbulent Diffusion Flame Close to Blowout.* **27th Symposium (Int.) on Combustion,** 1998: p. 1139-1148.

158. Gore, J.P. *A Theoretical and Experimental Study of Turbulent Flame Radiation*, in *Mechanical Engineering*. 1986, **PhD Thesis:** Pennsylvania State University: Pennsylvania.

159. Pope, S.B. *Ten questions concerning the large-eddy simulation of turbulent flows.* New Journal of Physics, 2004. **6**: p. 1-24.

160. Strelets, M. *Turbulence modelling in convective flow of fires*. In Proceedings of the **4th International Seminar on Fire and Explosive Hazards**. 2004. Londonderry, Northern Ireland, UK.

161. Mran, M.J. and Shapiro, H.N. *Fundamentals of Engineering Thermodynamics*. 3rd edition 1998: John Wiley and Sons Ltd.

162. Bird, R.B., Stewart, W.E. and Lightfoot, E.N. *Transport Phenomena*. 1960: John Wiley and Sons.

163. Hirschfelder, J.O., Curtiss, C.F. and Bird, R.B. *Molecular Theory of Gases and Liquids*. 2nd edition 1964, New York: John Wiley and Sons.

164. Warnatz, J., Maas, U. and Dibble, R.W. *Combustion*. 3rd edition 2001, Berlin: Springler-Verlag.

165. Kuo, K.K. *Principles of Combustion*. 2nd edition 2005, New York: John Wiley and Sons.

166. Wilcox, D.C. *Turbulence Modelling for CFD*. 2nd edition 2000, California: KNI, Incorporation.

167. White, F.M. *Fluid Mechanics*. 2nd edition 1988: McGraw-Hill.

168. Pope, S.B. *An explanation of the turbulent round jet/plane jet anomaly.* AIAA, 1978. **16**.

169. Jones, W.P. and Launder, B.E. *The prediction of laminarisation with a two-equation model of turbulence.* International Journal of Heat Mass transfer, 1972. **15**: p. 301-314.

170. Spalding, D.B. *Concentration fluctuations in a round turbulent free jet.* Chemical Engineering Science, 1971. **26**: p. 95-107.

171. Spalding, D.B. *GENMIX: A General Computer Program for Two-dimensional Parabolic Phenomenon*. 1977, Oxford: Pergamon Press.

172. Wang, H. and Chen, Y. *PDF modelling of turbulent non-premixed combustion with detailed chemistry.* Chemical Engineering Science, 2004. **59**: p. 3477-3490.

173. Morse, A.P. *Axisymmetric turbulent shear flows with and without swirl*. 1977, University of London: London.

174. Moss, J.B., Stewart, C.D. and Syed, K. *Flow field modelling of soot formation at elevated pressure.* The Combustion Institute, Pittsburgh, 1988. **22nd Symposium (Int.) on Combustion**: p. 413-423.

175. Drysdale, D. *Introduction to Fire Dynamics*. 2nd edition 1998: Wiley, UK.

176. Cox, G. *Some measurements of fire turbulence.* Fire and Materials, 1976. **1**: p. 116-122.

177. Sparrow, E.M. and Cess, R.D. *Radiation Heat Transfer*. 1978: McGraw Hill Higher Education.

178. Abramowitz, M. and Stegun, I.A. *Handbook of Mathematical Functions*. 1972, New York USA: Dover Publications.

179. Edwards, D.K. and Balakrishnan, A. *Thermal Radiation by combustion gases.* International Journal of Heat and Mass Transfer, 1973. **16**.

180. Leckner, B. *Spectral and total emissivity of water vapour and carbon dioxide.* Combustion and Flame, 1972. **19**: p. 33-48

181. Modest, M.F. *Radiative heat transfer*. 2nd edition 2003, New York: McGraw-Hill.

182. Taine, J. and Soufiani, A. eds. *Gas IR radiative properties: from spectroscopic data to approximate models*. Advances in heat transfer, eds. Harnett, J.P. and Irvine, T. 1999, Academic Press: San Diego. **33**: p. 295-414.

183. Song, T.H. and Viskanta, R. *Interaction of radiation with turbulence: application to a combustion system.* Thermophysics and Heat Transfer, 1987. **1**: p. 56-62.

184. Foster, P.J. *The relation of time-mean transmission of turbulent flames to optical depth.* Journal of Institute of Fuel, 1969. **42**: p. 179-182.

185. Soufiani, A., Taine, J. and Mignon, P. eds. *Radiation effects on turbulent heat transfer in channel flows of infrared active gases*. Radiation heat transfer: fundamentals and applications, ed. Smith, A.M. et al. Vol. 137. 1990, ASME: New York. p. 141-148.

186. Sivathanu, Y.R. and Faeth, G.M. *Generalized state relationships for scalar properties in nonpremixed hydrocarbon/air flames.* Combustion and Flame, 1990. **82**: p. 211-230.

187. Musonge, P. and Jones, W. *Closure of the reynolds stress and scalar flux equations.* Physic of Fluids, 1988. **31**.

188. Hossain, M.S. and Rodi, W. *Influence of buoyancy on the turbulence intensities in horizontal and vertical Jets*, in *Heat transfer and buoyant convection*,, Spalding, D.B. and Afgan, N. Editors. 1976, Washington: Hemisphere Publishing Corporation. p. 39-51.

189. Fairweather, M., Jones, W.P. and Lindstedt, R.P. *Predictions of a turbulent reacting jet in a cross-flow.* Combustion and Flame, 1991: p. 361-375.

190. Cumber, P.S., Fairweather, M. and Ledin, H.S. *Application of wide band radiation models to non-homogeneous combustion systems.* International Journal of Heat and Mass Transfer, 1998. **41**: p. 1573-1584.

191. Fairweather, M., Jones, W.P., Ledin, H.S. and Lindstedt, R.P. *Predictions of soot formation in turbulent non-premixed propane flames.* The Combustion Institute, Pittsburgh, 1992. **24th Symposium (Int.) on Combustion**: p. 1067-1074.

192. Chai, J.C., Haeok, S.L. and Patankar, S.V. *Ray effect and false scattering in the discrete ordinates method.* Numerical Heat Transfer, 1993. **Part B**: p. 373-389.

193. Liu, L.H., Xu, X., Chen, Y.L. and Wang, H.F. *Fluctuating characteristics of radiative source term in hydrogen turbulent jet diffusion flame.* Journal of Quantitative Spectroscopy and Radiative Transfer, 2004. **87**: p. 193-201.

194. Lockwood, F.C. and Shah, N.B. *A New Radiation Solution Method for Incorporation in General Combustion prediction procedures.* The Combustion Institute, Pittsburgh, 1981. **18th Symposium (Int.) on Combustion**: p. 1405-1413.

195. Docherty, P. and Fairweather, M. *Predictions of radiative transfer from non-homogeneous combustion products using the discrete transfer method.* Combustion and Flame, 1988. **71**: p. 79-87.

196. Siegel, R. and Howell, J.R. *Thermal Radiation Heat transfer*. 3rd edition 1992, Washington: Hemisphere Publishing Corporation.

197. Fairweather, M., Jones, W.P. and Lindstedt, R.P. *Predictions of radiative transfer from a turbulent reacting jet in a cross-wind.* Combustion and Flame, 1992. **89**: p. 45-63.

198. Cumber, P.S. *Improvements to the discrete transfer method of calculating radiative heat transfer.* International Journal of Heat and Mass Transfer, 1995. **38**: p. 2251-2258.

199. Henson, J.C. and Malalasekera, W.M.G. *Comparison of the Discrete Transfer and Monte Carlo methods for radiative heat transfer in three-dimensional, non-homogeneous, scattering media* Numerical Heat Transfer, 1997. **32**: p. 19-36.

200. Abdel-Gayed, R.G., Bradley, D. and Lau, A.K.C. *The straining of premixed turbulent flames.* The Combustion Institute, Pittsburgh, 1988. **22nd Symposium (Int.) on Combustion**: p. 731-738.

201. Onokpe, O. and Cumber, P.S. *Modelling lifted hydrogen jet fires using the boundary layer equations.* Applied Thermal Engineering, 2009. **29**: p. 1383-1390.

202. Janicka, J. and Peters, N. *Prediction of turbulent jet diffusion flame lift-off using a PDF transport equation.* The Combustion Institute, Pittsburgh, 1982. **19th Symposium (Int.) on Combustion**: p. 367-374.

203. Kollmann, W. *The PDF approach to turbulent flow.* Theoretical Computational Fluid Dynamics 1, 1990: p. 249-285.

204. Lockwood, F.C. and Naguib, A.S. *The prediction of the fluctuations in the properties of free, round jet, turbulent diffusion flames.* Combustion and Flame, 1975. **24**: p. 109-124.

205. Richardson, J.N., Howard, H.C. and Smith, R.W. *The Relation between Sampling Tube Measurements and Concentration Fluctuations in a Turbulent Gas Jet.* in **4th Symposium on Combustion.** 1953. p. 814-817

206. Ma, C.Y., Hampartsoumian, E., Mahmud, T., Fairweather, M. and Gaskell, P.H. *Prediction of lifted, non-premixed turbulent flames using a mixedness-reactedness flamelet model with radiation heat loss.* Combustion and Flame, 2002. **128**: p. 60-73.

207. Grosshandler, W.L. *RADCAL: A Narrow-band model for Radiation Calculation in a Combustion Environment*. 1983, National Institute of Standards and Technology: Gaithersburg. p. 1-52.

208. Gore, J.P. and Faeth, G.M. *Structure and spectral radiation properties of turbulent ethylene/air diffusion flames.* **21st Symposium (Int.) on Combustion**, 1988. p. 1521-1531.

209. Faeth, G.M. and Jeng, S.M. *Species Concentrations and Turbulence properties in bouyant methane diffusion flame.* Journal of Heat Transfer, 1984. **106**: p. 721-727.

210. Marstein, C.H. *Radiative properties of plastic fires.* The Combustion Institute, Pittsburgh, 1979. **17th Symposium on Combustion**: p. 1063-1073.

211. Cumber, P.S. *Efficient calculation of the radiation heat flux surrounding a jet fire.* Fire Safety Journal, 2009. **44**: p. 580-589.

212. Crauford, N.L., Liew, S.K. and Moss, J.B. *Experimental and numerical simulation of a buoyant fire.* Combustion and Flame, 1985. **61**: p. 63-77.

213. Nishida, O. and Mukohara, S. *Characteristics of soot formation and decomposition in turbulent diffusion flames.* Combustion and Flame, 1982. **47**: p. 269-279.

214. Marquis, A.J. *Jets in a Crossflow*. 1986, British Gas.

215. Dianat, M., Fairweather, M. and Jones, W.P. *Predictions of axisymmetric and two-dimensional impinging turbulent jets.* International Journal of Heat and Fluid Flow, 1996. **17**: p. 530-538.

Appendices

Appendix A

A1 Reynolds stress transport equations

The transport equations have been described in some detail in the main text. Nevertheless, the form in which the equations were cast is not the one in which the equations are coded in the computer programs. This appendix shows the Reynolds stress, scalar flux, and scalar dissipation rate equations in their tensor notation.

A1.1 The Reynolds stress equation

The equations are written in Favre-averaged form. The terms and constants are those of Jones and Musonge [187]

$$\frac{\partial \bar{\rho}\widetilde{u_i''u_j''}}{\partial t}+\bar{\rho}\widetilde{u_i''u_l''}\frac{\partial \tilde{U}_i}{\partial x_l}+\bar{\rho}\widetilde{u_j''u_l''}\frac{\partial \tilde{U}_j}{\partial x_l}=C_s\frac{\partial}{\partial x_l}\left[\frac{k}{\varepsilon}\widetilde{u_l''u_m''}\frac{\partial \widetilde{u_i''u_j''}}{\partial x_m}\right]$$
$$-\bar{\rho}C_1\frac{2\varepsilon}{q^2}\left(\widetilde{u_i''u_j''}-\frac{1}{3}\delta_{ij}q^2\right)$$
$$+\bar{\rho}C_2\delta_{ij}\widetilde{u_l''u_m''}\frac{\partial \tilde{U}_l}{\partial x_m}$$
$$+\bar{\rho}C_3\left(\widetilde{u_j''u_l''}\frac{\partial \tilde{U}_i}{\partial x_l}+\widetilde{u_i''u_l''}\frac{\partial \tilde{U}_j}{\partial x_l}\right)$$
$$+\bar{\rho}C_4\left(\frac{\partial \tilde{U}_i}{\partial x_l}+\frac{\partial \tilde{U}_j}{\partial x_l}\right)\frac{q^2}{2}$$
$$-\bar{\rho}\left(\frac{3}{2}C_2+C_3\right)\left(\widetilde{u_j''u_l''}\frac{\partial \tilde{U}_l}{\partial x_i}+\widetilde{u_i''u_l''}\frac{\partial \tilde{U}_l}{\partial x_j}\right)$$

where

$$C_s=0.220, C_1=1.500, C_2=-0.529, C_3=0.674, C_4=-0.122 \text{ and } C_5=0.300$$

A1.2 The scalar flux equations

The equations are written in their Favre-averaged form. The terms and constants are those proposed by Jones and Musonge [187].

$$\frac{\partial \bar{\rho}\widetilde{u_i''\phi}}{\partial t} + \bar{\rho}\widetilde{u_i''u_j''}\frac{\partial \tilde{\phi}}{\partial x_j} + \bar{\rho}\widetilde{u_i''\phi_j}\frac{\partial \tilde{U}_i}{\partial x_j} = C_s\frac{\partial}{\partial x_j}\left[\frac{q^2}{2\varepsilon}\widetilde{u_j''u_l''}\frac{\partial \widetilde{u_i''\phi}}{\partial x_l}\right]$$
$$-2\bar{\rho}C_{\phi_1}^*\frac{2\varepsilon}{q^2}\widetilde{u_i''\phi} + \bar{\rho}C_{\phi_2}b_{ij}q^2\frac{\partial \tilde{\phi}}{\partial x_j}$$
$$+\bar{\rho}C_{\phi_s}\widetilde{u_j''\phi}\frac{\partial \tilde{U}_i}{\partial x_j} + \bar{\rho}C_{\phi_4}b_{ik}\widetilde{u_j''\phi}\frac{\partial \tilde{U}_k}{\partial x_j}$$
$$+\bar{\rho}C_{\phi_5}b_{jk}\widetilde{u_j''\phi}\frac{\partial \tilde{U}_k}{\partial x_i} + \bar{\rho}C_{\phi_6}b_{jk}\widetilde{u_j''\phi}\frac{\partial \tilde{U}_i}{\partial x_j}$$

Where

$$b_{ij} = \frac{\widetilde{u_i''u_j''}}{q^2} - \frac{1}{3}\delta_{ij}$$

and

$$C_{\phi_1}^* = \frac{C_{\phi_1}}{\left(1 + C_{\phi_1}^{'}\right)\sqrt{b^2}}$$

The constants take the following values

$$C_s = 0.220$$
$$C_{\phi_1} = 3.000$$
$$C_{\phi_1}' = 3.000$$
$$C_{\phi_2} = -1.022$$
$$C_{\phi_3} = 2.071$$
$$C_{\phi_4} = -4.987$$
$$C_{\phi_5} = 4.300 \qquad \textit{and}$$
$$C_{\phi_6} = -0.835$$

A1.3 The scalar dissipation equation

The scalar dissipation equation was proposed by Jones and Musonge [187]

$$\frac{\partial \bar{\rho}\varepsilon_\phi}{\partial t}+\frac{\partial \bar{\rho}\tilde{U}_l\varepsilon_\phi}{\partial x_l}=C_s\frac{\partial}{\partial x_j}\left[\frac{q^2}{2\varepsilon}\widetilde{u_j''u_l''}\frac{\partial \varepsilon_\phi}{\partial x_l}\right]-\bar{\rho}C_{D_1}\frac{\varepsilon_\phi^2}{\phi^2}-\bar{\rho}C_{D_2}\frac{2\varepsilon}{q^2}$$
$$-\bar{\rho}C_{D_3}\frac{2\varepsilon}{q^2}\widetilde{u_i''\phi}\frac{\partial \tilde{\phi}}{\partial x_i}-\bar{\rho}C_{D_4}\frac{2\varepsilon_\phi}{q^2}\widetilde{u_i''u_j''}\frac{\partial \tilde{U}}{\partial x_j}$$

Where

$$\begin{aligned}&C_s=0.22\\&C_{D_1}=2.00\\&C_{D_2}=1.80\\&C_{D_3}=1.70\\&\textit{and}\\&C_{D_4}=1.40\end{aligned}\qquad\text{(A.1)}$$

Appendix B

The mixture fraction and State relationship

B1.1 Derivation of the mixture fraction

At any spatial location, the composition of the gas-phase is either pure oxidant (air), pure fuel (hydrogen), or a mixture of the two. For reasons that will become apparent later in this appendix, it is convenient to introduce a quantity known as the mixture fraction (Z). It is a numerical construct used in the analysis of non-premixed combustion systems to describe the degree of scalar mixing between fuel and oxidant. It is a local quantity within the flow field that varies both spatially and temporally.

The mixture fraction is best understood by visualizing a homogeneous control volume containing a finite quantity of mass in a gaseous state. In a two-feed system consisting of a fuel stream and an oxidant stream, the mass in this control volume originated either as fuel or as oxidant. The mixture fraction in this control volume is classically defined as "the fraction of mass present that originated in the fuel stream".

Let m_1 be a certain quantity of mass that came from the fuel stream. Likewise, m_2 is a certain quantity of mass that originated in the oxidant stream. This nomenclature is typical: a subscript 1 denotes a quantity originating in the fuel stream, and a subscript 2 denotes a quantity that began in the oxidant stream. The total amount of mass present is $m_1 + m_2$. By introducing this nomenclature, the verbal definition of the mixture fraction given above can be expressed mathematically as:

$$Z = \frac{m_1}{m_1 + m_2} \tag{B.1}$$

In a non-reacting mixture of pure fuel (hydrogen) and pure oxygen, the mass fraction of fuel is equal to the value of Z, and the mass fraction of oxygen is equal to the value of $1 - Z$. However, both the fuel and oxidant stream may contain inert substances such as nitrogen. Let $Y_{F,1}$ be the mass fraction of fuel in the fuel stream (unity for pure fuel in this case hydrogen) and let $Y_{O_2,2}$ be the mass fraction of oxygen in the oxidant stream.

In this generalised case, the mass fraction of fuel in a completely unburnt mixture of fuel and oxidant (designated Y_F'') is

$$Y_F'' = Y_{F,1} Z \tag{B.2}$$

Similarly, the mass fraction of oxygen, designated Y_{O_2}'' is :

$$Y_{O_2}'' = Y_{O_2,2}\left(1 - Z\right) \tag{B.3}$$

Equations (B.2) and (B.3) give the relationship between the mixture fraction and mass fraction of fuel and oxygen during mixing of fuel and oxidant in absence of combustion. These are important building blocks for the analysis of reacting systems. Now introduce a reaction describing the complete combustion of hydrogen fuel to form water vapour:

$$\nu_F' H_2 + \nu_{O_2}' O_2 \rightarrow \nu_{H_2O}'' H_2O \tag{B.4}$$

The stoichiometric coefficients in equation (B.4) can be defined in terms of ν_F' as follows:

$$\nu_{O_2}' = \frac{1}{2}\nu_F' \tag{B.5}$$

$$\nu_{H_2O}'' = \nu_F' \tag{B.6}$$

Consider the system described by equation (B.4) in the absence of any reaction, that is, with frozen reactants. This is a stoichiometric mixture consisting of $\nu_F' = \nu_{H_2}'$ moles of fuel, $\nu_O' = \nu_{O_2}'$ moles of oxygen, and zero mole of water vapour. The mole fractions of fuel (hydrogen) and oxygen are:

$$X_{H_2} = \frac{\nu'_{H_2}}{\nu'_{O_2} + \nu'_{H_2}} \tag{B.7}$$

$$X_{O_2} = \frac{\nu'_{O_2}}{\nu'_{O_2} + \nu'_{H_2}} \tag{B.8}$$

In combustion problems it is more convenient to work in terms of mass fraction rather than mole fraction. The reason for this is that mass is perfectly conserved during combustion process, but moles are not necessarily conserved. For this reason the mole fractions in (B.7) and (B.8) are rewritten as mass fractions:

$$Y_{O_2} = \frac{\nu'_{O_2} M_{O_2}}{\nu'_{O_2} M_{O_2} + \nu'_{H_2} M_{H_2}} \tag{B.9}$$

$$Y_{H_2} = \frac{\nu'_{H_2} M_{H_2}}{\nu'_{O_2} M_{O_2} + \nu'_{H_2} M_{H_2}} \tag{B.10}$$

Dividing equation (B.9) by (B.10) and multiplying by Y_{H_2} gives an expression that relates the oxygen mass fraction to the fuel mass fraction:

$$Y_{O_2} = Y_{H_2} \frac{\nu'_{O_2} M_{O_2}}{\nu'_{H_2} M_{H_2}} \tag{B.11}$$

Define s as the stoichiometric oxygen-to-fuel mass ratio:

$$s = \frac{\nu'_{O_2} M_{O_2}}{\nu'_{H_2} M_{H_2}} \tag{B.12}$$

Combining equations (B.11) and (B.12) gives:

$$Y_{O_2} = s Y_{H_2} \tag{B.13}$$

Up to this point, we have been considering a non-reacting mixture of fuel and oxygen. As the reaction in equation (B.4) proceeds from left to right, the reactants are consumed and products are generated. From equation(B.13), the change in the oxygen mass fraction dY_{O_2} is linearly proportional to the change in fuel mass fraction dY_{H_2} by the factor s:

$$dY_{O_2} = s dY_{H_2} \tag{B.14}$$

Now allow the reaction to proceed from a completely unburnt state, designated as u, to any state of combustion between completely unburnt and completely burnt, designated as b. This is equivalent to integrating equation (B.14) from state u to state b:

$$\begin{aligned} \int_u^b dY_{O_2} &= s\int_u^b dY_{H_2} \\ Y_{O_2}^b - Y_{O_2}^u &= sY_{H_2}^b - sY_{H_2}^u \\ sY_{H_2}^b - Y_{O_2}^b &= sY_{H_2}^u - Y_{O_2}^u \end{aligned} \tag{B.15}$$

As a point of rigour, it is worth noting that equation (B.15) is valid for homogeneous systems in the absence of diffusion. It is valid for spatially inhomogeneous systems such as diffusion flames, only if the diffusivities of the fuel and oxygen are equal. The traditional definition of the mixture fraction can be derived by substituting equations (B.2) and (B.3) into equation (B.15)

$$\begin{aligned} sY_{H_2}^b - Y_{O_2}^b &= sY_{H_2,1}Z - Y_{O_2,2}(1-Z) \\ sY_{H_2}^b - Y_{O_2}^b &= sY_{H_2,1}Z - Y_{O_2,2} + Y_{O_2,2}Z \\ sY_{H_2,1}Z + Y_{O_2,2}Z &= sY_{H_2}^b - Y_{O_2}^b - Y_{O_2,2} \\ Z\left(sY_{H_2,1} + Y_{O_2,2}\right) &= sY_{H_2}^b - Y_{O_2}^b - Y_{O_2,2} \\ Z &= \frac{sY_{H_2}^b - Y_{O_2}^b - Y_{O_2,2}}{sY_{H_2,1} + Y_{O_2,2}} \end{aligned} \tag{B.16}$$

At stoichiometric conditions, both $Y_{H_2}^b$ and $Y_{O_2}^b$ are zero because all the fuel and oxygen are consumed. Consequently, from equation (B.16) the stoichiometric value of the mixture fraction is

$$Z_{st} = \frac{Y_{O_2,2}}{sY_{H_2,1} + Y_{O_2,2}} \tag{B.17}$$

B1.2 State relations: Complete combustion

First, consider the stoichiometric combustion of one mole of hydrogen fuel in an oxidant stream consisting only of nitrogen and oxygen:

$$H_2 + \nu_{O_2}\left(O_2 + \frac{X_{N_2}^{\infty}}{X_{O_2}^{\infty}} N_2\right) \rightarrow \nu_{H_2O} H_2O + \nu_{O_2} \frac{X_{N_2}^{\infty}}{X_{O_2}^{\infty}} N_2 \tag{B.18}$$

Now consider the generalised reaction in which excess fuel and oxygen are allowed to exist:

$$H_2 + \frac{1}{\phi}\nu_{O_2}\left(O_2 + \frac{X_{N_2}^{\infty}}{X_{O_2}^{\infty}} N_2\right) \rightarrow \left(1 - \frac{1}{\phi}\right) H_2 + \frac{1}{\phi}\left[\nu_{O_2} - \frac{\nu_{H_2O}}{2}\right]\left(O_2 + \frac{X_{N_2}^{\infty}}{X_{O_2}^{\infty}} N_2\right) + \frac{1}{\phi}\nu_{H_2O} H_2O \tag{B.19}$$

The equivalent ratio can be related to the mixture fraction as:

$$\phi = \frac{Z}{1-Z}\frac{1-Z_{st}}{Z_{st}} \tag{B.20}$$

The system is fuel-lean for $0 < \phi < 1$, stoichiometric at $\phi = 1$, and fuel-rich for $1 < \phi < \infty$. Equations (B.19) and (B.20) can be used to relate the species composition of a non-premixed combustion system in the complete combustion, fast chemistry limit to the mixture fraction. The mass fractions of the five species included in this analysis are shown below in Figure B-1.

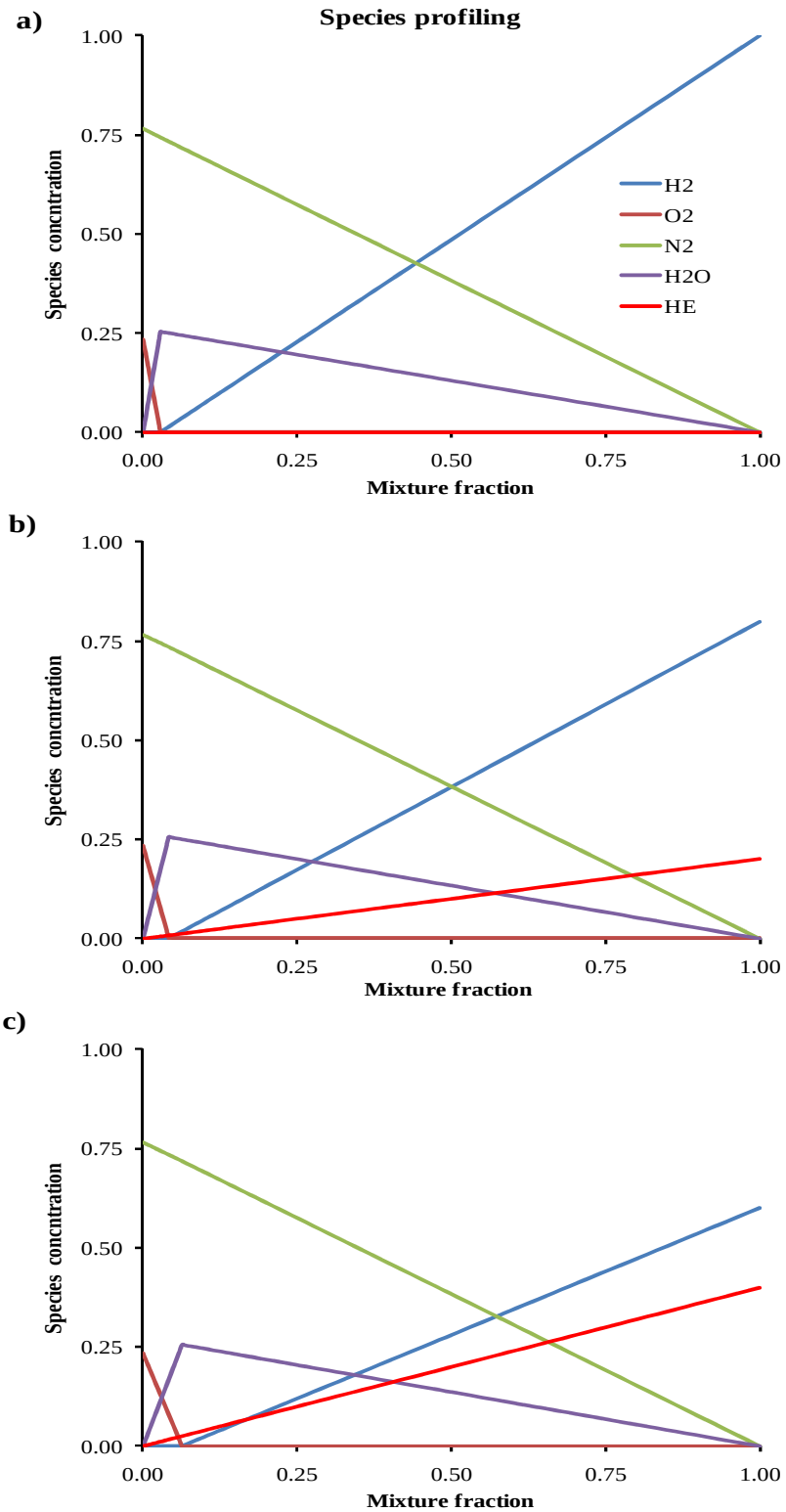

B. 1: Species profiling showing plot of species concentration against mixture fraction a) undiluted hydrogen flame b) 20% helium dilution of hydrogen flame and c) 40% helium dilution of hydrogen flame

Appendix C

Description of computer codes

There are quite a few different types of computer codes available for fluid flow simulations. The choice of code is crucial; they are not all good for all purposes. The nature of the problem, that is whether parabolic, elliptic or hyperbolic, will have to be taken into account.

C1 Introduction

The present investigation has looked at basically three types of flow problems, a laminar diffusion flame where the equations were cast in a boundary layer form, three turbulence diffusion flames, where the flow is parabolic, and finally turbulence radiating diffusion flames, where the flow is equally in parabolic form as well.

The Genmix code, developed by Spalding [171], has been used extensively over the years, for example Crauford [212] and Jeng [148], among others have made use of Genmix. The partial differential equations are cast in their boundary layer form in Genmix. By this we mean that the flow is represented by a boundary layer, which is allowed to develop through the domain. One of the main attractions with this representation is that all equations are of parabolic kind, and hence a change in a dependent variable at a point c cannot propagate upstream of that point. In the physical sense, this is strictly untrue, certain pressure changes might conceivably travel upstream, against the preferred direction of flow, say if the flow is subsonic, and the curvature of the stream lines is far greater than the boundary layer thickness. However, this is not a constraint when simulating the turbulence propane diffusion flames as described by Nishida and Mukohara [213]. The laminar flame code is also of Genmix type, for example, parabolic partial differential equations' are discretised. Nevertheless, in most other respects the codes differ considerably. The laminar code incorporates a one-step chemical kinetic scheme, a different way of refining the grid, and source term linearisation technique.

C2. Computational grid – Parabolic code

It is uneconomical, and problems are likely to arise when trying to use a uniform Cartesian grid, for boundary layer type problems. Many nodes end up outside the boundary layer and where the edge of the boundary layer crosses the grid line between two adjacent nodes; one must then work out how much of the cell is inside the computational cell, and change the coefficients accordingly. It would be ideal to have nodes only within the boundary layer, the region of interest. One possibility would be to use a stream function approach which replaces the Cartesian x-y co-ordinate system with a x-ψ system, where ψ is the stream function. However, this turns out to be just as wasteful as a Cartesian grid, because there will be nodes outside the boundary layer. If a sensible co-ordinate transformation is made, all nodes will be located within the boundary layer, and more importantly as the grid expand the nodes are relocated, but the number of nodes in the boundary layer stays constant. This has major advantages. The x-ψ co-ordinate system can be transformed into x-ω co-ordinates, where ω some function of x, specified by the user, is in fact, ω is a non-dimensional stream function. There are a number of different choices of co-ordinate systems which are more or less suited for the job.

The Genmix code has incorporated the x-ω system, thus all nodes are within the boundary layer. The ω is as said previously a function of x,

$$\omega = \frac{\psi - \psi_1}{\psi_E - \psi_1}, \quad 0 \le \omega \le 1 \tag{C.1}$$

The continuity and scalar-transport equations can be cast in a boundary layer form:

$$\frac{\partial \overline{\rho}\tilde{U}}{\partial x} + \frac{1}{r}\frac{\partial r\overline{\rho}\tilde{V}}{\partial r} = 0 \tag{C.2}$$

$$\overline{\rho}\tilde{U}\frac{\partial \phi}{\partial x} + \overline{\rho}\tilde{V}\frac{\partial \phi}{\partial r} = \frac{1}{r}\frac{\partial}{\partial r}\left[r\Gamma_\phi \frac{\partial \phi}{\partial r}\right] + \tilde{S}_\phi \tag{C.3}$$

Where ϕ stands for a dependent variable, that is U, for one of the Reynolds stresses, and S_ϕ is the source term. If a new coordinate system (x,ψ) is introduced where ψ is the stream function

$$r\rho U = \frac{\partial \psi}{\partial y}, \quad and \; r\rho V = \frac{\partial \psi}{\partial x} \tag{C.4}$$

The stream function does not have the properties required, and consequently it is vital to introduce a dimensionless stream function, (x,ω),

$$\left(\frac{\partial}{\partial x}\right)_\psi = \left(\frac{\partial}{\partial x}\right)_\omega + \left(\frac{\partial \omega}{\partial x}\right)_\psi \left(\frac{\partial}{\partial \omega}\right) \tag{C.5}$$

$$\left(\frac{\partial}{\partial \psi}\right)_x = \left(\frac{\partial}{\partial x}\right)\left(\frac{\partial x}{\partial \psi}\right)_x + \left(\frac{\partial \omega}{\partial \psi}\right)_x \left(\frac{\partial}{\partial \omega}\right) \tag{C.6}$$

The first term of the right hand side of equation (C.6) is zero, because x is held constant. Equations (C.5) and (C.6) together with (C.1) can then be combined to yield:

$$\left(\frac{\partial}{\partial x}\right)_\psi = \left(\frac{\partial}{\partial x}\right)_\omega - \left[\frac{d\psi_1}{dx} + \omega \frac{d(\psi_E - \psi_1)}{dx}\right] \frac{1}{(\psi_E - \psi_1)} \frac{\partial}{\partial \omega} \tag{C.7}$$

This with the following definitions of mass entrainment rates into the solution domain can be made to cover just the region of interest.

$$r_I m_I = -\frac{d\psi_1}{dx}, \quad and \quad r_E m_E = -\frac{d(\psi_E - \psi_I)}{dx} \tag{C.8}$$

and the final version of the transport equation can be written as

$$\frac{\partial \phi}{\partial x}+\left(\frac{r_I m_I+\omega\left(r_E m_E-r_I m_I\right)}{\left(\psi_E-\psi_I\right)}\right)\frac{\partial \phi}{\partial \omega}=\frac{\partial}{\partial \omega}\left[\frac{\rho U r^2 \Gamma_\phi}{\left(\psi_E-\psi_I\right)^2}\frac{\partial \phi}{\partial \omega}\right]+\frac{S_\phi}{\rho U} \tag{C.9}$$

or cast in a more compact form

$$\frac{\partial \phi}{\partial x}+\left(a+\omega b\right)\frac{\partial \phi}{\partial \omega}=\frac{\partial}{\partial \omega}\left[c\frac{\partial \phi}{\partial \omega}\right]+d \tag{C.10}$$

where

$$a=\frac{r_I m_I}{\left(\psi_E-\psi_I\right)}$$

$$b=\frac{r_E m_E-r_I m_I}{\left(\psi_E-\psi_I\right)}$$

$$c=\frac{\rho U r^2 \Gamma_\phi}{\left(\psi_E-\psi_I\right)^2}$$

and

$$d=\frac{S_\phi}{\rho U}$$

C3. Different types of boundary conditions

It is necessary to supply boundary conditions. The way these conditions are implemented depends on the grid layout. There are two different ways, firstly, the physical boundary coincides with the computational domain and secondly, the physical boundary is located half-way between the end nodes. The solutions will be identical for any one problem despite the choice of grid layout. The only difference lies in how the boundary conditions are implemented.

A variable can be set to a specific value at the boundary; this is called a Dirichlet condition. However, if a gradient condition is applied instead, then it is a von Neumann (or just Neumann) condition. Therefore, a zero gradient refers to a von Neumann condition where the gradient equals zero. The terms Dirichlet and von Neumann, are referred to implicitly in the description of the boundary conditions below

The transport equation of interest in the present study, are partial differential equations of at most second order, and there are thus only five different types of boundary. Firstly, the inflow is normally given by either a measured profile or an educated guess. This is a Dirichlet condition. The second type is the outflow, which in some cases will be specified by a measured profile, if known, but more often than not there is lack of information and a zero gradient is assumed. Consequently, the outflow is a von Neumann type condition. Another relevant type is the symmetry plane. Axisymmetric flows will require the introduction of a symmetry plane. This is beneficial since one can either reduce the number of nodes or keep the number of nodes the same but make the grid finer. There is no transport across the plane of symmetry, for example, the velocity normal to the plane is zero, while all other variables have a zero gradient.

The fourth kind of boundary type, constant pressure, causes a lot of problems. The idea is to go far enough away from the flow so that the pressure gradient is zero. This is also known as the entrainment boundary. The problems mentioned arise at the corner where the constant pressure plane meets with a zero gradient plane. In effect, one condition on the pressure is imposed in the axial direction and another in the radial direction. A particular emphasis will be put on this type of boundary because it is a likely source of non-convergence. Constant pressure boundaries are commonly used but it is rare for the papers to contain a description of how the boundary condition was implemented. The last type of boundary condition considered is that of a solid wall. It has been customary in the past to assume that a law of the wall holds, the velocity near the wall can be characterised as a function of the distance from the wall. Marquis [214] argued that the $k-\varepsilon$ model would handle the near-wall region but at the expense of an increase in the number of nodes in the boundary layer. This requirement would be prohibitively expensive in terms of CPU time. The implementation of higher-order closure models, that is, Reynolds stress models, has indicated that the law of the wall has some serious shortcomings, that is, the description is not sufficiently realistic. A specific problem is that of wall reflections of pressure, Dianat et al [215].

Appendix D

RADCAL

The program RADCAL [207] solves for the radiation intensity along optical paths in a non-homogeneous absorbing/emitting medium. We present a description of the RADCAL code as provided by Grosshandler. The spectral radiation intensity (I) received at the origin along a line of sight (of pathlength L) through a non-homogeneous (in temperature and concentration) absorbing/emitting gas, in local thermodynamic equilibrium, may be derived from

$$I_w = \int_0^U \kappa_w I_{w,b} \exp\left(-\int_0^u \kappa_w du' \right) du \tag{D.1}$$

Where κ_w is the spectral absorption coefficient for the gas, $I_{w,b}$ is the Planck blackbody distribution function, and U is the density pathlength defined by

$$du = \frac{\rho}{\rho_0} dl = \frac{P}{P_0} \frac{T_0}{T} dl \qquad U = \int_0^L \frac{\rho(l)}{\rho_0} dl \tag{D.2}$$

The major barrier to solution of equation (D.1) is the form of the function κ_w, for the gases this is provided by the narrow-band model discussed in chapter three. The principal bands present in the spectra from combustion products are those due to water vapour at 1.38, 1.88 and 2.7μm. The statistical model with equal line strengths is used to model the emission from water vapour molecules. Individual line broadening is primarily due to collisions between the radiating molecules. Thus a Lorentz line shape is assumed, with the small contribution from Doppler broadening taken as additive. The statistical model considers that all spectra lines comprising the band are randomly distributed. The two important parameters describing this band are the mean line strength to spacing parameter $\left(\overline{S/d}\right)$ and the mean inverse line spacing $\left(\overline{1/d}\right)$. For water vapour the parameters are experimentally derived and are given by Ludwig et al. [126] as a function of temperature and wave-number.

The statistical model gives the following expression for the spectral absorption coefficient in a homogeneous gas of pathlength l

$$\kappa_{w,H} = \overline{S/d}\left[1+\frac{\overline{S/dl}\,\rho/\rho_0}{4\gamma_L\overline{1/d}}\right]^{-0.5} \tag{D.3}$$

Where γ_L is the half-width of the broadened line. Nevertheless, this expression is only valid along a homogeneous path. The Curtis-Godson approximation [127] replaces $\left(\overline{S/d}\right)$ and $\left(\overline{1/d}\right)$ with appropriate averages for non-homogeneous path. Using the Curtis-Godson approximation, the absorption coefficient at a location l, for radiation directed towards the origin, can be written as

$$\kappa_{w,CG}(l) = \overline{S/d}_{CG}\left[1+\frac{\left(\int_0^l \frac{\rho(l')}{\rho_0}dl'\right)\left(\overline{S/d}_{CG}\right)^2}{4\int_0^1 \gamma_L\overline{1/d}(l')\overline{S/d}(l')\rho(l')/\rho_0 dl'}\right]^{-0.5} \tag{D.4}$$

Where the Curtis-Godson average of the line strength to spacing parameter $\left(\overline{S/d}_{CG}\right)$ is defined as

$$\overline{S/d}_{CG} = \frac{\int_0^l \overline{S/d}(l')\rho(l')/\rho_0 dl'}{\int_0^l \rho(l')/\rho_0 dl'} \tag{D.5}$$

The optical depth along a non-homogeneous path may be written as

$$X_w(l) = \int_0^l \kappa_w(l')\frac{\rho(l')}{\rho_0}dl' \tag{D.6}$$

For a mixture of gases the total optical depth is determined by summing the individual optical depths of the various species. Thus this mixture optical depth is given by

$$X_{w,Mix}(l) = \int_0^l \left[\sum_t \kappa_{w,t}(l') P_t(l') \right] \frac{T_0}{P_0 T(l')} dl' \tag{D.7}$$

The spectral transmittance may be defined from the optical depth

$$\tau_w(l) = e^{-X_w(l)} \tag{D.8}$$

Equation (D.1) may be written in terms of this transmittance

$$I_w = -\int_1^{\tau_w(L)} I_{w,b}(T)\, d\tau_w \tag{D.9}$$

This is the form of the radiative transfer equation solved numerically by RADCAL. The integration in equation (D.9) is replaced by a summation over the *N* homogeneous elements

$$I_w = -\sum_{j=1}^{N} I_{w,b}(T_j)\left(\tau_{w,j} - \tau_{w,j-1}\right) \tag{D.10}$$

Where $\tau_{w,j}$ is the narrow-band average transmissivity for the gas mixture over cell *j* .